CUKUROVA UNIVERSITY

INSTITUTE OF NATURAL AND APPLIED SCIENCES

PhD THESIS

# Analytical Modeling and Experimental Validation of the Flexural Behavior of Composite Face-Layered Sandwich Beams Using Novel Engineering Approaches

**Ahmet ÇETİN**

*Mechanical Engineering Department*

December, 2023

**CUKUROVA UNIVERSITY**

**INSTITUTE OF NATURAL AND APPLIED SCIENCES**

# PhD THESIS APPROVAL

# Analytical Modeling and Experimental Validation of the Flexural Behavior of Composite Face-Layered Sandwich Beams Using Novel Engineering Approaches

**Ahmet ÇETİN**

***Mechanical Engineering Department***

This Doctorate Thesis was evaluated by the following Jury Members on 25/12/2023 and was approved by unanimity ~~/ majority of votes~~.

Jury : Prof. Dr. Necdet GEREN (Advisor) ……

: Prof. Dr. Naki TÜTÜNCÜ ……

: Assoc. Prof. Dr. Kerimcan ÇELEBİ ……

: Assoc. Prof. Dr. Erinç ULUDAMAR ……

: Assoc. Prof. Dr. Çağrı UZAY ……

**This Thesis was written in the Department of Mechanical Engineering, Institute of Natural and Applied Sciences.**

**Thesis Number:**

**Prof. Dr. Sadık DİNÇER**
**Director**
**Institute of Natural and Applied Sciences**

**This work was supported by the Scientific Research Project Unit of Çukurova University.**
**Project ID: FBA-2020-13140**

**Note:** The usage of the presented specific declarations, tables, figures, and photographs either in this thesis or in any other reference without citation is subject to "The law of Arts and Intellectual Products" number of 5846 of Turkish Republic

**CONTENTS**

ABSTRACT ..... I
ÖZ ..... II
EXTENDED ABSTRACT ..... III
GENİŞLETİLMİŞ ÖZET ..... IX
ACKNOWLEDGEMENTS ..... XV
LIST OF TABLES ..... XVI
LIST OF FIGURES ..... XVIII
SYMBOLS AND ABBREVIATIONS ..... XXVI
1. INTRODUCTION ..... 1
1.1. Composite materials ..... 1
1.2. Sandwich structures ..... 4
1.3. Design of sandwich structures ..... 6
2. PRELIMINARY WORK ..... 11
2.1. Methods used for the design of the composite face layer of sandwiches ..... 11
2.2. Analytical methods used for plain woven fabric composites ..... 19
2.3. The Methods for Sandwich Design ..... 22
2.3.1. Experimental sandwich design methods ..... 22
2.3.2. Numerical sandwich design methods ..... 27
2.3.3. Analytical sandwich design methods ..... 30
2.4. Significance and goal of the study ..... 40
3. MATERIAL AND METHOD ..... 43
3.1. Materials used for sandwich structures ..... 43
3.1.1. Plain woven carbon fabrics ..... 43
3.1.2. Matrix materials ..... 43
3.1.3. PVC core materials ..... 44
3.2. Development of practical engineering approach by conducting novel analytical model ..... 45
3.2.1. Modeling of plain woven fabric composite face layer ..... 49
3.2.2. Approaches used to obtain flexural properties of sandwiches ..... 63
3.3. Experimental studies to verify the developed engineering approaches ..... 71
3.3.1. Fabrication of plain woven fabric composite plates using various methods ..... 72
3.3.2. Fabrication of sandwiches ..... 77
3.3.3. Preparation of test specimens ..... 79
3.3.4. Plain woven fabric composite tensile tests ..... 86
3.3.5. Plain woven fabric composite bending tests ..... 87
3.3.6. Core compression tests ..... 87

3.3.7. Sandwich flexural tests ..... 88
4. RESULTS AND DISCUSSIONS ..... 89
4.1. The results of the developed analytical method with engineering approaches ..... 89
4.1.1. The plain woven fabric composite properties obtained with the practical engineering approach ..... 89
4.1.2. The results of sandwich beam models ..... 108
4.2. Comparison and validation of developed analytical engineering approaches with experimental results and models in the literature ..... 116
4.2.1. Comparison of the results of practical engineering approach for plain woven fabric composite face layer ..... 116
4.2.2. The comparison of compression test results of foam core with the data sheet of the core ..... 134
4.2.3. Comparison and validation of developed engineering approaches for sandwich beams with flexural test results and models in the literature ..... 135
5. CONCLUSIONS ..... 159
REFERENCES ..... 163
CURRICULUM VITAE ..... 177

**CUKUROVA UNIVERSITY**
**INSTITUTE OF NATURAL AND APPLIED SCIENCES**

**PhD THESIS**

# Analytical Modeling and Experimental Validation of the Flexural Behavior of Composite Face-Layered Sandwich Beams Using Novel Engineering Approaches

**Ahmet ÇETİN**

***Advisor: Prof. Dr. Necdet GEREN***

***Department of Mechanical Engineering***

## ABSTRACT

In this study, analytical engineering approaches are developed to predict the flexural performance of sandwich beams fabricated of PVC foam core and plain woven fabric composite face material under bending loads. Firstly, a simple and practical engineering approach is developed to estimate the strength and elasticity properties of the composite. The results obtained from the practical engineering approach were compared with models from the literature and experimental test data from the present study. In the next stage of the study, engineering approaches were developed for the flexural performance of sandwiches with fiber-reinforced composite. Existing models in the literature require the modulus of elasticity of the face material of the sandwich. Although the elastic modulus, such as traditional steel and aluminum, is known, the average modulus of elasticity of layered composite materials varies according to the fiber material, direction, weave structure, and type of resin material. Therefore, the moduli of elasticity required for the models had to be obtained experimentally. However, the stiffness properties and average moduli of elasticity of fiber-reinforced composites can be obtained theoretically by composite mechanics. The mechanical properties of the composite face material are determined by a practical engineering approach developed in this study, and then they are integrated into the developed approaches to estimate the sandwich beam's flexural performance. Thus, flexural performance parameters such as flexural stiffness, core yield load, and the maximum load the sandwich beam can carry are obtained without the need for experimental data of the face material. The practical engineering approach developed in this work not only made the prediction of the above parameters much easier, it also eliminated the need for testing and finding the moduli of elasticity by experiments.

The results obtained from the approaches developed for the sandwich were compared with models in the literature and experimental test data from the present study. As a result, it is seen that the engineering approaches developed for layered plain woven fabric composite plates and sandwich beams provided reliable and accurate results.

**Keywords**: Plain woven fabric composite, Sandwich plate, Flexural stiffness, Analytical approaches, Experimental verification

**ÇUKUROVA ÜNİVERSİTESİ**
**FEN BİLİMLERİ ENSTİTÜSÜ**

**DOKTORA TEZİ**

# Kompozit Yüzey Katmanlı Sandviç Kirişin Eğilme DavranışlarınınYenilikçi Mühendislik Yaklaşımları Kullanarak Analitik Modellenmesi ve Deneysel Olarak Doğrulanması

**Ahmet ÇETİN**

***Danışman: Prof. Dr. Necdet GEREN***

***Makine Mühendisliği Anabilim Dalı***

**ÖZ**

Bu çalışmada, düz dokuma kumaş kompozit yüzey ve PVC köpük çekirdek malzemeli sandviç kirişlerin eğilme yükleri altında eğilme performanslarınını tahmin eden analitik mühendislik yaklaşımları geliştirildi. Öncelikle, katmanlı düz dokuma kumaş kompozit plakaların elastikiyet ve mukavemet özelliklerini tahmin için pratik ve kullanışlı bir pratik mühendislik yaklaşımı geliştiririldi. Bu yaklaşımından elde edilen sonuçlar literatürde bulunan modellerden ve çalışmada yapılan deneysel test verileriyle karşılaştırıldı. Çalışmanın diğer aşamasında elyaf takviyeli kompozit yüzey malzemeli sandviçlerin eğilme performansları için mühendislik yaklaşımları geliştirildi. Literatürde bulunan mevcut modellerde sandviçin yüzey malzemesinin elastikiyet modülü değerine ihtiyaç duyulur. Geleneksel çelik aliminyum gibi yüzey malzemelerinin elastikiyet modülleri bilinmesine rağmen katmanlı kompozit malzemelerin ortalama elastikiyet modülleri elyaf malzemesi, yönü, örgü yapısı ve reçine malzemesi türüne göre değişir. Bu yüzden; günümüze kadar, modeller için gerekli kompozitin elastikiyet modülleri deneysel verilerden elde edilmiştir. Ancak elyaf takviyeli kompozitlerin rijitlik özellikleri ve ortalama elastikiyet modülleri kompozit mekaniğinden elde edilebilmektedir. Bu çalışma, yüzey malzemesinin mekanik özelliklerini pratik mühendislik yaklaşımı ile elde ettikten sonra sandviç kirişin eğilme performansını tahmin eden yaklaşımlara entegre etmiştir. Böylece eğilme rijitliği, çekirdek malzeme akma kuvveti ve kırılma modlarına göre maximum taşıyabileceği yük gibi eğilme performansları kompozitin deneysel verilerine gerek kalmadan elde edilebilmektedir. Böylece, bu çalışmada geliştirilen pratik mühendislik yaklaşımı, yukarıdaki parametrelerin tahminini çok kolay hale getirdiği gibi, aynı zamanda deneysel bir çalışma ile test etme ve elastisite modüllerini bulma ihtiyacını da ortadan kaldırmıştır.

Sandviç için geliştirilen yaklaşımın sonuçları, literatürde bulunan modellerden ve çalışmada yapılan testlerden elde edilen verilerle karşılaştırıldı. Karşılaştırmalar sonucunda katmanlı düz dokuma kumaş kompozit plaka ve sandviç kirişler için geliştirilen mühendislik yaklaşımlarının güvenilir ve doğru sonuçlar verdiği gösterilmiştir.

**Anahtar Kelimeler**: Düz dokuma kumaş kompozit, Sandviç plaka, Eğilme rijitliği, Analitik yaklaşımlar, Deneysel doğrulama

## EXTENDED ABSTRACT

As today's technologies require materials with unique properties that traditional materials such as ceramics, metals and polymeric materials cannot achieve, the trend strategy for developing new materials aims to develop materials with hybrid properties that combine multiple existing materials. The remarkable properties of fiberglass and carbon-based composite materials at different extremes have encouraged researchers to create hybrid structures. These structures offer advantages such as better strength, lower density, and higher modulus of elasticity compared to conventional materials. Although they offer higher strength values than metals, their stiffness is generally lower. Therefore, to achieve high stiffness, a low-weight core material is usually placed between two composite plates to obtain a sandwich. Structurally, it resembles an I-beam. The facesheets support bending loads in two dimensions while the core transfers the pressure between them. The use of fiber-reinforced composites has significantly influenced the popularity of sandwich materials. Due to their low weight, foam materials are commonly used as core materials for sandwich panel applications. When designing sandwich structures, attention is paid to minimizing weight and ensuring high performance under tensile and flexural conditions.

The mechanical behavior of sandwich structure designs against conditions such as low-speed impact and flexural loading is performed by experimental, numerical, and analytical design methods. Experimental design is a process used to maximize precision and produce specific results. However, the disadvantages of using an experimental setup, such as high cost, long testing time, and the limited number of iterations, may prevent reaching the ideal result. Due to the time-consuming nature of numerical methods, developing closed-form analytical solutions is more efficient than applying numerical methods and performing experiments. Over the years, analytical methods have been used to estimate sandwich structure behavior. Analytical studies for sandwich design have focused on determining the mechanisms of linear displacement (collapse) in the force direction depending on the flexural stiffness and strength of the sandwich. Studies on the design of sandwich structures require the analysis of the face material's elastic modulus. This is done to determine the stiffness and displacement mechanisms of the structures. While the modulus of elasticity of metallic materials is known, the elastic properties of composite materials vary depending on properties such as fiber, matrix, fiber structure, and fiber volume fraction. For this reason, analytical studies that prefer composite structures have required obtaining the face material's elastic modulus by performing experiments. This study aims to analytically predict the flexural performance of sandwich plates made of layered carbon plain woven fabric composite and PVC foam materials. The study aims to develop an engineering approach that does not depend on the composite material's experimental test results when predicting the sandwich beam's flexural performance. First, a practical engineering approach is developed to predict the mechanical properties of layered plain-oven fabric composite plates. Then, engineering approaches are developed using the analytical results obtained from this model to predict the flexural properties of sandwich plates. Thus, the need for face material

experimental data, which is required when predicting the flexural properties of sandwich plates, is totally eliminated.

The mechanical properties of unidirectional and angled fiber-reinforced layered composite plates can be predicted by Classical Laminate Theory (CLT). However, owing to the complexity of the weave architecture between the warp and weft yarns, analytical modeling of plain woven fabric composite materials is quite challenging. The practical use of these models is also complex due to the complexity of the models and time-consuming analytical procedures. Most models developed for the fabric have focused on single-ply fabric and analytical assumptions to predict micro properties. However, application requirements are often realized with multilayer plates. Existing models have not been able to meet the needs of designers producing laminated composite plates using stacked fabrics. Therefore, in this study, a practical engineering approach is developed, a simple and understandable approach that can predict the mechanical properties of layered plain woven fabrics. This approach relies on the engineering fiber fraction representing the undulation angle and elliptical cross-sectional area of warp and weft yarns. The engineering fiber fraction is defined and integrated into the rule of mixture equations used in composite micromechanics. Thus, the micromechanical properties of the composite are obtained without complex trigonometric and integral operations. As with the mosaic model, which is the simplest model developed for the fabric, the single-ply composite was considered a cross-ply (0/90) laminate in this approach. Thus, it is assumed that there is a cross-layered composite plate with a known micromechanical structure. The cross-ply plate orientation was determined according to the fabric's layer number. The stiffness matrices ([A], [B], [D]), average moduli of elasticity, and strength values of the multilayer of the composite plate were obtained by applying CLT. The stiffness matrices of single-ply composite plates were also obtained with the Slice Array Model (SAM) (Naik and Ganesh, 1992), which requires trigonometric and integral solutions in its calculations. Axial and flexural stiffnesses obtained from both models were compared. In the comparison, the differences in the results obtained from the models are less than 5%. It was shown that the practical engineering approach, which is simpler and easier to implement in layered composite, provides results similar to the SAM model in the literature. A comparison was also made with an empirical model presented in the literature by Wang et al. (2019), which gives the strength values of the plate under tensile loads. Unlike the model, the practical engineering approach presented strength values for weft and warp yarns. It determines that the plate will fail in the range of these two strength values. The fracture accuracy of the plate in these two strength ranges was determined. For this purpose, the experimental and empirical solutions of the model presented in the literature were compared with the failure range results, and their accuracy was proved. Comparisons were also made with experimental test results to prove the reliability of the approach. The study produced plates using five production methods: hand lay-up, low vacuum, infusion, mold compression, and high vacuum. All composite plates were produced with four carbon plain woven fabric layers and epoxy resin. These plates were identified as MT1 (hand lay-up), MT2 (low vacuum), MT3 (infusion), MT4 (mold compression), and MT5 (high vacuum), respectively. Flexural and

tensile test specimens, at least five of each plate, were obtained and tested. The experimental maximum loads of the plates under tensile loading were found to be between the predicted maximum load values for weft and warp yarns. Correspondingly, the experimental tensile strengths are also between the predicted maximum strength values for the weft and warp yarns. It confirms that the strength prediction of the approach developed in the current thesis is highly accurate. Comparing the experimental and analytical modulus of elasticity shows that the difference between the two is less than 5%. Thus, the obtained experimental and analytical stress-strain and load-strain curves closely match. Flexural loading was carried out according to the three-point bending test conditions. The load-deflection curves determined from the experimental and approximation curves also overlap. The maximum bending loads are also very close. The flexural modulus of elasticity and flexural strengths are very close, too. The difference between the flexural moduli of elasticity is 5% or less. The analytical zigzag method presents the stress values between the layers at maximum loading. The average of the analytical stress variations between the layers of the plates were very close to the experimental predictions. Applying the approach developed in this study to composite plates proved successful based on literature and experimental comparisons.

For the flexural stiffness of sandwiches, it is necessary to obtain the sandwich plate stiffness matrices ($[A]^l$, $[B]^l$, $[D]^l$) from the stiffness matrices of fiber-reinforced composites. In the engineering approach developed in this thesis, the effect of the core material on the flexural stiffness is neglected due to its very low mechanical properties. The flexural stiffness of the sandwich varies depending on the distance of facesheets from the neutral axis. In this context, the parallel axis theorem was used to determine the moments of inertia of the faces concerning the neutral axis. Thus, sandwich plate stiffness matrices were obtained depending on the beam's thickness and the face material's stiffness matrices. The bending stiffness ($bD_{11}$) of the sandwich plate was obtained with the bending stiffness matrix ($[D]^l$). Modifications were made to the equation determining the deflection performance of a two-point simply supported sandwich beam under a point load applied to its center. The term *EI* present in homogeneous isotropic beam bending equations was replaced with the $bD_{11}$ for composites. In this way, the loading deflection curve of the sandwich beam can be obtained by purely analytical approaches under flexural loading. However, while beams under flexural loading are rigid up to the core yield load, the load-deflection curves have a non-linear form after this force. They maintain this form until the maximum load they can carry. At maximum loading, they collapse in failure modes such as core shear and indentation. Therefore, the study aimed to obtain the core yield, core shear, and indentation loads by analytical methods. Although analytical studies predicting these loads have been carried out in the past, the mechanical properties of the fiber-reinforced composite material are predicted by experimental methods. In this thesis, new modified approaches were developed by integrating the average moduli of elasticity and strength values obtained from composite mechanics into the developed model. Core yield and indentation loads were predicted without experimental data on the face material. Sandwich beams with fiber-reinforced plates were fabricated to determine the accuracy of the new engineering approaches developed for

sandwich plates. Twenty-one sandwich plates of different types were produced by the high vacuum (MT5) method according to parameters such as thickness and density of the core material, number of layers of the face material, and span length of the beam. At least five three-point bending test specimens were obtained from these plates and tested. The sandwich plates were produced with four-layer or eight-layer plain woven fabric composite material. Core materials of 10, 20, and 30 mm thickness were used. PVC foams used as core materials have three different densities (48 kg/m$^3$, 80 kg/m$^3$, 130 kg/m$^3$). Hence, a total of 105 test specimens were made. Three-point bending tests were carried out at 100 mm and 250 mm span lengths. Sandwich beams were identified in the study by the coding DsTxFyLz. The symbol "D" represents the density of the PVC foam core material, "T" is the thickness of the core material, "F" is the number of layers of the face material, and "L" is the span length. The results obtained from the models developed for the sandwich were compared with the models in the literature and to the experimental test results. The bending stiffness was obtained from the sandwich beam theory developed by Allen (1969) from the literature. The modulus of elasticity of the face material in the model was taken from the experimental results of the MT5 composite plate. The results were compared with the results obtained from the analytical engineering approach developed in the study. The difference between the analytical results is less than 0.5%. The difference between the flexural stiffnesses obtained from the analytical engineering approach and the experimental flexural stiffnesses was less than 4.8%. When the Allen model and experimental results were compared, the difference was 6.2% or less. The flexural stiffness predicted by the approach developed here is closer to the experimental test results. The core yield load of the sandwich beams was obtained by the model developed by Shuaeib and Soden (1997) with the help of the experimental data of the MT5 plate. The results were compared with those obtained from the new approach developed in this study by modifying Shuaeib and Soden (1997) model. The difference between the original and developed modified models' results was less than 0.5%. These very small differences indicate that the core yield load of a sandwich beam with layered composite face material can be obtained without the need for experimental tests. Comparing the results of the modified approach and the loads at which the linearity of the experimental load-deflection curve is ending, the difference is 6.8% or less. The difference between the original model and the experimental data results is 6.4% or less. Thus, the differences between the two models and the experimental results are very close. Two different load-deflection curves were obtained with the developed model and analytical models in the literature based upon the results of flexural stiffness and yield load of the core material. These curves were compared with the curves of the experimental results. It is shown in the figures that the three different curves generated for all sandwich beams in the study overlap until the end of the linear region. Since PVC foam materials are isotropic and the beam's cross-sectional area is constant, this study did not modify the analytical approach to predict core shear failure load. However, Steeves and Fleck (2004a) developed a model that requires the modulus of elasticity of the facesheet material to predict the indentation failure mode. Therefore, the fiber-reinforced composite surface was modified according to the average modulus of elasticity values obtained from the composite mechanics.

Indentation loads were obtained from the modified and original model. The results obtained from analytical approaches were compared, and the differences were found to be less than 0.5%. The results of the modified approach and the maximum loads from the experimental results were also compared. The differences between the results can be up to 15%. When the experimental and the original model results were compared, it was shown that the difference can again be up to 15%. The differences between the experimental and the analytical models' results are quite close. The high errors here may be due to the lack of structural assumptions in the original model. In this sense, a new approach can be developed by integrating the results obtained from the composite mechanics of the facesheet material to predict the maximum indentation loads.

## GENİŞLETİLMİŞ ÖZET

Günümüz teknolojileri, seramik, metal ve polimerik malzemeler gibi geleneksel malzemelerin elde edemeyeceği benzersiz özelliklere sahip malzemelere ihtiyaç duyduğu için yeni malzemeler geliştirme trend stratejisi, birden fazla mevcut malzemeyi birleştiren hibrit özellikli malzemeler geliştirmeyi amaçlıyor. Cam elyafı ve karbon bazlı kompozit malzemelerin farklı uçlardaki dikkat çekici özellikleri, araştırmacıları hibrit yapılar oluşturmaya teşvik etmiştir. Bu yapılar geleneksel malzemelerle karşılaştırıldığında daha iyi mukavemet, daha düşük yoğunluk ve daha yüksek elastikiyet modülü gibi avantajlar sunar. Metallere göre daha yüksek mukavemet değerleri sunmalarına rağmen rijitlikleri genellikle daha düşüktür. Bu nedenle, yüksek rijitlik elde etmek için genellikle iki kompozit plaka arasına düşük ağırlıklı bir çekirdek malzeme yerleştirilerek sandviç elde edildi. Yapısal olarak bir I-kirişine benzemektedir. Yüzey levhaları iki boyutta eğilme yüklerini desteklerken çekirdek aralarındaki basıncı aktarır. Fiber takviyeli kompozitlerin sandviç yüzey malzemesi olarak kullanılması sandviç malzeme popülerliğini önemli ölçüde etkiledi. Düşük ağırlıklarından dolayı da köpük malzemeler sandviç panel uygulamalarında çekirdek malzeme olarak yaygın kullanılmaktadır. Sandviç yapılar tasarlanırken ağırlığın en aza indirilmesine, ayrıca gerilme ve eğilme koşulları altında performansın yüksek olmasına dikkat edilir.

Sandviç yapı tasarımları düşük-hızlı darbe ve eğilme yüklemeleri gibi durumlara karşı mekanik davranışı deneysel, sayısal ve analitik tasarım yöntemleriyle yapılır. Deneysel tasarım kesinliği en üst düzeye çıkarmak ve spesifik sonuçlar üretmek için kullanılan bir süreçtir. Ancak, deney düzeneği kullanmanın yüksek maliyeti, uzun test süresi ve sınırlı sayıda yineleme gibi dezavantajları olması ideal sonuca ulaşmayı engelleyebilmektedir. Sayısal yöntemlerin zaman alıcı doğası nedeniyle kapalı form analitik çözüm geliştirmek, sayısal yöntemleri uygulamaktan ve deney yapmaktan daha verimlidir. Yıllar geçtikçe sandviç yapıların davranışını tahmin etmek için analitik yöntemlerden yararlanılmıştır. Sandviç tasarımına yönelik analitik çalışmalar, sandviçin eğilme rijitliği ve mukavemetine bağlı olarak kuvvet yönünde doğrusal yer değiştirme (çökme) mekanizmalarının belirlenmesine odaklanmıştır. Literatürde sunulan çalışmalar, tasarladıkları sandviç yapıların rijitlik özelliğini ve doğrusal yer değiştirme mekanizmasını tahmin edebilmek için yüzey malzemesinin elastik modülüne gerek duyarlar. Metalik malzemelerin elastisite modülleri bilinirken, kompozit malzemelerin elastik özellikleri elyaf, matris, elyaf yapısı ve elyaf hacim oranı gibi özelliklere bağlı olarak değişmektedir. Bu nedenle yüzey malzemesi olarak kompozit yapıları tercih eden analitik çalışmalar deneysel testler yaparak yüzey malzemesinin elastik modülünü elde etmiştir. Bu çalışma, tabakalı karbon düz dokuma kumaş kompozit yüzey malzemesi ve PVC köpük malzemelerden üretilen sandviç plakaların eğilme performanslarını analitik olarak tahmin edebilmeyi amaçlamaktadır. Çalışmada, sandviç kirişin eğilme performansları tahmin edilirken kompozit yüzey malzemesinin deneysel testlerine bağımlı kalmayan bir mühendislik yaklaşımı geliştirilmek istendi. Öncelikle katmanlı düz dokuma kumaş kompozit plakaların mekanik özelliklerini tahmin edebilen pratik mühendislik yaklaşımı geliştirildi. Sonrasında bu modelden elde

edilen analitik sonuçların kullanılarak sandviç plakaların eğilme özelliklerinin tahmin edilebildiği mühendislik yaklaşımları geliştirildi. Böylece sandviç plakaların eğilme özellikleri tahmin edilirken gerekli olan yüzey malzemesi deneysel verilerine ihtiyaç ortadan kaldırıldı.

Tek yönlü ve açılı elyaf takviyeli katmanlı kompozit plakaların mekanik özellikleri klasik lamina teorisiyle (CLT) tahmin edilebilmektedir. Ancak, atkı ve çözgü iplikleri arasındaki örgü mimarisinin karmaşıklığı nedeniyle, düz dokuma kumaş kompozit malzemelerin analitik modellemesi oldukça zordur. Bu modellerin pratik kullanımı da modellerin karmaşıklığı ve zaman alan analitik prosedürler nedeniyle zordur. Düz dokuma kumaş için geliştirilen modellerin çoğu, mikro özellikleri tahmin etmek için tek katlı kumaş ve analitik kabullere odaklanmıştır. Ancak uygulama gereksinimleri genellikle çok katmanlı plakalarla gerçekleştirilir. Mevcut modeller üst-üste dizilmiş katmanlı kumaşlar kullanarak lamine kompozit plakalar üreten tasarımcıların ihtiyaçlarını karşılayamamıştır. Bu yüzden, bu çalışmada katmanlı düz dokuma kumaşların mekanik özelliklerini tahmin edebilen basit ve anlaşılabilir bir yaklaşım olan pratik mühendislik yaklaşımı geliştirildi. Bu yaklaşımda çözgü ve atkı iplikçiklerinin ondülasyon açısı ve eliptik kesit alanlarını temsil eden mühendislik elyaf fraksiyonu tanımlandı. Kompozit mikro mekaniğinde kullanılan karışım kuralı denklemlerine mühendislik elyaf fraksiyonu entegre edildi. Böylelikle karmaşık trigonometrik ve integral işlemlerine gerek duyulmadan düz dokuma kumaş kompozitin mikro mekanik özellikleri elde edildi. Düz dokuma kumaş için geliştirilmiş en basit model olan mozaik modelde olduğu gibi bu yaklaşımda da tek katlı düz dokuma kumaş kompozit çapraz katlı ($0^0/90^0$) iki katmanlı plaka olarak kabul edildi. Böylece mikro mekanik yapısı bilinen çapraz katlı katmanlı bir kompozit plaka olduğu kabulü varsayıldı. Düz dokuma kumaşın katman sayısına göre çapraz katlı plaka oryantasyonu belirlendi. CLT uygulanarak çok katlı düz dokuma kumaş kompozit plakanın rijitlik matrisleri ([A], [B], [D]), ortalama elastikiyet modülleri ve mukavemet değerleri elde edildi. Düz dokuma kumaş tabakalar için literatürde güvenilir olmasına rağmen, hesaplamalarında trigonometrik ve integral çözümlemeleri gerektiren *Slice Array Model* (SAM) (Naik and Ganesh, 1992), ile tek katlı kompozit plakaların rijitlik matrisleri elde edildi. Her iki modelden elde edilen aksiyal ve eğilme rijitlikleri karşılaştırıldı. Karşılaştırmada modellerden elde edilen sonuçların farklılıkları %5 in altındadır. Daha basit ve katmanlı düz dokuma kumaş kullanılan kompozitlerde uygulanabilirliği daha kolay olan pratik mühendislik yaklaşımının, literatürdeki SAM modeli ile yakın sonuçlar sunduğu gösterildi. Ayrıca çekme yükleri altında plakanın mukavemet değerlerini veren literatürde Wang et al. (2019) tarafından sunulan bir ampirik bir modelle de karşılaştırma yapılmıştır. Modelden farklı olarak pratik mühendislik yaklaşımı atkı ve çözgü iplikçikleri için iki farklı mukavemet değeri sunulmuştur. Plakanın bu iki mukavemet değer aralığında kırılacağını yaklaşık olarak belirlemektedir. Plakanın bu iki mukavemet değer aralığında kırılma doğruluk tespiti yapıldı. Bu amaçla modelin literatürde sunduğu deneysel ve ampirik çözümleri kırılma aralığı sonuçlarıyla karşılaştırıldı ve doğruluğu kanıtlandı. Pratik mühendislik yaklaşımının güvenilirliğini kanıtlamak için deneysel test sonuçlarıyla da karşılaştırmalar yapılmıştır. Çalışmada el yatırma, düşük vakumlama, infüzyon, kalıpla sıkıştırılma ve yüksek vakum altında beş farklı üretim

yönteminde plakalar üretildi. Tüm kompozit plakalar dört katmanlı karbon düz dokuma kumaş ve epoksi reçine ile üretilmiştir. Bu plakalar çalışmada sırasıyla MT1 (el yatırma), MT2 (düşük vakumlama), MT3 (infüzyon), MT4 (kalıpla sıkıştırılma) ve MT5 (yüksek vakum) olarak tanımlandı. Her plakadan en az beşer adet olmak üzere eğme ve çekme test numuneleri elde edildi ve testleri gerçekleştirildi. Plakaların çekme yüklemesi altında deneysel maksimum yükleri, atkı ve çözgü iplikçikleri için tahmin edilen maksimum yük değerleri arasında bulundu. Buna bağlı olarak deneysel çekme mukavemetleri de atkı ve çözgü iplikçikleri için tahmin edilen maksimum mukavemet değerleri arasındadır. Bu, Doktora tez çalışmamda geliştirdiğimiz pratik mühendislik yaklaşımının ön gördüğü mukavemet tahminini doğrulamaktadır. Deneysel elastikiyet modülü ve analitik elastikiyet modülü karşılaştırıldığında ise ikisi arasındaki farkın %5'in altında olduğu görülmüştür. Böylece, elde edilen deneysel ve analitik gerilme-gerinim (uzama) ve yük-uzama eğrileri de üst üste çakışmıştır. Eğilme yüklemeleri ise üç noktadan eğilme test şartlarına göre yapılmıştır. Deneysel ve yaklaşımdan elde edilen yük-sehim eğrileri üst üste çakışmıştır. Maksimum eğilme yükleri de çok yakındır. Eğilme elastikiyet modülü ve eğilme mukavemetleri de birbirlerine oldukça yakındır. Eğilme elastikiyet modüllüleri arasındaki fark %5 ve altındadır. Maksimum yüklemede katmanlar arasındaki gerilme değerleri analitik zigzag yöntemiyle sunulmuştur. Plakaların katmanlar arasındaki analitik stres geçişlerinin ortalaması deneysel tahminlere oldukça yakın çıkmıştır. Bu çalışmada geliştirilen pratik mühendislik yaklaşımının kompozit plakalarda uygulamasının, literatür ve deneysel karşılaştırmalar neticesinde başarılı bir yaklaşım olduğunu ispatlamıştır.

Sandviçlerin eğilme rijitlikleri için elyaf takviyeli kompozitlerin rijitlik matrislerinden, sandviç plaka rijitliği matrislerinin ($[A]^{l}$, $[B]^{l}$, $[D]^{l}$) elde edilmesi gereklidir. Tez çalışmasında geliştirilen mühendislik yaklaşımında çekirdek malzemesinin çok düşük mekanik özelliklerinden dolayı eğilme rijitliğine etkisi ihmal edildi. Yüzey plaka test kirişlerinin eğilme rijitliği sandviç kirişin nötr eksene uzaklığına bağlı olarak kirişin eğilme rijitliği değişkenlik gösterir. Bu bağlamda yüzeylerin nötr eksene ilişkin atalet momentlerini belirlemek için paralel eksen teoreminden faydalanıldı. Böylece kirişin kalınlığı ve yüzey malzemesinin rijitlik matrislerine bağlı olarak sandviç plaka rijitlik matrisleri elde edildi. Eğme rijitlik matrisi ($[D]^{l}$) ile de sandviç plakanın eğilme rijitliği ($bD_{11}$) elde edildi. İki noktadan basit destekli sandviç kirişin merkezine uygulanan noktasal yük altında sehim performansını belirleyen denklemde değişiklikler yapıldı. $EI$ yerine $bD_{11}$ eğilme rijitliği terimi ile değiştirildi. Bu sayede eğilme yükü altındaki sandviç kirişin yükleme sehim eğrisi tamamen analitik yaklaşımlarla elde edilebilir hale geldi. Ancak, eğilme yükü altında kirişler çekirdek akma yükleme kuvvetlerine kadar rijitken, bu kuvvetten sonra yük sehim eğrileri lineer olmayan bir formdadırlar. Bu formu taşıyabilecekleri maksimum yüke kadar sürdürmektedirler. Maksimum yüklemede de çekirdek kayması, batma/ezilme gibi kırılma modlarında çökmektedirler. Bu yüzden çalışma; çekirdek akma, çekirdek kayması, batma yüklerini de analitik yöntemlerle elde etmeyi amaçladı. Bu yükleri tahmin eden analitik çalışmalar geçmişte yapılmış olmasına rağmen, elyaf takviyeli plaka yüzey malzemesinin mekanik özellikleri deneysel yöntemlerle tahmin edilmektedir. Bu tez çalışmasında kompozit mekaniğinden elde edilen ortalama elastikiyet modülleri

ve mukavemet değerleri geliştirilen modele entegre edilerek modifiye edilmiş yeni yaklaşımlar elde edilmiştir. Çekirdek akma, batma yükleri yüzey malzemesinin deneysel datalarına gerek kalmadan tahmin edildi. Sandviç plakalar için geliştirilen yeni mühendislik yaklaşımlarının doğruluğunu belirlemek için elyaf takviyeli plaka yüzeyli sandviç kirişler üretildi. Yirmi bir farklı sandviç plaka; çekirdek malzemenin yoğunluğu, kalınlığı, yüzey malzemesinin katman sayısı, kirişin span uzunluğu gibi parametrelere göre yüksek vakumlama (MT5) yöntemi ile üretildi. Bu plakalardan en az beşer adet üç noktadan eğme test numunesi elde edildi ve testleri gerçekleştirildi. Sandviç plakalar üretilirken dört katmanlı veya sekiz katmanlı düz dokuma kumaş kompozit yüzey malzemesi kullanıldı. 10, 20, ve 30 mm kalınlıklarda çekirdek malzemeler kullanıldı. Çekirdek malzeme olarak kullanılan PVC köpükler üç farklı yoğunluğa sahiptir (48 kg/m$^3$, 80 kg/m$^3$, 130 kg/m$^3$). Üç noktadan eğilme testleri ise 100 mm ve 250 mm span uzunluklarında gerçekleştirildi. Sandviç kirişler çalışmada D*s*T*x*F*y*L*z* kodlamasıyla tanımlanmıştır. "D" sembolu, PVC köpük çekirdek malzemenin yoğunluğunu, "T" çekirdek malzemenin kalınlığını, "F" yüzey malzemesinin katman sayısını ve "L" span uzunluğunu temsil eder. Sandviç için geliştirilen modellerden elde edilen sonuçlar literatürde bulunan modeller ve deneysel sonuçlarla karşılaştırıldı. Eğilme rijitliği Allen (1969) tarafından geliştirilmiş literatürdeki sandviç kiriş teorisi ile elde edildi. Modelde yüzey malzemesinin elastikiyet modülü MT5 kompozit plakasının deneysel sonuçlarından alındı. Sonuçlar, çalışmada geliştirilen analitik mühendislik yaklaşımından elde edilen sonuçlarla karşılaştırıldı. Elde edilen eğilme rijitlikleri arasındaki fark %0.5 'in altındadır. Analitik mühendislik yaklaşımından elde edilen ve deneysel eğilme rijitlikleri karşılaştırılınca %4.8'in altında farklar oluştu. Allen modeli ve deneysel sonuçlar karşılaştırıldığında ise fark %6.2 ve altında çıkmıştır. Burada geliştirilen yaklaşımla tahmin edilen eğilme rijitliği deneysele daha yakın çıkmıştır. Sandviç kirişlerin çekirdek malzemesinin akma yükü MT5 plakasının deneysel verileri yardımıyla Shuaeib and Soden'nin (1997) geliştirdiği modelle elde edildi. Elde edilen sonuçlar, bu çalışmada Shuaeib and Soden (1997) modelinin modifiye edilmesiyle geliştirilen yeni yaklaşımdan elde edilen sonuçlarla karşılaştırıldı. Orijinal model ve modifiye edilen yeni model sonuçları arasındaki fark %0.5 den düşük bulunmuştur. Bu çok düşük farklar gösteriyor ki deneysel testlere gerek kalmadan tabakalı kompozit yüzey malzemesine sahip bir sandviç kirişin çekirdek malzemesi akma yükü elde edilebilir. Modifiye edilen yaklaşım sonuçları ve deneysel yük-sehim eğrisinde lineerliğin bozulduğu yükler karşılaştırıldığında fark %6.8 ve altındadır. Orijinal modelden elde edilen sonuçlar ve deneysel veriler karşılaştırıldığında fark %6.4 ve altındadır. Böylece, iki modelin deneysel sonuçlarla karşılaştırılması sonucunda meydana gelen farklar çok yakındır. Eğilme rijitliği ve çekirdek malzeme akma yükü sonuçlarına göre geliştirilen model ve literatürdeki analitik modellerle iki farklı yük-sehim eğrisi elde edildi. Bu eğriler deneysel sonuçların eğrileriyle karşılaştırıldı. Çalışmadaki bütün sandviç kirişler için oluşturulan üç farklı eğrinin, lineer bölge bitişine kadar üst üste çakıştığı figürlerde gösterildi. PVC köpük malzemeler izotropik ve kirişin kesit alanı sabit olduğundan bu çalışmada çekirdek kayması kırılma madunundaki maksimum yüklemeyi tahmin eden analitik yaklaşım için geliştirme yapılmadı. Ancak batma/ezilme kırılma modu yükünü tahmin için Steeves and Fleck (2004a) tarafından

geliştirilmiş model yüzey malzemesinin elastikiye modülüne ihtiyaç duymaktadır. Bu yüzden elyaf takviyeli kompozit yüzey malzemenin kompozit mekaniğinden elde edilen ortalama elastikiyet modül değerlerine göre yeniden modifiye edilmiştir. Modifiye edilen ve orijinal modelden batma yükleri elde edildi. Her iki analitik yaklaşımdan elde edilen sonuçlar karşılaştırıldığında farklar %0.5'in altındadır. Modifiye edilen yaklaşım sonuçları ve deneysel sonuçlardan alınan maksimum yükler de karşılaştırıldı. Sonuçlar arasında farklılıklar %15'e kadar çıkabilmektedir. Orijinal model ve deneysel sonuçlarda karşılaştırıldığında farkın yine %15'lere kadar çıkabildiği gösterilmiştir. Her iki analitik modelin de deneysel sonuçlarla olan farklılıkları oldukça yakındır. Burada hataların yüksek olmasının sebebi orijinal modelin yapısal kabullerde eksiklikleri olabilir. Bu anlamda maksimum batma yüklerini tahmin için yüzey malzemesinin kompozit mekaniğinden elde edilmiş sonuçları entegre edilerek yeni bir yaklaşım geliştirilebilir.

**ACKNOWLEDGEMENTS**

First, I would like to thank my supervisor, Prof. Dr. Necdet GEREN, sincerely for sharing his valuable knowledge, experience, and support with me during my studies and while writing my doctoral thesis. Secondly, I would like to thank my esteemed mentor, Prof. Dr. Naki TÜTÜNCÜ, for sharing his valuable knowledge and experience in analytical studies with me, and giving me a new vision.

I would like to thank Assoc. Prof. Dr. Çağrı UZAY for sharing his experience in producing sandwich and composite materials with me. I want to thank Assoc. Prof. Dr. Sefa YILDIRIM for allowing me to use the KOMPro software he developed for reinforced composite mechanics calculations. I would like to thank my thesis committee member Assoc. Prof. Dr. Kerimcan ÇELEBİ for his advice and motivation. I would like to thank my thesis jury member, Assoc. Prof. Dr. Erinç ULUDAMAR, for his contributions. I would like to thank my dear colleague Durmuş Can ACER for his motivation, valuable friendship, and help in producing experimental samples. I would like to thank our valuable technician, Sefa MERAL, for his help in preparing the experimental samples.

I would like to thank all the Mechanical Engineering Department staff, the Scientific Research Project depeartment (BAP) unit staff, and the Teaching Staff Training Program (ÖYP) staff. Furthermore, I would like to thank the ÖYP and BAP units for their financial support.

Lastly, I am grateful to my precious parents, my mother Eşşe ÇETİN and my father Nizamettin ÇETİN, for all the support they have given me throughout my education. I would like to express my gratitude to my beloved wife Fatma Tuğba ÇETİN for her support and friendship in my academic and social life. I am especially grateful for having my beloved daughter, Gül Lina ÇETİN, who is the source of extra motivation and light of life for me.

**LIST OF TABLES**


Table 3.1. Mechanical properties of AIREX C70 foam materials ..... 45
Table 3.2. Technical specifications data of low vacuum pump ..... 74
Table 3.3. Technical specifications data of high vacuum pump ..... 77
Table 3.4. Carbon plain woven fabric laminates thickness and span length ..... 81
Table 3.5. Sandwich beam configuration details constituting the thesis study ..... 85
Table 4.1 Mechanical properties of on-axis plain woven fabric composite ..... 90
Table 4.2. Stiffness matrixes of four-layer plain woven fabric composite ..... 90
Table 4.3. Compliance matrixes of four-layer plain woven fabric composite ..... 91
Table 4.4. Tensile reserve factors R of the plate under 1 N tensile load, and maximum load bearing capacity ..... 92
Table 4.5. Average elastic modulus and strength results obtained with the proposed practical approach for plain woven fabric composite ..... 98
Table 4.6. Flexural reserve factors R of the beams under 1 N flexural load and maximum flexural load bearing capacity ..... 100
Table 4.7. Experimentally and analytically obtained flexural properties of four-ply woven plain fabric composite laminate beams ..... 103
Table 4.8. Analytically obtained stress values on layer surfaces of plain woven fabric composite beams ..... 105
Table 4.9. Analytical results of the flexural stiffness sandwich plates for the five manufacturing methods ..... 109
Table 4.10. Analytical core yield force results of sandwich configurations ..... 110
Table 4.11. Analytical failure mode force results and expected failure modes of sandwich configurations ..... 115
Table 4.12. Axial Stiffness ($A_{11}^{s}$) of UD cross-play (0-90) and single-ply plain woven fabric composite (lamina) ..... 117
Table 4.13. Bending Stiffness($D_{11}^{s}$) of UD cross-play (0-90) and single-ply plain woven fabric composite (lamina) ..... 117
Table 4.14. Comparison of SAM and the practical approach for axial stiffness ($A_{11}^{s}$) of single-ply plain woven fabric composite plate ..... 118
Table 4.15. Comparison of bending stiffness ($D_{11}^{s}$) of single-ply plain woven fabric composite plate based on SAM and the developed practical approach ..... 118
Table 4.16. Comparison of tensile strength values between the experimental literature examples and the present approach ..... 119
Table 4.17. Maximum tensile loads obtained from experimental and practical engineering approach ..... 121

Table 4.18. Comparison of tensile modulus data obtained from both experiments and analytical approach for four-layer plain woven fabric composite plate ..... 125
Table 4.19. Comparison of the experimental strength results with the proposed practical approach for four-layer plain woven fabric composite plate..... 125
Table 4.20. Experimental and analytical maximum flexural load results of plain woven fabric composite plates ..... 128
Table 4.21. Experimental flexural strength results of plain woven fabric composite ..... 130
Table 4.22. Experimentally and analytically obtained flexural properties of four-ply woven plain fabric composite laminate beams ..... 131
Table 4.23. Comparison of flexural stiffness of sandwich plates configuration obtained by engineering approach (developed approach), and Allen's method in literature..... 137
Table 4.24. Experimental flexural stiffness results of sandwich plates..... 137
Table 4.25. Comparison of flexural stiffness of sandwich plates obtained by experiment, engineering approach, and Allen's method..... 138
Table 4.26. Comparison of core yield loads obtained from the original and modified models.... 139
Table 4.27. Comparison of core yield loads obtained from the original and modified models with experimental results..... 140
Table 4.28. Comparison of core shear loads obtained from analytical models with experimental results..... 153
Table 4.29. Comparison of indentation loads obtained from the original and modified model ... 155
Table 4.30. Comparison of indentation loads obtained from the original and modified models with experimental results..... 156

**LIST OF FIGURES**


Figure 1.1. The dispersed and matrix phase of composite materials. ..... 2
Figure 1.2. Schematic diagram of production methods of composite ..... 3
Figure 1.3. Representation of a type of sandwich structure. ..... 4
Figure 1.4. The sandwich structure is subjected to various deformation and flexural loads. ..... 6
Figure 1.5. A sandwich beam exhibits a bending moment of M, N's normal force, and V's shear force ..... 6
Figure 1.6. Sandwich beam under bending ..... 8
Figure 1.7. The sandwich structure failure modes are presented in detail ..... 9
Figure 2.1. The facesheet and core of the sandwich panel are made of plywood ..... 12
Figure 2.2. Schematic illustration of timber sandwich panel ..... 13
Figure 2.3. Failure modes: (a-b) core shear failure (c-d) top facesheet crushing failure with debonding and buckling ..... 14
Figure 2.4. The failure modes of the specimens were (a) flatwise and (b) edgewise ..... 15
Figure 2.5. The process of creating sandwich panels using a honeycomb-filled orthogrid core is shown in this diagram ..... 16
Figure 2.6. Test details a) The laser acquisition system's position and the acoustic emission sensors' position b) The results of a mechanical-acoustic coupling study ..... 17
Figure 2.7. The sandwich structure features inner and outer layers: a) classic concept, b) the hybrid structure shows the intermediate layers ..... 23
Figure 2.8. The diagram shows the fabrication process of the sandwich ..... 24
Figure 2.9. Sandwich structure with core material reinforced with carbon or glass rods ..... 24
Figure 2.10. The sandwich structures were modeled in three types ..... 25
Figure 2.11. Corrugated core shapes were utilized in designing and constructing composite sandwich panels ..... 25
Figure 2.12. Designed and manufactured corrugated sandwich beam sample ..... 26
Figure 2.13. This illustration shows the manufacturing process of SrPP structures ..... 27
Figure 2.14. A diagram showing existing a) Cross-laminated timber panel, b) Peeling Core Sandwich, and c) Bamboo Core Sandwich panel ..... 29
Figure 2.15. Diagram showing the layout of the sandwich panel ..... 29
Figure 2.16. The force-displacement diagrams compare the numerical and experimental results ..... 30
Figure 2.17. Load-deflection diagram of sandwiches under three-point bending loading ..... 33
Figure 2.18. The collapse modes A and B are used for the core shear of a sandwich beam in a three-point bending process ..... 36
Figure 3.1. Image of carbon plain woven fabric ..... 43

Figure 3.2. MGS L160 resin and MGS H160 hardener ..... 44
Figure 3.3. AIREX C70 foams are used as core material ..... 44
Figure 3.4. Plenary flow chart illustrating the overall approach for the analytical and experimental studies to obtain and verify the mechanical properties of the sandwich beam ..... 46
Figure 3.5. The detailed flow chart for Part 1 in Figure 3.4 shows the step-by-step procedure to find the mechanical properties of carbon fiber composite face sheet and validate the properties by experimental study. ..... 47
Figure 3.6. The detailed flow chart for Part 2 in Figure 3.4 shows the step-by-step procedure to find the mechanical properties of the carbon fiber composite sandwich beam and the validation of the properties by the experimental study. ..... 48
Figure 3.7. a) muffle furnace b) burn-off tests specimens prepared from plain woven fabric composite plate ..... 50
Figure 3.8. Cross sections for a) Woven plain fabric composites unit cell, b) Yarn geometry details, c) Yarn cross-sectional area at the midpoint of undulation ..... 51
Figure 3.9. Stress distribution under the two-dimensional unidirectional lamina ..... 54
Figure 3.10. The beam is under a bending moment, and the axial load ..... 56
Figure 3.11. (a) Beam configuration under three-point bending loading (b) beam internal load ..... 59
Figure 3.12. a) Front sectional and b) half front sectional view of the sandwich plate ..... 64
Figure 3.13. Schematical presentation of the sandwich beam under a three-point bending loa ..... 66
Figure 3.14. The deflection of a sandwich beam is computed by taking into account both the shear component $vs$ and the bending component $vb$. ..... 67
Figure 3.15. Core yield condition in the sandwich beam under three-point bending load ..... 69
Figure 3.16. Core shear failure in the sandwich beam under a three-point bending load ..... 70
Figure 3.17. Indentation failure in the sandwich beam under a three-point bending load ..... 71
Figure 3.18. Hand Lay-up production method (a) schematic explanation (b) laboratory production photo ..... 73
Figure 3.19. Vacuum bagging production method (a) schematic explanation (b) laboratory production photo ..... 74
Figure 3.20. Vacuum-assisted resin infusion production method (a) schematic explanation (b) laboratory production photo ..... 75
Figure 3.21. Compression molding production method (a) schematic explanation (b) laboratory production photo ..... 76
Figure 3.22. The pump with high vacuuming power used in the thesis ..... 77
Figure 3.23. Schematic view of the vacuum bag method for the sandwich plate ..... 78
Figure 3.24. (a) Sandwich panels curing under vacuum, (b) Sandwich panel after curing ..... 78

Figure 3.25. Schematic presents the dimensions of plain woven fabric composite plates and specimens for axial tensile test ..... 79
Figure 3.26. (a) Schematical presentation of the assembly of the tabs and tensile specimen (b) plain woven fabric composite specimens prepared for axial tensile tests ..... 80
Figure 3.27. Schematic presents the dimensions of plain woven fabric composite plates and specimens for a three-point bending test ..... 81
Figure 3.28. Plain woven fabric composite specimens prepared for three-point bending testin ..... 82
Figure 3.29. PVC foam specimens prepared for compression testing ..... 82
Figure 3.30. Schematic presents the dimensions of the sandwich plate for a three-point bending test of (a) short beam and (b) long beam ..... 84
Figure 3.31. Explanation of abbreviation codes of sandwich beams ..... 85
Figure 3.32. Sandwich beam preparation process for the three-point bending test ..... 86
Figure 3.33. Carbon plain woven fabric composite plate axial tensile test setup ..... 86
Figure 3.34. Carbon plain woven fabric composite plate three-point bending test setup ..... 87
Figure 3.35. Compression test setup of PVC foam core material ..... 88
Figure 3.36. Sandwich three-point bending test setup a) long-span length (b) short-span lengt ..... 88
Figure 4.1. Analytical tensile load-extension curve of MT1 plate obtained with the practical engineering approach..... 94
Figure 4.2. Analytical tensile load-extension curve of MT2 plate obtained with the practical engineering approach..... 94
Figure 4.3. Analytical tensile load-extension curve of MT3 plate obtained with the practical engineering approach..... 94
Figure 4.4. Analytical tensile load-extension curve of MT4 plate obtained with the practical engineering approach..... 95
Figure 4.5. Analytical tensile load-extension curve of MT5 plate obtained with the practical engineering approach..... 95
Figure 4.6. Analytical tensile stress-strain curve of MT1 plate obtained with the practical engineering approach..... 96
Figure 4.7. Analytical tensile stress-strain curve of MT2 plate obtained with the practical engineering approach..... 96
Figure 4.8. Analytical tensile stress-strain curve of MT3 plate obtained with the practical engineering approach..... 97
Figure 4.9. Analytical tensile stress-strain curve of MT4 plate obtained with the practical engineering approach..... 97
Figure 4.10. Analytical tensile stress-strain curve of MT5 plate obtained with the practical engineering approach..... 97

Figure 4.11. Plain woven fabric composite plate layer configuration as cross-ply for bending loading ..... 99
Figure 4.12. Analytical flexural load-deflection curve of MT1 plate obtained with the practical engineering approach..... 102
Figure 4.13. Analytical flexural load-deflection curve of MT2 plate obtained with the practical engineering approach..... 102
Figure 4.14. Analytical flexural load-deflection curve of MT3 plate obtained with the practical engineering approach..... 102
Figure 4.15. Analytical flexural load-deflection curve of MT4 plate obtained with the practical engineering approach..... 103
Figure 4.16. Analytical flexural load-deflection curve of MT5 plate obtained with the practical engineering approach..... 103
Figure 4.17. Internal stress distribution along the thickness of the MT1 plate was obtained with the practical engineering approach ..... 107
Figure 4.18. Internal stress distribution along the thickness of the MT2 plate was obtained with the practical engineering approach ..... 107
Figure 4.19. Internal stress distribution along the thickness of the MT3 plate was obtained with the practical engineering approach ..... 107
Figure 4.20. Internal stress distribution along the thickness of the MT4 plate was obtained with the practical engineering approach ..... 108
Figure 4.21. Internal stress distribution along the thickness of the MT5 plate was obtained with the practical engineering approach ..... 108
Figure 4.22. Load-displacement curves of sandwiches designed with 48 kg/m$^3$ density core and 4-ply plain woven fabric composite at 100 mm span range under three-point bending ..... 111
Figure 4.23. Load-displacement curves of sandwiches designed with 48 kg/m$^3$ density core and 4-ply plain woven fabric composite at 250 mm span range under three-point bending ..... 111
Figure 4.24. Load-displacement curves of sandwiches designed with 80 kg/m$^3$ density core and 4-ply plain woven fabric composite at 100 mm span range under three-point bending ..... 112
Figure 4.25. Load-displacement curves of sandwiches designed with 80 kg/m$^3$ density core and 4-ply plain woven fabric composite at 250 mm span range under three-point bending ..... 112
Figure 4.26. Load-displacement curves of sandwiches designed with 130 kg/m$^3$ density core and 4-ply plain woven fabric composite at 100 mm span range under three-point bending ..... 112

Figure 4.27. Load-displacement curves of sandwiches designed with 130 kg/m$^3$ density core and 4-ply plain woven fabric composite at 250 mm span range under three-point bending ..... 113
Figure 4.28. Load-displacement curves of sandwiches designed with 20 mm thickness cores and 8-ply plain woven fabric composite at 100 mm span range under three-point bending ..... 113
Figure 4.29. Failure mechanism maps of sandwich beams designed from (a) high-density and (b) medium-density PVC foam core (Steeves and Fleck, 2004b) ..... 116
Figure 4.30. Load-extension curves of MT1 (manufactured with hand lay-up) specimens ..... 120
Figure 4.31. Load-extension curves of MT2 (manufactured in the vacuum bag with a low-capacity vacuum pump) specimens ..... 120
Figure 4.32. Load-extension curves of MT3 (manufactured with vacuum-assisted resin infusion) specimens ..... 120
Figure 4.33. Load-extension curves of MT4 (manufactured with compression molding) specimens ..... 121
Figure 4.34. Load-extension curves of MT5 (manufactured in the vacuum bag with a high-capacity vacuum pump) specimens ..... 121
Figure 4.35. Stress-strain curves of MT1 (manufactured with hand lay-up) specimens ..... 123
Figure 4.36. Stress-strain curves of MT2 (manufactured in the vacuum bag with a low-capacity vacuum pump) specimens ..... 123
Figure 4.37. Stress-strain curves of MT3 (manufactured with vacuum-assisted resin infusion) specimens ..... 123
Figure 4.38. Stress-strain curves of MT4 (manufactured with compression molding) specimens ..... 124
Figure 4.39. Stress-strain curves of MT5 (manufactured in the vacuum bag with a high-capacity vacuum pump) specimens ..... 124
Figure 4.40. Flexural load-deflection curves of MT1 (manufactured with hand lay-up) specimens ..... 126
Figure 4.41. Flexural load-deflection curves of MT2 (manufactured in the vacuum bag with a low-capacity vacuum pump) specimens ..... 127
Figure 4.42. Flexural load-deflection curves of MT3 (manufactured with vacuum-assisted resin infusion) specimens ..... 127
Figure 4.43. Flexural load-deflection curves of MT4 (manufactured with compression molding) specimens ..... 127
Figure 4.44. Flexural load-deflection curves of MT5 (manufactured in the vacuum bag with a high-capacity vacuum pump) specimens ..... 128
Figure 4.45. Flexural stress-strain curves of MT1 (manufactured with hand lay-up) specimen ... 129

Figure 4.46. Flexural stress-strain curves of MT2 (manufactured in the vacuum bag with a low-capacity vacuum pump) specimens ..... 129
Figure 4.47. Flexural stress-strain curves of MT3 (manufactured with vacuum-assisted resin infusion) specimens ..... 129
Figure 4.48. Flexural stress-strain curves of MT4 (manufactured with compression molding) specimens ..... 130
Figure 4.49. Flexural stress-strain curves of MT5 (manufactured in the vacuum bag with a high-capacity vacuum pump) specimens ..... 130
Figure 4.50. Internal stress distribution along the thickness of MT1 specimens manufactured with hand lay-up ..... 132
Figure 4.51. Internal stress distribution along the thickness of MT2 specimens manufactured in the vacuum bag with a low-capacity vacuum pump ..... 132
Figure 4.52. Internal stress distribution along the thickness of MT3 specimens manufactured with vacuum-assisted resin infusion specimens ..... 132
Figure 4.53. Internal stress distribution along with the thickness of MT4 specimens manufactured with compression molding ..... 133
Figure 4.54. Internal stress distribution along with the thickness of MT5 specimens manufactured in the vacuum bag with a high-capacity vacuum pump ..... 133
Figure 4.55. 48 kg/m$^3$ density PVC foam compression stress-strain curve ..... 134
Figure 4.56. 80 kg/m$^3$ density PVC foam compression stress-strain curve ..... 134
Figure 4.57. 130 kg/m$^3$ density PVC foam compression stress-strain curve ..... 135
Figure 4.58. Comparison of experimental and analytical force-deflection curves of D48T10F4L100 coded sandwich beam ..... 141
Figure 4.59. Comparison of experimental and analytical force-deflection curves of D48T20F4L100 coded sandwich beam ..... 142
Figure 4.60. Comparison of experimental and analytical force-deflection curves of D48T30F4L100 coded sandwich beam ..... 142
Figure 4.61. Comparison of experimental and analytical force-deflection curves of D75T10F4L100 coded sandwich beam ..... 142
Figure 4.62. Comparison of experimental and analytical force-deflection curves of D75T20F4L100 coded sandwich beam ..... 143
Figure 4.63. Comparison of experimental and analytical force-deflection curves of D75T30F4L100 coded sandwich beam ..... 143
Figure 4.64. Comparison of experimental and analytical force-deflection curves of D130T10F4L100 coded sandwich beam ..... 143
Figure 4.65. Comparison of experimental and analytical force-deflection curves of D130T20F4L100 coded sandwich beam ..... 144

Figure 4.66. Comparison of experimental and analytical force-deflection curves of D130T30F4L100 coded sandwich beam ..... 144
Figure 4.67. Comparison of experimental and analytical force-deflection curves of D48T20F8L100 coded sandwich beam ..... 144
Figure 4.68. Comparison of experimental and analytical force-deflection curves of D75T20F8L100 coded sandwich beam ..... 145
Figure 4.69. Comparison of experimental and analytical force-deflection curves of D130T20F8L100 coded sandwich beam ..... 145
Figure 4.70. Comparison of experimental and analytical force-deflection curves of D48T10F4L250 coded sandwich beam ..... 146
Figure 4.71. Comparison of experimental and analytical force-deflection curves of D48T20F4L250 coded sandwich beam ..... 147
Figure 4.72. Comparison of experimental and analytical force-deflection curves of D48T30F4L250 coded sandwich beam ..... 147
Figure 4.73. Comparison of experimental and analytical force-deflection curves of D75T10F4L250 coded sandwich beam ..... 147
Figure 4.74. Comparison of experimental and analytical force-deflection curves of D75T20F4L250 coded sandwich beam ..... 148
Figure 4.75. Comparison of experimental and analytical force-deflection curves of D75T30F4L250 coded sandwich beam ..... 148
Figure 4.76. Comparison of experimental and analytical force-deflection curves of D130T10F4L250 coded sandwich beam ..... 148
Figure 4.77. Comparison of experimental and analytical force-deflection curves of D130T20F4L250 coded sandwich beam ..... 149
Figure 4.78. Comparison of experimental and analytical force-deflection curves of D130T30F4L250 coded sandwich beam ..... 149
Figure 4.79. Images of sandwiches with 10 mm core thickness and four-ply plain woven fabric composite facesheet at failure under three-point bending load ..... 150
Figure 4.80. Images of sandwiches with 10 mm core thickness and four-ply plain woven fabric composite facesheet at failure under three-point bending load ..... 151
Figure 4.81. Images of sandwiches with 10 mm core thickness and four-ply plain woven fabric composite facesheet at failure under three-point bending load ..... 152
Figure 4.82. Demonstration of the use of failure maps of sandwich beams made of PVC foam core material ..... 157

**SYMBOLS AND ABBREVIATIONS**

$(\varepsilon_m^1)_{ult}$ : Matrix ultimate tensile strain

$A_{11}^s$ : Axial stiffness of single-ply PWFC

$A_{yarn}$ : Yarn cross-sectional area

$b_f$ : Width of facesheet

$D_{11}$ : Longitudinal unit bending stiffness

$D_{11}^f$ : Laminate bending stiffness for four (f) ply of PWFC

$D_{11}^s$ : Longitudinal bending stiffness term of sandwich

$D_f$ : Analytic unit bending stiffness

$E_1$ : Longitudinal modulus of lamina

$E_2$ : Transverse modulus of lamina

$E_{av}$ : Plate average elastic modulus

$E_B$ : Bending Modulus

$E_c$ : Compression elastic modulus of core

$E_f$ : Experimental elastic modulus of facesheet

$E_F$ : Fiber tensile elastic modulus

$E_m$ : Matrix tensile elastic modulus

$E_x, E_y$ : Laminate elastic modulus

$G_{12}$ : On-axis shear modulus

$G_f$ : Fiber shear modulus

$G_m$ : Matrix shear modulus

$h_f$ : Fill thickness

$h_w$ : Warp thickness

$I_f$ : Moment of inertia of facesheet

$k_x, k_y\ k_{xy}$ : Curvature

$L_u$ : Undulation length of warp

$P_1$ : Core yield load

$P_2 = P_i$ : Maximum indentation failure load

$P_{Fy}$ : Maximum face yielding failure load

$P_S$ : Maximum shear failure load

$P_W$ : Maximum wrinkling failure load

$Q_{11}$ : Lamina Stiffness

$Q_{ij}$ : Stiffness coefficients

$Q_w$ : Undulation angle

$t_f$ : Facesheet thickness

$v_{12}$ : On-axis poison ratio

$v_f$ : Fiber poison ratio

$V_f$ : Volume fraction

$V_f^E$ : Engineering fiber volume fraction

$V_f^O$ : Overall fiber volume fraction

$V_f^Y$ : Yarn fiber volume fraction

$v_m$ : Matrix Poison's ratio

$X_1$ : Longitudinal strength

$Y_1$ : Transverse strength

$\alpha_{11}$ : Axial compliance

$\delta_{11}$ : Bending compliance

$\delta_{11}^f$ : Bending compliance for four (f) ply of WPFC

$\varepsilon_x, \varepsilon_x, \gamma_{xy}$ : Internal Strains

$\sigma_{\varepsilon_{max}^f}^m$ : Matrix tensile strength at fiber maximum strain

$\sigma_c$ : Compression core yield strength

$\sigma_f$ : Flexural stress

$\sigma_{fill}^T$ : Fill yarn tensile strength

$\sigma_{max}^f$ : Fiber tensile strength

$\sigma_{warp}^T$ : Warp yarn tensile strength

[A], [B], [D] : Composite plate stiffness matrices

$[A]^l$, $[B]^l$, $[D]^l$ : Sandwich Plate stiffness matrices

ASTM : American Society for Testing and Materials

b : Specimen width

b : width of sandwich

c : Core thickness

CCAM : Composite cylinder assemblage model

CLT : Classical Laminate Theory

$d$ : Fiber diameter

d : Sandwich thickness

FEA : Finite element analysis

FEM : Finite element model

FML : Fiber metal laminate

FRP : Glass fiber-reinforced polymers

g : Yarn gap

GFRP : Glass fiber-reinforced polymer

h : Specimen thickness

HL : Hand lay-up

k : Foundation modulus

L : Span length

m : Slope of the tangent to the initial of the load-deflection curve

MT1 : Composite plate manufactured by hand lay-up

MT2 : Composite plate manufactured by low vacuum bag

MT3 : Composite plate manufactured by infusion

MT4 : Composite plate manufactured by mold compression

MT5 : Composite plate manufactured by high vacuum bag

PET : Polyethylene terephthalate

PU : Polyurethane

PVC : Polyvinyl chloride

PWFC : Plain woven fabric composite

RTM : Resin transfer molding

s : Fiber distance

SAM : Slice array model

SRC : Self-reinforced polymer composite

SrPP : Self-reinforced polypropylene composites

t : Plate thickness

UD : Unidirectional composite

VARTM : Vacuum-assisted resin transfer molding

VIP : Vacuum infusion processing

w : Width of fill yarn

# 1. INTRODUCTION

## 1.1. Composite materials

Today's technologies require materials with unique properties that cannot be achieved by traditional materials such as ceramics, metal, and polymeric materials. Therefore, finding the correct type of material for materials used in transportation, aerospace, and underwater applications is significant. For instance, aircraft engineers are looking for lightweight, hard-wearing structural materials that resist corrosion (Callister and Rethwisch, 2016). New materials can be expensive and uncertain, and the gains from their development can be incremental rather than significant. The trend strategy of developing novel materials aims to combine multiple existing materials to create hybrid properties. For example, the remarkable properties of glass-fiber and carbon-based composite materials at different extremes have encouraged researchers to look into creating hybrid structures (Ashby, 2016). Compared to conventional materials, composite structures offer advantages, including better strength, lower density, and higher modulus. One of the first structural materials that were widely used was fiberglass-reinforced plastics. Advanced materials such as carbon and graphite are commonly used in aerospace. Also, certain composite materials, such as carbon/epoxy, are commonly used in aircraft structures. Various structural elements made from composite materials are used in various forms of construction, such as marine structures and automotive. They are also utilized in producing golf clubs, tennis rackets, and skis. The increasing number of aircraft applications of composite materials has been attributed to the lower cost of materials and the technological advancements in the field. The structural weight of vehicles is a primary concern for car manufacturers, so the use of low-weight composite components has continued to grow. Although glass fiber-reinforced polymers (FRPs) are still the dominant type of automotive composite, the cost of carbon fibers has decreased in recent years (Gibson, 2016).

A structural material composed of two or more components that are not soluble in each other is known as a composite. One is called the reinforcing (dispersed) phase, while the other is called the matrix phase (shown the Figure 1.1) (Callister and Rethwisch, 2012). Referring to the reinforcing phase, fibers, particles, or flakes can be made from it. Matrix phase materials, such as epoxy and steel, are usually continuous. Various types of fibers, including glass, graphite, and aramid, have high specific modulus values compared to metals like steel and aluminum. Compared to metals, composite materials with matrixes and fibers have lower strength and modulus. The mechanical properties of such materials are affected by different factors. While long and continuous fibers are easy to machine, short fibers cannot be fully controlled. High strength and stiffness are usually gained from fibers oriented in one direction. The fibers' material mainly influences a composite's strength and rigidity.

The matrixes are used to bind the fibers and keep them from getting damaged by environmental elements. They also distribute the load to the fibers. The matrix with lower mechanical

properties than steel or aluminum influences composites' mechanical properties such as fatigue strength, transverse modulus, compressive strength, and interlaminar shear strength (Kaw, 2005).

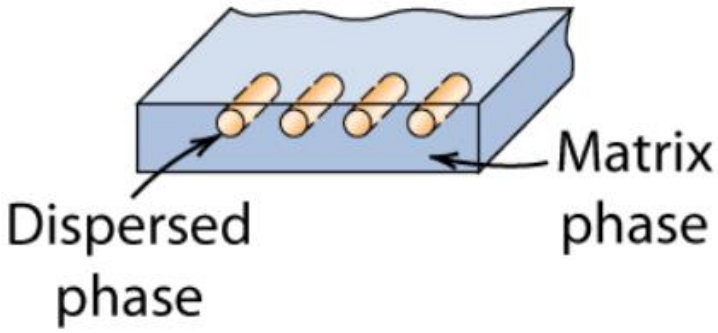



Figure 1.1. The dispersed and matrix phase of composite materials (Callister and Rethwisch, 2012).

Based on the matrix phase, the composite can be categorized into three types: metal matrix, polymer matrix, and ceramic matrix. Polymer matrixes are commonly used in commercial composite materials. They are referred to as resin solutions. Depending on the raw materials used, various polymers can be formed. The most common types include epoxy, polyester, vinyl ester, phenolic, and polyimide (Jose and Joseph, 2012). Most commonly, the resins used are epoxy. These organic liquids are characterized by their low molecular weight. They are made up of epoxide groups. Although epoxy is more expensive than other types of plastic matrix, it is still widely used due to its high strength, low flow rates ideal for the wetting of fibers, and low volatility during the curing process (Kaw, 2005).

The process of producing composite fiber products differs from that of plastics and metals. Fiber composite products are carried out simultaneously with the thermosetting process. The thermosetting resin matrix is usually formed during the final stage of the production process. This process can be carried out by various methods, such as hand lay-up, resin transfer molding, vacuum bagging, and pultrusion (Agarwal et al., 2017). These production methods are presented schematically in Figure 1.2.

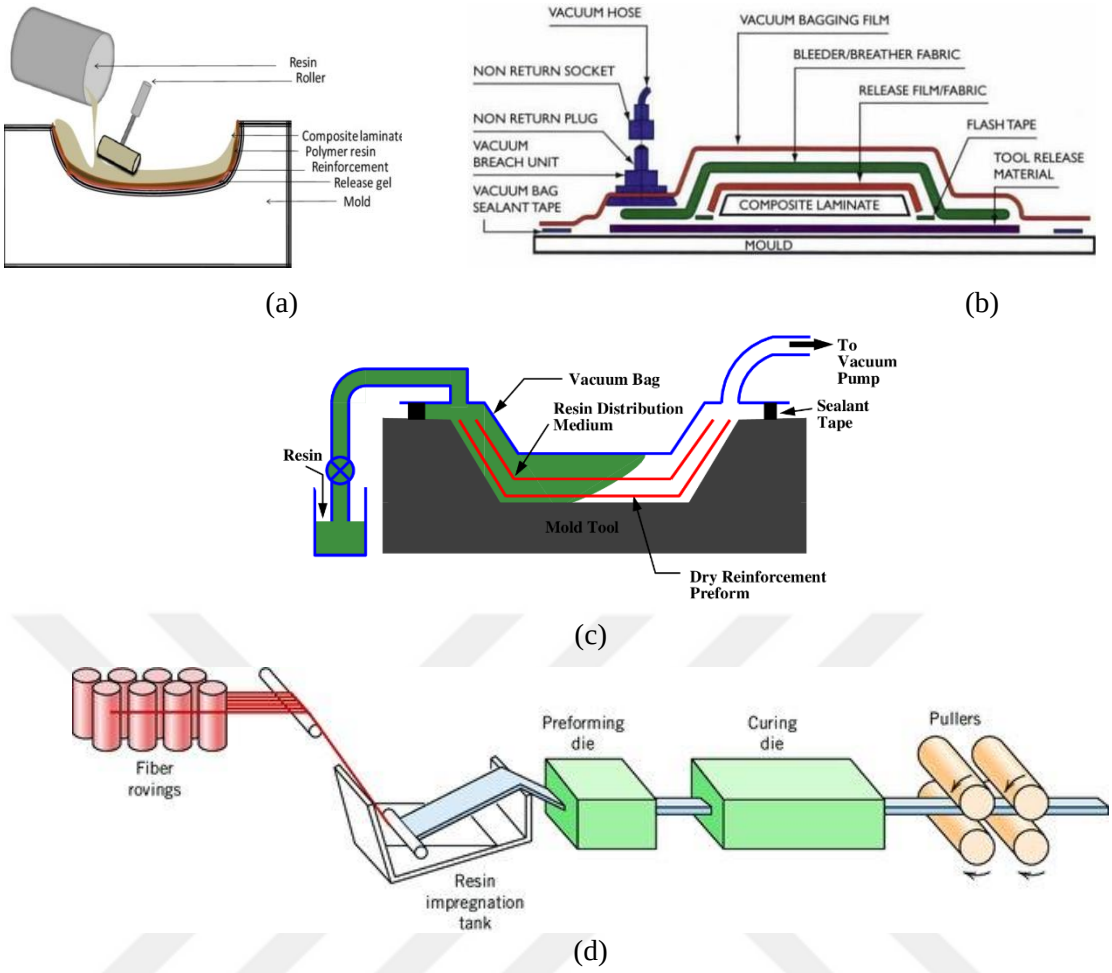



Figure 1.2. Schematic diagram of production methods of composite a) Hand Lay-up (Aljibori et al., 2016), b) vacuum bagging (Naik M et al., 2013), c) resin transfer molding (Song, 2003), d) pultrusion (Callister and Rethwisch, 2012).

The hand lay-up process is one of the simplest and oldest methods used to manufacture large and small fiber-reinforced products. Creating a resilient mat or roving begins with placing the appropriate materials inside an open mold. Then, the resin is poured and brushed. Matrixes such as epoxies and polyesters are commonly used for processing composite materials. The curing time can vary due to the type of resin used (Kar, 2016). The next method is vacuum bag molding with similar processes, which impregnated fiber with epoxy with hand lay-up before vacuuming. The resin air-trapped in the laminate is removed through a vacuum. After it has been fabricated, a release film is placed over the top of the laminate, and a bleeder ply is used to absorb any excess resin. Polyester, non-woven nylon, and fiberglass cloth are some materials used in this process. The process of merging laminates involves creating a vacuum under the bag, which then pressures the material to a certain level. This process allows for high reinforcement and better adhesion than hand lay-up (Kar, 2016). Resin transfer molding (RTM) involves impregnating resin and fibers in a closed mold. This process requires the use of dry-fiber reinforcement and liquid resin to fill the cavities in the mold. Air can escape through the inlets and outlets of an RTM mold. Once the resin supply has been

removed, the outlet and mold inlets are sealed, and the resin is cured (Agarwal et al., 2017). A process known as pultrusion is used to produce continuous profiles of composite materials. It is similar to manufacturing thermoplastic and aluminum products but pulls it from the die instead of pushing it out through pressure. This method can produce various structural profiles, such as tubes and rods (Agarwal et al., 2017).

### 1.2. Sandwich structures

A sandwich panel is a representation of the hybrid concept. In various applications, such as aircraft, trains, portable structures, and sports equipment, sandwich panels are commonly used to reduce weight (Ashby, 2016). A structural sandwich is made by placing a thick and lightweight core between two thin facesheet made of metal or fiber material. This type of structure resembles an I-beam. The facesheets support the bending loads in two dimensions while the core transfers the pressure between them (Carlsson and Kardomateas, 2011). Representative sandwich construction is given in Figure 1.3.

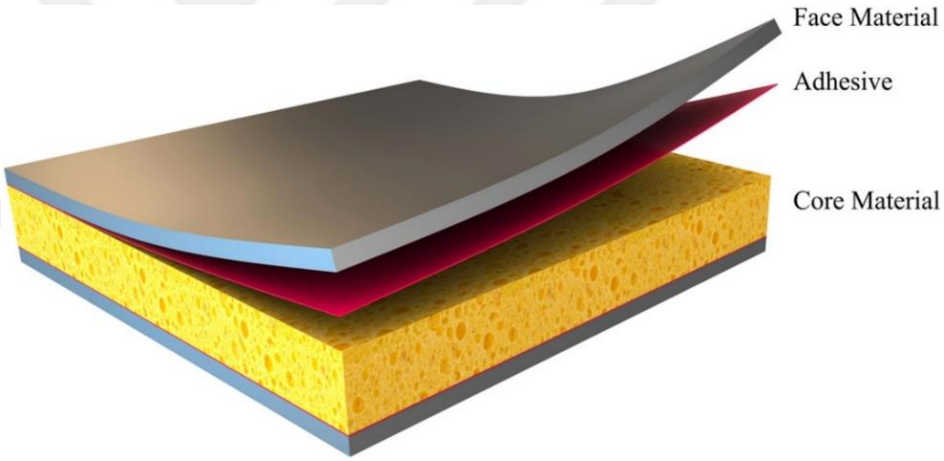



Figure 1.3. Representation of a type of sandwich structure (Khan et al., 2020).

The face materials can be categorized into two main groups: metallic and non-metallic. The former includes metallic materials such as stainless steel, steel, and aluminum. The strength properties of these materials vary, while the stiffness variation is limited. The latter include non-metallic materials such as cement, plywood, and reinforced plastic. Since the introduction of fiber composites, one of the reinforced materials, their use in sandwich construction has dramatically impacted the process. One of the main reasons for this is that they offer higher strength ratings than metals, but their rigidity is typically less. Therefore, a low-weight core is usually placed between two composite plates to achieve high rigidity (Zenkert, 1995). The various core materials used in sandwich construction include cellular structural foams, web and lattice trusses, honeycombs, solid cores, 3D woven fabric components, and microsphere mats. A web core or lattice truss is a metal sandwich structure made by welding the skin and core together. The three-dimensional structure of

the materials is called a lattice network, which reduces the structure's mass and improves strength and rigidity. The various types of honeycomb core materials are categorized as metallic and non-metallic. The former includes materials such as aluminum and stainless steel. On the other hand, the non-metallic ones include fibers made from plastic, paper, and phenolic resin. Light wood and plastic foam are examples of microcellular solid core materials. The foam cores include various plastic and rubber materials such as polyethylene terephthalate (PET), polyurethane (PU), Polyvinyl chloride (PVC), and styrene-butadiene rubber (SBR) (Ma and Elkin, 2021). The foam materials have low densities and are usually realized through conventional processes. Due to their low weight, foam cores can be used in various sandwich panel applications. However, once they are cured, these structures can endure significant loads. Although it has good mechanical properties, the thermoplastic PVC used for sandwich applications tends to soften at high temperatures. Cross-linked PVC foams, on the other hand, have higher rigidity and strength. Although rigid, the foam used for sandwich applications can extend its initial length by up to 10%. It is higher than other materials, such as polystyrene and polyurethane (Krishnasamy et al., 2022).

After the Second World War, the sandwich was incorporated into various moving vehicles, such as military and commercial vessels, power boats, trucks, buses, and trailers. In addition, the wind energy industry has started using sandwich structures to make large wind turbine blades, and this is the largest market for this type of construction. Marine products made from composite sandwich materials include hulls, deck panels, furniture, and bulkheads for lifeboats, racing yachts, and leisure vessels. Some submarines and military vessels also utilize this type of construction for their structural components. These include the walls, topside structures, and doors. The deck and hull are the most structural parts of a marine vessel. The high strength and stiffness of composite sandwich materials make them ideal for aerospace vehicles and aircraft that need lightweight and robust constructions. Various composite materials and the increasing number of core sandwich components made from foam and honeycomb have contributed to the development of aviation structures. Airbus aircraft also feature composite sandwich structures such as doors, wing panels, and cover structures (Ma and Elkin, 2021). Subway structures can be found in ground vehicles such as trains, buses, and trucks. Since the 1980s, sandwich technology has been used to construct locomotives' front cabs. These structures have high energy absorption and impact resistance. Sandwich panels are commonly used for the structural components of passenger rail cars, such as the roof, floor, and sidewalls. In the case of buses, using sandwich composite body panels can reduce the vehicle's weight by about 2,000 kg. This weight reduction can improve the passenger capacity and extend the range of the vehicle. The structural components of a low-floor bus, such as the roof, floor, and body shell, are made of sandwich panels (Ma and Elkin, 2021). In addition, they can be used for the roof, wall, and floor of express services trucks and couriers (Pruez et al., 2013). For decades, sandwich panels have been used in civil engineering projects for their low weight and high thermal insulation. For instance, the Stockholm Globe Arena uses these panels as part of its load-carrying structure. Examples include

garage doors and windmill housing (Zenkert and Fund, 1997). Structural panels of extruded or expanded polystyrene are increasingly used to construct sophisticated buildings. These are often integrated with other components, such as windows and doors (Davies, 2001).

### 1.3. Design of sandwich structures

Before designing a sandwich structure, it is essential to analyze its various mechanical properties. This process helps minimize the weight and improve performance under stress and flexural conditions. The deflection and stress of a sandwich structure are two of the most critical factors that can affect its performance. They can also forecast damages and prevent bending and edgewise buckling failures. The face is subjected to compression and tension, responsible for the sandwich's strength. The function of cores is supporting the facesheets, preventing them from collapsing. Core also experiences various degrees of vertical and shear stress, as shown in Figure 1.4. The rigidity of the sandwich structure is mainly due to the core placed between the faces. However, it also transmits shear to the other parts of the structure. In Figure 1.5, a sandwich beam shows the various bending moments in the structure (Ma and Elkin, 2021).

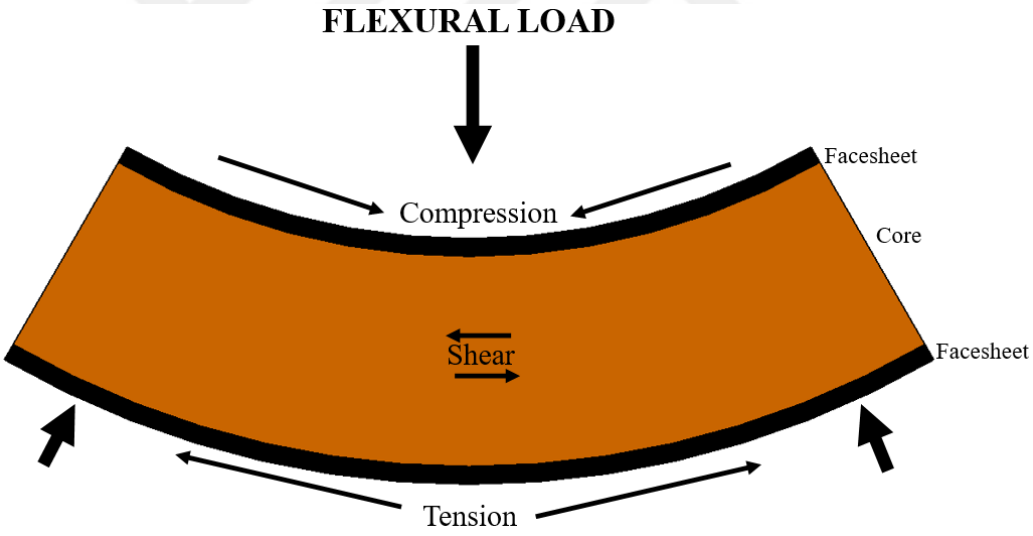



Figure 1.4. The sandwich structure is subjected to various deformation and flexural loads.

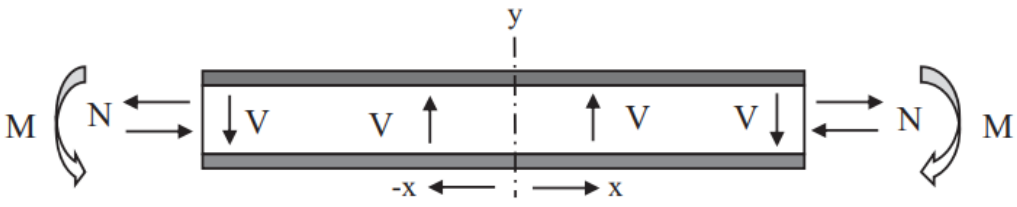



Figure 1.5. A sandwich beam exhibits a bending moment of M, N's normal force, and V's shear force (Ma and Elkin, 2021).

It is generally assumed that the transverse deformations of sandwich beams should be considered in the design of structures. However, in classical engineering theory, these are only minor additions to the overall deformation of the beams with high shear stiffness. In other cases, using a two or three-dimensional elasticity theory is the only way to account for these deformations (Zenkert, 1995). The deformation of the sandwich structure, such as a beam or a plate, is always composed of two parts (bending and shear). Usually, in classical studies of structures with a homogeneous cross-section, the emphasis is only on the bending part unless the member has a short span. However, in cases where the shear stiffness is low, this component should be included. For example, a sandwich with thin faces may have two superimposed deformation components. A structural component subjected to high shear forces will eventually deform without changing its volume. This deformation can be categorized as in-plane and transverse (Karlsson and TomasÅström, 1997). When studying the transverse shear deformation effects on the faces, it is essential to consider the thinness of the faces. For instance, if the deformation takes place without the presence of bending of the faces around their neutral axes, then it does not need to be resisted. This treatment is similar to the principle of partial deflections. In-plane stresses are caused by bending (Delawa, 1990). The properties of a beam subjected to bending can be computed using the ordinary bending theory. This method assumes that the cross-sections of the unloaded beam remain constant when bending takes place. The flexural rigidity of a beam is computed by considering the second moment of area and the modulus elasticity. Although the sandwich beams are made up of various parts, its flexural rigidity refers to the rigidity of the core and face components (Allen, 1969). The standard theories of beam bending treat the shear-flexible and the shear-rigid models. The former focuses on the deformation caused by the forces (Heyman, 1998). The concept of the shear strain is derived utilizing the infinitesimal rectangle beam element, which is subjected to the effects of pure shear stress. The characteristics of a thick beam, such as a sandwich, are described in the Timoshenko theory (Öchsner, 2021). The Timoshenko beam theory is similar to engineering beam theory except that it now requires that transverse shear deformations be considered (Zenkert, 1995). The Timoshenko beam equation is presented below (Timoshenko, 1921).

$$EI\frac{d^2\emptyset}{dx^2} + K_s GA\left(\frac{dw^T(x)}{dx} - \emptyset(x)\right) = 0 \tag{1.1}$$

The deformations of the sandwich beam are given in Figure 1.6 regarding their representative elements in the Timoshenko beam theory. The displacement fields of the top and bottom layers should be considered when ignoring the slippage between the face and core layers. The face layers carry the bending and in-plane stresses of a sandwich beam. However, the core carries only transverse shear stress, with negligible in-plane and bending stresses (Fadaee, 2019).

A sandwich structure's structural stability can vary depending on the construction and loading conditions (Hause, 2021). Therefore, the strength of sandwich beams, as well as stiffness, is one of the essential factors considered when designing them. For instance, the stiffness and strength should be considered if the beams are designed for three-point or four-point bending (Ashby et al., 2002). Various factors can cause the failure of a sandwich beam owing to bending and compression. These include face yielding, core shear, wrinkling, and the facesheet's indentation, shown in Figure 1.7.

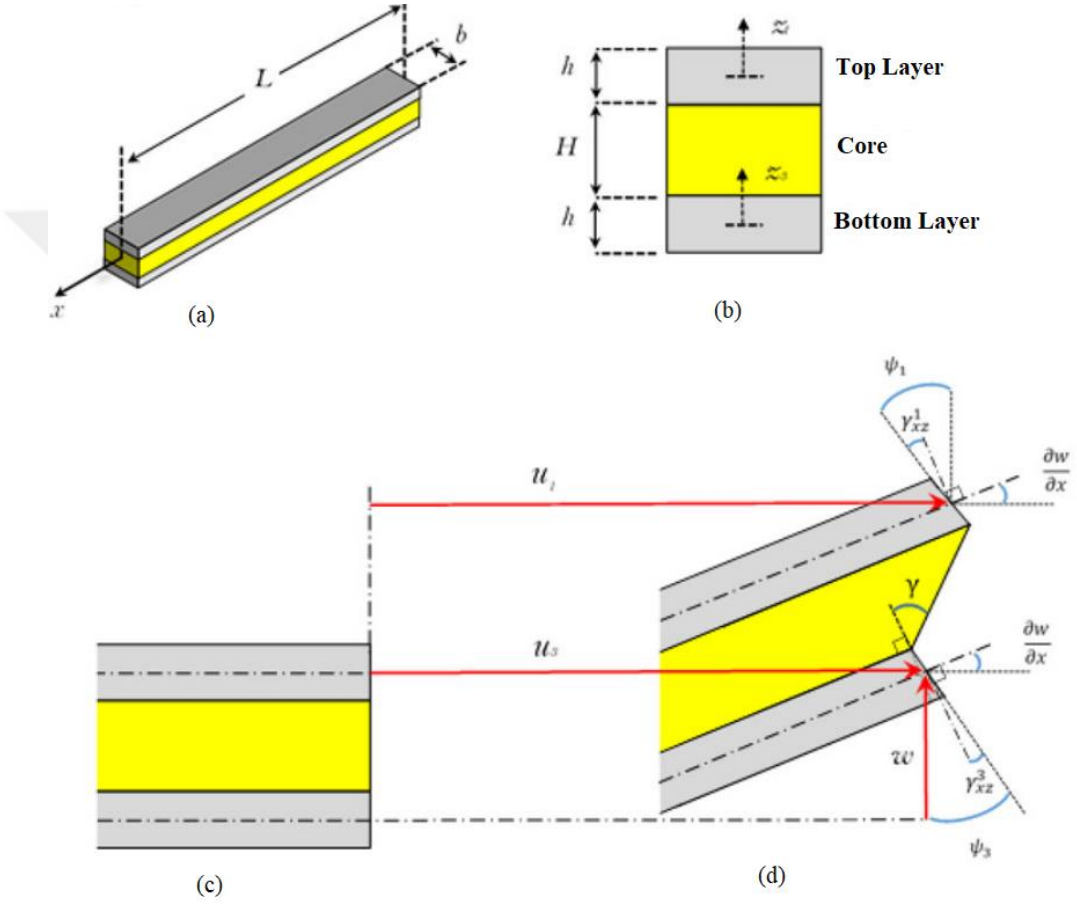



Figure 1.6. Sandwich beam under bending (a) 3D view (b) Cross-section (c) Before flexural deformation, and (d) shear and bending deformation after loading (Fadaee, 2019).

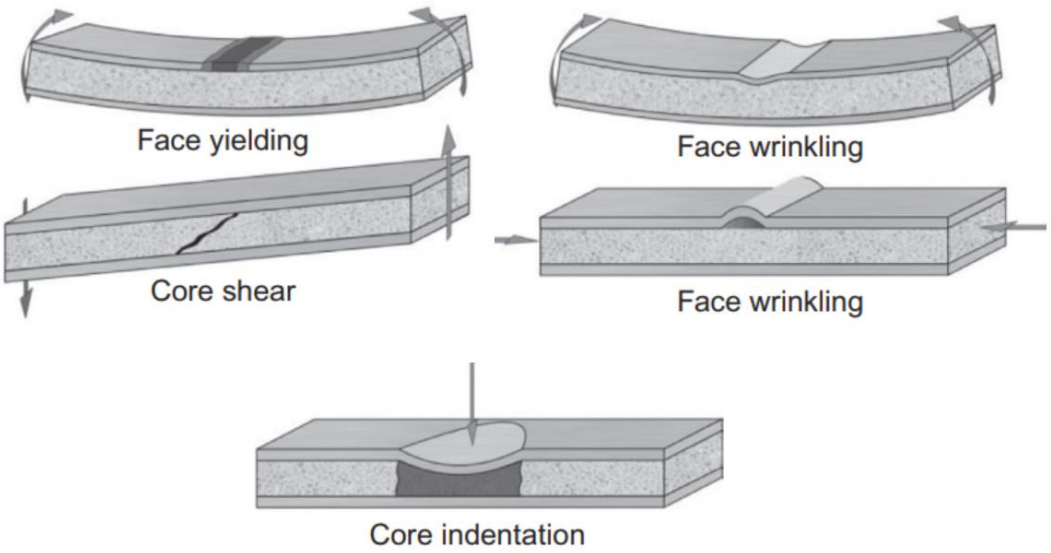



Figure 1.7. The sandwich structure failure modes are presented in detail (Oterkus et al., 2016).

The face yield of a beam or sandwich panel depends on the strength of the material used to make it. This determines the limit load that the panel or beam can carry. The easiest way to determine this is by assuming that the plastic collapses when the facesheets exceed the strength of the material (Ashby et al., 2002). Core failures were observed in sandwich beams subjected to three-point bending. This is because the primary mode of transport of the applied shear load is the core. Therefore, when the stress level reaches the critical value of the core material, it can cause failure (Daniel and Gdoutos, 2010). Wrinkling can be regarded as the result of the facesheet's short-wavelength collapse under stress. This type of failure can be caused by the loss of the beam's stiffness. The interaction between the core and the face causes the wrinkling phenomenon. The critical load that a sandwich panel can achieve is determined by the stiffnesses of its core and face (Daniel et al., 2002). In the case of composite sandwich beams, indentation can occur under heavy loads, especially in soft cores. This can cause high local stress levels (Daniel et al., 2009). Indentation depends entirely on design parameters, such as face thickness, core thickness, face and core material properties, and support span length (Balıkoğlu and Demircioğlu, 2022; Li et al., 2016; Li et al., 2020; Mao et al., 2016; Uzay and Geren, 2022). The indentation causes the sandwich structure to carry less load than the ultimate flexural load (Newaz et al., 2019). This may be attributed to the local buckling phenomenon in the flexural loading zone (Dhaliwal and Newaz, 2020; Lee and Tsotsis, 2000; Lyckegaard et al., 2004). Therefore, indentation failure can restrict the efficient use of sandwich structures (Li et al., 2016).

## 2. PRELIMINARY WORK

### 2.1. Methods used for the design of the composite face layer of sandwiches

Metallic and non-metal are the two main types of face layer materials. While the metallic face layer comprises aluminum, stainless steel, and steel, the non-metal includes plywood and fiber composites (Zenkert, 1995).

Cai et al. (2018) investigated the drum peel, bending, and positive-pressure tests performed on aluminum sandwich panels with aluminum honeycomb core and aluminum alloy. They obtained that the face layer was composed of a compressive force that transfers axial forces to the core layer. This case helped improve the overall tensile strength of aluminum honeycomb panels. The aluminum face layer was the most critical component of the aluminum honeycomb panel sandwich's flexural-tensile tests. The enhanced flexural-tensile properties could be achieved by increasing the face layer's thickness.

When subjected to three-point bending, the failure behavior of sandwich beam with double-layer aluminum foam was studied by Yuan et al. (2022). The beam comprises a closed-cell aluminum alloy foam core and 5052H32 aluminum alloy face material. They observe the combination of indentation with core shear and face yield with indentation, as well as main failures such as face yield, core shear, and indentation. The results indicate that the thickness significantly impacts the initial failure rates of sandwich beams with double-layering.

Taghipoor et al. (2020) conducted a numerical and experimental study of the effects of low-speed impact on the structural performance of the sandwich panels' steel face layer and lattice core. The study demonstrated a highly efficient sandwich absorption structure with lattice cores. It is composed of low-weight materials and has excellent energy absorption. Furthermore, the finite element and experimental study results revealed that the two had a high agreement.

The studies above show that metallic faces are still used in sandwich structure design. However, innovations were made in the core element instead of the design in the metallic structure. As a result, foams with different densities, honeycombs with different structures, and lattices are designed as core materials. However, only thickness and material selection are presented as design criteria for metallic skins. While sandwich structures are under loads such as impact and bending, the face carries main loads such as tensile compression and impact resistance. Therefore, making differences in the structure and strength of the face material allows more diversity in the design of the sandwich structure. Furthermore, it is possible to design a facesheet according to the purpose by using non-metallic materials.

Kavermann and Bhattacharyya (2019) conducted experimental work on the static behavior of a sandwich core made of corrugated plywood. For the experiments, sandwich panel specimens were made by attaching an epoxy adhesive to the joints of the plywood facesheets and the corrugated core. The produced sandwich plate is shown in Figure 2.1. The sandwich structures were made from

6-ply $(0/90/0)_s$, 5-ply (0/90/0/90/0), and 3-ply (0/90/0) laminated plywood panels. The panels used 0.6 mm thick New Zealand pine veneers bonded with a two-component PVAc glue. The mechanical properties of the core material were evaluated in compression. This process could have various failure modes, such as delamination and local hinging. Corrugation walls and plywood adhesive could be used to address these issues. Shear cracking occurred in bending the corrugation core when the load point was under indentation, causing the failure.



Figure 2.1. The facesheet and core of the sandwich panel are made of plywood (Kavermann and Bhattacharyya, 2019).

Darzi et al. (2020a) demonstrated the structural strength of load-bearing timber walls made of bamboo cores and plywood faces. The light timber sandwich panel was made by attaching two plywood faces to the rings of a bamboo core (Figure 2.2). These structural laminates were made from plantation pine in New Zealand and Australia. The mechanical properties of plywood combined with the orthotropic properties of each veneer.

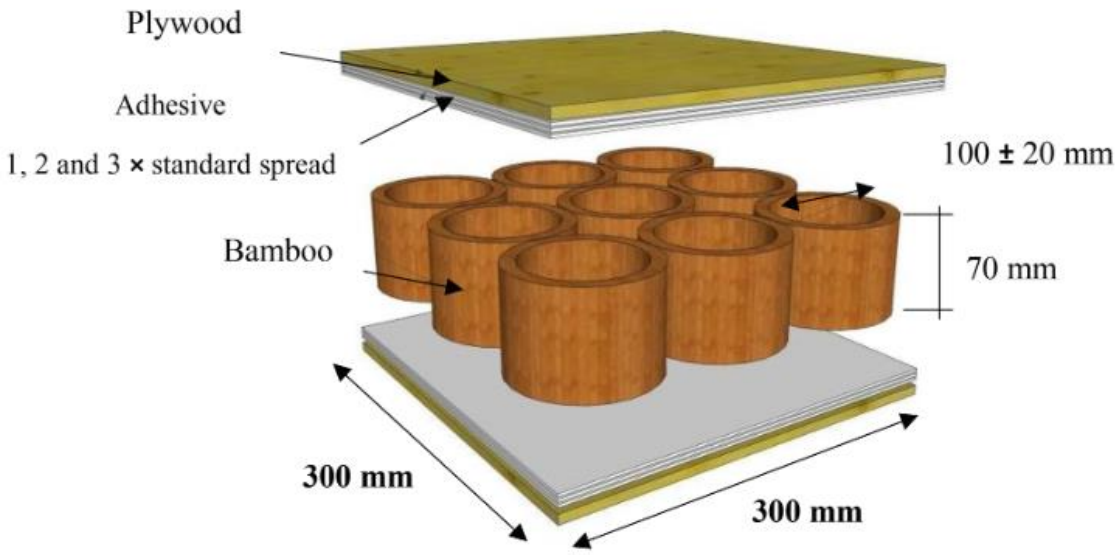



Figure 2.2. Schematic illustration of timber sandwich panel (Darzi et al., 2020a).

Darzi et al. (2020b) demonstrated the bending and shear characteristics of the composite sandwich panels in another study. The panels were also made using plywood skins and bamboo rings. They concluded that the manufacturing strategy and core layout of bamboo core and peeler core panels could help improve their performance against Cross-laminated Timber panels regarding their strength and stiffness. Adding timber boards between the plywood and the peeler cores could also improve their fire performance.

Peliński and Smardzewski (2020) studied the bending behavior of lightweight sandwich beams made of wood used in the cellular core and plywood faces. The study on the structural properties of lightweight sandwich beams using plywood facings revealed favorable mechanical properties. They also exhibited a good absorption capacity.

In recent years, plywood or metal sheets have been used as face material in sandwich studies. However, fiber-based composites are the most widely used and efficient forms for sandwich structures. One of the main advantages of fiber-reinforced composites is that they are easier to make than metal face. Another advantage of these is that they have anisotropic properties, which can vary depending on the load. Engineers typically view this as an initial challenge, but it is advantageous because it allows them to tailor their properties (Zenkert, 1995). Also, composites have different architectural forms of continuous fibers, and essential component reinforcement materials can be used for different applications and processes. Various fabrics for sandwiches are used in composite lamination, such as unidirectional, bi-axial, twill, and woven (Ma and Elkin, 2021).

Liu et al. (2015) studied the bending properties of composite sandwich structures under temperature effects. The sandwich used in their study was made using a combination of pre-formed pyramidal truss cores and unidirectional carbon/epoxy prepregs. The top and bottom faces were made using 14-plies carbon/epoxy prepregs. They revealed that temperature affected the bending

performance of composite sandwich structures. For instance, as the temperature increased, the load on the bending component decreased.

Bey et al. (2015) studied the impact of three-point bending fatigue loading on the mechanical properties of sandwich composites. Two types of sandwiches with varying facesheets were made in their study. The first one was made from a combination of unidirectional glass fibers (677 g [90 × 30] × 0.85 cm) with $[0]_4$ staking sequence. The other one was made from unidirectional glass fibers (677 g [90 × 30] × 0.85 cm) with a $[0/90_2/0]$ staking sequence. They noted that independent of the loading conditions, the life of the $[0/90_2/0]$ sandwich lasted longer than $[0]_4$.

Yu et al. (2019) developed a model to estimate the failure modes and stress levels of composite sandwich structures under different three-point bending conditions. The analytical model preferred using unidirectional carbon fiber for the facesheet of the sandwich structure. Their model has considered the various critical stresses in a sandwich and provided a variety of damage criteria to predict its initial failure modes.

MacDonnell and Sadeghian (2020) presented the analytical and experimental results of works on the behavior of reinforced sandwich beams made with glass fiber-reinforced polymer. The materials used to construct the facesheet were epoxy resin and unidirectional fiberglass fabric. While testing sandwich specimens, they observed two primary failure modes: crushing core shear and the top face deformation (Figure 2. 3).

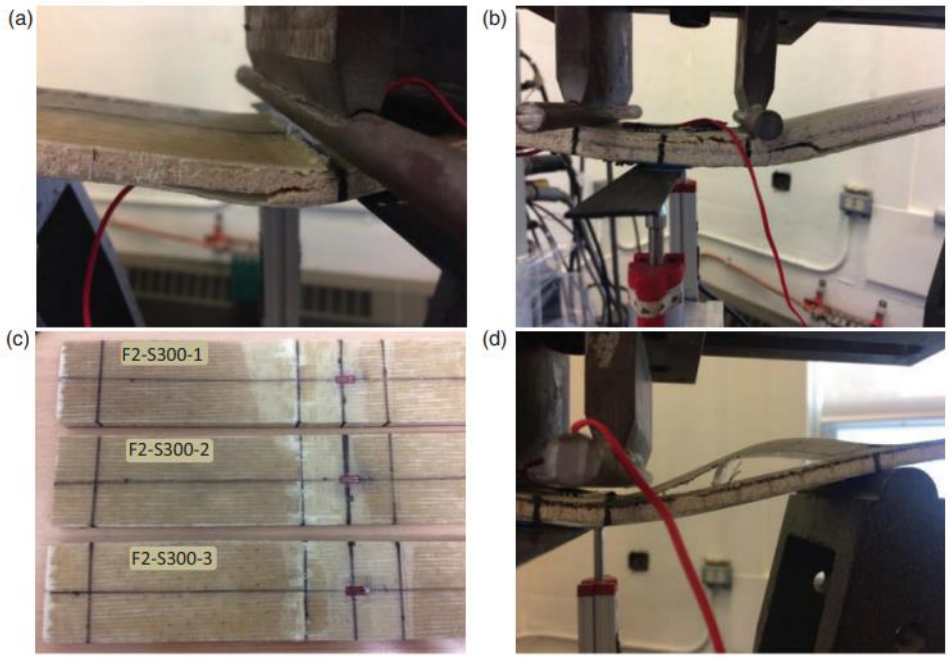



Figure 2.3. Failure modes: (a-b) core shear failure (c-d) top facesheet crushing failure with debonding and buckling (MacDonnell and Sadeghian, 2020).

Non-crimp biaxial fabrics composite exhibited similar tensile behavior to unidirectional fabric because the bias-direction yarns of the composite materials did not undulate (Ahmed et al.,

2020). A bi-axial fiber comprises two layers, usually at 0/90 or ±45, and is bonded together using thick stitch techniques (Chen et al., 2016). The structure utilizes a combination of low-cost processing and unidirectional laminates for enhanced strength and fiber modulus (Truong et al., 2005).

Manalo et al. (2010) presented that the structural fiber sandwich beams which exhibited flexible behavior in the flat and edgewise positions (Figure 2.4). The facesheets of the sandwich comprised two layers of bi-axial (0/90) E-CR glass (E-Glass Corrosion Resistant) fiber fabrics, which have a total thickness of 1.8 millimeters. The study revealed that a composite sandwich panel could provide a high-performance structural laminate beam. In addition, it suggested that the beams should be placed in a flatwise position to carry compressive and tensile stresses.




Figure 2.4. The failure modes of the specimens were (a) flatwise and (b) edgewise (Manalo et al., 2010).

Najafi et al. (2012) aimed to investigate the influence of fabrication methods on the strength of sandwich composites. The sandwich composites made of E-glass, Kevlar, and Endgrain wood as their core were fabricated using vacuum infusion and hand lay-up processes. The materials used to produce sandwich composites include E-glass mats, bi-axial E-glass, bi-axial Kevlar fabric, and isophthalic polyester resin. They obtained that the high compressive strength of sandwich composites made using vacuum infusion processing (VIP) was superior to that of hand lay-up (HL) methods. The compressive strength of these materials was 28.27 MPa for the VIP and 15.02 MPa for the HL.

Awad et al. (2012) focused on the behavior of laminated and single-layer glass fiber reinforced sandwich beams with different spans and cross sections. These beams' top and bottom face layers are of 3 mm. thickness. The plies of the layers are made of bi-axial E-CR glass, having 0/90 orientations. The study revealed that the failure mode of the sandwich beams affected the total depth variations and shear span.

Qi et al. (2017) presented a paper that explored the structural flexibility of composite sandwich beams made from a combination of glass fiber-reinforced face material and pine wood core. The glass-fiber-reinforced manufactured HS-2101-G100 unsaturated polyester resins and bi-axial glass fiber laminates (800 g/m$^2$). It was also made up of three layers of stitched bi-axial fiber

fabric, each with a thickness of around 1 mm. According to the researchers, the composite sandwich beams exhibited a larger deflection in flatwise bending tests than in sidewise bending procedures.

Textile composites are suitable for producing composite materials with better dimensional stability and moldability than unidirectional composites. Woven-fabric-reinforced composites, which have high mechanical strength and flexibility, are best to produce structures ideal in the textile composite. Compared to unidirectional composites, woven fabrics offer more balanced properties. As a result, woven-fabric-reinforced composites have increased significantly in naval construction, aerospace, and automobile engineering. The composites use standard woven fabrics such as plain, satin, and twill (Vidal-sallé and Boisse, 2012).

Shi et al. (2014) presented a study on the strength and flexibility of a carbon fiber-reinforced aluminum sandwich enhanced with an aluminum grid; the sandwich structure is given in Figure 2.5. The face material was made using a 2X2 twill woven of carbon fiber (200 gr/m$^2$). They found that the core structure of the ortho grid filled with carbon fiber-faced composite was higher than that of the grid or honeycomb sandwich. However, the improved energy absorption, strength, and load characteristics indicated that this structure could be used for thin-walled engineering applications.

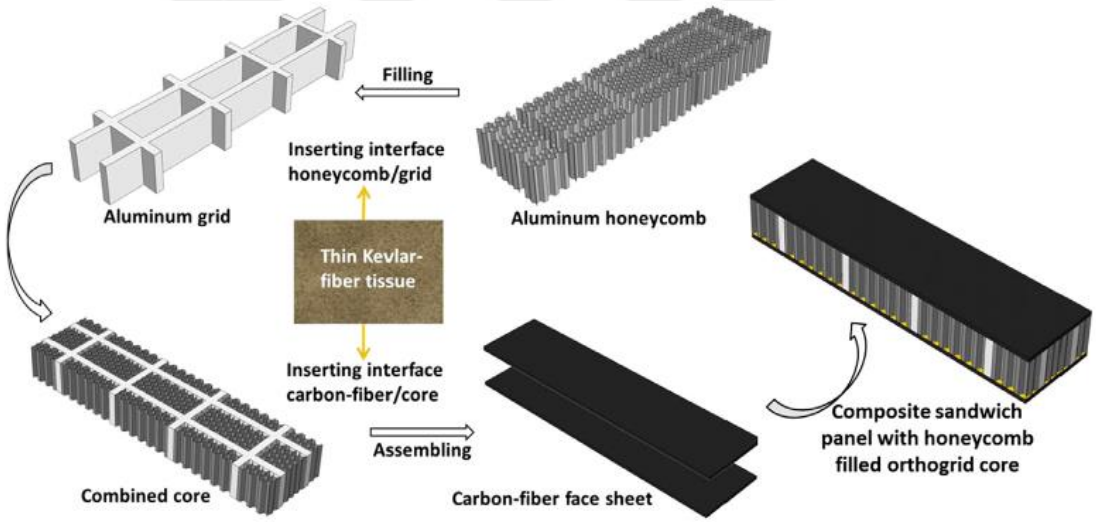



Figure 2.5. The process of creating sandwich panels using a honeycomb-filled orthogrid core is shown in this diagram (Shi et al., 2014).

Betts et al. (2021) studied the impact on the flexural characteristics of sandwich panels made with polyisocyanurate foam cores and flax fiber-reinforced polymer faces. The faces was fabricated using a wet lay-up process and a balanced 2x2 twill woven fiber fabric. After the impact, the beams' residual flexural strength and stiffness were compared to those of intact specimens. The beams exhibited remarkable resilience since the impact did not alter their structural properties.

Harizi et al. (2021) analyzed the three-point bending behavior of various carbon-fiber-reinforced thermoplastic sandwich composites with a mechanical-acoustic coupling approach (Figure 2.6). The faces were made from reinforced thermoplastic polyphenyl sulfone resins using

2X2 twill woven carbon fabrics, and various core materials, such as aluminum, polyetherimide, and honeycomb, were used to produce sandwich panels. They obtained that the two design methods exhibited similar properties of fibrous reinforcements when subjected to three-point bending tests. However, the variations in the core's composition affected the results. Before the failure, the absorbed energy of the sandwich layers was calculated. It was revealed that the Polyetherimide cores were more energy-efficient than those of Nomex and Aluminum.

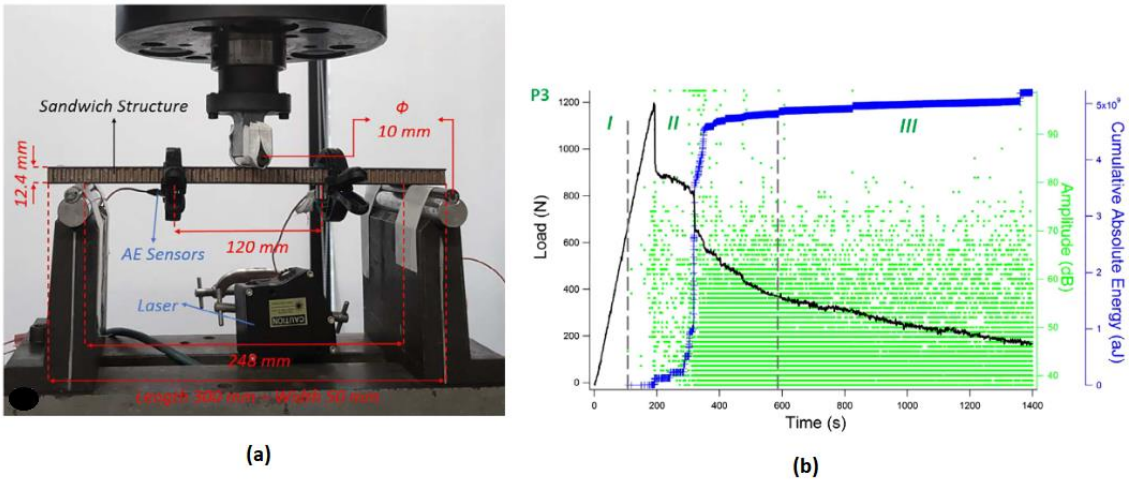



Figure 2.6. Test details a) The laser acquisition system's position and the acoustic emission sensors' position b) The results of a mechanical-acoustic coupling study (Harizi et al., 2021).

The experimental and numerical analyses of the various aspects of composite sandwich panels were performed by Thiagarajan and Munusamy (2022). The panels were subjected to compression-wise and quasi-static edgewise loads. Bi-directional 2X2 twill woven carbon fiber has been chosen due to its excellent mechanical properties. It has a strength of 4000 MPa and a tensile modulus of 240 GPa. A flexural test specimen exhibited delamination of only a single layer at the loading face, even after failure. The other layers were intact even after the test failed. During edgewise compression, the sandwich was subjected to severe compression. The tension side exhibited high delamination, but the compression side failed due to a bending effect.

Plain woven is the most widely preferred type of reinforcement for woven fabric composites (Pandita et al., 2003). It is popular for structural applications (Adumitroaie and Barbero, 2012). Plain weave offers better abrasion resistance, pilling resistance, and high tensile strength than other woven fabric types. The mechanical properties of plain weaves have improved owing to the decrease in the number of floating yarns (yarn or yarns omitted in weaving) and the increase in the number of weft and warp yarns (Jahan, 2017).

According to Ivañez et al. (2010), a 3D model was created to study the dynamic flexural behavior of sandwich beams, which include a foam and composite. In addition, they carried out dynamic three-point bending tests, which were utilized to check the reliability of the computer model. The face materials were made using a combination of plain woven E-glass fibers and polyester resin.

The researchers discovered that the upper surface was most likely to fail due to its high deflection and curvature.

Umer et al. (2012) investigated an experimental and numerical study of the flexural behavior of composite sandwich structures incorporating VARTM technology. The face materials were reinforced using a plain woven glass fabric with an areal weight of 818 grams. The core materials used for the sandwich were both non-porous H130 and H250 foams. The behavior of sandwich panels made of different core thicknesses and foam densities was studied using four- and three-point bending tests. The tests were then simulated using a finite element model. The results indicated that the simulations performed accurately predicted the failure loads.

Karahan et al. (2013) noted that the foam density and the thickness of three-dimensional woven sandwich composites were studied under three-point bend conditions. The sandwich panel's top and bottom faces have been reinforced using a plain woven E-glass material. Authors revealed that compared to foam core sandwich composites, which are commonly used, 3D sandwich composites offer superior mechanical properties. They were more stable and could withstand the load that came from bending. In addition, unlike conventional materials, the pile yarns and foam in the core could support each other when subjected to bending loads, which helps prevent core breakage.

Wei et al. (2020) discussed the three-dimensional structure of the failure mechanism map for all-composite hexagonal honeycomb sandwich beams and their bending characteristics. The face materials were produced with the plain woven carbon fiber/epoxy prepreg with a thickness of 0.2 mm. The core of the honeycomb structure was also made from the same carbon fiber. They revealed that a three-dimensional map was created to visualize the various phases of a failure process. The map could identify the transitional path from one failure mode to another.

In a study conducted on naval ships' sandwich structures, Gargano et al. (2022) analyzed the impacts of an explosion on the structure's structural performance. The sandwich panels were made of facesheets composed of woven plain E-glass or carbon fibers with a vinyl ester matrix. Its core material was a closed-cell PVC foam with a 130 $kg/m^3$ density. In explosive blast test conditions, the resistance of glass fiber sandwich panels to deformation during out-of-plane movement was higher than that of carbon fiber ones. Also, glass fiber is more resistant to damage than carbon fiber.

This section summarized studies on face materials used in the literature while designing sandwiches in recent years. Many types of materials are used in sandwich design. Metallic materials, such as aluminum and steel, mainly use lattice or honeycomb core materials. However, they are insufficient in applications that require face material mechanical diversity. Fiber-reinforced composites are the most widely used in non-metallic materials with face material mechanical diversity because they are more applicable and more accessible to produce than plywood. In addition, fiber-reinforced composites are structurally diverse, and the most common are those formed from unidirectional, bi-axial, woven fabrics. While unidirectional composite materials provide excellent

longitudinal strength, they are weak in the transverse direction. They can be produced in two layers (0,90) to provide high strength in both directions, but this is a cost and production-time-increasing process. Therefore, bi-axial fibers with the same mechanical properties in both directions have been developed instead of unidirectional fiber. However, woven fabrics, which are textile composites, are usually preferred in composite production due to dimensional stability and moldability. Woven fabrics are diversified as 8-harness satin, 4-harness satin, twill, and plain as knitted structures. Twill and plain are primarily used as face materials in sandwich structures. However, the properties of plain wovens, such as absorption resistance, pilling resistance, and high tensile strength, are better than other woven fabrics. Therefore, this thesis chose this fabric architecture as the face material. Although they are widely used, it is difficult to predict their mechanical properties due to their complex architecture. In the past decades, many analytical studies have presented models for determining the mechanical properties of these composites. These models are detailed in the next section.

### 2.2. Analytical methods used for plain woven fabric composites

A plain woven textile composite is a fiber-reinforced material produced by weaving longitudinal (warp) and transverse yarns (fill or weft) (Bhattacharjee and Roy, 2020). They have better formability and delamination resistance, producing complex shapes (Dixit et al., 2014; Gao et al., 2019; Ishikawa and Chou, 1982; Kubo et al., 2018). However, due to the complexity of the design of textile composites, the analytical capabilities are limited to predict their properties (Wang et al., 2018; Yang and Zeng, 2018).

Chou and Ishikawa presented the analytical models that could investigate the properties of woven materials, such as the bridging model, the fiber undulation model, and the mosaic model (Ishikawa and Chou, 1983a, b; Ishikawa and Chou, 1982). The first and benchmark models they proposed used a one-dimensional approach. They then simplified it using the series and parallel models. The analytical model results were higher than the experimental ones, considering that the woven fabric was considered unidirectional (UD). The new undulation model considered the various factors that affect the strength and stiffness of a woven fabric. It was developed using the iso-stressed model's extension. Although it requires a complex solution, it assumes that the undulation occurs in one direction. The third model was suggested due to the advantages of the previous two models when determining the strength and stiffness of UD fabrics. It was modified to take into account the undulation and mosaic models. The experiments were conducted on 8-harness satin fabrics. The proposed model could not provide a good evaluation of woven composites. According to Tang and Whitcomb (2003), the design of the weave architecture of composite materials significantly affects their mechanical results even when they have the same fiber volume fractions and cross-sections.

Raju and Wang (1994) updated the undulation model to accommodate zero undulation and isotropic cases. The value of the fiber volume fraction was not specified, whether it was the overall

volume or the volume fraction of yarn. A numerical study conducted by Tan et al. (1999) revealed that the mechanical properties of yarn and its volume fraction were related.

Naik and Ganesh (1992), Naik and Shembekar ( 1992b), and Naik and Ganesh (1996) presented two-dimensional models of the yarn cross-section. They took into account the gap between the yarns that are adjacent to each other and the continuity of the yarns along the fill and warp directions. They suggested using a parallel-series or a series-parallel model depending on the iso-strain conditions. The results of the study were then compared with those of the experiments. It was concluded that the former model is more accurate when calculating in plain elastic parameters. The method, known as the slice array model (SAM) (Naik and Ganesh, 1992) is reliable, it requires several complicated geometric calculations to arrive at an elliptical yarn cross-section and an undulation angle. The suggested approach also requires precise values of various parameters to arrive at solutions, such as the gap between fibers, undulation angle, length of the yarn, and thickness of the yarn. The slice array model equations are summarized below (Naik and Ganesh, 1992),

The local off-axis angle in the fill yarn;

$$\vartheta_f(1) = \tan^{-1}\left(\frac{\pi h_w}{2(w+g)}\sin\frac{\pi x}{(w+g)}\right) \tag{2.1}$$

The local off-axis angle in the warp yarn;

$$\vartheta_w(2) = \tan^{-1}\left(\frac{\pi h_w}{2(w+g)}\sin\frac{\pi y}{(w+g)}\right) \tag{2.2}$$

Compliances are;

$$S_{11}(\vartheta) = \frac{1}{E_1(\vartheta)} = \frac{m^4}{E_1} + \left(\frac{1}{G_{12}} - \frac{2v_{12}}{E_1}\right)m^2n^2 + \frac{n^4}{E_1} \tag{2.3}$$

$$S_{22}(\vartheta) = \frac{1}{E_2(\vartheta)} = \frac{1}{E_2} \tag{2.4}$$

$$S_{12}(\vartheta) = \frac{v_{21}(\vartheta)}{E_2(\vartheta)} = \frac{v_{12}}{E_2}m^2 + \frac{v_{22}}{E_2}n^2 \tag{2.5}$$

$$S_{66}(\vartheta) = \frac{1}{G_{12}(\vartheta)} = \frac{m^2}{G_{12}} + \frac{n^2}{G_{22}} \tag{2.6}$$

$m = \cos\vartheta$ and $n = \sin\vartheta$, $\vartheta$=undulation angle

Extensional stiffness:

$$A_{ij}^{sl}(y) = \sum_{k=1}^{4} hx_k(x,y)(\bar{Q}_{ij})_k \quad (2.7)$$

Extensional stiffness of unit-cell

$$A_{ij} = \frac{2}{(w+g)} \int_0^{(w+g)/2} A_{ij}^{sl}(y)\, dy \quad (2.8)$$

Tanov and Tabiei (2000) investigated two different micromechanical models designed to analyze plain weave fabric composites. The first model considered the volume element of a woven garment, while the second model considered the sub-cells made up of homogeneous materials. The stiffness of a volume cell was computed by considering the values of the various sub-cells. Udhayaraman and Mulay (2017) noted that the model was complex and time-consuming.

Wen and Aliabadi (2011) aimed to create a mesh-free micromechanical model to evaluate the performance of woven fabric composite moduli. They claimed that the proposed method was straightforward to implement and significantly more efficient than the other methods when solving complex numerical problems. Moreover, unlike the finite element method, the mesh-free approach did not require formal elements. However, It was initially believed that using the meshless method was complex and would involve the distribution of homogenous matrixes (Udhayaraman and Mulay, 2017).

Udhayaraman and Mulay (2017) revealed that a multi-scale approach is used for modeling the constitutive properties of plain weave textiles. The main contributions of this work were the development of a parallel-series model that could calculate the UD lamina's material properties in the transverse direction, the use of a new approach to calculate the volume of yarns, and the analysis of the composites' homogenized properties. In addition, the results of this work indicated that the constant and sinusoidal approaches of the Voigt model could be used to calculate the effective properties of the composite.

Akkerman (2005) noted that the plain woven fabric materials he studied had been subjected to several layers of continuous lamination. According to Mallikarachchi (2019), most research on developing two-ply composite has focused on single-ply on-axis and analytical models to predict its micro properties. The requirements for space applications are usually made of thin films. These are usually made up of one to six layers of composite. The relative positioning of the layers influences the out-of-plane behavior of these materials.

### 2.3. The Methods for Sandwich Design

The mechanical behavior of a sandwich structure against situations such as low-velocity impact and flexural loadings is determined in three ways. These are experimental, numerical, and analytical solution methods.

#### 2.3.1. Experimental sandwich design methods

While sandwich structures are being developed with experimental methods, the changed parameter is compared with the old version, and its contribution to the design is discussed. In sandwich structures, improvements are made in facesheet or core design.

Hosur et al. (2005) investigated the characterization of hybrid faces and foam-filled sandwich composites for low-velocity impact testing. Various face materials were used to make sandwich structures, such as carbon/epoxy, glass/epoxy, and hybrid (carbon and glass epoxy). The load-carrying capabilities of composite sandwich materials were significantly improved by adding hybrid and glass fiber. The impact of sandwich composites made of glass or epoxy was considered the least damaged type. The hybrid constructions between glass and laminates containing carbon and epoxy performed well.

Liu et al. (2017) presented that a new sandwich panel with a low-velocity impact response was developed using a combination of aluminum foam core and FML face materials. The faces were made using materials such as E-glass fibers and aluminum sheets. The impact behavior of sandwich panels with different core thicknesses was studied to see how their foam composition affects their velocity impact. The panels with two face configurations were analyzed to study the stacking sequence effect on the panels, which were a sequence of layers of Al sheet and a single ply of plain E glass prepreg, and a representation of two layers of Al alloy and two plies of woven glass prepregs, respectively. Increasing the sandwich panels' foam thickness could result in higher energy absorption. Also, the facesheets' thickness could increase significantly.

Uzay and Geren (2020a) studied the flexural characteristics of a low-density PVC foam core sandwich. They utilized the hybridization of carbon fibrer/epoxy facings and the wire mesh sheets made of thin stainless steel. After the failure of wire mesh sandwiches, their bending load capacity decreased. The wire mesh sheets carried the resulting increased bending loads. Also, the hybrid approach to forming wire mesh sheets using carbon/epoxy composites could benefit FMLs. This method involved using perforated mesh steel integrated with a carbon fiber matrix.

Geren et al. (2021) revealed the effects of modified sandwich structures with carbide microparticles in the epoxy matrix on their low-velocity behavior. The modified sandwich structures were made using a combination of carbon/epoxy and PVC foam materials. The micro-participating materials used for the construction of the structures were Boron carbide. They were dispersed into the epoxy resin in varying loading ratios to study their impact on the crash resistance of the low-density foam core structure. The experiments were performed at different energy levels ranging from

10 to 25 J. The study results revealed that using Boron carbide additives could benefit areas prone to low-velocity impacts.

Mamalis et al. (2008) developed a novel hybrid sandwich structure made from polymeric and metallic materials to avoid some of the main advantages of these materials. The hybrid structure is formed by adding an intermediate layer between the facesheet and the core (Figure 2.7). This new concept utilizes low-density foams, thin metallic faces, and intermediate layers for improved impact and debonding behavior.

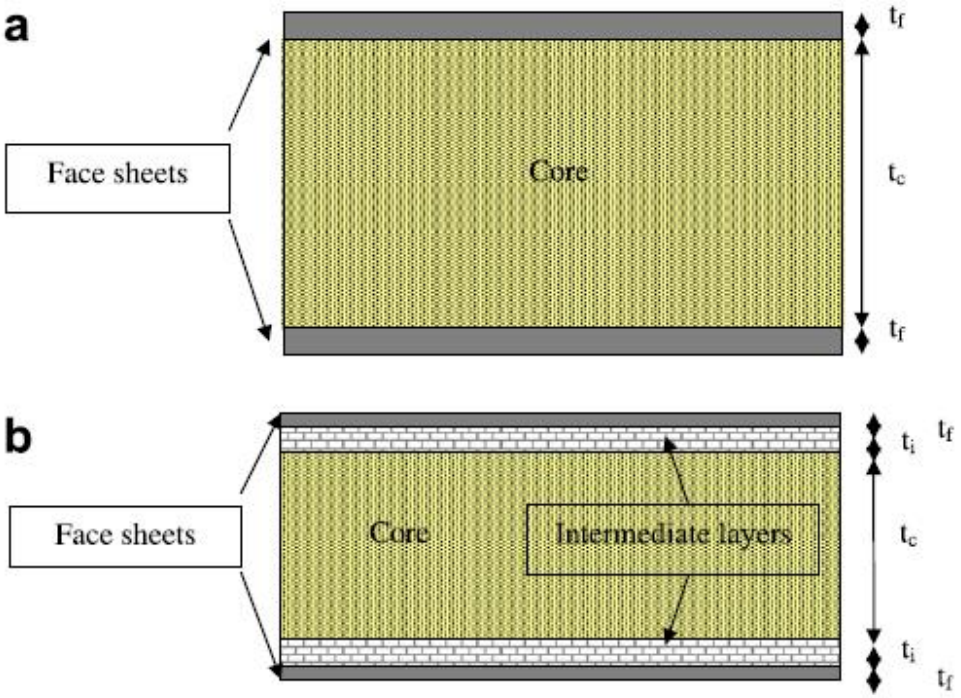



Figure 2.7. The sandwich structure features inner and outer layers: a) classic concept, b) the hybrid structure shows the intermediate layers (Mamalis et al., 2008).

Ashraf et al. (2021) investigated the mechanical properties of a sandwich structure made of a honeycomb and a glass/flax hybrid composite. The reinforcement of E-glass and flax in woven mats was used to create the composite structures. They focused on the hybrid sandwich structure's tensile, flexural, and edgewise compression properties. The researchers noted that the sandwich using the hybrid facesheet in its outer layer glass exhibited better modulus and tensile strength than the flax composite. The normalized hybrid fiber-reinforced glass composite exhibited a compressive strength of 90%. Compared to the flax composite, the hybrid increased the sandwich structure's flexural facing stress by 25%.

Wang et al. (2010) investigated the construction and design of a sandwich structure reinforced with composite columns. Their study paper comprised vertical composite columns mechanically connected to the facesheets. The columns were then embedded in the foam core (Figure 2.8.). They presented some findings of the investigation. The column-shaped sandwich structure

could effectively overcome the delamination and low strength of traditional sandwiches. The advantages of composite sandwich materials with column-shaped foam were apparent in their load-carrying capacity.

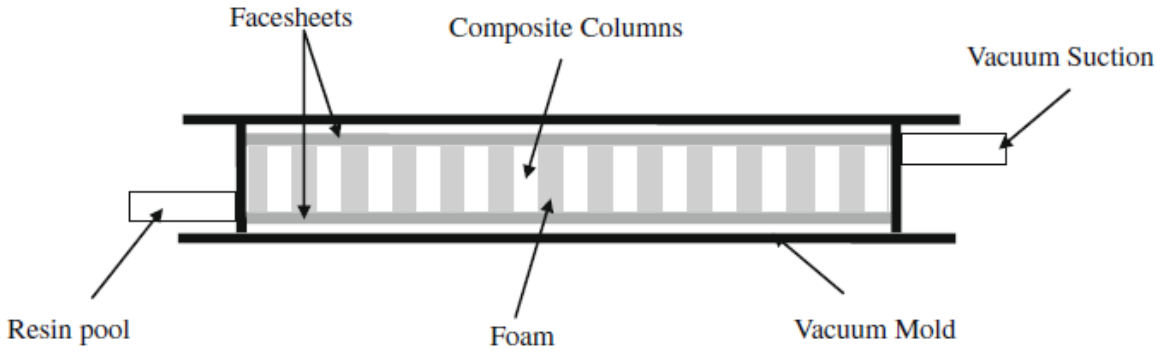



Figure 2.8. The diagram shows the fabrication process of the sandwich (Wang et al., 2010)

Haldar and Bruck (2014) made a synthetic sandwich using a combination of carbon fiber, epoxy, and polymeric foam reinforced with carbon rods. The goal was to improve the sandwich's energy absorbance and flexural behavior. The three-point bend test revealed that the core with carbon rod reinforcements composite sandwich's enhanced mechanical strength was higher than the conventional core.

Selver and Kaya (2019) presented a study using Z-pins inserted in foam cores to improve the flexure characteristics of sandwiches with carbon or glass composite. The panels used six layers of woven carbon or glass face materials. The foam core was also reinforced with rods that were 3 mm in diameter and had carbon/vinylester and glass/vinyl-ester composite (Figure 2.9). Their flexural loads and strength increased significantly after adding carbon and glass rods to the sandwich composites. In addition, carbon rods were better than glass rods in terms of their flexural properties due to their better bonding with facesheet and core.

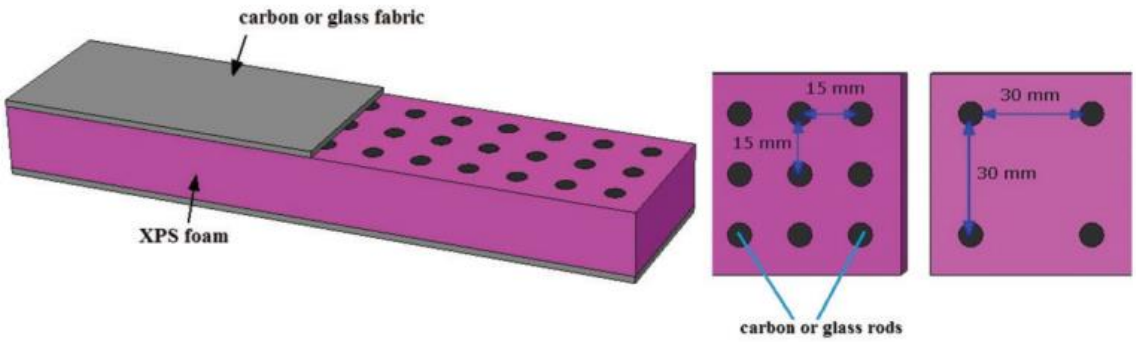



Figure 2.9. Sandwich structure with core material reinforced with carbon or glass rods (Selver and Kaya, 2019)

Three different types of all-fiber reinforced sandwich structures were created by Mohamed et al. (2015) using the VARTM process. These structures used different core designs, such as the box, PU rectangular, and trapezoidal foam (Figure 2.10). A new generation of thermoset urethane resin systems and woven glass fiber fabricated sandwich structures. Core shear, edgewise compression, and flatwise compression tests were performed. The core shear test results revealed that the Type-2 sandwich panel model has the highest bending capacity. In addition, they exhibited the highest load under edgewise and flatwise compression.

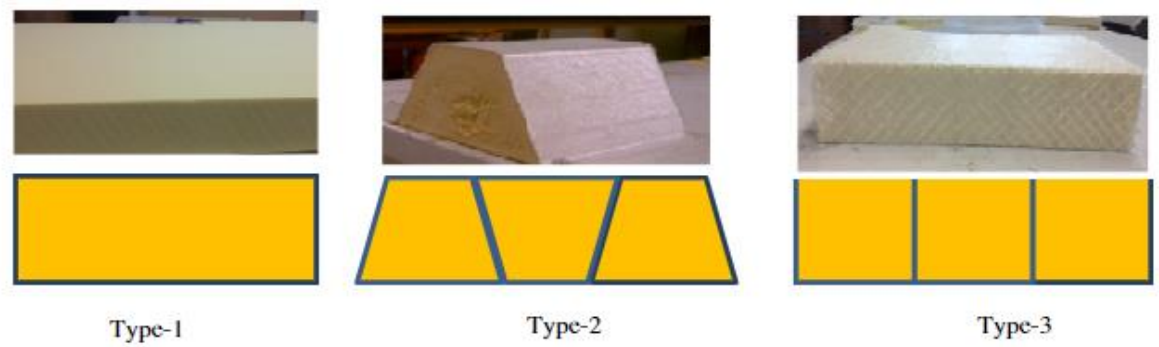



Figure 2.10. The sandwich structures were modeled in three types (Mohamed et al., 2015).

Taghizadeh et al. (2019) worked on the compressive behavior of infilled sandwich panels made of PVC foam. The panels were characterized by their corrugated core shapes, which were trapezoidal, rectangular, and triangular (Figure 2.11). The results indicated that the nose shape and geometry mainly influenced the failure modes of complex corrugated core composite structures. They could help prevent structures from collapsing.

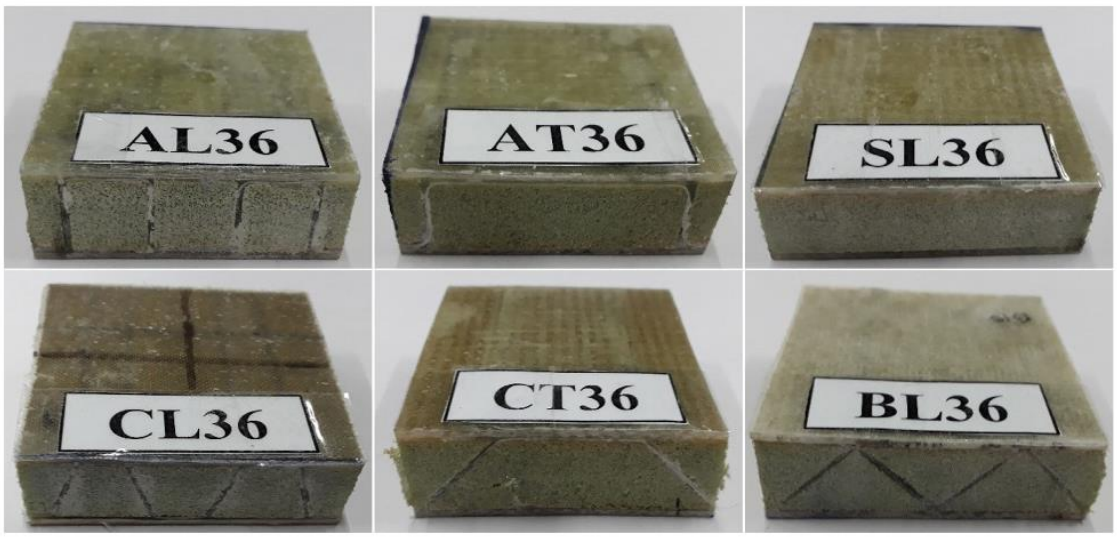



Figure 2.11. Corrugated core shapes were utilized in designing and constructing composite sandwich panels (Taghizadeh et al., 2019).

Zhang et al. (2013) studied a corrugated sandwich composite's (Figure 2.12.) energy absorption and bending strength to determine the design features of lightweight load-bearing structures that can be used in transportation applications. The sandwich coupon used long fiber, woven fabric, glass, and carbon fibers. The facesheets and core were then bonded using epoxy. The increase in the core-sheet thickness and the corrugation angle resulted in a stronger sandwich structure. However, increasing the bond length resulted in weaker bending strength. Also, the foam insertion technique in hybrid composite coupons allowed them to absorb medium energy compared to carbon fiber and glass fiber. It also performed well in terms of crush force efficiency.

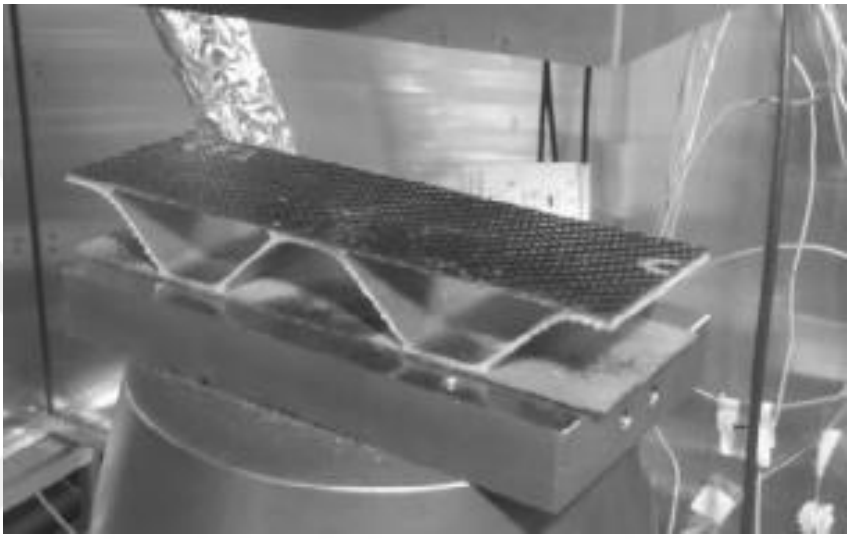


Figure 2.12. Designed and manufactured corrugated sandwich beam sample (Zhang et al., 2013).

Through a process known as ex-situ consolidation, Ali et al. (2021) were able to create SrPP (self-reinforced polypropylene composites) sandwich beams ideal for producing high-volume SRC (Self-reinforced polymer composites) structures. The three-point bending of SrPP sandwich beam was performed on a non-symmetric mass arrangement between the facesheet and core. Their study aimed to examine this distribution's effects on the product's energy absorption capacity and flexural properties. The manufacturing process of SrPP structures involved heating the sheet and mold, applying pressure, and translating the calculated step into a mold. Corrugated SrPP sheets were used as a core, and profiles were passed through roller pads to ensure the product was dimensionally stable. Polymer adhesive was also used to join the faces and core. The process of making sandwich beams using SrPP is shown in Figure 2.13. They concluded that the beams with higher core mass proportions exhibited higher energy absorption capacity. However, these beams could not improve performance due to the interface's delamination and the parent material's compressive failure.

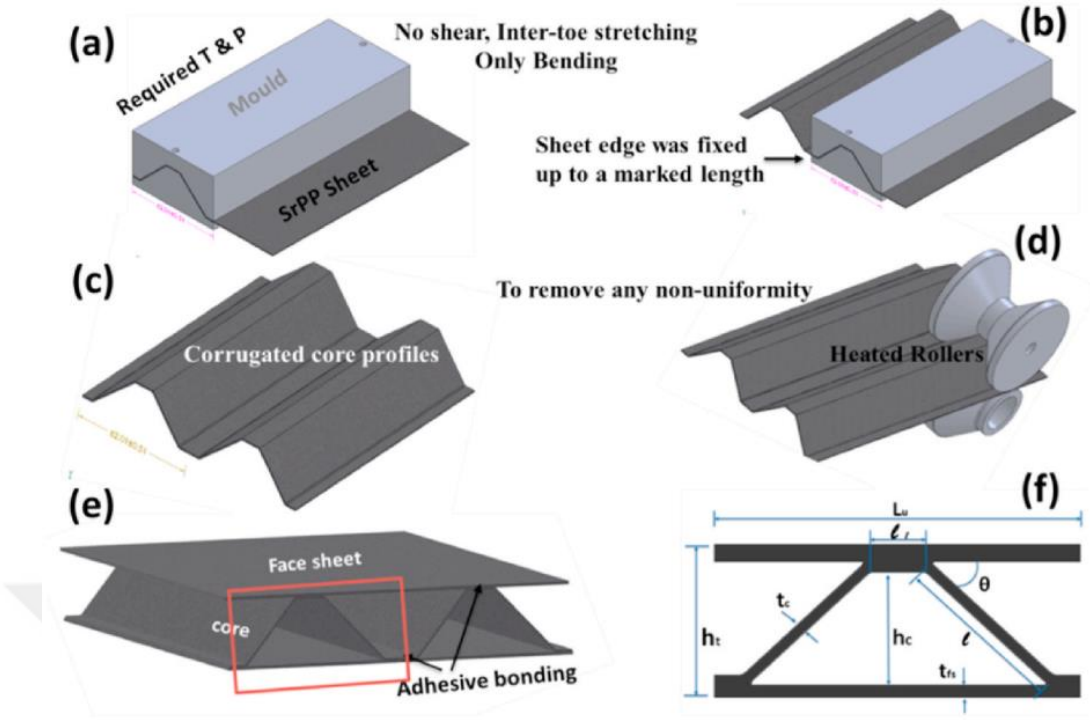



Figure 2.13. This illustration shows the manufacturing process of SrPP structures (Ali et al., 2021).

### 2.3.2. Numerical sandwich design methods

The finite element method is popular for numerically solving structural analysis problems, heat transfer, and fluid flow. The concept of finite elements refers to dividing a large system into simpler parts (Logan, 2002).

Mines and Alias (2002) investigated the progressive collapse of polymers' sandwich beams using the ABAQUS/standard finite element code. The paper discussed the various properties that need to be input into the numerical model. The paper also covered the various effects of multi-axial crushing and laminate damage on the upper face. The study's results revealed that a three-dimensional variation of the Hashin failure model was required to analyze the facesheets. The model also had to be used to study the tensile strength of the foam.

Theotokoglou et al. (2008) revealed a numerical study on the effects of a flexible loading technique on fractured sandwich composites. The position of the crack initiation of a sandwich beam was estimated using a static finite element analysis. In addition, the analysis considered the angle of the core debonds parallel to its beam axis. Their results revealed the understanding of propagation and initiation of a fatigue crack within the sandwich beams' foam core.

Sharaf and Fam (2012) put effort into modeling sandwich panels using a numerical model. The numerical model considered various aspects of the flexible behavior of sandwich panels fabricated of woven glass fiber and foam. The core structure included various density foams and glass fiber-reinforced polymer rib configurations. The validated model was obtained through the experimental database of results. It predicted the various failure modes and flexural responses of the

panels. The ribs were the structural component that allowed the compression skin to exert its full compressive strength. Under concentrated loads, the facesheets could get wrinkled, while those with relatively distributed loads tend to fail because of excessive shear deformation. Also, a parametric study revealed that the reduction in the longitudinal rib spacing could increase the flexural strength of the panels. It stabilized the panel's rib spacing to a ratio of 2.93.

Yazici et al. (2014) investigated the impact of foam on the blast resistance of corrugated steel sandwich panels through a combination of methods: high-speed photography of shock tube testing and numerical simulation. The results of the FEM and experimental studies were shown that the corrugations tended to bend and elasticize before plastic deformation. The foams applied between the cells improved the bending and corrugation rigidity of the core. In addition, the foam filling significantly increased the sandwich panel's blast resistance.

Wang et al. (2015a) investigated the failure mechanism of the PMI foam core sandwich beams under bending. A numerical model of this structure was developed, which predicts the damage propagation for foam core. The validation experiments also detected a complex failure process using a high-speed video camera. The results of numerical simulations and tests support the reliability of the predicted failure of the core sandwich beam of the PMI foam.

Studziński et al. (2018) presented experimental and numerical studies on the sandwich panel with a hybrid core. It featured steel facesheets and a core with mineral wool, foam, and a combination of these materials. The numerical analysis used to study the sandwich panel's materials properties was based on the results of the experimental data. The results of the laboratory tests supported the use of the FE model in determining the sandwich panel's material properties. It allowed the determination of the correct strain and stress distributions in each layer.

Chen et al. (2018) presented a paper that was a numerical analysis of the effects of the stress behavior of a reinforced foam core lattice-web sandwich panel on its flexibility. They used the softwares ANSYS and LS-DYNA to analyze the effects of a lattice-web composite sandwich panel's load distribution and stress response under intense loading conditions. The results of the investigations were analyzed and validated with FE model. The paper showed that the addition of thick facesheets and lattice webs could achieve the enhanced load-carrying capacity of the composite sandwich panel. However, the foam densities did not affect the midspan deflection and the load-carrying efficiency of the structure.

Darzi et al. (2018) revealed a numerical model to investigate the flexural strength of ultra-light composite sandwich panels. The study used a modified Ritz method and formulated sandwich beam theories to analyze the stiffness of thick faces and core sandwich panels. The panels' ultimate failure and capacity modes were then predicted using multidimensional and nonlinear analysis tools. The study's results revealed that the bending stiffness of the Peeling Core Sandwich and the Bamboo Core Sandwich panels was similar to that of Cross-Laminated Timber panels at the same depths

(Figure 2.14). The panels' ultimate capacities were obtained using finite element analysis, considering the effects of various materials and geometric factors.

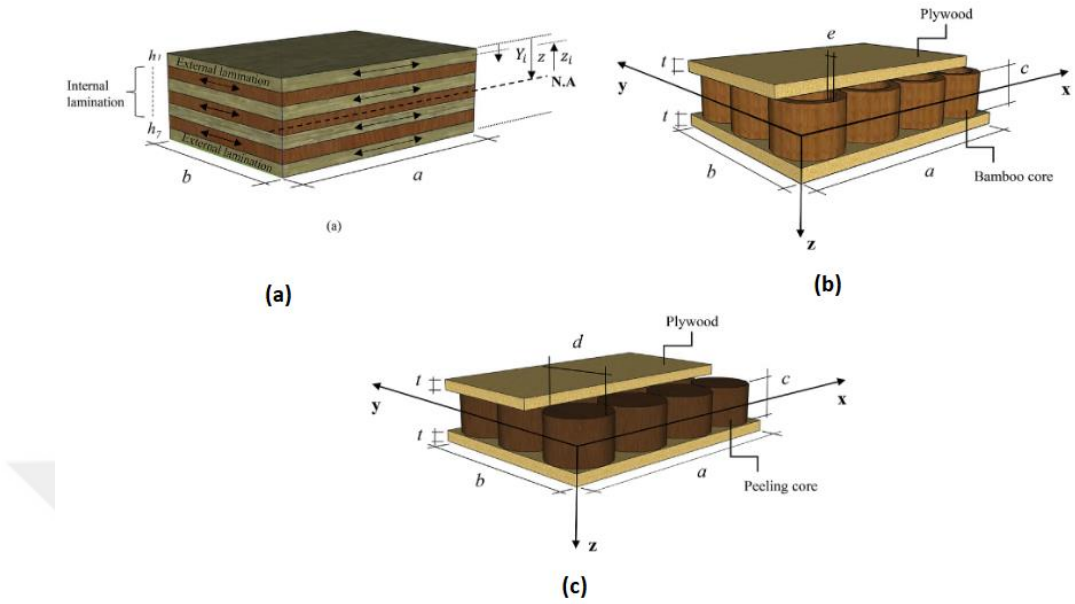



Figure 2.14. A diagram showing existing a) Cross-laminated timber panel, b) Peeling Core Sandwich, and c) Bamboo Core Sandwich panel (Darzi et al., 2018)

Uzay et al. (2022a) developed a method to optimize the design of low-density PVC foam core sandwiches using multidimensional optimization and finite element analysis. In addition, they aimed to model the sandwich panel using FEA, which could provide helpful and accurate mechanical test results. The various sandwich configurations were subjected to a numerical TPB evaluation in an ANSYS environment. Various sandwiches were modeled using PVC foam materials with different densities and woven carbon fiber fabric (Figure 2.15). The results of an FEA study on the sandwich panels were validated with those of literature studies. In addition, using mathematical expressions to determine the bending load capacity and mass of low-density foams was made possible by eliminating the need for expensive experiments.

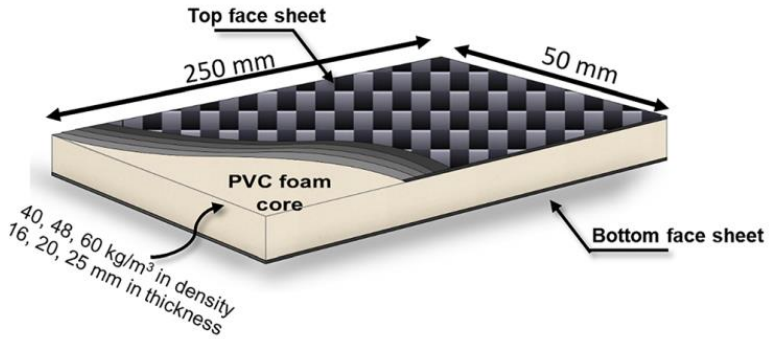



Figure 2.15. Diagram showing the layout of the sandwich panel (Uzay et al., 2022a).

Vahidi Bidhendi et al. (2022) studied delamination between the core and face of sandwich structures using hybrid corrugated cores (trapezoidal, square, and triangular types) via numerical analysis, validating the experimental result. The structures were exposed to three-point loading. The ABAQUS software and the cohesive zone modeling method for numerical analysis were used by combining these two tools. The increase in the crack length could lead to a higher strain energy release rate in the studied systems. In addition, the charts tended to drop after reaching their peak energy release rate. Load–displacement curve of the specimens was also extracted and compared to the data from experimental sources (Figure 2.16).

A numerical method is often used for multi-dimensional problems or complex geometry problems. The predictions can be very accurate if the data handling and boundary conditions are well-known. However, if the goal is to produce the best possible results, analytical methods should be used instead of numerical ones. It also requires a high level of programming and mathematical formulation. Moreover, the computational time needed for a given problem is often long, even with powerful computers (Buschow, 2001).

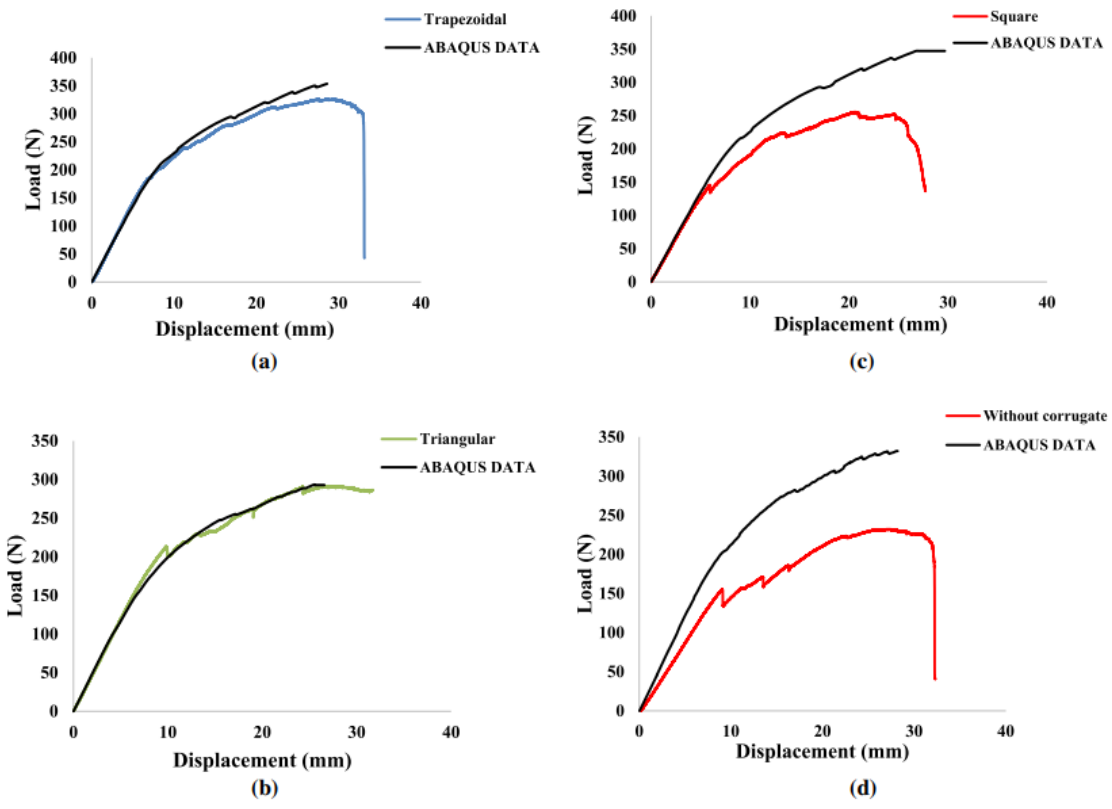



Figure 2.16. The force-displacement diagrams compare the numerical and experimental results (Vahidi Bidhendi et al., 2022)

### 2.3.3. Analytical sandwich design methods

Analytical methods provide good transparency between the calculated results and the input data. They also reduce the time needed to program and model complex problems (Buschow, 2001).

Due to the time-consuming nature of numerical methods, developing a closed-form analytical solution is more efficient than conducting experiments (Mahbod and Asgari, 2019). Over the years, analytical methods have been utilized to estimate the behavior of sandwich structures (Zhu et al., 2018). Sandwich beams are commonly used in bending loading cases because of their high bending strength, stiffness, and low-weight. Therefore, analytical design strategies for sandwich beams have been developed according to stiffness and strength properties (Steeves and Fleck, 2004a).

The deflection of a sandwich beam can be obtained by adding the bending ($w_1$) and shear ($w_2$) deflections. Depending on the stiffness, the total deflection equation is as follows.

$$w = w_1 + w_2 = \frac{PL^3}{48EI} + \frac{PL}{4AG} \tag{2.9}$$

$$w = w_1 + w_2 = \frac{P(l-s)^2+(l+2s)}{48EI} + \frac{P(l-s)}{4AG} \tag{2.10}$$

$$EI = \frac{E_f b t_f d^2}{2} + \frac{E_f b t_f^3}{6} + \frac{E_c b t_c^3}{12} \sim \frac{E_f b t_f d^2}{2} \tag{2.11}$$

$$AG = \frac{b d^2 G_c}{c} \sim b d G_c \tag{2.12}$$

Equation 2.9 uses three-point bending, and Equation 2.10 uses four-point bending. While the product known as *AG* refers to the shear stiffness of the sandwich, *EI* refers to bending stiffness (Allen, 1969).

Theotokoglou (1996) analyzed the strength of sandwich beams with E-glass/polyester laminates and PVC-core. The flexural rigidity of the sandwich beam calculations was made according to the equations above. The mechanical properties of the face materials were taken from the literature. Their analytical results aligned with the literature's findings.

Chen et al. (2001) studied the collapse modes of plastic sandwich beams. It involved using cold-worked aluminum sheets and an aluminum alloy foam. The analytical formulas were presented to calculate sandwich beams' collapse strength and stiffness. They were based on the elastic-plastic isotropic properties of the core and face materials. The sandwich beam was loaded with four-point bending through circular rolling wheels. Equations 2.10, 2.11, and 2.12, given above, were used while designing the sandwich beams according to their stiffness.

McCormack et al. (2001) identified the failure of the sandwich beams made of metallic foam cores. They estimated the linearity of the load-deflection curve for three-point bending loading with Equations 2.9, 2.11, and 2.12.

Steeves and Fleck (2004b) revealed a study to analyze the collapse mechanisms for supported sandwich beams using a combination of PVC foam and woven glass composite. The total deflections

were computed using the Allen formulas (given above). Tension tests of woven glass specimens were carried out to obtain mechanical properties.

Mostafa et al. (2014) aimed to investigate the failure mode and flexural behavior of composite sandwich panels, which are mainly used in marine applications. The panels were fabricated with glass fiber-reinforced composite and PVC foam. A four-point bending test was also performed to study the panel's flexibility under quasi-static load conditions. The flexural stiffness of the sandwich was calculated by considering Equation 2.11. The elastic properties of the GFRP were evaluated by testing them under various types of compressive, tensile, and shear loads. The results of the tests were then used in theoretical and numerical simulations.

Mostafa et al. (2015) revealed the behavior of sandwich panels constructed with PU foam and glass-fiber composite when subjected to flexural static load. The experimental results were compared with those of the classical sandwich theories. The flexural stiffness of the sandwich was calculated with Equation 2.11. The face material elastic properties required for calculations were experimentally obtained.

Wang et al. (2015b) developed sandwich panels with GFRP facesheets and a foam-GFRP web core. The study's goal was to estimate the bending strength of the panels using a combination of analytical methods. The formulas for calculating the mid-span deflection, shear modulus, and bending stiffness were also developed. Allen's approach was used in the calculation of the bending stiffness. The tensile strength, tension, and compressive strength of a GFRP were evaluated utilizing experimental tests.

Zhang et al. (2020a) revealed the effects of a low-velocity impact and the deformation of hybrid sandwich beams using an aluminum foam core. The facesheets were fabricated from carbon fiber-reinforced composite. The CFRP's bending and tensile tests were performed to measure their mechanical properties. The mid-span deflection of the sandwich beams was determined according to Allen's formulas.

Wang et al. (2020) investigated the flexural behavior of three grid structures made of wood and reinforced with epoxy composite cores. The study focused on the micro-surface modification of composites and the bending behaviors of sandwich structures. The total deflection and stiffness of the sandwich beam were computed using the Allen model under three-point bending.

Zhang et al. (2020b) described the structural collapse of a fully supported and geometrically asymmetric hybrid sandwich beam using a combination of aluminum carbon fiber and foam. The bending rigidity of the asymmetric cross-section was determined with equation 2.13, derived by Zenkert (1995). Based on Equation 2.9, the midspan deflection was calculated. The nominal tensile stress levels of the composite were evaluated using quasi-static tests.

$$D = EI = \frac{E_f h_t h_b d^2}{h_t + h_b} \tag{2.13}$$

Mei et al. (2022) worked on the three-point bending behavior of a foam-filled sandwich panel made of CFRP X-core. This group aimed to develop analytical formulas suitable for use in various fields. They used Allen's (Mei et al., 2022) approach for the total deflection of a bending beam due to the superposition of the core shear deformation and the pure bending deformation. The authors obtained the stiffness properties of the face material from the tensile test results they performed in a previous study (Mei et al., 2021).

Xie et al. (2022) analyzed the flexural properties of a foam-filled sandwich panel manufactured from polyethylene terephthalate under four-point bending loadings. In addition, the different core and face thicknesses were analyzed to determine their impact on these characteristics. An analytical model was used to forecast structures' bending stiffness and failure modes. The total displacement of a structure at the mid-point is expressed in terms of Equation 2.10. The mechanical properties of the face material were obtained with experimental test data.

Dariushi and Sadighi (2013)studied the bending characteristics of sandwich beams made with FML (fiber metal laminate) facesheets. Various materials were used to manufacture sandwich specimens, such as aluminum 1050 sheets, unidirectional glass fiber, epoxy resin for the skins, PU foam, and ethylene vinyl acetate foam for the core. They aimed to comprehensively analyze the deformation of sandwich beams using a combination of classical laminate theory and nonlinear geometric and elastic material relations. It also generated an explicit expression for symmetric beams. They obtained a deformation equation as,

$$w = w_1 + w_2 = \frac{PL^3}{48.7bD_{11}} + \frac{PL}{4.9bkA_{55}} \tag{2.14}$$

Where, $w_1$ and $w_2$ are total deflection of the sandwich beam, bending stiffness deflection, and shear deflection, respectively.

The presented technique was similar to the classical sandwich beam theory developed by Allen (1969). The experiments' results generally agreed with the predictions of the analytical models when the beam deflection was very small (Figure 2.17).

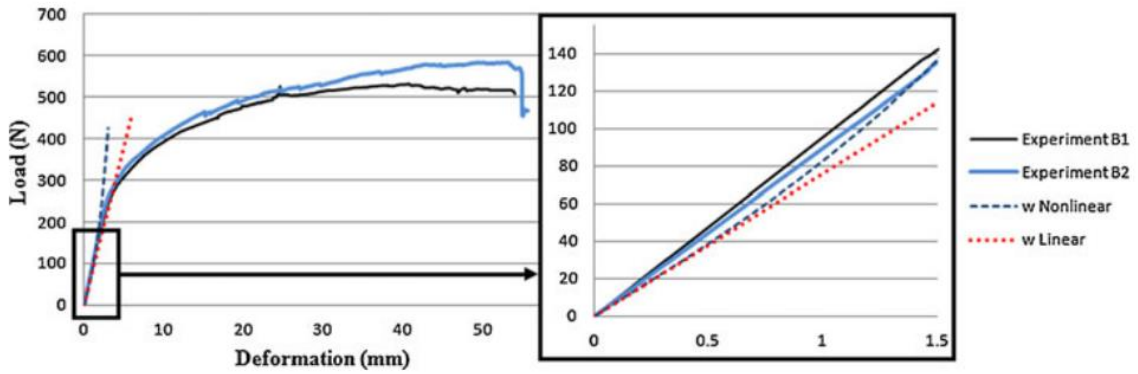



Figure 2.17. Load-deflection diagram of sandwiches under three-point bending loading (Dariushi and Sadighi, 2013)

On the other hand, the strength of sandwich beams is also considered in their design, as well as stiffness. Although they are lightweight and have high flexural stiffness, sandwich beams can still experience failure, such as indentation, core shear, face yield, and wrinkles (Ashby et al., 2002). Therefore, analytical studies have also been developed to account for these strength-based failure problems.

The wrinkles are caused by the short wavelength elastic strain in the top facesheet, which the underlying core resists (Steeves and Fleck, 2004a). As a result, several authors developed closed-form solutions for addressing the critical wrinkling stress of the sandwich structure when designing and analyzing structures. The result developed by Hoff and Mautner (1945) states that critical stress is a function of the structure materials properties. It is generally considered to apply to an isotropic core (Wadsworth et al., 2009). The general wrinkling maximum force formula is given in Equation 2.15., which was derived by Hoff and Mautner (1945) as

$$P_w = \frac{2bt_f d}{L} \sqrt[3]{E_f E_c G_c} \tag{2.15}$$

Wadsworth et al. (2009) revealed that the facesheet of damaged honeycomb sandwich structures was wrinkled. This study extended an analytical expression depending on Equation 2.15 due to the depth of the core material's crushed regions. The results of this study revealed that the sub-surface damage to the core material significantly decreased the support provided by the facesheet. The model provided a means of assessing the various fundamental parameters that govern the wrinkling process.

Staal et al. (2009) presented a method to accurately predict the failure loads in unlaminated honeycomb sandwich panels subjected to bending. Although the past wrinkling method was limited, it could be used to analyze future failure loads. The model was based on the two linear stress studies that were conducted in parallel. The first predicted the stress of an undamaged panel, while the second indicated the failure stress for a large impact dent with a subsurface damage layer. Horrigan and Staal (2010) also presented a closed-form analytical framework that could predict critical stresses in various dimensions. They also found an expression for the vital wrinkling wavelength in a given closed-form solution, an extension of the previous work (Staal et al., 2009).

Kheirikhah et al. (2012) studied a new high-order theory and a finite element model for analyzing bi-directional sandwich plate wrinkles. The boundary conditions and motion equations were derived from the minimum potential energy principle. The paper also presented an analytical solution for analyzing the compressive loads of supported sandwich plates with a biaxial in-plane structure. The results of the finite element method agreed with the analytical approaches. Furthermore, the increase in the load ratio and constant geometrical parameters reduced the dimensionless wrinkling loads.

In a study conducted by Birman et al. (2019), they noted that the thin facings of certain sandwich structures can get wrinkled due to the use of a bi-modular elastic framework. The paper suggested extending the Hoff method to address this issue. One of the solutions was the classical Hoff method, which indicates that the core's stiffness is equivalent to compression. The second case shows that the difference in the stiffness of the core's compression and tension is large enough to be assumed to be infinite. The mismatch between the two factors could affect the wrinkles' mode. The researchers noted that a higher stress level might be caused by a stiffer bi-directional structure or a more rigid face. In addition, the energy that is absorbed during the wrinkles' development could be reduced by the increased stiffness.

When the average stress level in the face exceeds its yield stress, the face begins to yield and is determined with Equation 2.16. Finally, the face-yielding limit load is computed with Equation 2.17. This equation compares a sandwich beam's plastic moment to the applied moment (Allen, 1969).

$$\sigma_y^f = \frac{M(t+\frac{c}{2})E_f}{(EI)_{eq}} \tag{2.16}$$

$$P_{Fy} = 4\frac{\sigma_y^f bdt_f}{L} \tag{2.17}$$

McCormack et al. (2001) identified the failure of the sandwich beams with the use of metallic foam cores. They used equations 2.16 and 2.17 above to calculate the yield failure loads of the facesheet, which were made from aluminum alloy. The cores of these beams were made of 8% aluminum foam, and the cell size was 4.5 millimeters.

Banghai et al. (2015) subjected the mechanism for the failure of sandwich beams to bending at three points. They assumed a facesheet was elastic-plastic, and only when it had a full plastic deformation did it show the face yield because aluminum alloy was used to make the sandwich beams. So, they also used Equations 16 and 17 to get the critical face yield strength.

Vitale et al. (2017) revealed the mechanical properties of synthetic and natural fiber-reinforced sandwich panels under three-point bending. The mechanical properties of different facesheet combinations were analyzed using analytical models. Yielding collapse loads were calculated using the Allen approach. The skin plate was subjected to uniaxial tensile tests at a 2 mm/min speed to obtain yielding stress.

It was assumed the core would collapse uniformly, with little additional strength from the facesheets for core shear failure. However, skins can provide additional strength when the core collapses. There are two limiting cases: the skins bend elastically when the beam collapses, or they develop plastic hinges. This method was unsuitable for use with strong faces, as the plastic shear of

a core would be accompanied by the elastic bending of faces (Steeves and Fleck, 2004a). The most basic model developed for core shear failure load is given in Equation 2.18 (Allen, 1969; Zenkert, 1995). The model that predicts the collapse of sandwich based on core shear understates its peak strength due to its failure to consider the bending strength of faces (Steeves and Fleck, 2004b).

$$P_s = 2bd\tau_c \tag{2.18}$$

Lim et al. (2004) studied the failure modes of sandwich beams with foam cores when subjected to impact and static loads with simple analysis and experimental methods. The static three-point bending test was conducted to determine the failure modes and load capabilities of foam core sandwich beams concerning their core densities and geometry. The core shear collapse force was computed by considering Equation 2.18.

Rice et al. (2006) explored the collapse of reinforced foam sandwich panels with pin-reinforced foam core structures. The pins were made from either carbon fiber, titanium, or steel. They were inserted into the foam's outer surface and extended from the facesheet to the body. Analytical models were developed to determine the collapse strength of sandwich beams under three-point bending, as well as experimental work. The stress level that exceeds the core shear strength of a sandwich panel during its bending phase can trigger a collapse mode. They adopted the general shear failure approach because facesheet strength did not affect the collapse force.

Ashby et al. (2002) also developed two approaches for core shear for metal facesheets with yield strength. These were Mode A and Mode B, shown in Figure 2.18. The core shear failure maximum loads can be determined by Equations 2.19 and 2.20.

$$F_A = \frac{2bt^2}{l}\sigma_y^f + 2bc\tau_y^c\left(1 + \frac{2H}{l}\right) \tag{2.19}$$

$$F_B = \frac{4bt^2}{l}\sigma_y^f + 2bc\tau_y^c \tag{2.20}$$

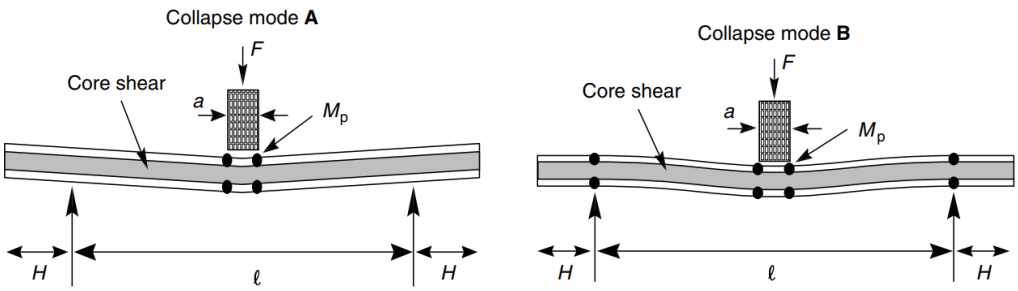



Figure 2.18. The collapse modes A and B are used for the core shear of a sandwich beam in a three-point bending process (Ashby et al., 2002).

Crupi and Montanini (2007) investigated that aluminum foam sandwiches collapsed under dynamic and static three-point bending. The aluminum foam sandwich was made using a combination of aluminum and lightweight foam. The study's authors utilized Mode A and Mode B to analyze core shear failures. Crupi et al. (2012) aimed to analyze the impact and bending response of two typologies of aluminum honeycomb structures on different cell sizes. They also used Mode A and B when calculating core shear failure load. Zhang et al. (2014) studied the failure behavior of metal foam core-supported sandwich beams with asymmetric structures. Due to three-point bending, the asymmetric sandwich beams exhibit initial failure modes, such as face yield, indentation, and core shear Mode A and B. They used Equations 2.19 and 2.20 in their calculations for core shear.

Research have shown that analytical methods can predict indentation behavior in the past few decades (Zhu et al., 2018). Shuaeib and Soden (1997) developed an analytical model that could estimate the failure load of indentations. The model depended on the elastic-plastic Winkler-type foundation model developed by Zingone (1968). It was based on the elastic beam's support structure, which is an elastoplastic core. The phenomenon referred to supporting an elastic beam (composite facesheets) using a foundation (core) made of elastoplastic materials. The developed model determined the sandwich beam's elastic limit load ($P_1$) using Equations 2.21, 2.22, and 2.23, given below. The maximum indentation failure load ($P_2$) was then determined by splitting the sandwich beam into plastic deformation and elastic regions with numerical convergence. The researchers then used the data collected by tests to verify their analytical model. In addition, experiments were performed to obtain the elasticity properties of the composite material for Equations 2.22.

$$P_1 = \frac{2\sigma_c b}{\lambda} \tag{2.21}$$

where,

$$\lambda = \left(\frac{k}{4E_f I_f}\right)^{\frac{1}{4}} \tag{2.22}$$

with foundation modulus k defined as;

$$k = \frac{E_c b}{c} \tag{2.23}$$

Steeves and Fleck (2004a, b) studied the sandwich beams' failure mechanisms with three-point bending loading. They created an analytical model that considers the various factors that can affect indentation failures, such as elastic facesheets and a rigid, ideally plastic core. The proposed governing equation considered the local bending of the indentation zone along its length. The force Equation 2.24 used to calculate the indentation failure load ($P_2$) was obtained from the governing

formula. Thus, they tried to attain $P_2$ by implementing the model in a way that did not require a numerical solution. They confirmed the analytical model's findings after conducting experiments on sandwich beams made of various materials, such as PVC foam and woven glass/epoxy composite (Steeves and Fleck, 2004b). The elasticity properties of woven glass were obtained with tension and compression tests.

$$P_i = P_2 = bt_f\left(\frac{\pi^2 dE_f\sigma_c^2}{3L}\right)^{1/3} \tag{2.24}$$

For decades, the analysis of the indentation failure loads of sandwich beams has been carried out using the Shuaeib-Soden and Steeve-Fleck methods. Gdoutos et al. (2002) aimed to analyze the impact of indentation on a composite sandwich panel. The two cases were presented: a sandwich panel with a carbon/epoxy face and a PVC foam core on a rigid base. The other case was a sandwich beam with a symmetrical face and core materials. The analytical model was represented as an elastic beam resting on a plastic foundation. The compressive and longitudinal stress-strain behavior of the carbon/epoxy material was obtained from experimental data.

Zenkert et al. (2004) explored the effects of static indentation on foam core sandwich beams. The analytical model was based on the assumption that the foam core's compressive behavior was elastic. The indentation response's elastic component was described in the framework of the Winkler model. This study aimed to extend the scope of the indentation framework's ability to predict the reaction of foam core after it has been unloaded. It also aimed to analyze the residual strain levels and the crushed core zone's extent. The bending stiffness of the face laminates was obtained with three-point bending tests.

Tagarielli et al. (2004) observed composite sandwich beams' collapse using three-point bending loading. The composite structure comprised a foam core and glass, vinyl ester facesheets.

Mohan et al. (2005) performed the four-point bending test of the sandwich beam with different configurations to identify the failure modes, such as core shear and indentation. The formulas for identifying the various failure modes were then obtained. They identified the mechanism by which indentation failure could occur in the foam core by analyzing its elastic beam properties according to the Steeves-Fleck model. The researchers utilized sandwich structures made of aluminum foam and alumina.

Mamalis et al. (2008) presented a new type of hybrid sandwich structure that combines the advantages of polymeric and metallic materials; details of the structure are given in Figure 2.9. This study aimed to investigate the various configurations of panel structures using a simplified analytical method. The simplification developed for indentation was based on Equation 2.24.

Sadighi and Pouriayevali (2008) explored the impact on the sandwich beam's low-velocity transverse configuration using composite materials with cores and faces, such as Epoxy, E-glass, and

PVC. In addition, the Winkler foundation theories that Shuaeib-Soden developed for sandwich beams had been used regarding the three-point loading, the indentation of the sandwich beams, and the indentation of the laminated beam (Shuaeib and Soden, 1997). Finally, the properties of the composite laminates were obtained by testing them; they were made with epoxy and woven glass using the vacuum bag and hand layup techniques.

Quispitupa et al. (2009) conducted a design analysis of a sandwich with mixed bending modes. They used a plastic yield model developed by Steeve-Fleck to analyze the indentations in sandwich beams made with elastic surfaces. As a result, they revealed that the design methodology for sizing mixed-mode-bending sandwich studs was presented to enable the debond fracture.

Russell et al. (2011) revealed the analytical expressions to determine the various collapse mechanisms of sandwich beams, which were fabricated square honeycombs and identical carbon fiber composite materials. The indentation failure maximum load was calculated using Equation 2.16, which Steves and Fleck developed. The mechanical properties of the composite were obtained from these materials' quasi-static compressive and tensile test data.

Minakuchi et al. (2012) investigated that the facesheet's relaxation and formation were caused by transverse loading on sandwich structures. Under indentation loading, they utilized fully backed sandwich beams designed to interact with the deformation of the skins and the core's stretching and crushing. They utilized the Winkler foundation method for analytically developed methods.

Analytical studies for sandwich design have focused on determining the collapse mechanisms based on the bending stiffness and strength of the sandwich. The stiffness performance of the sandwich structure affects the deformation under bending loading. Deformation equations 2.9 and 2.10, attributed to Allen (1969), were used in the literature studies. These equations are derived from the Timoshenko beam theory. In Timeshenko beam theory, the beam has a shear deformation coefficient according to the cross-sectional geometry, such as circular, square, and rectangular. For sandwich structures, the shear effect coefficient is assumed to be one (1). Thus, equations 2.9 and 2.10 are obtained. Allen also presented how to calculate the stiffness value of the sandwich (*EI*) structure analytically by the classical sandwich theory with Equation 2.11 given earlier. The studies presented in the literature obtained the stiffness values of the sandwich structures they designed using this equation. The modulus of elasticity of the face material ($E_f$) is needed in this equation. The moduli of elasticity of metallic materials are known, whereas the elastic properties of composite materials vary. Therefore, studies that prefer composite structures as the face material have obtained the $E_f$ by performing experimental tests, except in Dariushi, and Sadighi (2013)where they used FML composite material as a facesheet and obtained the collapse equation using classical laminate theory. Their equation 2.14 was very similar to equation 2.9 presented by Allen (1969). In addition, the force-deflection curves in the linear region overlapped with the experiments (Figure 2.19). This study has paved the way for solving a sandwich collapse problem in sandwich design with purely analytical solutions without requiring composite experimental test data.

On the other hand, analytical approaches have been developed that calculate critical collapse loads of sandwiches due to failure modes such as wrinkling, face yield, core shear, and indentation. These approaches have used mechanical properties and characteristics of core and face materials. However, as in the case of calculating the stiffness of the sandwich, experimental tests have been used to determine the elastic modulus of composite materials.

### 2.4. Significance and goal of the study

In the present study, sandwich beams will be designed using the PVC foam core and the composite face layer of plain woven carbon fibers. Designed sandwich beams whose mechanical properties are predicted by analytical methods will be verified by experimental study. The study's analytical prediction will determine the face layer's mechanical properties with micro and macro mechanical approaches used in layered composite mechanics. Most analytical approaches in the literature on two-ply plain woven fabric development have focused on the single-ply axis and analytical models to predict its micro properties (Mallikarachchi, 2019). Thin plates are used in space applications, and the requirements for these are usually six to eight layers. The relative position of the layers can influence their out-of-plane behavior. The analytical studies also focused on determining the mechanical properties of specific plain woven composites. The computational models used for the study are complex and on the micromechanical level.

Firstly, this study provides a practical and simple analytical method to determine layered plain woven composite plates' flexural and axial properties. The mechanical properties of the two-dimensional (2D) fabric are analyzed using the yarn volume fraction ($V_f^y$) and geometric shapes. The micromechanical properties of the single-ply WPFC plate were determined with The Composite Cylinder Assemblage Model (CCAM) (Hashin, 1983; Hashin et al., 1972). Later, the composite was assumed to be a cross-ply lamina (0/90), and the flexural and axial properties of composite laminates were determined by applying classical laminate theory. The analytical findings of the approach were compared with those of the experiments to verify its reliability and accuracy. The experimental studies include laminate productions, tensile, and three-point bending tests. The carbon fiber/epoxy laminates are going to be produced by applying five different manufacturing methods: High and low vacuum bagging, hand lay-up, compression molding, and infusion. Different manufacturing methods aim to obtain various test specimens with individual features such as fiber volume fraction ($V_f$). This approach allows the investigation of the generality of the proposed practical engineering model by comparing the analytical solutions with experimental data.

In the second phase of the thesis, sandwich beams are designed according to their stiffness and strength properties. Equation 2.9, derived from Timoshenko's beam theory, determines the deformation of sandwich beams under three-point bending loading. The stiffness value of the sandwich beam used in this equation is obtained by equation 2.11 in the traditional sandwich theory. The elastic of the composite face layers has been obtained experimentally in the literature studies so

far. The neutral axis is the center of the sandwich beam, and the facesheets carrying the bending loading affect the structure's stiffness depending on the sandwich's thickness. Therefore, the sandwich's stiffness value can be obtained using the parallel axis theorem. This method requires the composite bending stiffness, axial stiffness, and coupling term values to calculate the sandwich beam's stiffness. The stiffness value of the designed sandwich can be determined by obtaining these values with the “practical engineering approach” developed in this study for multilayer plain woven composite plates.

Moreover, the study aims to predict the collapse mechanisms of sandwich beams under flexural loading. The primary failure mode can be detected by calculating the maximum limit loads. Core shear and indentation failure modes generally occur in sandwiches made of foam core. Therefore, the work focused on these failure modes and the determination of the elastic limit load. When calculating the core shear failure load of sandwiches made of composite plates, the effect of facesheet shear can be neglected, and equation 2.18 is often used. However, elastic limit and maximum indentation loads are affected by the elasticity of the face material. Although the fundamental equations in 2.21 and 2.24 have been developed and are widely used, some shortcomings need improvement. While these equations are used for composite sandwiches, the modulus of elasticity is still obtained by performing experimental tests of the face material. In this study, these equations are modified to make stiffness terms derived from composite mechanics applicable. With the engineering approach developed in the study, the stiffness terms of the composite can be easily calculated, and the failure loads can be calculated using the modified equations. Thus, failure forces can be predicted without depending on any experimental data.

The results of this study will enable sandwich beam producers or designers to predict the mechanical properties of the sandwich beam analytically before production. Experimental testing for faceeshet will not be required during the designing process.

# 3. MATERIAL AND METHOD

## 3.1. Materials used for sandwich structures

In this thesis, carbon plain woven fabric, one of the textile composite fiber materials, was chosen for the face layer material. Closed-form PVC foam material was preferred for the core material. Epoxy resin material was used as the fibers, face layer, and core surface binder.

### 3.1.1. Plain woven carbon fabrics

3K continuous plain woven carbon fiber fabrics were used for the laminated fiber-reinforced plastic (FRP) composites. The fabrics featured a 200 g/m$^2$ areal density and a 0.2 mm ply thickness. The warp and fill yarns of these fabrics are 2 mm wide. The warp yarn's undulation length is 2 mm. The continuous carbon fibers of these fabrics have a density of approximately 1790 kg/m$^3$. They have a tensile strength of 3800 MPa, a strain factor of 1.6, and a modulus of 240 GPa (Dost Kimya, 2014).



Figure 3.1. Image of carbon plain woven fabric

### 3.1.2. Matrix materials

The matrix was made using a mixture of MGS L160 and MGS H160, which had a weight ratio of 100:25, as shown in Figure 3.2. The manufacturer's technical documentation indicates that the matrix has a density of approximately 1190 kg/m$^3$. Its various characteristics, such as tensile strength, flexural strength and flexibility, and strain, are around 75 MPa, 3.4 GPa, 125 MPa, and 4.5% (Dost Kimya, 2009). This type of epoxy matrix is ideal for areas where lightweight and bending rigidity is required.



Figure 3.2. MGS L160 resin and MGS H160 hardener

### 3.1.3. PVC core materials

AIREX C70 is a high-quality closed-cell foam that provides exceptional strength and stiffness. It has superior toughness. This non-friable material is highly water-resistant, and it exhibits excellent anti-chemical properties. Its fine cell structure also provides a good bonding surface. AIREXC70 is compatible with most manufacturing processes and resins. It can be used as a core material for sandwich structures subjected to dynamic and static loads. Its unique lightweight properties make it ideal for applications that prioritize lightweight. AIREX C70 foam with three different densities and thicknesses has been selected as the core material, given in Figure 3.3. The manufacturer provided the mechanical properties of the foams with densities of 48, 75, and 130 kg/m³ used in the study and presented in Table 3.1.

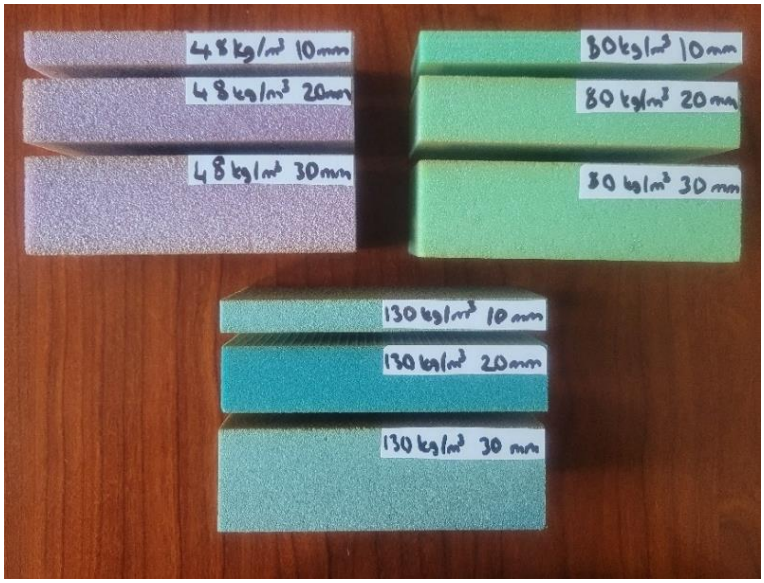


Figure 3.3. AIREX C70 foams are used as core material

Table 3.1. Mechanical properties of AIREX C70 foam materials (Metyx, 2020)

| **Properties of AIREX C70** | **Unit** | **C70.48** | **C70.75** | **C70.130** |
|---|---|---|---|---|
| Density | $kg/m^3$ | 48 (min 43) | 80 (min 72) | 130 (min120) |
| Compressive strength | MPa | 0.60 (min 0.50) | 1.45 (min 1.10 ) | 3.0 (min 2.6) |
| Compressive modulus | MPa | 48 (min 35) | 104 (min 80) | 170 (min 145) |
| Tensile strength in the plane | MPa | 0.95 (min 0.80) | 2.0 (min 1.6) | 4.0 (min 3.0) |
| Tensile modulus in the plane | MPa | 35 (min 28) | 66 (min 50) | 115 (min 95) |
| Shear strength | MPa | 0.55 (min 0.50) | 1.2 (min 1.0) | 2.4 (min 2.1) |
| Shear modulus | MPa | 16 (min 14) | 30 (min 24) | 54 (min 45) |

### 3.2. Development of practical engineering approach by conducting novel analytical models

A systematic procedure illustrating the overall approach for the analytical and experimental studies to obtain and verify the mechanical properties of the sandwich beam given in Figure 3.4 will be followed in this study. As seen in Figure 3.4, the study has two main parts: analytical and experimental. In the first step of the analytical study, the face sheet's axial and flexural mechanical properties produced from plain woven carbon fabric will be predicted by the engineering approach (EA) developed in this work. Detailed steps are shown in Figure 3.5. If these predictions are validated with experimental results, the second step of the study will be initiated. In the second analytical step, the behavior of the sandwich structure such as force-displacement and failure mode will be predicted under bending load from three-point tests. In this step, the mechanical properties of the face material, such as the bending stiffness predicted in the first part, will be compared to evaluate the developed EA. A step-by-step procedure is given in Figure 3.6. If predictions for force-displacement and failure modes such as indentation and core shear are validated experimentally, the study will have met the ultimate goal. Thus, the proposed approach aims to predict the flexural behaviors of the composite sandwich beam avoiding the lengthy and costly experimental work.

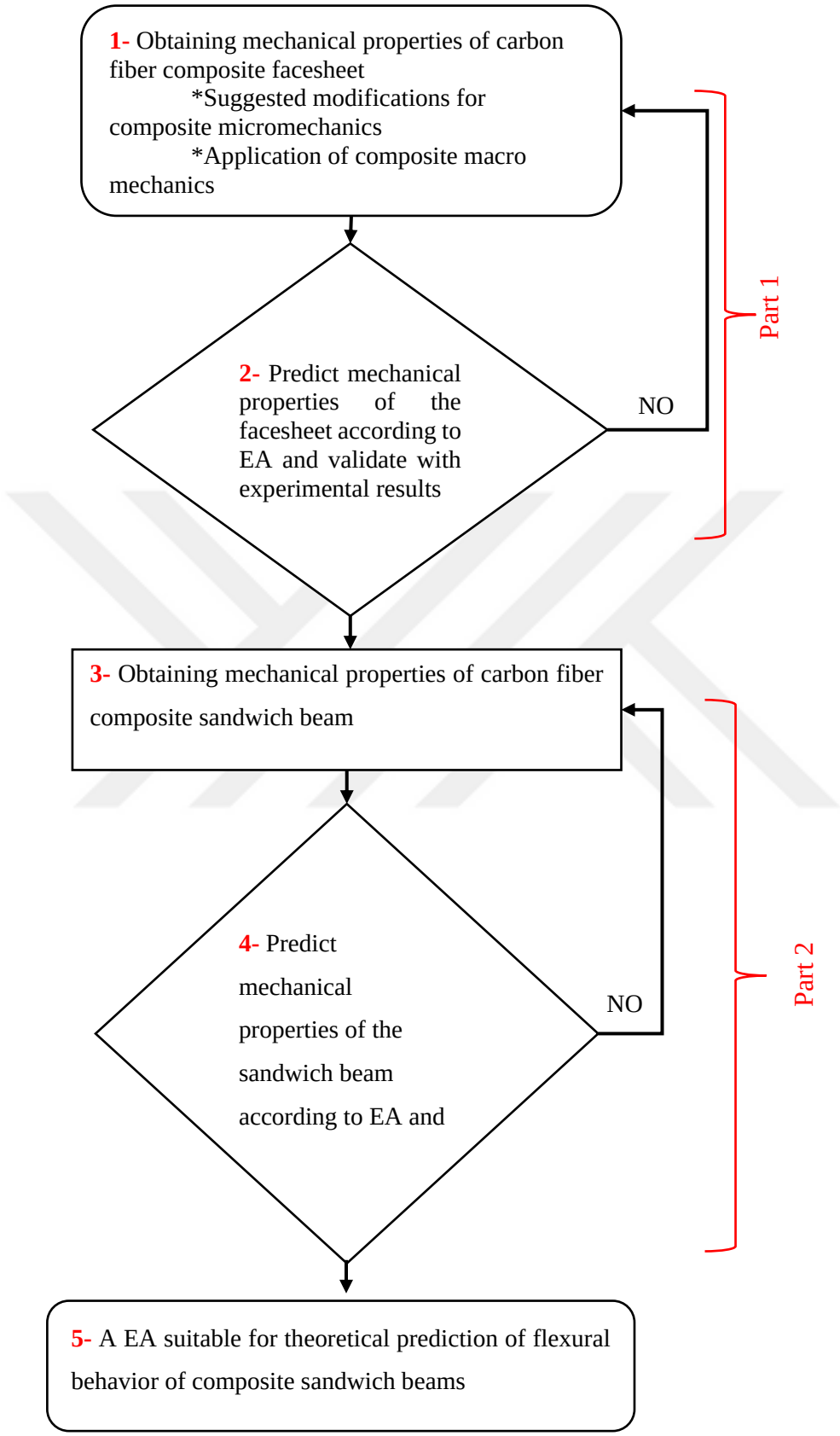



Figure 3.4. Plenary flow chart illustrating the overall approach for the analytical and experimental studies to obtain and verify the mechanical properties of the sandwich beam

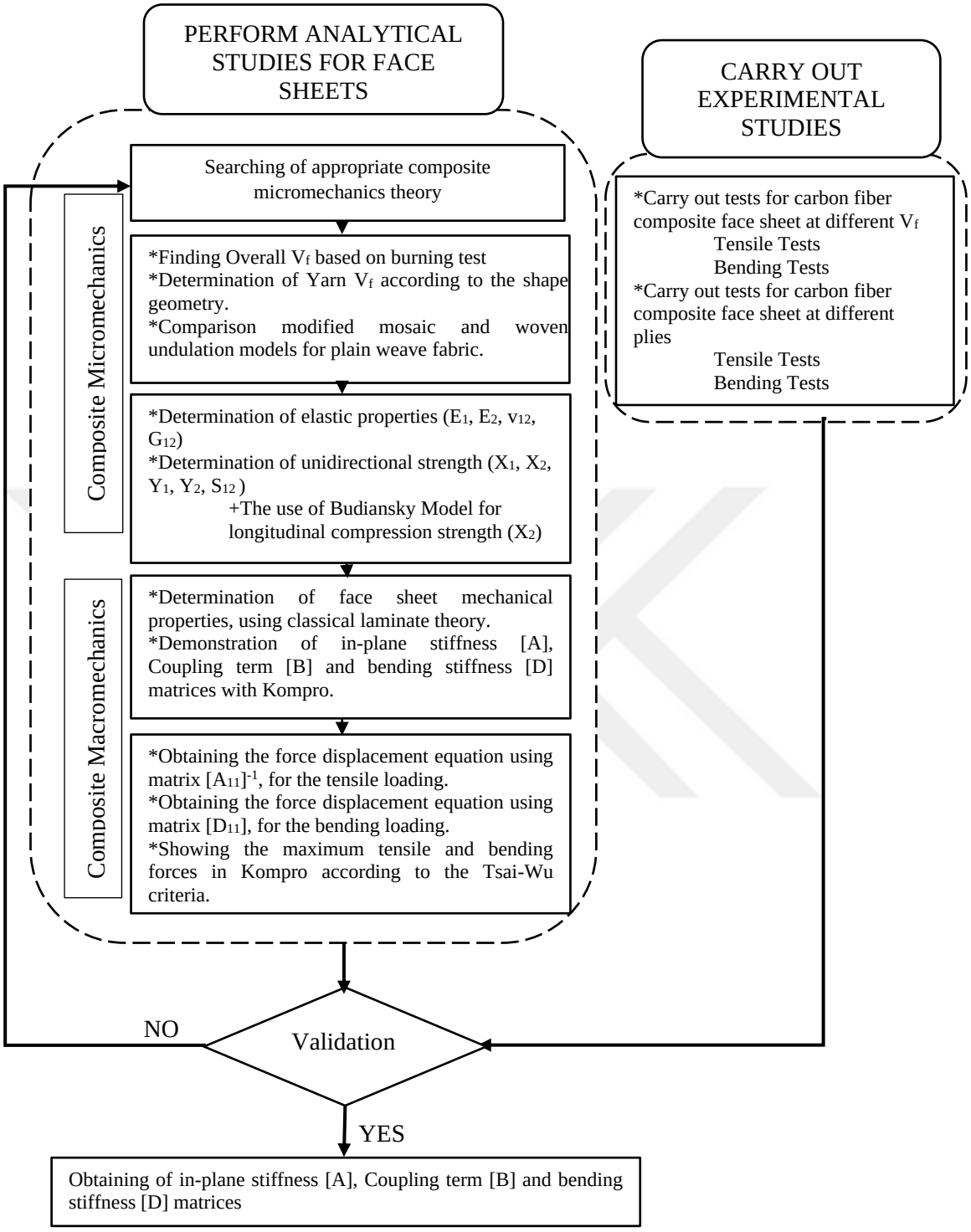



Figure 3.5. The detailed flow chart for Part 1 in Figure 3.4 shows the step-by-step procedure to find the mechanical properties of carbon fiber composite face sheet and validate the properties by experimental study.

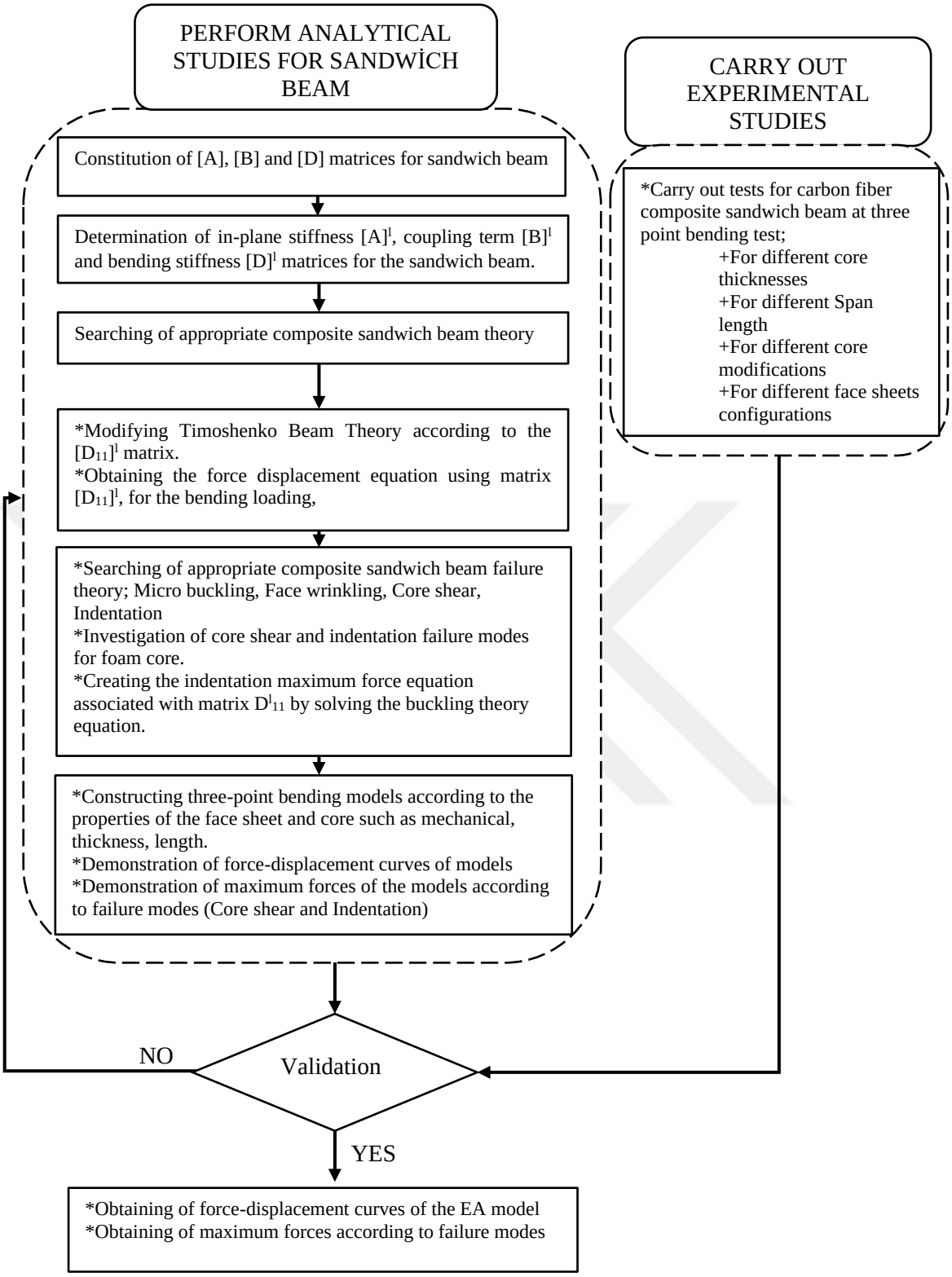



Figure 3.6. The detailed flow chart for Part 2 in Figure 3.4 shows the step-by-step procedure to find the mechanical properties of the carbon fiber composite sandwich beam and the validation of the properties by the experimental study.

### 3.2.1. Modeling of plain woven fabric composite face layer

Complex structure of plain woven fabric makes it difficult to determine its mechanical properties. In the past, some analytical studies have been conducted on the subject. Most research on developing two-ply these fabrics has focused on the analytical models and single-ply axes (Mallikarachchi, 2019). This study has developed a model to obtain the mechanical properties of the layered plain woven fabric composite plate by first considering the microstructure for a layer and then the macrostructure for the laminate.

*Micromechanical approaches used to obtain properties of plain woven fabric composite face layer*

All the micromechanics models of plain woven fabric composite derived during the 1980s were complex and difiicult to implement. Therefore, there existed a need to develop a practical method to predict the micromechanical properties of these composites (Karkkainen and Sankar, 2006; Xiong et al., 2009). The microstructure of heterogeneous materials significantly affects their macro-scale behavior (Gopinath and Batra, 2018). Therefore, the need for modeling was also stated recently (Wang et al., 2019). The current study utilized the geometric shape and yarn volume fraction of 2D plain weave fabric to develop a practical engineering approach.

- Estimating the overall fiber volume fraction with burning test

The fiber volume fraction ($V_f$) is a parameter utilized in designing and constructing composite materials. It refers to the fraction of the total fiber volume in a given composite material (Hull, 1981). The fraction of reinforced fiber utilized in a composite is significant in assessing its mechanical properties. Therefore, the higher the fiber volume ratio, the better the mechanical properties of the composite (Endruweit et al., 2013). The burn-off tests were performed to determine the $V_f$ of the composite materials. It was used successfully by Abdelal and Donaldson (2017). The burn-off tests were conducted in a muffle furnace at 500 degrees Celsius, given in Figure 3.7a. The procedure used followed ASTM D 3171-99 (International, 2017b). Seven different specimens were prepared in rectangular dimensions and with a surface area greater than 625 $mm^2$, as shown in Figure 3.7b. The matrix portion of a known fiber-reinforced composite material is removed during combustion in a furnace. The remaining residue, fiber material, is then cooled and weighed. The matrix and fiber weight fractions were calculated by comparing the initial mass of the specimen with its fiber mass after the burn-off test. Equation 3.1 (Kaw, 2005) determines the $V_f$ values. The weight fractions of a matrix and fiber obtained after burn-off tests are $w_m$ and $w_f$, respectively.

$$V_f = \frac{{}^{w_f}/_{\rho_f}}{\left({}^{w_f}/_{\rho_f}\right)+\left({}^{w_m}/_{\rho_m}\right)} \tag{3.1}$$



(a)




(b)

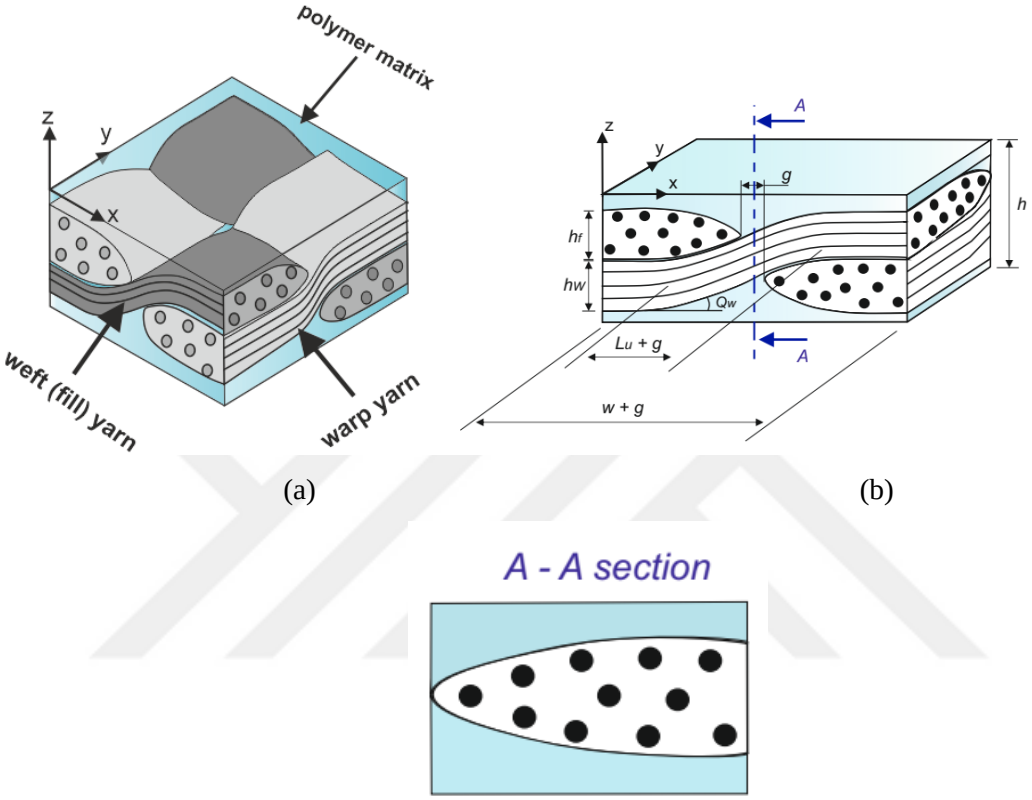
Figure 3.7. a) muffle furnace b) burn-off tests specimens prepared from plain woven fabric composite plate

The fiber volume fraction of a woven fabric composite is called the overall volume fraction ($V_f^o$), which is the ratio of the total amount of fibers to the total amount of woven composite lamina (Naik and Shembekar, 1992). $V_f^o$ can be easily determined with Equation 3.1 utilizing burn-off tests.

- Estimating the yarn fiber volume fraction according to yarn geometry

The plain woven fabric comprises weft and warp yarns, which are weaved to create a layer. Yarn, used in textile fabric construction, comprises fibers grouped or twisted together by strands. Figure 3.8a shows the interlacing relationship between the two yarns in the composite cell. The woven structure is more resilient and performs better in transverse and longitudinal directions (Stier

et al., 2015). However, this material's longitudinal strength is lower than that of a unidirectional fabric composite with the same yarn volume fraction ($V_f^y$) due to its elliptical cross-sectional area and undulation angle (Ishikawa and Chou, 1982). $V_f^y$ refers to the ratio of the volume of fibers to the volume of yarn (warp/weft). The volume of yarn can be determined by the numerical integration of the shape functions, the shape details of yarn are given in Figure 3.8b.




(a) (b)

(c)

Figure 3.8. Cross sections for a) Woven plain fabric composites unit cell, b) Yarn geometry details, c) Yarn cross-sectional area at the midpoint of undulation (Çetin et al., 2023)

The $V_f^y$ of composite is computed by knowing its $V_f^o$ and volume of yarn (Naik and Shembekar, 1992). The $V_f^O$ is first obtained by the burn-off test, and then the $V_f^y$ is calculated using Equations 3.2 and 3.3 (Cox and Flanagan, 1997; Naik, 1994).

$$A_{yarn} = \frac{h_f}{2}\left[w - L_u\left(1 - \frac{2}{\pi}\right)\right] \tag{3.2}$$

$$V_f^y = \frac{wt}{A_{yarn}} V_f^o \tag{3.3}$$

The undulation angle (in Figure 3.8b) reduces the longitudinal strength and leads to the loss of the on-axis properties of the composite. In addition, the reduction in the cross-sectional area of elliptical yarn (section A-A in Figure 3.8c) also decreases the units' longitudinal strength.

- Developing a model called engineering fiber volume fraction

The mechanical properties of plain woven fabric composites will be determined much more simply with a novel approach using the Composite Cylinder Assemblage Model (CCAM) along with Classical Laminate Theory (CLT).

The primary assumptions to formulate the approach are outlined below:

- Modeling PWFC like Cross-ply,
- Considering PWFC as 2D,
- Considering the Yarn cross-section area as elliptical,
- Neglecting the gap between the yarns,
- Warp and fill yarns have equal geometric structure and mechanical properties,
- Theoretically, no void formation was assumed (Mehdikhani et al., 2018).

The mechanical properties of unidirectional composite materials can be accurately estimated depending on their overall volume fraction. However, due to the fiber structure, predicting an ideal solution using the overall volume fraction of plain woven fabric is not feasible. After all, matrix spaces, not including fiber, are found in the cellular structure of the fabric (Figure 3.8). Therefore, the yarn volume fraction is higher than the overall volume fraction. Furthermore, it has been shown that the fiber fraction of a yarn decreases by almost half when the elliptical cross-sectional area and undulation angle are considered. The representative volume element is given in Figures 3.8b and 3.8c. Reducing the fiber fraction of representative volume elements could affect the woven composite stiffness and strength. So, the engineering volume fraction ($V_f^E$), defined in the present study, can be determined by dividing $V_f^y$ by two (Çetin et al., 2023; Uzay et al. 2023). Thus, $V_f^E$ may be used to find the micromechanical properties of the composite materials, which are considered cross-ply, using the CCAM.

- Modeling and modification of on-axis properties with engineering fiber volume fraction

Elastic properties of the on-axis ply (Longitudinal modulus ($E_1$), Transverse modulus ($E_2$), Poison's ratio ($v_{12}$), and Shear modulus ($G_{12}$) were determined with Composite Cylinder Assemblage Model (CCAM) (Jones, 1998), also called the rule of mixture.

The equations provided by Jones (1998) were modified by replacing $V_f$ with the $V_f^E$. In the case of using $V_f$ the elastic properties may be erroneous. When $V_f^y$ or $V_f^O$ is used, the results always

differ from experimental findings. This is why the use of the new term, $V_f^E$, is a strong necessity for woven plain fabric composite. The modified equations are provided below.

$$E_1 = E_f V_f^E + E_m(1 - V_f^E) \tag{3.4}$$

$$E_2 = \frac{E_f E_m}{E_m V_f^E + E_f\left(1 - V_f^E\right)} \tag{3.5}$$

$$v_{12} = v_f V_f^E + v_m\left(1 - V_f^E\right) \tag{3.6}$$

$$G_{12} = \frac{G_f G_m}{G_m V_f^E + G_f\left(1 - V_f^E\right)} \tag{3.7}$$

- Modeling and modification of on-axis strength with engineering fiber volume fraction

Longitudinal $(X_1)$, transverse $(X_1)$ tensile and transverse $(Y_2)$ compressive strengths are determined with the following equations (Gibson, 2011; Kaw, 2005) modified with $V_f^E$.

$$X_1 = \sigma_{max}^f V_f^E + \sigma_{\varepsilon_{max}}^m (1 - V_f^E) \tag{3.8}$$

$$Y_1 = E_2\left[\left[\frac{d}{s}\frac{E_m}{E_f} + \left(1 - \frac{d}{s}\right)\right](\varepsilon_m^1)_{ult}\right] \tag{3.9}$$

$$Y_2 = E_2\left[\left[\frac{d}{s}\frac{E_m}{E_f} + \left(1 - \frac{d}{s}\right)\right](\varepsilon_m^2)_{ult}\right] \tag{3.10}$$

$$\frac{d}{s} = \left(\frac{4V_f^E}{\pi}\right)^{1/2} \tag{3.11}$$

There are three typical failure modes for longitudinal compressive failure. These are breakage of the matrix or fiber-matrix bond, fiber shear failure, and micro buckling of the fibers (Gibson, 2011; Kaw, 2005). Naik and Kumar (1999) examined the unidirectional composite's compressive strength and compared it with prediction models available in the literature. According to the researchers, the Budiansky model could accurately predict a composite's unidirectional compressive strength once the plate parameter has been identified (Budiansky, 1983). Therefore, in this thesis, this model is used to predict the unidirectional compressive strength and is detailed in the following,

$$X_2 = \frac{G_{12}}{\left(1+\left(\bar{\emptyset}/\gamma_y^m\right)\right)} \tag{3.12}$$

$\bar{\emptyset}$ is defined misalignment angle of fiber and was observed between 0 and $2^0$ (Yurgartis 1987). $\gamma_y^m$ is matrix strain.

*Approaches used to obtain macro mechanical properties of plain woven fabric composite face layer*

The micromechanical properties of the composite, which is assumed to be cross-ply (0/90), can be determined via the equations (3.4 and 3.12) given above, based on the $V_f^E$. The study in this section aims to determine the mechanical properties of a layered plate. CLT is used to determine the plate in the study because it is a widely used predictive tool that can be utilized to analyze the complex coupling effects of laminate composite (Shokrieh and Kamali Shahri, 2021). The in-plane stiffness [A], coupling term [B], and bending stiffness [D] matrices are obtained from CLT; these are the stiffness matrices in the equations that relate the physical load to the strain in the plate.

- Modeling of a layered-composite with classical laminate theory

  The general stress-strain relationship is shown as follows (Gibson, 2011; Kaw, 2005),

$$\{\sigma\} = [C]\{\varepsilon\} \tag{3.13}$$

The fiber-reinforced composite plate is considered a two-dimensional orthotropic material. Plane stress conditions for the unidirectional lamina are assumed to be $\sigma_3 = 0$, $\tau_{23} = 0$, and $\tau_{31} = 0$, as shown in Figure 3.9.

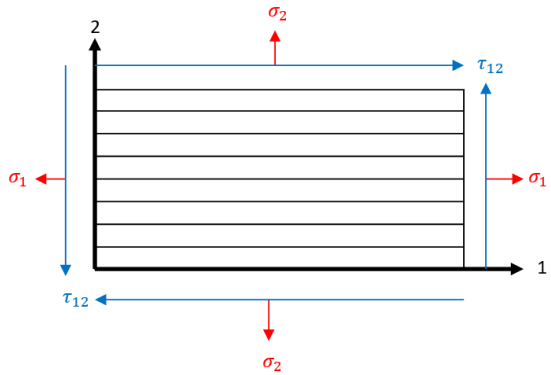



Figure 3.9. Stress distribution under the two-dimensional unidirectional lamina

Equation 3.13 is written for a specially-orthotropic unidirectional lamina as

$$\begin{bmatrix}\sigma_1\\ \sigma_2\\ \tau_{12}\end{bmatrix}=\begin{bmatrix}Q_{11} & Q_{12} & 0\\ Q_{21} & Q_{22} & 0\\ 0 & 0 & Q_{66}\end{bmatrix}\begin{bmatrix}\varepsilon_1\\ \varepsilon_2\\ \gamma_{12}\end{bmatrix} \tag{3.14}$$

The stiffness terms ($Q_{ij}$) is given below,

$$Q_{11}=\frac{E_1}{1-V_{21}V_{12}},\ Q_{22}=\frac{E_2}{1-V_{21}V_{12}},\ Q_{12}=Q_{21}=\frac{V_{12}E_2}{1-V_{21}V_{12}},\ \ Q_{66}=\ G_{12} \tag{3.15}$$

Due to their low strength and stiffness in transverse direction, some of the laminate's unidirectional components are placed at an angle. The stress-strain relationship between the components of a laminate at an angle ($\theta$) is (Gibson, 2011; Kaw, 2005),

$$\begin{bmatrix}\sigma_x\\ \sigma_y\\ \tau_{xy}\end{bmatrix}=[T]^{-1}\begin{bmatrix}\sigma_1\\ \sigma_2\\ \tau_{12}\end{bmatrix} \tag{3.16}$$

$[T]$ is transformation matrix expanded as,

$$[T]^{-1}=\begin{bmatrix}c^2 & s^2 & -2sc\\ s^2 & c^2 & 2sc\\ sc & -sc & c^2-s^2\end{bmatrix},c=Cos(\theta),\ s=\sin(\theta) \tag{3.17}$$

If Equation 3.14 is rewritten in Equation 3.16,

$$\begin{bmatrix}\sigma_x\\ \sigma_y\\ \tau_{xy}\end{bmatrix}=[T]^{-1}\begin{bmatrix}Q_{11} & Q_{12} & 0\\ Q_{21} & Q_{22} & 0\\ 0 & 0 & Q_{66}\end{bmatrix}\begin{bmatrix}\varepsilon_x\\ \varepsilon_y\\ \gamma_{xy}\end{bmatrix} \tag{3.18}$$

which yields

$$\begin{bmatrix}\sigma_x\\ \sigma_y\\ \tau_{xy}\end{bmatrix}=\begin{bmatrix}\bar{Q}_{11} & \bar{Q}_{12} & \bar{Q}_{16}\\ \bar{Q}_{21} & \bar{Q}_{22} & \bar{Q}_{26}\\ \bar{Q}_{61} & \bar{Q}_{62} & \bar{Q}_{66}\end{bmatrix}\begin{bmatrix}\varepsilon_x\\ \varepsilon_y\\ \gamma_{xy}\end{bmatrix} \tag{3.19}$$

The elements of the transformed stiffness matrix [ $\bar{Q}$] are referred to $\bar{Q}_{ij}$, and defined as,

$$\bar{Q}_{11}=Q_{11}c^4+Q_{22}s^4+2(Q_{12}+2Q_{66})c^2s^2,$$

$$\bar{Q}_{22} = Q_{11}s^4 + Q_{22}c^4 + 2(Q_{12} + 2Q_{66})c^2s^2,$$

$$\bar{Q}_{12} = \bar{Q}_{21} = (Q_{11} + Q_{22} - 4Q_{66})c^2s^2 + Q_{12}(c^2s^2),$$

$$\bar{Q}_{16} = \bar{Q}_{61} = (Q_{11} - Q_{12} - 2Q_{66})c^3s - (Q_{22} - Q_{12} - 2Q_{66})\, s^3c,$$

$$\bar{Q}_{26} = \bar{Q}_{62} = (Q_{11} - Q_{12} - 2Q_{66})s^3c - (Q_{22} - Q_{12} - 2Q_{66})\, c^3s,$$

$$\bar{Q}_{66} = (Q_{11} + Q_{22} - 2Q_{12} - 2Q_{66})c^2s^2 + Q_6(c^4 + s^4) \quad (3.20)$$

Above is the lamina theory, which gives the global and nominal stress-strain relationship of a fiber-reinforced composite lamina with known micromechanical properties. Plain woven fabric composites are assumed to be cross-ply, and composite plates in many applications consist of two or more lamina layers. It is called laminates.

- Modeling of load and moment relation with matrices [A], [B], and [D] for multilayer composites

If the beam is under the bending moment and axial load as shown in Figure 3.10, strain is written as (Gibson, 2011; Kaw, 2005),

$$\varepsilon_{xx} = \varepsilon_0 + z\kappa \quad (3.21)$$

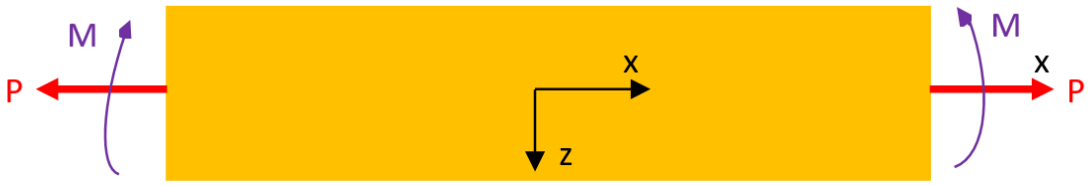



Figure 3.10. The beam is under a bending moment, and the axial load

Equation 3.21 is also valid for laminated beams, so its strains can be expressed as,

$$\begin{Bmatrix} \varepsilon_x \\ \varepsilon_y \\ \gamma_{xy} \end{Bmatrix} = \begin{Bmatrix} \varepsilon_x^0 \\ \varepsilon_y^0 \\ \gamma_{xy}^0 \end{Bmatrix} + z \begin{Bmatrix} \kappa_x \\ \kappa_y \\ \kappa_{xy} \end{Bmatrix} \quad (3.22)$$

Equation 2.19 is rewritten for a known thickness (z) of the lamina according to Equation 3.22. Thus, the equation giving the stress-strain relationship of the lamina is

$$\begin{bmatrix}\sigma_x\\ \sigma_y\\ \tau_{xy}\end{bmatrix}=\begin{bmatrix}\bar{Q}_{11} & \bar{Q}_{12} & \bar{Q}_{16}\\ \bar{Q}_{21} & \bar{Q}_{22} & \bar{Q}_{26}\\ \bar{Q}_{61} & \bar{Q}_{62} & \bar{Q}_{66}\end{bmatrix}\begin{Bmatrix}\varepsilon_x^0\\ \varepsilon_y^0\\ \gamma_{xy}^0\end{Bmatrix}+z\begin{bmatrix}\bar{Q}_{11} & \bar{Q}_{12} & \bar{Q}_{16}\\ \bar{Q}_{21} & \bar{Q}_{22} & \bar{Q}_{26}\\ \bar{Q}_{61} & \bar{Q}_{62} & \bar{Q}_{66}\end{bmatrix}\begin{Bmatrix}\kappa_x\\ \kappa_y\\ \kappa_{xy}\end{Bmatrix} \tag{3.23}$$

Stresses vary linearly in a given lamina depending on its thickness, but the stiffness terms of the lamina can vary from one lamina to another depending on its orientation and material. Therefore, the moments and forces applied to a laminate through its thickness can be integrated to give resultant moments and forces. Furthermore, it will allow us to identify the plate curvatures and midplane strain. The curvature and strains of the midplane are related to the applied loads and moments (Kaw, 2005). These are given below where $N_x, N_y,$ and $N_{xy}$ are x, y direction loads and shear load, respectively; and $M_x, M_y,$ and $M_{xy}$ are x, y direction moments and twisting moment.

$$N_x=\int_{-h/2}^{h/2}\sigma_x dz,\quad N_y=\int_{-h/2}^{h/2}\sigma_y dz,\quad N_{xy}=\int_{-h/2}^{h/2}\tau_{xy}dz, \tag{3.24}$$

$$M_x=\int_{-h/2}^{h/2}\sigma_x z dz,\quad M_y=\int_{-h/2}^{h/2}\sigma_y z dz,\quad M_{xy}=\int_{-h/2}^{h/2}\tau_{xy}z dz \tag{3.25}$$

Equations 3.24 and 3.25 are written in matrix form for a laminate as,

$$\begin{bmatrix}N_x\\ N_y\\ N_{xy}\end{bmatrix}=\sum_{k=1}^{n}\int_{h_k-1}^{h_k}\begin{bmatrix}\sigma_x\\ \sigma_y\\ \tau_{xy}\end{bmatrix}_k dz,\quad \begin{bmatrix}M_x\\ M_y\\ M_{xy}\end{bmatrix}=\sum_{k=1}^{n}\int_{h_k-1}^{h_k}\begin{bmatrix}\sigma_x\\ \sigma_y\\ \tau_{xy}\end{bmatrix}_k z dz, \tag{3.26}$$

Equation 3.23 is written in equation 3.26,

$$\begin{bmatrix}N_x\\ N_y\\ N_{xy}\end{bmatrix}=\left\{\sum_{k=1}^{n}\begin{bmatrix}\bar{Q}_{11} & \bar{Q}_{12} & \bar{Q}_{16}\\ \bar{Q}_{21} & \bar{Q}_{22} & \bar{Q}_{26}\\ \bar{Q}_{61} & \bar{Q}_{62} & \bar{Q}_{66}\end{bmatrix}\int_{h_k-1}^{h_k}dz\right\}\begin{bmatrix}\varepsilon_x^0\\ \varepsilon_y^0\\ \gamma_{xy}^0\end{bmatrix}+$$
$$\left\{\sum_{k=1}^{n}\begin{bmatrix}\bar{Q}_{11} & \bar{Q}_{12} & \bar{Q}_{16}\\ \bar{Q}_{21} & \bar{Q}_{22} & \bar{Q}_{26}\\ \bar{Q}_{61} & \bar{Q}_{62} & \bar{Q}_{66}\end{bmatrix}\int_{h_k-1}^{h_k}z dz\right\}\begin{bmatrix}\kappa_x\\ \kappa_y\\ \kappa_{xy}\end{bmatrix},$$

$$\begin{bmatrix}M_x\\ M_y\\ M_{xy}\end{bmatrix}=\left\{\sum_{k=1}^{n}\begin{bmatrix}\bar{Q}_{11} & \bar{Q}_{12} & \bar{Q}_{16}\\ \bar{Q}_{21} & \bar{Q}_{22} & \bar{Q}_{26}\\ \bar{Q}_{61} & \bar{Q}_{62} & \bar{Q}_{66}\end{bmatrix}\int_{h_k-1}^{h_k}z dz\right\}\begin{bmatrix}\varepsilon_x^0\\ \varepsilon_y^0\\ \gamma_{xy}^0\end{bmatrix}+$$
$$\left\{\sum_{k=1}^{n}\begin{bmatrix}\bar{Q}_{11} & \bar{Q}_{12} & \bar{Q}_{16}\\ \bar{Q}_{21} & \bar{Q}_{22} & \bar{Q}_{26}\\ \bar{Q}_{61} & \bar{Q}_{62} & \bar{Q}_{66}\end{bmatrix}\int_{h_k-1}^{h_k}z^2 dz\right\}\begin{bmatrix}\kappa_x\\ \kappa_y\\ \kappa_{xy}\end{bmatrix} \tag{3.27}$$

in matrix form,

$$\begin{bmatrix} N \\ M \end{bmatrix} = \begin{bmatrix} A & B \\ B & D \end{bmatrix} \begin{bmatrix} \varepsilon \\ k \end{bmatrix},$$

$$\begin{bmatrix} N_x \\ N_y \\ N_{xy} \\ M_x \\ M_y \\ M_{xy} \end{bmatrix} = \begin{bmatrix} A_{11} & A_{12} & A_{16} & B_{11} & B_{12} & B_{16} \\ A_{21} & A_{22} & A_{26} & B_{21} & B_{22} & B_{26} \\ A_{61} & A_{62} & A_{66} & B_{61} & B_{62} & B_{66} \\ B_{11} & B_{12} & B_{16} & D_{11} & D_{12} & D_{16} \\ B_{21} & B_{22} & B_{26} & D_{21} & D_{22} & D_{26} \\ B_{61} & B_{62} & B_{66} & D_{61} & D_{62} & D_{66} \end{bmatrix} \begin{bmatrix} \varepsilon_x \\ \varepsilon_y \\ \varepsilon_{xy} \\ k_x \\ k_y \\ k_{xy} \end{bmatrix} \quad (3.28)$$

The three matrices used in calculating stiffness and extensional properties are known as extensional [A], coupling [B], and bending stiffness [D] in equation 3.28. These matrices are defined as,

$$A_{ij} = \sum_{k=1}^{n} \left(\bar{Q}_{ij}\right)_k (h_k - h_{k-1}), \quad i = 1,2,6;\ j = 1,2,6,$$
$$B_{ij} = \frac{1}{2} \sum_{k=1}^{n} \left(\bar{Q}_{ij}\right)_k (h_k^2 - h_{k-1}^2), \quad i = 1,2,6;\ j = 1,2,6,$$
$$D_{ij} = \frac{1}{3} \sum_{k=1}^{n} \left(\bar{Q}_{ij}\right)_k (h_k^3 - h_{k-1}^3), \quad i = 1,2,6;\ j = 1,2,6, \quad (3.29)$$

By determining the [A], [B], and [D] matrices, the force and strain relationship of multilayer fiber-reinforced composite plates is determined. *k* refers to the lamina in the laminate, and *h* refers to the distance of the lamina interfaces to the neutral axis.

All the above calculation processes in the present work have been performed using a local software based on CLT as designed by Yildirim and Tutuncu (2014). This program is called KomPro. The KomPro is a user-friendly software for solving static problems in the design and evaluation of composite plates.

*Modeling of plain woven fabric composite face layer under axial loading*

If the laminate is only subjected to tensile load ($N_x$), the other forces ( $N_y, N_{xy}$) are zero. But, shear strain ($\gamma_{xy}$), axial strain ($\varepsilon_x$), and transverse strain might occur in the laminate. Therefore, in order to get the relationship between $\varepsilon_x$ and $N_x$, the matrix in Equation 3.28 has been transformed into a new form for symmetrical laminate,

$$\begin{bmatrix} \varepsilon_x \\ \varepsilon_y \\ \gamma_{xy} \end{bmatrix} = \begin{bmatrix} \alpha_{11} & \alpha_{12} & \alpha_{16} \\ \alpha_{21} & \alpha_{22} & \alpha_{26} \\ \alpha_{61} & \alpha_{62} & \alpha_{66} \end{bmatrix} \begin{bmatrix} N_x \\ 0 \\ 0 \end{bmatrix} \quad (3.30)$$

where $[\alpha_{ij}]$ is the inverse of the $[A_{ij}]$. The axial strain is expressed as, $\varepsilon_x = \alpha_{11} N_x$

$N_x$ and $\varepsilon_x$ are explicitly written as $N_x=P/b$ and $\varepsilon_x=\delta/L$, respectively, and the force ($P$) displacement ($\delta$) equation 3.30 can be transformed as follows (Uzay et al., 2023)

$$\delta = \alpha_{11} \frac{PL}{b} \tag{3.31}$$

The average axial elastic modulus ($E_{av}$) of laminated composites is shown in the following:

Stress due to axial loading

$$\sigma_{max} = \frac{F}{A} \tag{3.32}$$

Composite laminate axial stress equation,

$$(\sigma_{av})_x = E_{av}\varepsilon^0 = \frac{N_x}{h} \tag{3.33}$$

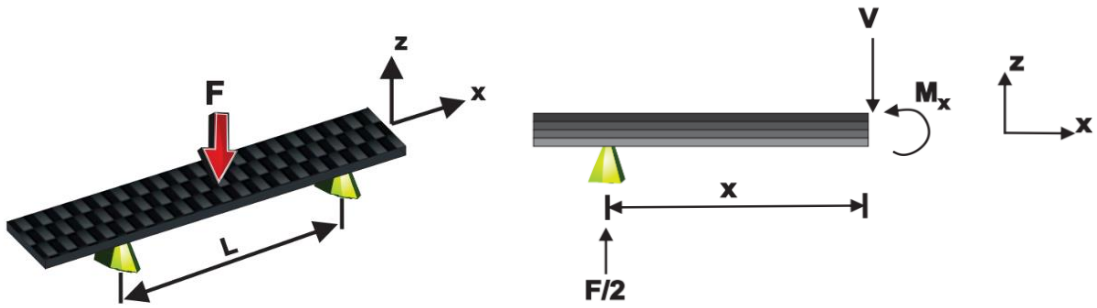
Where,

$$E_{av} = \frac{N_x}{h}\frac{1}{\varepsilon^0} = \frac{N_x}{h}\frac{1}{N_x\alpha_{11}} \tag{3.34}$$

$$E_{av} = \frac{1}{h\alpha_{11}} \tag{3.35}$$

*Modeling of plain woven fabric composite face layer under flexural loading*

A simply supported beam from a laminate plate is created under the midpoint loading in Figure 3.11a. Shear forces (V) and the bending moment ($M_x$) are shown in Figure 3.11b for the beam.




(a) (b)

Figure 3.11. (a) Beam configuration under three-point bending loading (b) beam internal loads (Çetin et al., 2023)

The general set of equations formulating the relationship between the laminates loading and strain and curvature is given in Equation 3.28. According to the loading condition in Figure 3.11, the equation can be written as follows.

$$\begin{bmatrix} M_x \\ 0 \\ 0 \end{bmatrix} = \begin{bmatrix} B_{11} & B_{12} & B_{16} \\ B_{12} & B_{22} & B_{26} \\ B_{16} & B_{26} & B_{66} \end{bmatrix} \begin{bmatrix} \varepsilon_x^0 \\ \varepsilon_y^0 \\ \gamma_{xy}^0 \end{bmatrix} + \begin{bmatrix} D_{11} & D_{12} & D_{16} \\ D_{12} & D_{22} & D_{26} \\ D_{16} & D_{26} & D_{66} \end{bmatrix} \begin{bmatrix} k_x \\ k_y \\ k_{xy} \end{bmatrix} \tag{3.36}$$

The compliance matrix ($\begin{bmatrix} \alpha & \beta \\ \beta^- & \delta \end{bmatrix}$), as the inverse of the stiffness matrix $\left(\begin{bmatrix} A & B \\ B & D \end{bmatrix}\right)$, is used due to $k_y$, and $k_{xz}$ not equal to zero. Equation 3.36 is transformed into the following as,

$$\begin{bmatrix} k_x \\ k_y \\ k_{xy} \end{bmatrix} = \begin{bmatrix} \beta_{11}^- & \beta_{12}^- & \beta_{16}^- \\ \beta_{12}^- & \beta_{22}^- & \beta_{26}^- \\ \beta_{16}^- & \beta_{26}^- & \beta_{66}^- \end{bmatrix} \begin{bmatrix} 0 \\ 0 \\ 0 \end{bmatrix} + \begin{bmatrix} \delta_{11} & \delta_{12} & \delta_{16} \\ \delta_{12} & \delta_{22} & \delta_{26} \\ \delta_{16} & \delta_{26} & \delta_{66} \end{bmatrix} \begin{bmatrix} M_x \\ 0 \\ 0 \end{bmatrix} \tag{3.37}$$

Establishing the relations $k_x = w^{II}$ and $M_x = Fx/2b$ (b : width of the beam) the deflection may be determined. The followings are the solution steps (Çetin et al., 2023),

$$w^{II} = k_x = \delta_{11} \frac{Fx}{2b} \tag{3.38}$$

$$w^{I} = \delta_{11} \frac{Fx^2}{4b} + C1 \tag{3.39}$$

$$w = \delta_{11} \frac{Fx^3}{12b} + C1x + C2 \tag{3.40}$$

The boundary conditions are $w_{(0)} = 0,\ w^I_{(L/2)} = 0$, the solution is,

$$w = \delta_{11} \frac{Fx^3}{12b} - \delta_{11} \frac{FL^2}{16b} x \tag{3.41}$$

The maximum deflection is obtained at the midpoint $x = (L/2)$ as,

$$w_{max} = \delta_{11} \frac{FL^3}{48b} \tag{3.42}$$

Average bending elastic modulus ($E_{av}$) of the laminated composites is now to be determined. Maximum stress for pure bending is,

$$\sigma_{max} = \frac{Mc}{I} \tag{3.43}$$

Bending maximum stress of composite laminate,

$$(\sigma_{av})_x = E_{av} z k_x \tag{3.44}$$

Assuming $\sigma_{max} = (\sigma_{av})_x$ , z=c,

$$\frac{Mc}{I} = E_{av} z k_x, \qquad \frac{M}{I} = E_{av} k_x, \tag{3.45}$$

The laminate beam has a rectangular cross-sectional area,

$$\frac{M}{\left(\frac{bh^3}{12}\right)} = E_{av} k_x \, , \qquad \frac{M}{b} = M_x \tag{3.46}$$

Where,

$$\frac{12M_x}{h^3 k_x} = E_{av} \, , \quad k_x = M_x \delta_{11} \tag{3.47}$$

And so, $E_{av}$ is obtained,

$$E_{av} = \frac{12}{h^3 \delta_{11}} \tag{3.48}$$

Finally, the stress for each lamina can be defined as,

$$(\sigma_{max})_l = (Q_{11})_l \, z \, k_{max} \tag{3.49}$$

*Plain woven fabric composite face layer failure analysis with Tsai Wu Criterion*

The material failure criterion, known as the Tsai-Wu failure theory, analyzes anisotropic composites with varying compression and tension strengths (Tsai and Wu, 1971). Details of the theory are given in the following,

The failure criterion is

$$F_1\sigma_1 + F_2\sigma_2 + F_{11}\sigma_1^2 + F_{22}\sigma_2^2 + F_{66}\tau_{12}^2 + 2F_{12}\sigma_1\sigma_2 = 1 \quad (3.50a)$$

where

$$F_1 = \frac{1}{X_1} - \frac{1}{X_2},\ F_2 = \frac{1}{Y_1} - \frac{1}{Y_2},\ F_{11} = \frac{1}{X_1X_2},\ \ F_{22} = \frac{1}{Y_1Y_2},$$

$$F_{66} = \frac{1}{S_{12}}, \qquad F_{12} = \frac{1}{2}\sqrt{F_{11}F_{22}} \quad (3.50b)$$

Equation 3.50a is rewritten with the reserve factor R as (Tutuncu, 1995).

$$(F_{11}\sigma_1^2 + 2F_{12}\sigma_1\sigma_2 + F_{22}\sigma_2^2 + F_{66}\tau_{12}^2)R^2 + (F_1\sigma_1 + F_2\sigma_2)R - 1 = 0 \quad (3.51)$$

Letting,

$$(F_{11}\sigma_1^2 + 2F_{12}\sigma_1\sigma_2 + F_{22}\sigma_2^2 + F_{66}\tau_{12}^2) = a,\ (F_1\sigma_1 + F_2\sigma_2) = b,\ 1\text{=c} \quad (3.52)$$

The following equation is obtained:

$$aR^2 + bR - c = 0 \quad (3.53)$$

The roots are

$$R_1 = \frac{-b+\sqrt{b^2+4ac}}{2a}, \quad R_2 = \frac{-b-\sqrt{b^2+4ac}}{2a} \quad (3.54)$$

One is positive $(R_1)$, while the other is negative $(R_2)$. The positive value of R will be used. It should be greater than one to ensure the safety of lamina or laminate. The negative value corresponds to the the reserve factor with the applied loads are reversed in direction.

The present study's failure strengths of plain woven fabric composites are solved with Kompro.

### 3.2.2. Approaches used to obtain flexural properties of sandwiches

The flexural capability of the sandwich is directly related to its bending stiffness. The flexural stiffness of the sandwich structure is related to the mechanical properties of the face material, its thickness, and its distance from the neutral axis of the sandwich. The contribution of mechanical properties of core materials such as low-density foam to the bending stiffness is negligible and, therefore, neglected. For example, Equation 2.11 in Chapter 2 shows that the modulus of elasticity of the core is neglected in the calculation of bending stiffness. When determining the bending stiffness, the modulus of elasticity of the face material is needed. In the previous studies, the composite face materials were subjected to experiments to determine their elastic modulus. However, the first part of this chapter details how analytical methods are used to obtain the mechanical properties of composite plates. Also, a practical engineering approach is developed to determine the mechanical properties of plain woven fabric composite plates quickly. This part will explain how the analytical values of the composite obtained from composite mechanics are adapted to the sandwich plate to obtain the bending stiffness.

*Constitution of $[A]^l$, $[B]^l$, and $[D]^l$ matrices for the sandwich beam with parallel axis theorems*

Figure 3.12a shows a front-sectional view of a sandwich plate. The face material of the plate in the figure is considered a fiber-reinforced composite. The mechanical properties of this material are determined according to the set of equations given in equation 3.29 and are assumed to be [A], [B], [D]. The parameter “d” represents the distance of the face material from the neutral axis of the sandwich plate.

The extensional, coupling, and bending stiffness matrices given in Equation 3.29 are rewritten according to the sandwich neutral axis (Figure 3.12b) as,

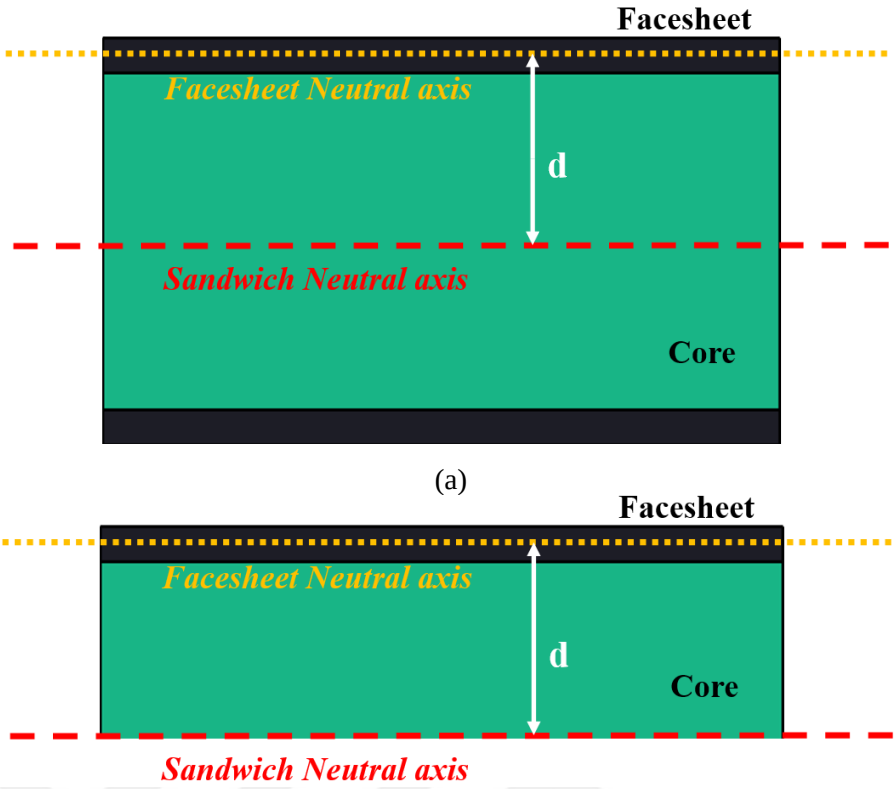



Figure 3.12. a) Front sectional and b) half front sectional view of the sandwich plate

$$[A]' = \sum_{k=1}^{n} (\bar{Q})_k \left((h_k + d) - (h_{k-1} + d)\right),$$

$$[B]' = \frac{1}{2}\sum_{k=1}^{n} (\bar{Q})_k \left((h_k + d)^2 - (h_{k-1} + d)^2\right),$$

$$[D]' = \tfrac{1}{3}\textstyle\sum_{k=1}^{n} (\bar{Q})_k \left((h_k + d)^3 - (h_{k-1} + d)^3\right), \qquad (3.55)$$

Expanded as,

$$[A]' = \sum_{k=1}^{n} (\bar{Q})_k \left(h_k - h_{k-1}\right),$$

$$[B]' = \frac{1}{2}\sum_{k=1}^{n} (\bar{Q})_k \left(h_k^2 + 2d(h_k - h_{k-1}) - h_{k-1}^2\right),$$

$$[D]' = \tfrac{1}{3}\textstyle\sum_{k=1}^{n} (\bar{Q})_k \left(h_k^3 - h_{k-1}^3 + 3d\left(h_k^2 - h_{k-1}^2\right) + 3d^2(h_k - h_{k-1})\right) \qquad (3.56)$$

If equation 3.56 is simplified, it can be rewritten in terms of [A], [B], and [D] as

$$[A]' = \sum_{k=1}^{n} (\bar{Q})_k \, (h_k - h_{k-1}) = [A],$$

$$[B]' = \frac{1}{2}\sum_{k=1}^{n} (\bar{Q})_k \left(h_k^2 - h_{k-1}^2\right) + 2d\frac{1}{2}\sum_{k=1}^{n} (\bar{Q})_k \, (h_k - h_{k-1}) = \ [B] + d[A],$$

$$[D]' = \tfrac{1}{3}\textstyle\sum_{k=1}^{n}(\bar{Q})_k \left(h_k^3 - h_{k-1}^3\right) + 2d\,\tfrac{1}{2}\sum_{k=1}^{n}(\bar{Q})_k \left(\, h_k^2 - h_{k-1}^2\right) + d^2 \sum_{k=1}^{n}(\bar{Q})_k \, (h_k - h_{k-1}) = [D] + 2[B] + d^2[A] \quad (3.57)$$

The stiffness properties of a symmetric sandwich with the same upper and bottom face material properties are obtained as follows (for symmetric laminate $[B] = 0$),

$$[A]^s = 2[A]', \ for \ [A]' = [A]^u = [A]^b,$$

$$[B]^s = 0, [B]^u = [B] + d[A], \ [B]^b = [B] + (-d)[A], \ [B] = 0,$$

$$[D]^s = 2[D]' = 2([D] + d^2[A]) \, , for \ [D]' = [D]^u = [D]^b \text{ and } [B] = 0, \quad (3.58)$$

$[A]^s, [B]^s$ and $[D]^s$ are defined as extensional, coupling, and bending stiffness matrices of sandwich, respectively. If a sandwich is loaded as in Figure 3.13 and the fiber directions are assumed to be in the x-axis direction (x= on-axis), the bending stiffness property of the sandwich structure is obtained as follows.

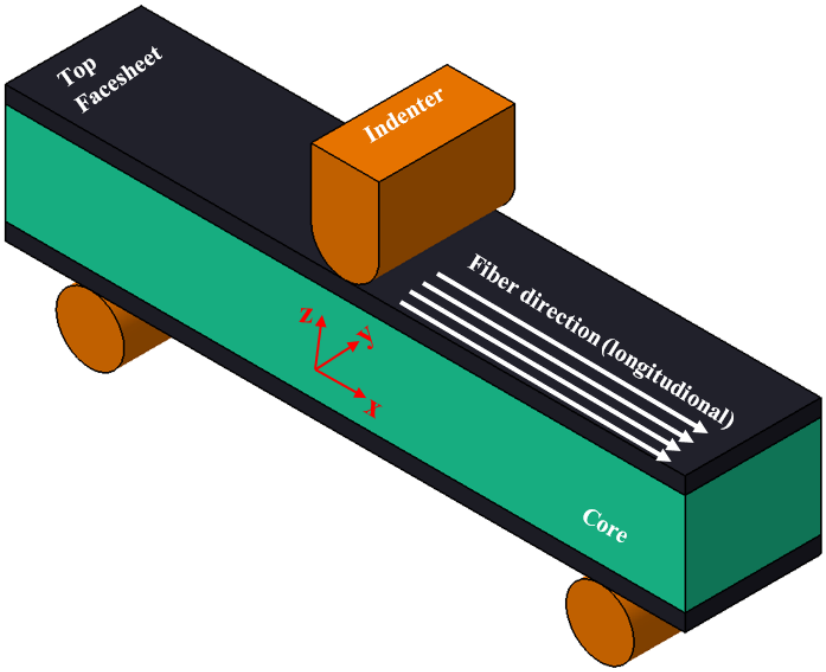



Figure 3.13. Schematical presentation of the sandwich beam under a three-point bending load

$$[D]^s = \begin{bmatrix} D_{11}^s & D_{12}^s & D_{16}^s \\ D_{21}^s & D_{22}^s & D_{26}^s \\ D_{61}^s & D_{62}^s & D_{66}^s \end{bmatrix} \tag{3.59}$$

$D_{11}^s$ is longitudinal direction bending stiffness term of sandwich,

$$D_{11}^s = 2D_{11}^{s\prime} = 2(D_{11} + d^2 A_{11}) \tag{3.60}$$

Thus, the bending stiffness property can be determined by Equation 3.60 for sandwich plates with fiber directions in the x-axis and loading in the z-axis direction, as in Figure 3.14. $D_{11}$ and $A_{11}$ are the terms for the bending and extensional stiffness of the facesheet in the longitudinal direction. These terms are calculated with the classical laminate theory. If the sandwich is made of plain woven fabric composite, they are calculated using the practical engineering approach developed in this study.

*Modifying Timoshenko beam theory with bending stiffness matrix of sandwich* $[D]^s$

A composite sandwich beam's deformation can be categorized into two parts depending on its radius of curvature and the strain in its constituent materials. The first type is deformation caused by bending, while transverse forces cause the shear. (Figure 3.14).

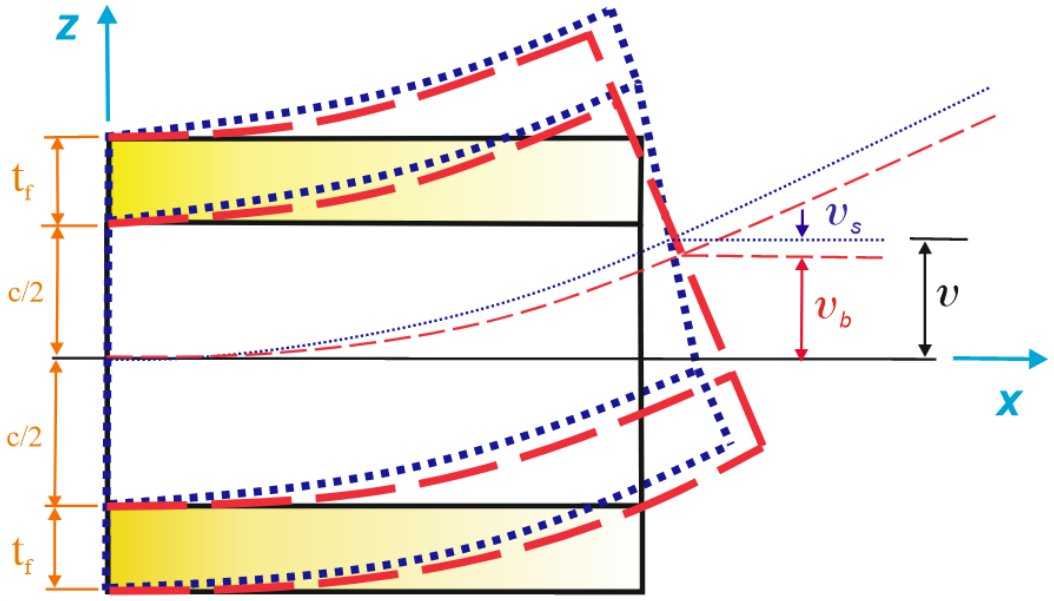



Figure 3.14. The deflection of a sandwich beam is computed by taking into account both the shear component $v_s$ and the bending component $v_b$.

The total deflection of a sandwich beam is computed by considering the various factors that affect its bending. The sum of the deflections is shown in Equation 3.62, which was derived from Equation 1.1 for simply-supported bending load (Allen and Neal, 2013; Timoshenko, 1941).

$$v = v_b + v_s = \frac{PL^3}{48EI} + \frac{\alpha_S PL}{4AG} \tag{3.61}$$

$\alpha_S$ is called the shear coefficient and assumed for sandwich beams equal to one (Timoshenko, 1941). Thus, equation 2.9 in chapter two, presented by Allen, is obtained. Recalling this equation again,

$$v = v_b + v_s = \frac{PL^3}{48EI} + \frac{PL}{4AG} \tag{3.62}$$

$EI$ is defined as the bending stiffness of the sandwich beams, which is usually determined in Equation 2.11. The equation depends on the composite materials' elastic modulus obtained experimentally. However, in Equation 2.58, the bending stiffness term per unit width of a sandwich plate with a fiber-reinforced composite can be calculated. If the width $b$ of a non-homogenous beam with a rectangular cross-section is assumed, the equivalent form can be written as (Vinson and Sierakowski, 2008),

$$EI = bD_{11} \tag{3.63}$$

Equation 3.63 can be easily explained with the deflection equation of a beam under a simply supported distributed load. Two different deflection equations can be written for this beam. In the

first approach, the beam is considered as symmetric orthotropic. The deflection equation for such a beam with width b obtained by CLT can be written as (Vinson and Sierakowski, 2008),

$$bD_{11}\frac{d^4u}{dx^4} = q \tag{3.64}$$

The deflection equation derived by the Classical Beam Theory for an isotropic homogeneous beam is (Rapp, 1992).

$$EI\frac{d^4u}{dx^4} = q \tag{3.65}$$

Comparing Equations 3.64 and 3.65, Equation 3.63 is checked for the rectangular cross-sectional area as,

$$bD_{11} = \frac{bh^3}{12}E = EI \tag{3.66}$$

For a sandwich,

$$EI = \ bD_{11}^{s} = 2bD_{11}^{s\ \prime} = 2b(D_{11} + d^2A_{11}) \tag{3.67}$$

If we rewrite equation 3.60 with $bD_{11}^{s}$, the following deflection equation is obtained,

$$v = v_b + v_s = \frac{PL^3}{48bD_{11}^{s}} + \frac{PL}{4AG} \tag{3.68}$$

With Equation 3.68, the bending behavior of any sandwich beam with composite under a simple bending load can be determined without experimental properties of face materials. Furthermore, this derived equation supports the developed equation in the work done by (Dariushi, and Sadighi, 2013) for FML face (Equation 2.14). However, this equation describes the force-displacement relationship in the linear region. In order to reveal the fundamental flexural characteristics of a sandwich beam, we need the linear limit force and fracture methods and forces, which will be studied in the next section.

*Modification of core yield load model for sandwich beams*

In the design of sandwich beams, strength is essential, as well as stiffness. Therefore, the core yield force ($P_1$) is the elastic limit of the sandwich beam and should be estimated. $P_1$ is determined with Equations 2.21-2.23 (Shuaeib and Soden, 1997). Equation 2.21-2.23 can be modified if the following explanation is followed. For the loading case of the sandwich, presented in Figure 3.15, the relationship between the moment and longitudinal curvature of facesheets is

established with the longitudinal bending stiffness ($D_{11}$) for symmetrical plates. Thin-walled bars could be easily handled by combining CLT and engineering bending theory (Rapp, 1992).

Accordingly, the following equations are obtained when equation 3.63 is adapted for the facesheet:

$$\alpha = \left(\frac{k}{4D_{11}b_f}\right)^{1/4} \tag{3.69}$$

$k$ is the element foundation of the foam given by equation 2. 21, and $\alpha$ now becomes,

$$\alpha = \left(\frac{E_c b}{4cD_{11}b_f}\right)^{1/4} \tag{3.70}$$

Noting that sandwich beam width ($b$) and facesheet width ($b_f$) are the same. If the $\alpha$ is rewritten in Equation 2.21, the final equation, giving $P_1$, is as follows:

$$P_1 = 2\sigma_c b_f \left(\frac{4cD_{11}}{E_c}\right)^{\frac{1}{4}} \tag{3.71}$$

Thus, the elastic limit of a sandwich produced from a composite face sheet, which has the term flexural stiffness ($D_{11}$), can comfortably be determined under simple bending loading.

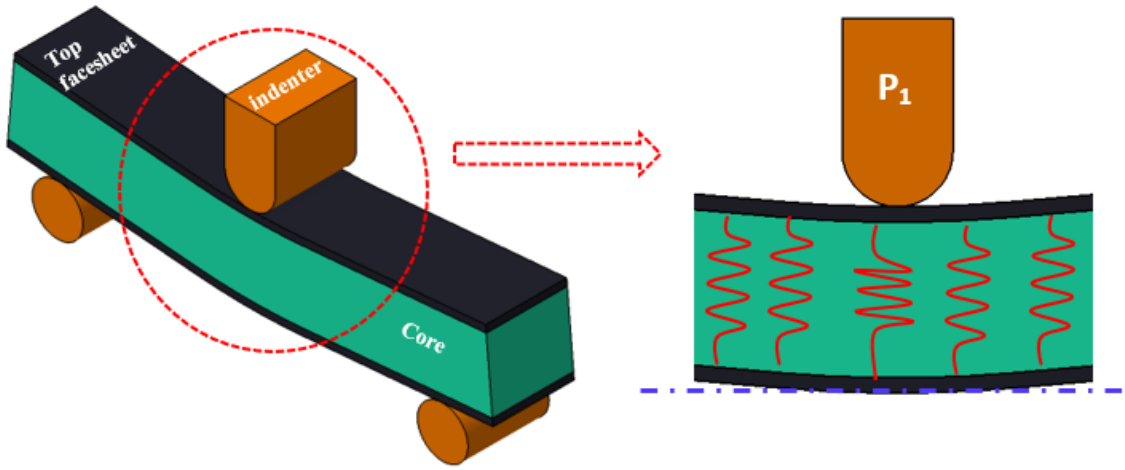



Figure 3.15. Core yield condition in the sandwich beam under three-point bending load

*Failure load determination methods for sandwich beam*

Although sandwich beams have high flexural stiffness (Zhang et al., 2019) and are lightweight (Funari et al., 2021), they have failure problems such as indentation, core shear, face

yield, and wrinkling (Zhang et al., 2020a). The strength performance of low-density core materials is considerably lower than that of high-strength face materials. Therefore, the face yield failure mode is not encountered in sandwich structures of low-density core and high-strength face materials. In this thesis, face yield and wrinkling failure modes were not analyzed in detail since low-density foam core material and high-strength composite were used to construct the sandwiches. However, the following sections thoroughly analyze core shear and indentation failure modes.

- Core shear failure methods

Figure 3.16 shows a core shear failure in sandwich beams subjected to three-point bending. The core is mainly used for carrying the applied shear load. When beams are subjected to three-point bending, the main component of the structure is subjected to excessive shear stress ($\tau_c$). Failure occurs when the stress level reaches its critical value (Gdoutos and Daniel, 2010). Studies that predicted core collapse analytically assumed that the core would collapse at a uniform shear strength (Sandifer, 1969; Vocke, 1967). Core shear failure is calculated by Equation 2.18.

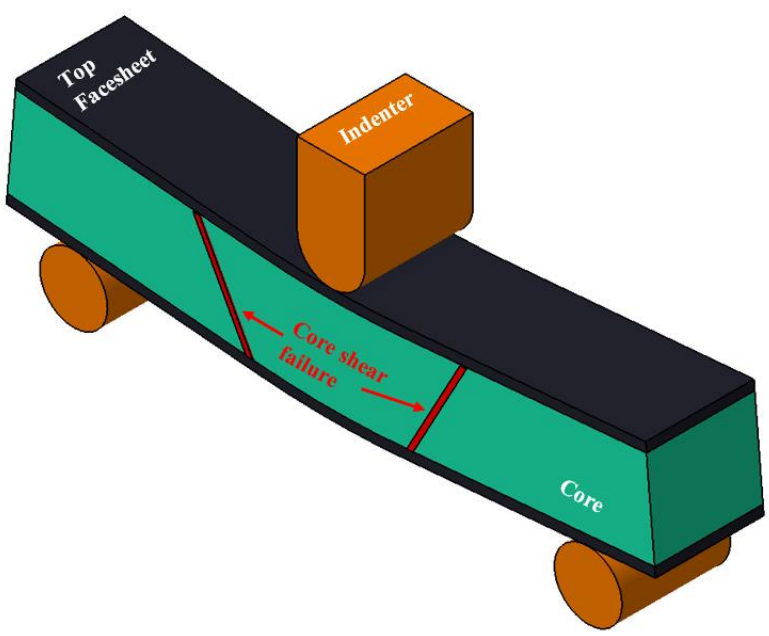



Figure 3.16. Core shear failure in the sandwich beam under a three-point bending load

- Modification of indentation failure methods

Steeves and Fleck (2004a) developed an indentation model for elastic facesheets and rigid ideally-plastic core according to the local bending occurring in the indentation zone (u) length (Figure 3.17). Equation 2.24 in the model gives the maximum indentation failure load ($P_2$) resulting from the solution of the governing equation (Steeves and Fleck, 2004a). If Equation 3.63 (Vinson and Sierakowski, 2008) is adapted for Equation 2.24, as Equation 3.74, the indentation failure loads can be predicted without requiring the experimental data for the FRP composite.

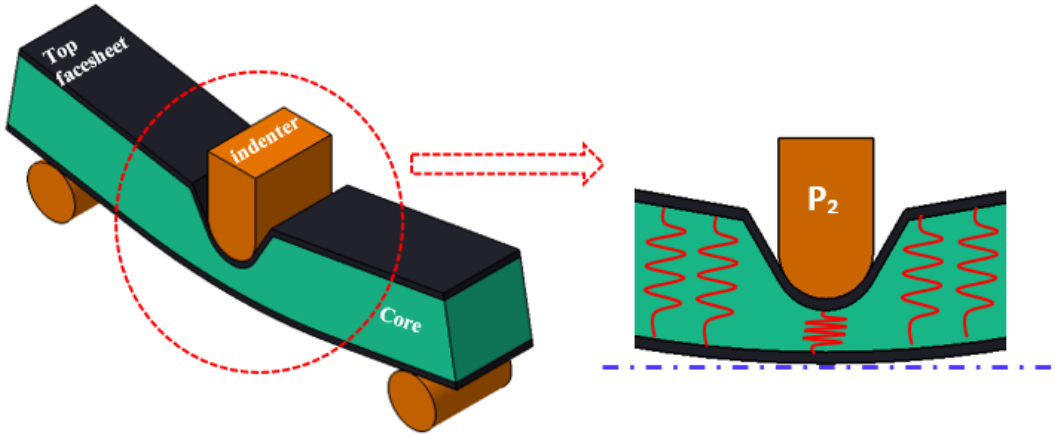



Figure 3.17. Indentation failure in the sandwich beam under a three-point bending load

The modification of Equation 2.24 is presented as follows,

$$P_2 = \left(\frac{4t_f^3 b_f^3 \pi^2 d E_f \sigma_c^2}{12L}\right)^{1/3} \tag{3.72}$$

Noting that the moment of inertia of the facesheet with a rectangular cross-sectional area is $I = b_f t_f^3/12$, then $P_2$ becomes

$$P_2 = \left(\frac{4b_f^2 \pi^2 d E_f I_f \sigma_c^2}{L}\right)^{1/3} \tag{3.73}$$

$D_{11} b_f$ is substituted for $E_f I_f$, then $P_2$ is

$$P_2 = \left(\frac{4b_f^2 \pi^2 d D_{11} b_f \sigma_c^2}{L}\right)^{1/3} = b_f \left(\frac{4\pi^2 d D_{11} \sigma_c^2}{L}\right)^{1/3} \tag{3.74}$$

### 3.3. Experimental studies to verify the developed engineering approaches

A novel engineering approach is developed to analytically determine the flexural behavior of sandwich beams made of plain woven fabric composite face sheets and low-density foam core under three-point bending loads. This chapter conducts tensile and bending experimental studies to validate the developed practical engineering approach. Also, experimental studies are carried out for different parameters such as foam density, sandwich thickness, face layer, and span length. The foams, fabric, and epoxy were obtained from suppliers as raw materials. Composite laminates and sandwich plates were manufactured at the Çukurova University Mechanical Engineering Department Composites Laboratory. The plates were prepared by cutting the test specimen dimensions with a table saw. All mechanical tests were carried out with Instron 8801 universal testing machine with 100 kN (%±0,002) load capacity.

### 3.3.1. Fabrication of plain woven fabric composite plates using various methods

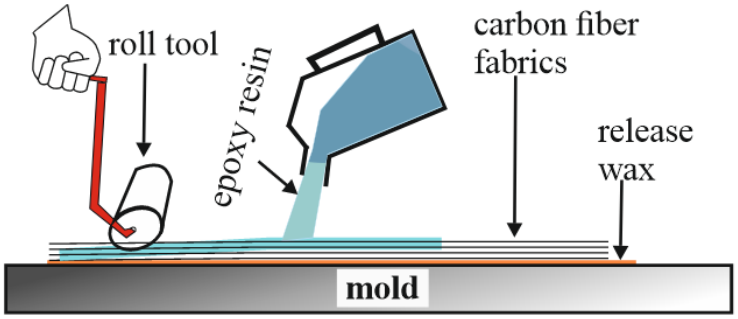
The proposed practical engineering approach is verified by producing standard test specimens and conducting tensile and bending tests. Five different manufacturing methods are utilized to obtain different types of composite samples with different volume fractions. These manufacturing methods are;

- Hand lay-up method (MT1),
- Vacuum bagging method with a low-capacity vacuum pump (MT2),
- Vacuum-assisted resin infusion method (MT3),
- Compression molding method (MT4).
- Vacuum bagging method with a high-capacity vacuum pump (MT5).

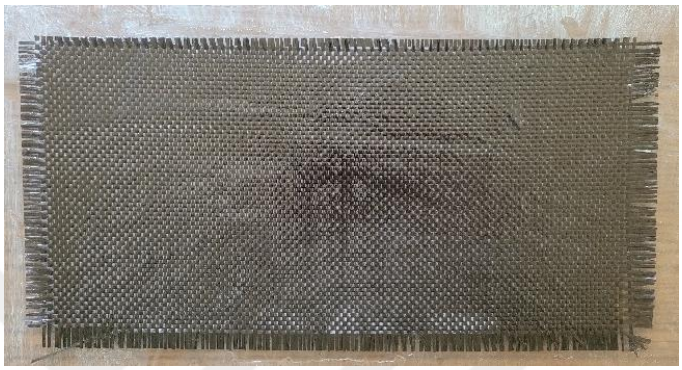
While MT1, MT2, MT3, and MT5 manufacturing techniques are applied with an open molding process, MT4 is applied with a closed molding process. All mold surfaces are chemically treated with a mold release. The cured laminates made with MT1 were subjected to ambient conditions, while those made with MT2, MT3, and MT5 were subjected to a vacuum environment (Çetin et al., 2023; Uzay et al., 2022b; Uzay et al., 2023). In the case of compression molding process, the fabrics are enclosed in two mold parts using screws. For all manufacturing techniques, the curing processes last for about 24 hours. All plates are produced as 4-layer carbon plain woven fabric. Detailed descriptions of production methods are given in the proceeding sections.

*Hand lay-up method*

Each fabric layer was manually resin-impregnated with a rolling tool called hand lay-up, shown in Figure 3.17. Then, as shown in Figure 3.18, a release agent vax is applied to a mold. Tempered glass with a thickness of 5 mm was used as a mold in the production. Polywax, a cream-like wax used to separate the components from the mold, was used as a release agent. First, a thin film is created by applying wax to the mold's surface using circular movements. This process is repeated three times until the desired thickness is achieved. After waxing, the first layer of fabric is placed in the mold, and some resin is poured. Then, the epoxy is spread on the fabric with a hand-sized sheet until the entire fabric absorbs it. Next, the second fabric is placed on top of the first, and the air gaps are removed with a roller. This process is repeated until all the layers are placed. After these processes, the plate is cured.




(a)

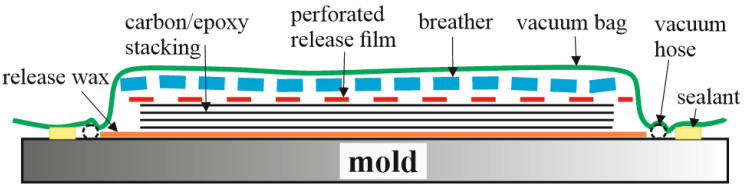


(b)

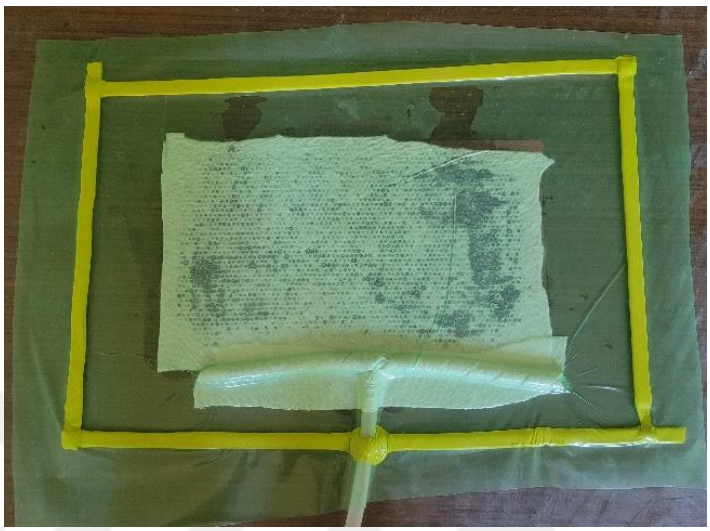
Figure 3.18. Hand Lay-up production method (a) schematic explanation (b) laboratory production photo

*Vacuum bagging method using a low-capacity vacuum pump*

In the vacuum bag method, waxing the mold and impregnating the fabrics with epoxy are the same processes as in the hand lay-up method. However, differences start after this process. First, a perforated release film is placed on the epoxy-impregnated fabrics. In this way, it removes the epoxy absorbed by the fiber fabrics under vacuum. Then, a breather layer with high epoxy absorbency capacity is placed on top. Thus, it absorbs and discards excess epoxy from the perforated release film. Then, the breather is surrounded by a spiral tube for vacuuming. Finally, the whole stack is sealed into the mold with the help of sealing tape in a vacuum bag. Then, the bag, which is disconnected from the external environment, is vacuumed with the help of a vacuum pump and cured. Figure 3.19a shows the schematics of the vacuuming method. Two vacuum pumps are used with different capacities to produce composite plates. The plates manufactured with the low vacuum pump is shown in Figure 3.19b. The specifications of this vacuum pump are given in Table 3.2.




(a)



(b)

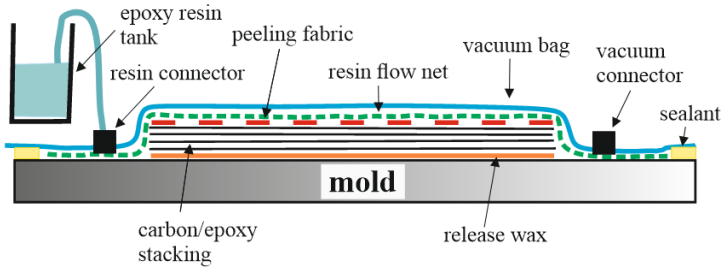
Figure 3.19. Vacuum bagging production method (a) schematic explanation (b) laboratory production photo

Table 3.2. Technical specifications data of low vacuum pump

| **Specifications** | **Values** | **Units** |
|---|---|---|
| Total final pressure | 0.2 | millibar |
| Nominal capacity speed | 5.95 | $m^3/h$ |
| Stage number | 1 | |
| Motor power | 0.248 | kW |
| Nominal RPM | 170 | n/min |
| Weight | 8 | kg |

*Vacuum-assisted resin infusion method*

Composite plate fabrication by vacuum-assisted resin infusion was carried out according to the schematic representation in Figure 3.20a. Four layers of dry carbon fabric were stacked on the glass mold prepared with poly wax. Peel-ply fabric and resin flow mesh were placed on the carbon fabrics. Spiral pipe and connector inlet were placed on the two end edges of the fabrics. One of the connectors provided a resin inlet, and the other was connected to the vacuum pump. The fabric pile was sealed with a vacuum bag with the help of sealing tape. First, the air was removed from the vacuum bag by vacuuming. Next, the resin inlet connector was opened, and the epoxy was sucked from the resin tank by vacuum to the epoxy dry fabric pile, Figure 3.20b. The resin flow valve was closed when the entire fabric pile was impregnated with epoxy. Finally, the plates were cured under a vacuum for 24 hours.




(a)

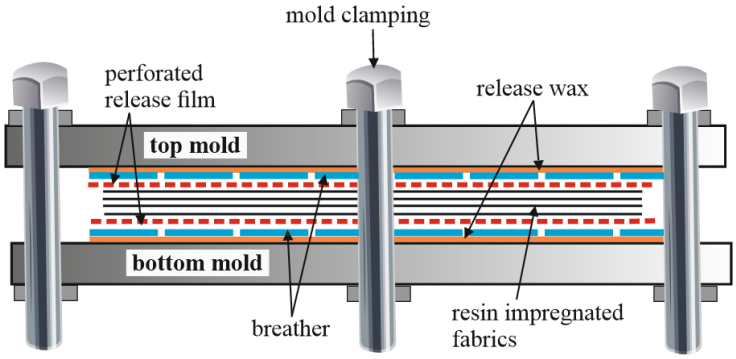


(b)

Figure 3.20. Vacuum-assisted resin infusion production method (a) schematic explanation (b) laboratory production photo

*Compression molding method*

Compression molding is another preferred production method, as shown in Figure 3.21. In this method, two 35X25 cm plexi glass molds with a thickness of 20 mm were used. Holes with a diameter of 14 mm were drilled around the perimeter of the molds for M12 screws. When starting production, a perforated release film is first placed on the bottom mold, and the fiber fabrics are impregnated with resin as in the hand lay-up method. Next, the upper layer is again covered with a perforated release film, and the upper mold is placed. The figure shows that the upper and lower molds are fixed between three steel L profiles. The profiles are tightened evenly with a torque wrench. The excess of epoxy absorbed by the fabric is thus expelled, and the curing process begins.




(a)



(b)

Figure 3.21. Compression molding production method (a) schematic explanation (b) laboratory production photo

*Vacuum bagging method using a high-capacity vacuum pump*

This production method is the same as the low-vacuum manufacturing process, but the vacuum pump that makes the vacuum during production is more powerful and can vacuum at a higher rate. The specific features of this vacuum pump (Figure 3.22) are given in Table 3.3. The fiber volume fraction of the composite plate produced will be better as more waste epoxy from the epoxy-impregnated fabric is removed. This will affect the mechanical properties of the produced plates.



Figure 3.22. The pump with high vacuuming power used in the thesis

Table 3.3. Technical specifications data of high vacuum pump

| **Specifications** | **Values** | **Units** |
|---|---|---|
| Nominal capacity speed | 8.5 | $m^3/h$ |
| Total final pressure | 0.01 | millibar |
| Stage number | 2 | - |
| Motor power | 3.7 | kW |
| Nominal RPM | 1400 | n/min |
| Weight | 13.2 | kg |

### 3.3.2. Fabrication of sandwiches

The vacuum bag method was preferred when manufacturing sandwich plates due to its advantages. First, it provides evenly-distributed compression pressure over the entire surface of the laminated sandwich material. Thus, problems such as crushing in some regions of the core material are prevented. Also, uniform the thickness of the sandwich panel is obtained. Another advantage is that the vacuum removes the excess impregnated epoxy from the sandwich structure. Finally, the facesheet and core interface are better bonded with high vacuum power, and more of the excess epoxy is removed from the structure.

Considering these advantages, all sandwich structures used in this study were fabricated using the vacuum bagging method. The specifications of the vacuum pump are given in Table 3.3. The production process of sandwiches is similar to that of composite plates in vacuum bagging, as shown in Figure 3.23.

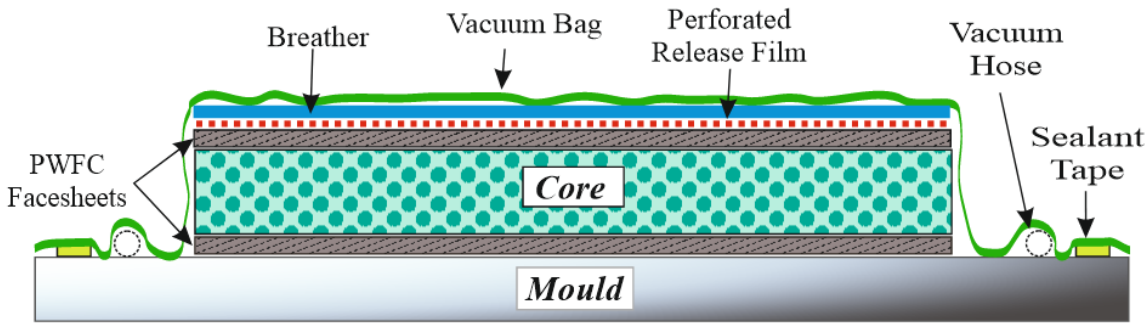



Figure 3.23. Schematic view of the vacuum bag method for the sandwich plate

In order to obtain a symmetric sandwich structure, the number of layers of the top and bottom composite plates was kept equal. When the bottom face layer stacking and epoxy impregnation process is finished, epoxy is spread on the bottom surface of the core material and placed on the bottom layer. Next, epoxy is spread on the top surface of the core material, and the top face layer is stacked. Then, perforated release film and breather are placed on the sandwich structure prepared by epoxy impregnation and stacking. Finally, the structure is sealed with a vacuum bag and cured under vacuum at 25 $^{0}$C for 24 hours (see Figure 3.24a). After 24 hours, the manufactured sandwich is removed from the mold and vacuumed (see Figure 3.24b).

In this thesis, AIREX C70 (High Specific Properties) PVC foam, carbon woven plain fabric (200 g/m$^2$), and epoxy (HEXION MGS L160) were used as raw materials for sandwich panel production. Six different PVC foams were used with three different thicknesses (30 mm, 20 mm, and 10 mm) and densities (48g/cm$^3$, 75 g/cm$^{3,}$ and 130 g/cm$^3$). Furthermore, two different span lengths (100 and 250 mm) were determined for the three-point bending of sandwich beams. In addition, 4- and 8-layer composite plates were preferred for the facesheet. Based on these variables, 21 different plates were produced.



(a) (b)

Figure 3.24. (a) Sandwich panels curing under vacuum, (b) Sandwich panel after curing

### 3.3.3. Preparation of test specimens

All test specimens were prepared following ASTM standards. A total of 10 plates were produced for tensile and bending tests for composite plate, while 21 plates were produced for sandwich bending tests in various configurations. All produced plates were cut with TÖRK MAKİNE A.Ş brand Törk 1500 model table saw.

*Plain woven fabric composite tensile test specimens*

In this thesis, five test specimens were cut and prepared from plates produced by five different manufacturing methods; the plate's specimen-cutting plan is presented in Figure 3.25. Test specimens were cut to dimensions following ASTM D 3039, which determined the in-plane tensile strength of high-modulus fibers reinforced polymer matrixes (International, 2017a).

Various materials configurations can be tested without tabs. These include multi-directional laminates, reinforced compounds, and fabrics. However, tabs are strongly recommended for unidirectional testing materials (International, 2017a). Since the composite plates tested contained fibers in the unidirectional direction, tabs were applied to the test specimens as shown in Figure 3. 26a. Tabs were made from 56x15mm and 1,5 mm-thick plain woven glass fabric composites according to the standards. The four tabs were glued to both surfaces and endpoints of a specimen with Loctite composite adhesive. Specimens cured for 24 hours were suitable for testing, as shown in Figure 3.26b.

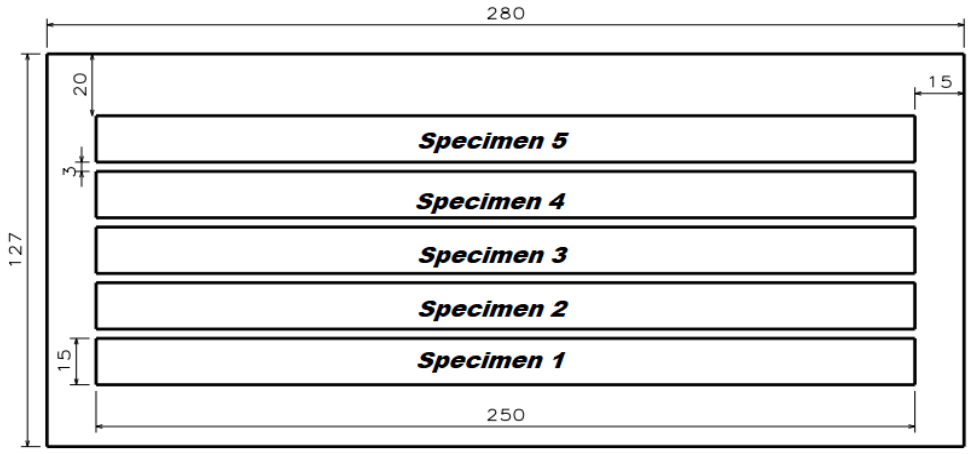
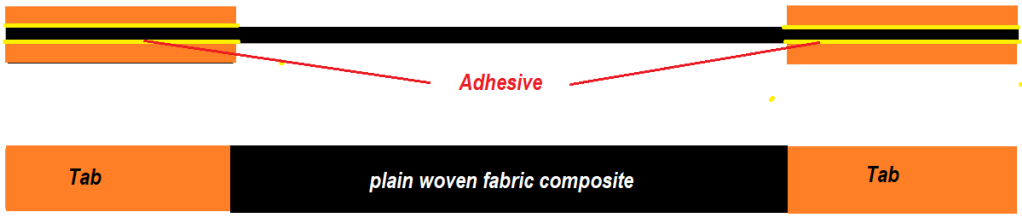



Figure 3.25. Schematic presents the dimensions of plain woven fabric composite plates and specimens for axial tensile test




(a)




(b)

Figure 3.26. (a) Schematical presentation of the assembly of the tabs and tensile specimen (b) plain woven fabric composite specimens prepared for axial tensile tests

*Plain woven fabric composite flexural test specimens*

In the bending tests, at least five test specimens were cut from the plates produced by five different methods; the plate specimen cutting plan is presented in Figure 3.27. Specimen dimensions were determined according to the ASTM D790 standard (ASTM, 2017). These standards aim to determine the flexural properties of unreinforced and reinforced plastics. They also include high-modulus composites and insulating materials molded into rectangular bars.

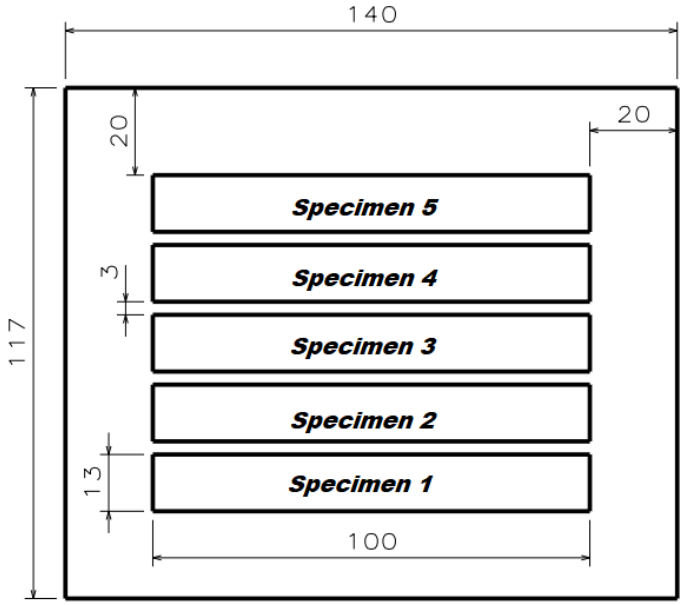


Figure 3.27. Schematic presents the dimensions of plain woven fabric composite plates and specimens for a three-point bending test

The recommended span-to-depth ratio for high-strength reinforced composites should be chosen so that the failure of the outer fibers is only caused by the bending moment. However, shear deformation can have a major influence on the modulus measurements of certain highly anisotropic materials, such as those with a span-to-depth ratio of 40:1. Therefore, to minimize the effects of this phenomenon, it is recommended that the span-to-depth ratio of these materials should be increased to 60:1. The thickness-span relationship of the test groups is given in Table 3.4.

Table 3.4. Carbon plain woven fabric laminates thickness and span length

| **Manufacturing Technique** | **Sample Code** | **Thickness (mm)** | **Span Length (mm)** |
|---|---|---|---|
| Hand lay-up | MT1 | 1.19 | 71.4 |
| Vacuum bag with a low-capacity vacuum pump | MT2 | 1.03 | 61.8 |
| Vacuum-assisted resin infusion | MT3 | 0.95 | 57 |
| Compression molding | MT4 | 0.90 | 54 |
| Vacuum bag with a high-capacity vacuum pump | MT5 | 0.82 | 49.2 |

The highest span length in the study was 71,4 mm. According to the standard, the sample should have a protrusion of at least 10% of the support opening at the ends. Therefore, the specimens were cut to 100 mm long for easy preparation and to comply with the test standard. The specimens ready for testing are shown in Figure 3.28.



Figure 3.28. Plain woven fabric composite specimens prepared for three-point bending testing

*PVC core test specimens*

Table 3.1 presents the mechanical properties of AIREX C70 (High Specific Properties) PVC foams used in this thesis. However, PVC foams with three different densities were subjected to compression testing to check this data's accuracy. Compression test specimens were prepared according to ASTM C365, which determines the modulus and compressive strength of the sandwich cores (International, 2016b). Five specimens were prepared as for each group with 30 mm thickness and 60X60 mm surface cross-section as shown in Figure 3.29.

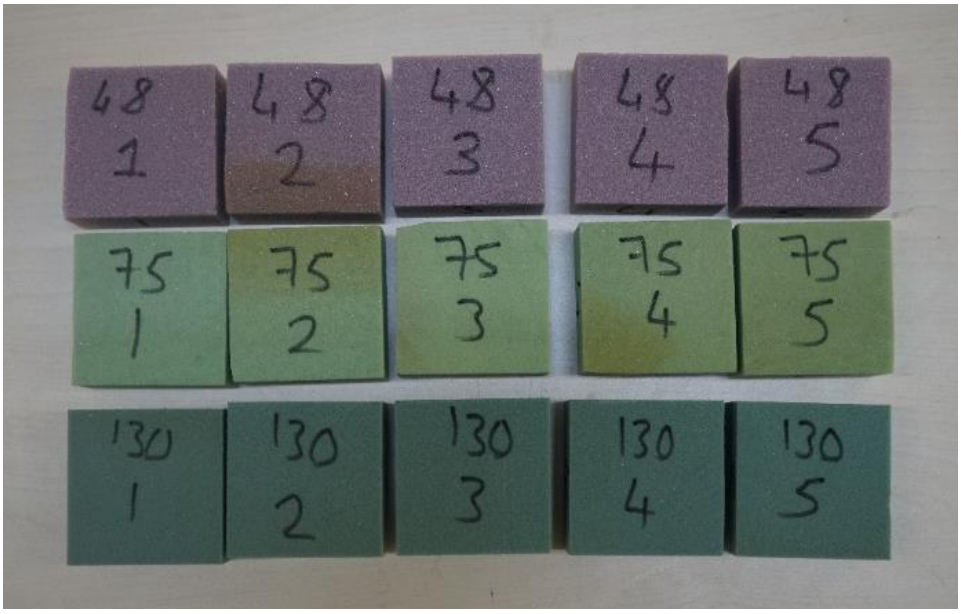
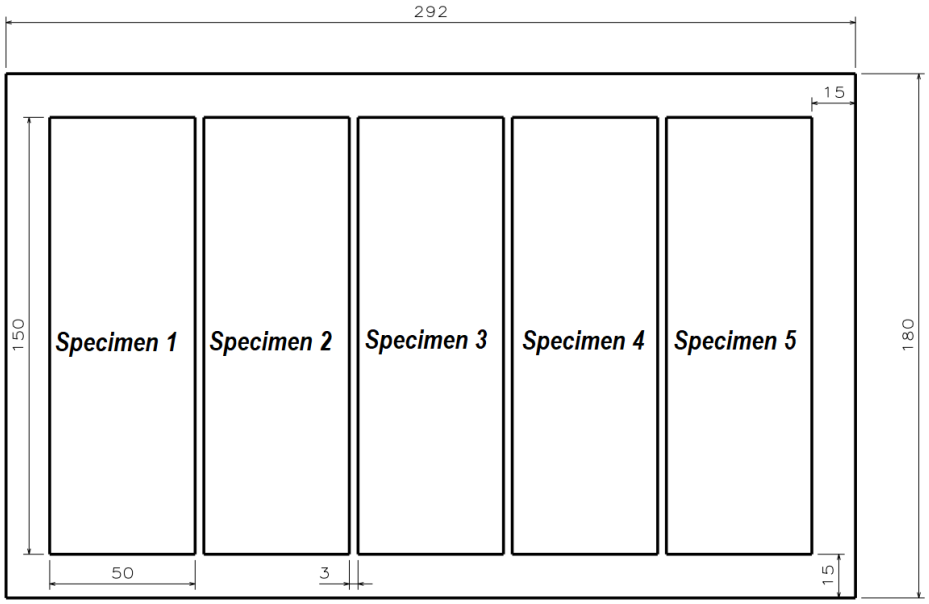


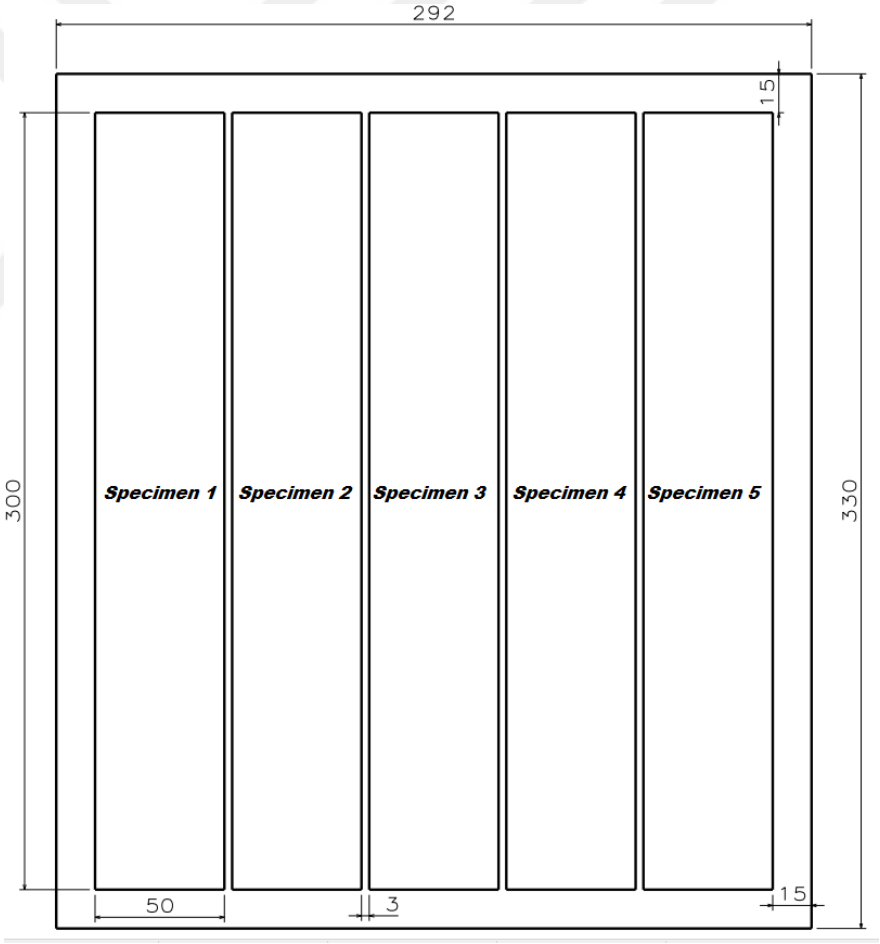

Figure 3.29. PVC foam specimens prepared for compression testing

*Sandwich beam test specimens*

Three-point bending test specimens were prepared following ASTM C 393 to obtain the flexural properties of flat sandwich structures (Materials, 2020). Two different sizes of sandwich plates were planned for two different span lengths (100 mm and 250 mm), as presented in Figure 3.30. Plates were produced so that five test specimens were obtained from each plate. The structural properties of the 21 different sandwich plate configurations are presented in Table 3.5. They were marked with abbreviation codes described in Figure 3.31. Finally, the specimens were prepared for testing by cutting them, as shown in Figure 3.32, using the diagram presented in Figure 3.30. In total, 105 test specimens were prepared.




(a)

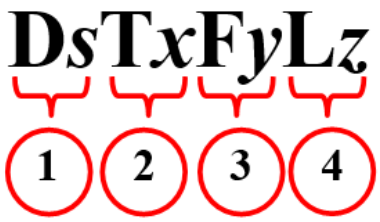



(b)

Figure 3.30. Schematic presents the dimensions of the sandwich plate for a three-point bending test of (a) short beam and (b) long beam

Table 3.5. Sandwich beam configuration details constituting the thesis study

| No | Configuration code | PVC foam density | Core thickness | Face Layer number | Total Length | Span length |
|---|---|---|---|---|---|---|
| | | kg/m$^3$ | mm | | mm | mm |
| 1 | D48T10F4L100 | 48 | 10 | 4 | 150 | 100 |
| 2 | D48T20F4L100 | 48 | 20 | 4 | 150 | 100 |
| 3 | D48T30F4L100 | 48 | 30 | 4 | 150 | 100 |
| 4 | D48T10F4L250 | 48 | 10 | 4 | 300 | 250 |
| 5 | D48T20F4L250 | 48 | 20 | 4 | 300 | 250 |
| 6 | D48T30F4L250 | 48 | 30 | 4 | 300 | 250 |
| 7 | D75T10F4L100 | 80 | 10 | 4 | 150 | 100 |
| 8 | D75T20F4L100 | 80 | 20 | 4 | 150 | 100 |
| 9 | D75T30F4L100 | 80 | 30 | 4 | 150 | 100 |
| 10 | D75T10F4L250 | 80 | 10 | 4 | 300 | 250 |
| 11 | D75T20F4L250 | 80 | 20 | 4 | 300 | 250 |
| 12 | D75T30F4L250 | 80 | 30 | 4 | 300 | 250 |
| 13 | D130T10F4L100 | 130 | 10 | 4 | 150 | 100 |
| 14 | D130T20F4L100 | 130 | 20 | 4 | 150 | 100 |
| 15 | D130T30F4L100 | 130 | 30 | 4 | 150 | 100 |
| 16 | D130T10F4L250 | 130 | 10 | 4 | 300 | 250 |
| 17 | D130T20F4L250 | 130 | 20 | 4 | 300 | 250 |
| 18 | D130T30F4L250 | 130 | 30 | 4 | 300 | 250 |
| 19 | D48T20F8L100 | 48 | 20 | 8 | 150 | 100 |
| 20 | D75T20F8L100 | 80 | 20 | 8 | 150 | 100 |
| 21 | D130T20F8L100 | 130 | 20 | 8 | 150 | 100 |




**1**
**D:** PVC foam core density,
***s:*** 48- 48 kg/m$^3$, 75- 80 kg/m$^3$, 130- 130 kg/m$^3$
**2**
**T:** Core thickness,
***x:*** 10- 10 mm, 20- 20 mm, 120-20 mm
**3**
**F:** Plain woven fabric layer number
***y:*** 4- 4 plain woven fabric layer, 8- 8 plain woven fabric layer
**4**
**L:** Span length
***z:*** 100- 100 mm , 250- 250 mm

Figure 3.31. Explanation of abbreviation codes of sandwich beams



Figure 3.32. Sandwich beam preparation process for the three-point bending test

### 3.3.4. Plain woven fabric composite tensile tests

Tests were performed following ASTM D 3039 standard procedures (Testing and Materials, 2008). First, the specimen is aligned longitudinally with the test direction and placed in the jaws of the testing machine. Next, the tabbed parts placed in the jaws were fixed by tightening with clamping screws (see Figure 3.33). The machine was run by setting the fixed head speed to 2 mm/min. The test stopped when the specimen suddenly broke away from the composite region. It was ensured that the specimens did not break in the tabs and peel off from the tab composite plate interface. Tests were performed at ambient temperature.



Figure 3.33. Carbon plain woven fabric composite plate axial tensile test setup

### 3.3.5. Plain woven fabric composite bending tests

Three-point bending tests of composite plate followed ASTM D 790 test procedures (Materials et al., 2009). The support spans of the fixator were fixed before starting each grub test by adjusting the span lengths given in Table 3.4. First, the specimen is placed centered on the support spans. The diameters of the loading and support rollers are 10 mm. Next, the cross-head motion speed (R) was adjusted as

$$R = ZL^2/6d \tag{3.75}$$

Where L, d, and Z are defined as span length, plate thickness, and rate of straining, respectively. Z is assumed to equal 0.01 according to the standard. The test was started once the cross-head speed was adjusted, as shown in Figure 3.34. The test was stopped once the layer on the plate's upper or lower surface has failed.




Figure 3.34. Carbon plain woven fabric composite plate three-point bending test setup

### 3.3.6. Core compression tests

PVC foam compression tests were carried out according to the ASTM C 365 standard procedure (International, 2016b). Firstly, rigid plates of 20 mm thickness were fixed to the upper and lower jaws of the machine. Then, the specimen was placed between the lower and upper jaw (see Figure 3.35). Next, the cross-head motion was set to 0.50 mm/min, and the test was started. During the test, it was ensured that the loading was evenly distributed over the specimen's surface. The tests were continued until the foam specimens were densified.




Figure 3.35. Compression test setup of PVC foam core material

### 3.3.7. Sandwich flexural tests

Three-point bending tests of sandwich beams were carried out according to the test procedure given in ASTM C 393 standard (International, 2016a). Support spans were set according to span lengths of 250 mm for long beams and 100 mm for short beams. The cross-head motion was set to 2 mm/min as it is recommended to reach the maximum load between 3 and 6 min. The test set up is shown in Figure 3.36. The tests were continued until the maximum load for which core densification occurred.




(a) (b)

Figure 3.36. Sandwich three-point bending test setup a) long-span length (b) short-span length

# 4. RESULTS AND DISCUSSIONS

The analytical results for the configurations determined in the study using the novel engineering approaches developed for sandwich beams under three-point bending load and plain woven fabric composite used as face material are presented with figures and tables. The results obtained with developed approaches were compared with experimental, and the model results in the literature.

## 4.1. The results of the developed analytical method with engineering approaches

The flexural properties of sandwich beams made of plain woven composite fabric face material and PVC foam core were calculated under a simple bending load, with the engineering approaches developed in this thesis. The engineering approaches were divided into two main parts, and estimations were made. Firstly, it analytically determined the properties of plain woven fabric composite. The second stage is related to the sandwich beam. The study explained the integration of stiffness matrices of the face material obtained from composite mechanics into the calculation of sandwich bending stiffness. Bending stiffness, failure modes and loads, elastic limit load, and force-deflection curves were determined as explained in the Materials and Methods section of the thesis.

### 4.1.1. The plain woven fabric composite properties obtained with the practical engineering approach

A practical engineering approach was developed in this work to predict the mechanical properties of plain woven fabric composite plates easily. This approach takes the composite as a cross-ply (0/90) laminate and defines the *engineering fiber volume fraction*. The approach calculates the on-axis properties (micro-mechanical) of composite using a rule-of-mixture approach modified with engineering volume fraction. Since the plates produced to control the model are made of four layers of fabric, the multilayer composite stiffness matrices were determined as eight-layer cross-ply with CLT. Axial and flexural behavior of the designed plates under axial and three-point bending loads were determined according to standard procedures.

*The results of micro and macro mechanical properties*

The $E_1$, $E_2$, $v_{12}$, $G_{12}$, $X_1$, $Y_1$, $X_2$, and $Y_2$, which are the mechanical properties of on-axis plain woven fabric composite ply, were determined from the analytical solutions given in Equations 3.4-3.12 depending on the engineering fiber volume fraction ($V_f^E$). The results are shown in Table 4.1. Although they are produced from the same fabric and resin, the values of the fiber volume fractions of the plates obtained from five different production techniques (MT1-MT5) are different.

Table 4.1. Mechanical properties of on-axis plain woven fabric composite

| **Lamina code** | **Physical Properties** | | **Elastic Properties** | | | | **Tensile and Compressive Strength Properties** | | | |
|---|---|---|---|---|---|---|---|---|---|---|
| | **One Ply thick.** | $\mathbf{V_f^E}$ | $\mathbf{E_1}$ | $\mathbf{E_2}$ | $\mathbf{G_{12}}$ | $\boldsymbol{\vartheta_{12}}$ | $\mathbf{X_1}$ | $\mathbf{Y_1}$ | $\mathbf{X_2}$ | $\mathbf{Y_2}$ |
| | mm | | GPa | GPa | GPa | - | MPa | MPa | MPa | MPa |
| MT1 | 0.2975 | 0.26 | 64.90 | 4.57 | 1.72 | 0.303 | 1030 | 58 | 1350 | 115 |
| MT2 | 0.2575 | 0.30 | 74.40 | 4.83 | 1.81 | 0.298 | 1180 | 55 | 1430 | 116 |
| MT3 | 0.2375 | 0.34 | 83.80 | 5.11 | 1.91 | 0.293 | 1330 | 52 | 1520 | 117 |
| MT4 | 0.2250 | 0.35 | 86.20 | 5.19 | 1.93 | 0.291 | 1360 | 52 | 1540 | 118 |
| MT5 | 0.2050 | 0.39 | 95.70 | 5.52 | 2.05 | 0.285 | 1510 | 49 | 1640 | 118 |

Since the plates were designed as four-ply plain woven based on the experimental control specimens, the plates were considered as eight-layer cross-ply laminates when calculating the macro mechanical properties. The on-axis characteristics of each group were taken from Table 4.1. The stiffness matrices ([A], [B], and [D]) that give the macro mechanical properties of multilayer composite plates are calculated by following equations 3.12-3.29. These stiffness matrices are used to calculate load values with known strain values, as presented in Equation 3.29. Stiffness matrices for five plates were calculated and presented in Table 4.2.

Table 4.2. Stiffness matrixes of four-layer plain woven fabric composite

| **Laminate code** | **[A]** | **[B]** | **[D]** |
|---|---|---|---|
| | **N/m** | **N** | **Nm** |
| MT1 | $\begin{bmatrix} 41.6 & 1.6 & 0.0 \\ 1.6 & 41.6 & 0.0 \\ 0.0 & 0.0 & 2.0 \end{bmatrix} 10^6$ | $\begin{bmatrix} -2.6 & 0.0 & 0.0 \\ 0.0 & 2.6 & 0.0 \\ 0.0 & 0.0 & 0.0 \end{bmatrix} 10^3$ | $\begin{bmatrix} 48.7 & 1.9 & 0.0 \\ 1.9 & 48.7 & 0.0 \\ 0.0 & 0.0 & 2.4 \end{bmatrix} 10^{-1}$ |
| MT2 | $\begin{bmatrix} 41.0 & 1.5 & 0.0 \\ 1.5 & 41.0 & 0.0 \\ 0.0 & 0.0 & 1.9 \end{bmatrix} 10^6$ | $\begin{bmatrix} -2.3 & 0.0 & 0.0 \\ 0.0 & 2.3 & 0.0 \\ 0.0 & 0.0 & 0.0 \end{bmatrix} 10^3$ | $\begin{bmatrix} 36.2 & 1.3 & 0.0 \\ 1.3 & 36.2 & 0.0 \\ 0.0 & 0.0 & 1.6 \end{bmatrix} 10^{-1}$ |
| MT3 | $\begin{bmatrix} 42.4 & 1.4 & 0.0 \\ 1.4 & 42.4 & 0.0 \\ 0.0 & 0.0 & 1.8 \end{bmatrix} 10^6$ | $\begin{bmatrix} -2.3 & 0.0 & 0.0 \\ 0.0 & 2.3 & 0.0 \\ 0.0 & 0.0 & 0.0 \end{bmatrix} 10^3$ | $\begin{bmatrix} 31.9 & 1.9 & 0.0 \\ 1.9 & 31.9 & 0.0 \\ 0.0 & 0.0 & 1.4 \end{bmatrix} 10^{-1}$ |
| MT4 | $\begin{bmatrix} 41.3 & 1.3 & 0.0 \\ 1.3 & 41.3 & 0.0 \\ 0.0 & 0.0 & 1.7 \end{bmatrix} 10^6$ | $\begin{bmatrix} -2.0 & 0.0 & 0.0 \\ 0.0 & 2.0 & 0.0 \\ 0.0 & 0.0 & 0.0 \end{bmatrix} 10^3$ | $\begin{bmatrix} 232.4 & 9.2 & 0.0 \\ 9.2 & 232.4 & 0.0 \\ 0.0 & 0.0 & 11.7 \end{bmatrix} 10^{-2}$ |
| MT5 | $\begin{bmatrix} 41.7 & 1.2 & 0.0 \\ 1.2 & 41.7 & 0.0 \\ 0.0 & 0.0 & 1.6 \end{bmatrix} 10^6$ | $\begin{bmatrix} -1.9 & 0.0 & 0.0 \\ 0.0 & 1.9 & 0.0 \\ 0.0 & 0.0 & 0.0 \end{bmatrix} 10^3$ | $\begin{bmatrix} 233.6 & 7.2 & 0.0 \\ 7.2 & 233.6 & 0.0 \\ 0.0 & 0.0 & 9.4 \end{bmatrix} 10^{-2}$ |

Some solutions may require the inverse of equation 3.28. In these cases, the inverse of stiffness matrices is taken, and compliance matrices are obtained. The compliance matrices of [A], [B], and [D] matrices are [α], [β], and [δ], respectively. The compliance matrices were also calculated with KomPro and are shown in Table 4.3.

Table 4.3. Compliance matrixes of four-layer plain woven fabric composite

| **Laminate code** | **[α]** | **[β]** | **[δ]** |
|---|---|---|---|
| | **m/N** | **1/N** | **1/Nm** |
| MT1 | $\begin{bmatrix} 2.4 & 0.0 & 0.0 \\ 0.0 & 2.4 & 0.0 \\ 0.0 & 0.0 & 48.9 \end{bmatrix} 10^{-8}$ | $\begin{bmatrix} 1.4 & 0.0 & 0.0 \\ 0.0 & -1.4 & 0.0 \\ 0.0 & 0.0 & 0.0 \end{bmatrix} 10^{-5}$ | $\begin{bmatrix} 2.1 & 0.0 & 0.0 \\ 0.0 & 2.1 & 0.0 \\ 0.0 & 0.0 & 41.4 \end{bmatrix} 10^{-1}$ |
| MT2 | $\begin{bmatrix} 2.5 & 0.0 & 0.0 \\ 0.0 & 2.5 & 0.0 \\ 0.0 & 0.0 & 53.6 \end{bmatrix} 10^{-8}$ | $\begin{bmatrix} 1.6 & 0.0 & 0.0 \\ 0.0 & -1.6 & 0.0 \\ 0.0 & 0.0 & 0.0 \end{bmatrix} 10^{-5}$ | $\begin{bmatrix} 28.6 & -1.9 & 0.0 \\ -1.9 & 28.6 & 0.0 \\ 0.0 & 0.0 & 600.6 \end{bmatrix} 10^{-2}$ |
| MT3 | $\begin{bmatrix} 2.5 & 0.0 & 0.0 \\ 0.0 & 2.5 & 0.0 \\ 0.0 & 0.0 & 55.1 \end{bmatrix} 10^{-8}$ | $\begin{bmatrix} 1.7 & 0.0 & 0.0 \\ 0.0 & -1.7 & 0.0 \\ 0.0 & 0.0 & 0.0 \end{bmatrix} 10^{-5}$ | $\begin{bmatrix} 32.5 & -1.0 & 0.0 \\ -1.0 & 32.5 & 0.0 \\ 0.0 & 0.0 & 732.8 \end{bmatrix} 10^{-2}$ |
| MT4 | $\begin{bmatrix} 2.5 & 0.0 & 0.0 \\ 0.0 & 2.5 & 0.0 \\ 0.0 & 0.0 & 57.5 \end{bmatrix} 10^{-8}$ | $\begin{bmatrix} 1.9 & 0.0 & 0.0 \\ 0.0 & -1.9 & 0.0 \\ 0.0 & 0.0 & 0.0 \end{bmatrix} 10^{-5}$ | $\begin{bmatrix} 42.78 & -1.2 & 0.0 \\ -1.2 & 42.78 & 0.0 \\ 0.0 & 0.0 & 852.3 \end{bmatrix} 10^{-2}$ |
| MT5 | $\begin{bmatrix} 2.5 & 0.0 & 0.0 \\ 0.0 & 2.5 & 0.0 \\ 0.0 & 0.0 & 59.5 \end{bmatrix} 10^{-8}$ | $\begin{bmatrix} 2.0 & 0.0 & 0.0 \\ 0.0 & -2.0 & 0.0 \\ 0.0 & 0.0 & 0.0 \end{bmatrix} 10^{-5}$ | $\begin{bmatrix} 42.71 & -1.4 & 0.0 \\ -1.4 & 42.71 & 0.0 \\ 0.0 & 0.0 & 1062.0 \end{bmatrix} 10^{-2}$ |

*The results of the analytical approach under axial loading*

The mechanical behavior of the plates under tensile load was investigated and provided in the following subsections. These are the load-extension curve, stress-strain curve, tensile modulus elasticity, and strength properties.

- Tensile Load-extension curves

The plates were designed according to the ASTM D 3039 standard used in the test standards. Widths of 15 mm, a total length of 250 mm, and the gauge length of 138 mm, excluding tab size, were accepted. The load extension relationship was calculated based on Equation 3.31. $\alpha_{11}$ values were obtained from Table 4.3. The load-displacement curve can be plotted with this relationship, but the maximum load must also be known. The maximum load can be obtained according to the Tsai-Wu criterion, details of which are in equation 3.50. This study calculated the reserve factor (given by equations 3.53-3.54) values obtained against 1 N loading. The reserve factor thus calculated corresponds to maximum estimated load values that the plates can carry (see Table 4.4). Since each layer will have different angles and properties in laminate composite structures, the maximum load values each layer and its surface can carry were calculated. The smallest load value that can be carried by 0 and 90 degrees is considered the maximum load value that the plate can carry.

Table 4.4. Tensile reserve factors R of the plate under 1 N tensile load, and maximum load bearing capacity

| **Laminate Code** | **Load** | **Nx** | **Plain woven Layer** | **Cross-ply Layer** | **Layer surface** | **R (Maximum allowable tensile load)** |
|---|---|---|---|---|---|---|
| | **N** | **N/mm** | | | | **x $10^3$ N** |
| MT1 | 1 | 66.66 | 1 | 0 | Top | 9.890 |
| | | | | | Bottom | **9.890** |
| | | | | 90 | Top | **7.854** |
| | | | | | Bottom | 7.854 |
| | | | 2 | 0 | Top | 9.890 |
| | | | | | Bottom | 9.890 |
| | | | | 90 | Top | 7.854 |
| | | | | | Bottom | 7.854 |
| | | | 3 | 90 | Top | 7.854 |
| | | | | | Bottom | 7.854 |
| | | | | 0 | Top | 9.890 |
| | | | | | Bottom | 9.890 |
| | | | 4 | 90 | Top | 7.854 |
| | | | | | Bottom | 7.854 |
| | | | | 0 | Top | 9.890 |
| | | | | | Bottom | 9.890 |
| MT2 | 1 | 66.66 | 1 | 0 | Top | 9.256 |
| | | | | | Bottom | **9.256** |
| | | | | 90 | Top | **6.860** |
| | | | | | Bottom | 6.860 |
| | | | 2 | 0 | Top | 9.256 |
| | | | | | Bottom | 9.256 |
| | | | | 90 | Top | 6.860 |
| | | | | | Bottom | 6.860 |
| | | | 3 | 90 | Top | 6.860 |
| | | | | | Bottom | 6.860 |
| | | | | 0 | Top | 9.256 |
| | | | | | Bottom | 9.256 |
| | | | 4 | 90 | Top | 6.860 |
| | | | | | Bottom | 6.860 |
| | | | | 0 | Top | 9.256 |
| | | | | | Bottom | 9.256 |

Table 4.4. continued.

| | | | | | | |
|---|---|---|---|---|---|---|
| MT3 | 1 | 66.66 | 1 | 0 | Top | 9.789 |
| | | | | | Bottom | **9.789** |
| | | | | 90 | Top | **6.484** |
| | | | | | Bottom | 6.484 |
| | | | 2 | 0 | Top | 9.789 |
| | | | | | Bottom | 9.789 |
| | | | | 90 | Top | 6.484 |
| | | | | | Bottom | 6.484 |
| | | | 3 | 90 | Top | 6.484 |
| | | | | | Bottom | 6.484 |
| | | | | 0 | Top | 9.789 |
| | | | | | Bottom | 9.789 |
| | | | 4 | 90 | Top | 6.484 |
| | | | | | Bottom | 6.484 |
| | | | | 0 | Top | 9.789 |
| | | | | | Bottom | 9.789 |
| MT4 | 1 | 66.66 | 1 | 0 | Top | 9.585 |
| | | | | | Bottom | **9.585** |
| | | | | 90 | Top | **6.142** |
| | | | | | Bottom | 6.142 |
| | | | 2 | 0 | Top | 9.585 |
| | | | | | Bottom | 9.585 |
| | | | | 90 | Top | 6.142 |
| | | | | | Bottom | 6.142 |
| | | | 3 | 90 | Top | 6.142 |
| | | | | | Bottom | 6.142 |
| | | | | 0 | Top | 9.585 |
| | | | | | Bottom | 9.585 |
| | | | 4 | 90 | Top | 6.142 |
| | | | | | Bottom | 6.142 |
| | | | | 0 | Top | 9.585 |
| | | | | | Bottom | 9.585 |
| MT5 | 1 | 66.66 | 1 | 0 | Top | 9.507 |
| | | | | | Bottom | **9.507** |
| | | | | 90 | Top | **5.560** |
| | | | | | Bottom | 5.560 |
| | | | 2 | 0 | Top | 9.507 |
| | | | | | Bottom | 9.507 |
| | | | | 90 | Top | 5.560 |
| | | | | | Bottom | 5.560 |
| | | | 3 | 90 | Top | 5.560 |
| | | | | | Bottom | 5.560 |
| | | | | 0 | Top | 9.507 |
| | | | | | Bottom | 9.507 |
| | | | 4 | 90 | Top | 5.560 |
| | | | | | Bottom | 5.560 |
| | | | | 0 | Top | 9.507 |
| | | | | | Bottom | 9.507 |

The load-displacement curves of the plates are presented in the following figures. Since fiber-reinforced composites are brittle materials, they are considered linear up to the maximum load and then are assumed to break suddenly.

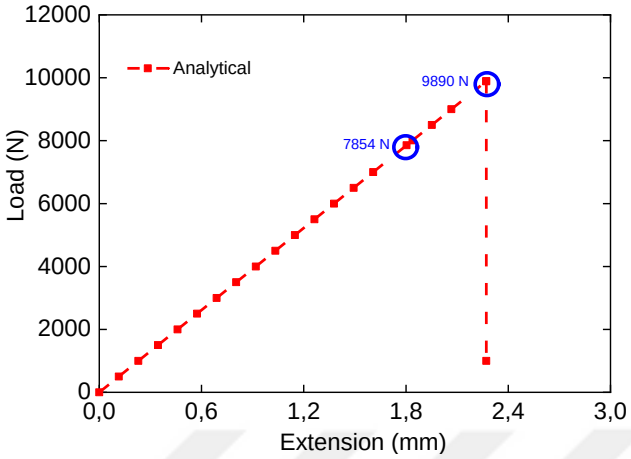



Figure 4.1. Analytical tensile load-extension curve of MT1 plate obtained with the practical engineering approach

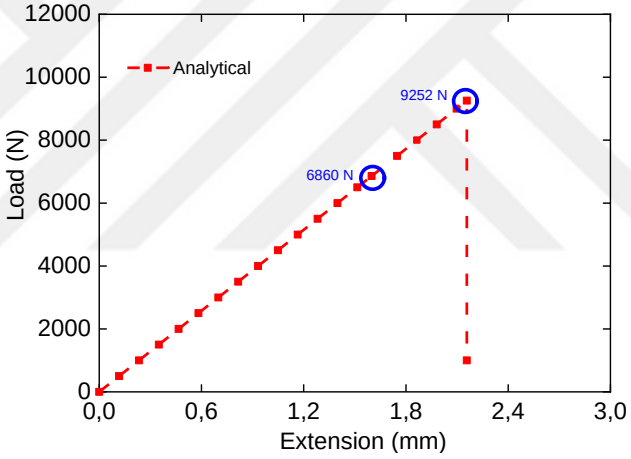



Figure 4.2. Analytical tensile load-extension curve of MT2 plate obtained with the practical engineering approach

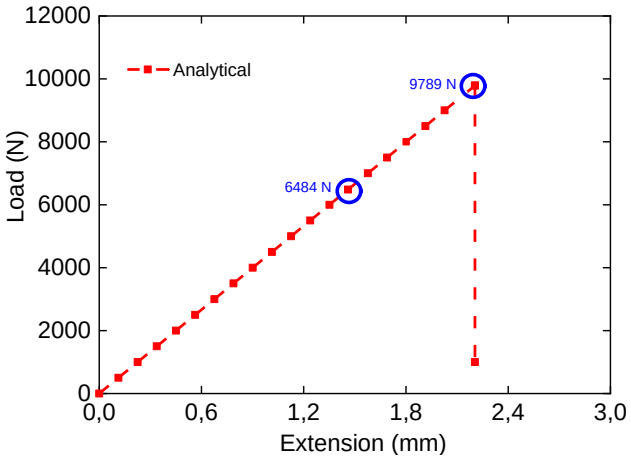



Figure 4.3. Analytical tensile load-extension curve of MT3 plate obtained with the practical engineering approach

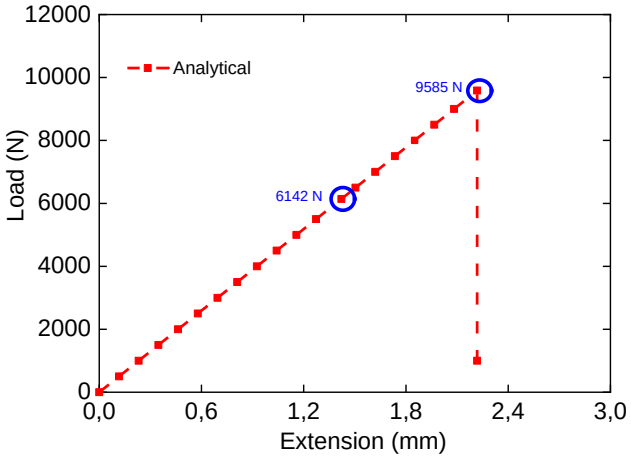



Figure 4.4. Analytical tensile load-extension curve of MT4 plate obtained with the practical engineering approach

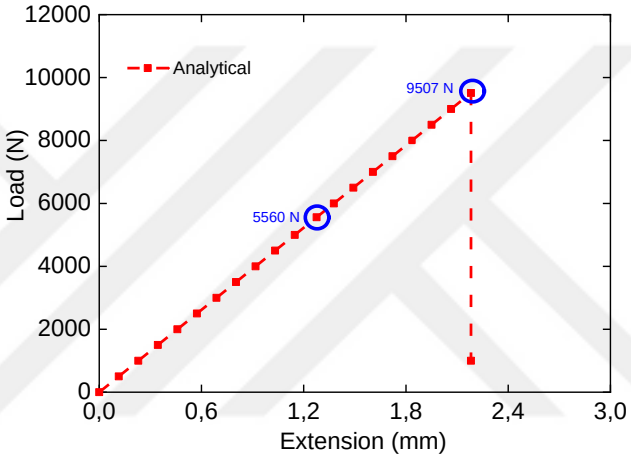



Figure 4.5. Analytical tensile load-extension curve of MT5 plate obtained with the practical engineering approach

Analytical tensile load-extension curves of the plates are given in Figures 4.1-4.5. Two load values are marked on the curves. The low force values in the curves are the maximum load capacity that the fibers in the transverse ($90^0$) direction can carry. For plain woven fabric, the yarns formed by the fibers in the transverse direction are called fill yarns. Therefore, these load values are the load values that the fill yarns of the plates can carry. The highest force values in the curves are the load values that the longitudinal ($0^0$) fibers along the loading can carry. For the fabric, the yarn formed by the fibers in the longitudinal direction is called warp yarn.

- Tensile stress-strain curves

Tensile stress-strain curves were calculated using the data from the force-displacement curves of Figures 4.1-4.5. Stress values were calculated using Equation 3.32, while the rectangular cross-sectional area of the plate was obtained based on the total thickness of the plates and the width of 15 mm. Strain values were calculated as an extension divided by the initial length, which is assumed to be 138 mm. Stress-strain values were calculated for each plate and plotted in Figures 4.6-

4.10. The figures also specify stress values as warp and fill stress. When the plate reaches the tensile fill yarn stress ($\sigma_{fill}^{T}$) value in loading, microfracture cracks start on the fill yarn. When the plate reaches the tensile warp yarn stress ($\sigma_{warp}^{T}$) value in loading, the longitudinal fibers in the warp tow fail, and the plate breaks. However, the residual stress of plain woven fabric composite is relatively high due to fiber architecture, such as undulation angle. Therefore, although the plate can withstand the stress above $\sigma_{fill}^{T}$ it breaks before reaching $\sigma_{warp}^{T}$.

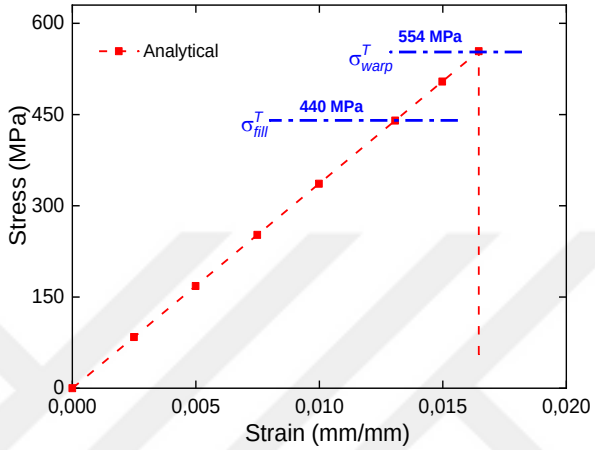



Figure 4.6. Analytical tensile stress-strain curve of MT1 plate obtained with the practical engineering approach

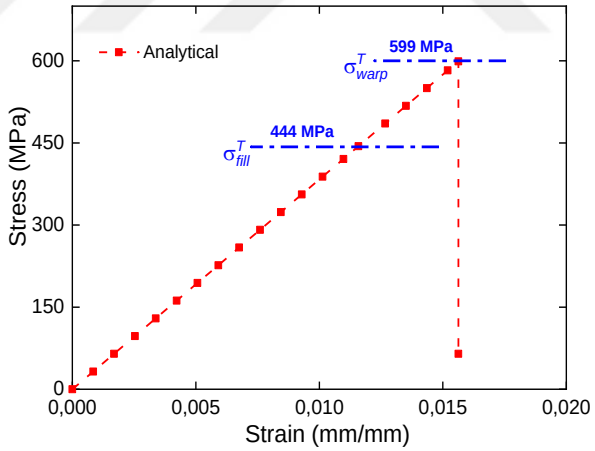



Figure 4.7. Analytical tensile stress-strain curve of MT2 plate obtained with the practical engineering approach

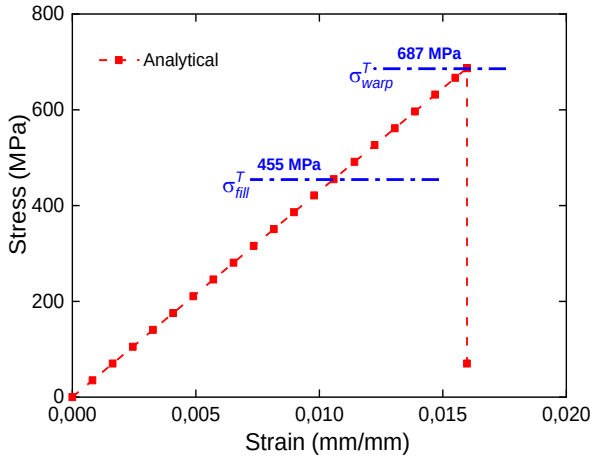



Figure 4.8. Analytical tensile stress-strain curve of MT3 plate obtained with the practical engineering approach

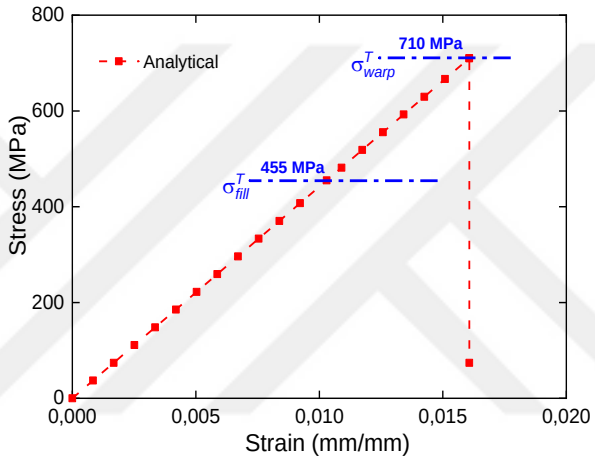



Figure 4.9. Analytical tensile stress-strain curve of MT4 plate obtained with the practical engineering approach

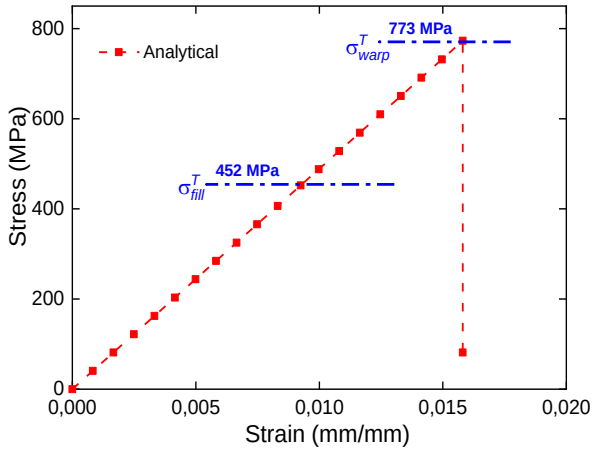



Figure 4.10. Analytical tensile stress-strain curve of MT5 plate obtained with the practical engineering approach

- Tensile modulus of elasticity and strength properties

Table 4.5 presents the obtained elastic modulus and strength values of the plates. The tensile elastic modulus of fiber-reinforced composite laminae is called the average elastic modulus ($E_{av}$). Because it has a layered structure, each layer may have a different elastic property due to fiber orientation and fiber materials. In the present study, plain woven fabric is considered a cross-ply in composite plates and contains transverse and longitudinal fibers in its layers. Therefore, it was assumed that its layers had different mechanical properties. The average elastic modulus of different layers of laminated plates is $E_{av}$. The $E_{av}$ depends on the laminate's longitudinal extension matrix terms ($A_{11}$, and $\alpha_{11}$) and is calculated by Equation 3.35. Since the warp and fill yarns of the fabric used in the study have the same physical structure of yarns, such as width sizes, undulation, thickness, and cross-sectional area, the elastic behavior of the laminates along x and y axes was considered equal to $E_{av}$.

Table 4.5. Average elastic modulus and strength results obtained with the proposed practical approach for plain woven fabric composite

| **Laminate code** | **Composite Laminates and $V_f$** | | | **Results of the Practical Engineering Approach** | | |
|---|---|---|---|---|---|---|
| | $\mathbf{V_f^O}$ | $\mathbf{V_f^Y}$ | $\mathbf{V_f^E}$ | $\mathbf{E_{av}= E_x=E_y}$ | $\boldsymbol{\sigma}_{\mathbf{warp}}^{\mathbf{T}}$ | $\boldsymbol{\sigma}_{\mathbf{fill}}^{\mathbf{T}}$ |
| | | | | **GPa** | **MPa** | **MPa** |
| MT1 | 0.34 | 0.52 | 0.26 | 34.8 | 554 | 440 |
| MT2 | 0.38 | 0.60 | 0.30 | 37.4 | 599 | 444 |
| MT3 | 0.43 | 0.68 | 0.34 | 43.3 | 687 | 455 |
| MT4 | 0.45 | 0.70 | 0.35 | 45.0 | 710 | 455 |
| MT5 | 0.50 | 0.78 | 0.39 | 49.3 | 773 | 452 |

*The results of analytical methods under flexural loading*

The flexural properties of plain woven fabric composite plates for the three-point bending loading shown in Figure 3.11 were calculated using the practical engineering approach. The dimensions and boundary conditions of the beams used in the calculations were determined according to the ASTM D790 standard. The beams were assumed to have a width of 13 mm and a span length of sixty times of their thickness. The cross-ply configuration of the composite plates consisting of four layers is assumed, as shown in Figure 4.11. The maximum load capacity that each layer of the beam can carry, load-displacement curves, average flexural elastic modulus, and stress values occurring in each layer at the maximum load that the beams can carry are presented in tables and figures.

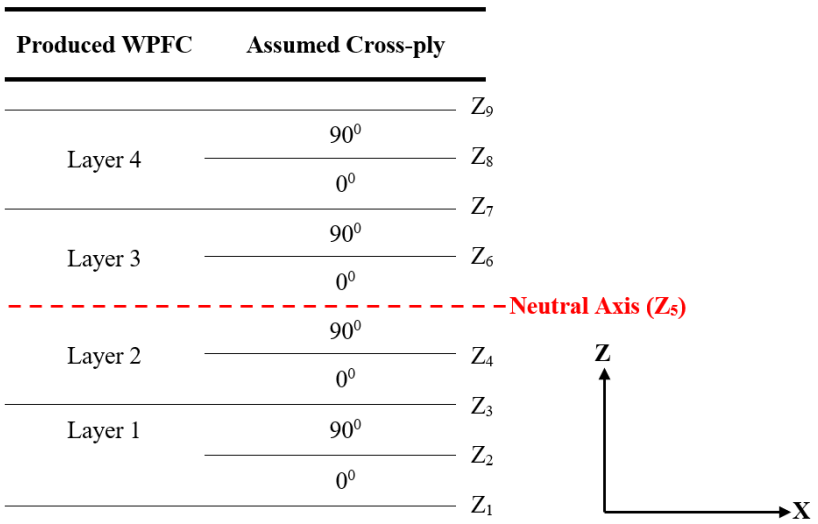



Figure 4.11. Plain woven fabric composite plate layer configuration as cross-ply for bending loading

- Bending load-midspan deflection

The load-deflection relationship of the composite beams was calculated with the deflection Equation 3.42, obtained from the differential equation solved according to the loading conditions in Figure 3.11. The values of the bending longitudinal compliance term ($\delta_{11}$) in the collapse equation were obtained from Table 4.3. The span length of the beam with a width of 13 mm was calculated based on the length-to-thickness ratio of 60:1. Load deflection curves can be drawn with Equation 3.42, but strength calculations are required for the maximum loads the beams can carry. Similar to the tensile loading case, Mx values of the beams are calculated under 1N load. Then, reserve factors were obtained for each layer of the composite plate's top and bottom surfaces. The results are shown in Table 4.6. Then, the inverse proportion was established with the 1N and reserve factors to obtain the maximum transverse loads where the reserve factor was equal to one. The calculated loads are also presented in Table 4.6

Table 4.6. Flexural reserve factors R of the beams under 1 N flexural load and maximum flexural load bearing capacity

| Lam. Code | Load | Span Length | Mx | Plain woven Layer | Cross-ply Layer | Layer surface | R (Maximum allowable flexural load) |
|---|---|---|---|---|---|---|---|
| | N | mm | N | | | | N |
| MT1 | 1 | 71.4 | 2.74 | 1 | 0 | Top | **83.8** |
| | | | | | | Bottom | 116.7 |
| | | | | | 90 | Top | 112.4 |
| | | | | | | Bottom | 183.7 |
| | | | | 2 | 0 | Top | 190.7 |
| | | | | | | Bottom | 520.1 |
| | | | | | 90 | Top | 503.4 |
| | | | | | | Bottom | 338.3 |
| | | | | 3 | 0 | Top | 674.1 |
| | | | | | | Bottom | 322.5 |
| | | | | | 90 | Top | 261.3 |
| | | | | | | Bottom | 94.3 |
| | | | | 4 | 0 | Top | 116.2 |
| | | | | | | Bottom | 70.9 |
| | | | | | 90 | Top | 57.5 |
| | | | | | | Bottom | **50.9** |
| MT2 | 1 | 61.8 | 2.38 | 1 | 0 | Top | **76.5** |
| | | | | | | Bottom | 106.3 |
| | | | | | 90 | Top | 105.9 |
| | | | | | | Bottom | 173.4 |
| | | | | 2 | 0 | Top | 173.8 |
| | | | | | | Bottom | 477.2 |
| | | | | | 90 | Top | 478.5 |
| | | | | | | Bottom | 311.7 |
| | | | | 3 | 0 | Top | 629.5 |
| | | | | | | Bottom | 320.5 |
| | | | | | 90 | Top | 244.9 |
| | | | | | | Bottom | 87.9 |
| | | | | 4 | 0 | Top | 114.8 |
| | | | | | | Bottom | 87.9 |
| | | | | | 90 | Top | 53.6 |
| | | | | | | Bottom | **50.3** |
| MT3 | 1 | 57.0 | 2.20 | 1 | 0 | Top | **77.1** |
| | | | | | | Bottom | 107.1 |
| | | | | | 90 | Top | 104.7 |
| | | | | | | Bottom | 171.7 |
| | | | | 2 | 0 | Top | 175.3 |
| | | | | | | Bottom | 482.6 |
| | | | | | 90 | Top | 476.4 |
| | | | | | | Bottom | 271.0 |
| | | | | 3 | 0 | Top | 612.8 |
| | | | | | | Bottom | 272.1 |
| | | | | | 90 | Top | 222.1 |
| | | | | | | Bottom | 78.5 |
| | | | | 4 | 0 | Top | 95.8 |
| | | | | | | Bottom | 58.2 |
| | | | | | 90 | Top | 47.8 |
| | | | | | | Bottom | **41.8** |

Table 4.6. continued.

| | | | | | | | |
|---|---|---|---|---|---|---|---|
| MT4 | 1 | 54.0 | 2.08 | 1 | 0 | Top | **65.4** |
| | | | | | | Bottom | 102.8 |
| | | | | | 90 | Top | 101.3 |
| | | | | | | Bottom | 166.1 |
| | | | | 2 | 0 | Top | 168.2 |
| | | | | | | Bottom | 463.4 |
| | | | | | 90 | Top | 461.3 |
| | | | | | | Bottom | 259.4 |
| | | | | 3 | 0 | Top | 593.3 |
| | | | | | | Bottom | 317.6 |
| | | | | | 90 | Top | 207.3 |
| | | | | | | Bottom | 74.1 |
| | | | | 4 | 0 | Top | 113.1 |
| | | | | | | Bottom | 68.8 |
| | | | | | 90 | Top | 49.4 |
| | | | | | | Bottom | **45.1** |
| MT5 | 1 | 49.2 | 1.90 | 1 | 0 | Top | **73.2** |
| | | | | | | Bottom | 101.6 |
| | | | | | 90 | Top | 96.3 |
| | | | | | | Bottom | 158.0 |
| | | | | 2 | 0 | Top | 166.5 |
| | | | | | | Bottom | 459.5 |
| | | | | | 90 | Top | 440.4 |
| | | | | | | Bottom | 230.6 |
| | | | | 3 | 0 | Top | 559.0 |
| | | | | | | Bottom | 318.2 |
| | | | | | 90 | Top | 185.9 |
| | | | | | | Bottom | 66.3 |
| | | | | 4 | 0 | Top | 112.9 |
| | | | | | | Bottom | 68.6 |
| | | | | | 90 | Top | 49.2 |
| | | | | | | Bottom | **40.3** |

Figures 4.12- 4.16 show the linear force-displacement curves for each beam up to the maximum load it can carry. On the curves, it is assumed that the first failure starts at the load called failure load of the compression side, where micro-fractures start from the fill yarns in the top layer of the beams. When the load value called failure load of the tensile side is reached, it is assumed that the warp yarns in the lower layer of the beams have entirely failed. Since the composite plates are brittle materials, they break entirely when the ultimate load is reached, as seen in the figures, and the load drops suddenly.

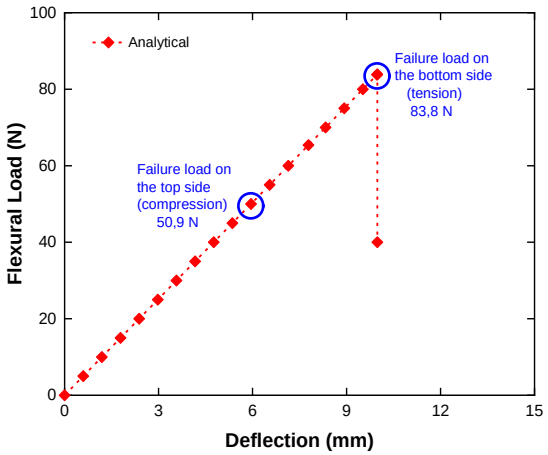



Figure 4.12. Analytical flexural load-deflection curve of MT1 plate obtained with the practical engineering approach

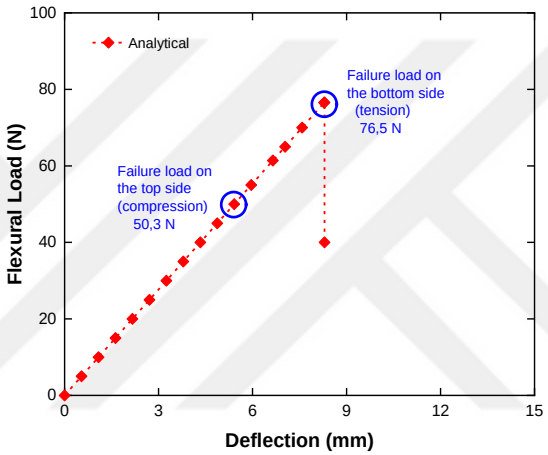



Figure 4.13. Analytical flexural load-deflection curve of MT2 plate obtained with the practical engineering approach

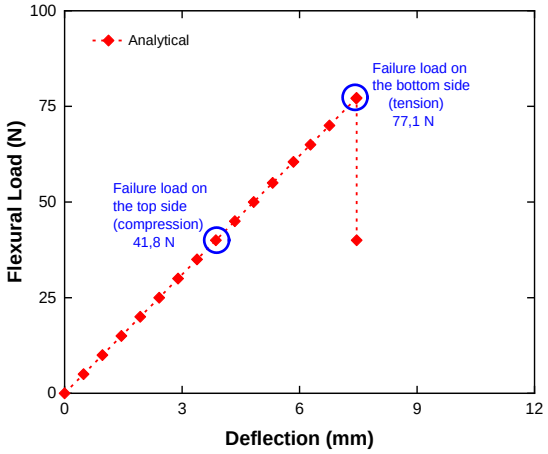



Figure 4.14. Analytical flexural load-deflection curve of MT3 plate obtained with the practical engineering approach

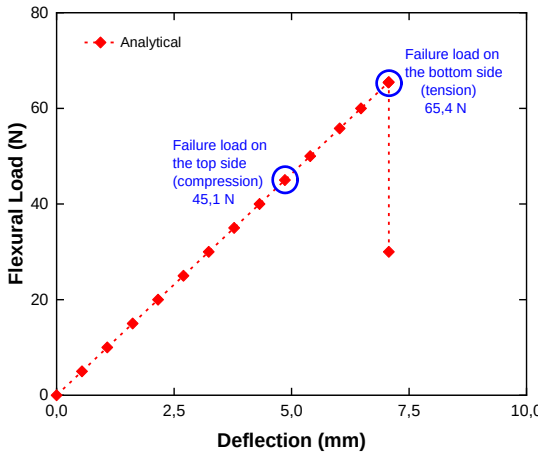



Figure 4.15. Analytical flexural load-deflection curve of MT4 plate obtained with the practical engineering approach

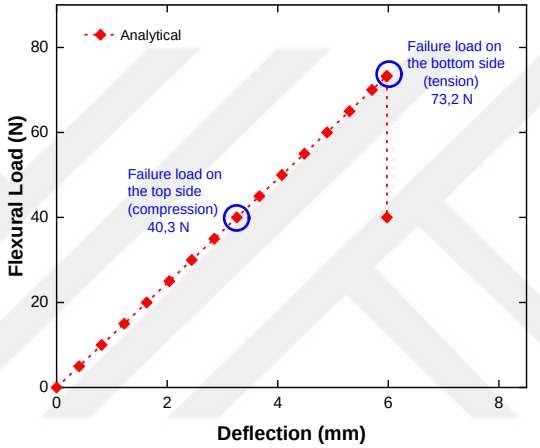



Figure 4.16. Analytical flexural load-deflection curve of MT5 plate obtained with the practical engineering approach

➢ Flexural modulus of elasticity

The flexural modulus ($E_{av}^{f}$) depends on the stiffness terms of longitudinal bending ($D_{11}, \delta_{11}$). The $E_{av}^{f}$ values of the beams were calculated by equation 3.48, and the results are presented in Table 4.7.

Table 4.7. Experimentally and analytically obtained flexural properties of four-ply woven plain fabric composite laminate beams

| **Laminate Codes** | **Composite Laminates and $V_f$** | | | **Results of the Practical Engineering Approach** | | |
|---|---|---|---|---|---|---|
| | $\mathbf{V_f^O}$ | $\mathbf{V_f^y}$ | $\mathbf{V_f^E}$ | $\mathbf{D_{11}^f}$ **(Nmm)** | $\boldsymbol{\delta_{11}^f}(\frac{\mathbf{1}}{\mathbf{Nmm}})$ | $\boldsymbol{E_{av}^f}$ **(GPa)** |
| MT1 | 0.34 | 0.52 | 0.26 | 4871 | 2.040 e-4 | 34.5 |
| MT2 | 0.38 | 0.60 | 0.30 | 3628 | 2.863 e-4 | 38.4 |
| MT3 | 0.43 | 0.68 | 0.34 | 3193 | 3.255 e-4 | 43.0 |
| MT4 | 0.45 | 0.35 | 0.35 | 2324 | 4.278 e-4 | 38.5 |
| MT5 | 0.50 | 0.39 | 0.39 | 2336 | 4.271 e-4 | 50.9 |

- Flexural internal stress distribution

The internal stress distribution inside the beams is assumed to be equal and in the same vectorial direction, according to Saint-Venant's principle, under tensile loads. Under bending loads, the values and vectorial directions of the internal stresses in the beam vary according to the position of the point relative to the neutral axis. Therefore, while the stress value is zero on the neutral axis, compressive stresses occur on the beam's upper side and tensile stresses on the lower side. The highest stresses occur on the top and bottom surfaces of the beam. For homogeneous beams, stresses increase outward from the neutral axis, and the highest stresses occur at the top and bottom surfaces of the beam. However, for fiber-reinforced composites, defined as inhomogeneous structures, the internal stress distribution does not increase linearly, and each layer is evaluated because each layer may have its structural differences, such as fiber material and orientation, that affect the stress-bearing capacity of the layer. Also, the layer's position on the neutral axis affects the stress it carries. Therefore, stress analysis is performed for each layer independently, and the internal stress distribution of the laminate is shown using the zig-zag method. The results of the stress analysis of each lamina as a cross-ply of the plain woven fabric composites designed in the study are presented in Table 4.8. Stress values were calculated with equation 3.49. The maximum $k_x$ value used in the equation was calculated according to the moment formed at the failure load of tensile side load value, assuming complete failure given in the curves in Figure 4.14-4.16, and Equation 3.47 was used. The stiffness values of each layer were calculated with equation 3.20, and the micromechanical properties were obtained from Table 4.1.

Table 4.8. Analytically obtained stress values on layer surfaces of plain woven fabric composite beams

| **Laminate Code** | **Plain Woven Layer** | **Cross-ply Layer** | **Layer surface** | **Z** | **z (mm)** | **Stress (MPa)** |
|---|---|---|---|---|---|---|
| MT1 | 1 | 0 | top | $Z_1$ | -0.588 | 897 |
| | | | bottom | $Z_2$ | -0.441 | 673 |
| | | 90 | top | $Z_2$ | -0.441 | 47 |
| | | | bottom | $Z_3$ | -0.294 | 31 |
| | 2 | 0 | top | $Z_3$ | -0.294 | 448 |
| | | | bottom | $Z_4$ | -0.147 | 224 |
| | | 90 | top | $Z_4$ | -0.147 | 15 |
| | | | bottom | $Z_5$ | 0 | 0 |
| | *Neutral axis (Z=0, Stress=0)* | | | | | |
| | 3 | 0 | top | $Z_5$ | 0 | 0 |
| | | | bottom | $Z_6$ | 0.147 | -224 |
| | | 90 | top | $Z_6$ | 0.147 | -15 |
| | | | bottom | $Z_7$ | 0.294 | -31 |
| | 4 | 0 | top | $Z_7$ | 0.294 | -448 |
| | | | bottom | $Z_8$ | 0.441 | -673 |
| | | 90 | top | $Z_8$ | 0.441 | -47 |
| | | | bottom | $Z_9$ | 0.588 | -63 |
| MT2 | 1 | 0 | top | $Z_1$ | -0,515 | 1087 |
| | | | bottom | $Z_2$ | -0,38625 | 815 |
| | | 90 | top | $Z_2$ | -0,38625 | 49 |
| | | | bottom | $Z_3$ | -0,2575 | 33 |
| | 2 | 0 | top | $Z_3$ | -0,2575 | 543 |
| | | | bottom | $Z_4$ | -0,12875 | 271 |
| | | 90 | top | $Z_4$ | -0,12875 | 16 |
| | | | bottom | $Z_5$ | 0 | 0 |
| | *Neutral axis (Z=0, Stress=0)* | | | | | |
| | 3 | 0 | top | $Z_5$ | 0 | 0 |
| | | | bottom | $Z_6$ | 0,12875 | -271 |
| | | 90 | top | $Z_6$ | 0,12875 | -16 |
| | | | bottom | $Z_7$ | 0,2575 | -33 |
| | 4 | 0 | top | $Z_7$ | 0,2575 | -543 |
| | | | bottom | $Z_8$ | 0,38625 | -815 |
| | | 90 | top | $Z_8$ | 0,38625 | -49 |
| | | | bottom | $Z_9$ | 0,515 | -66 |
| MT3 | 1 | 0 | top | $Z_1$ | -0,475 | 1059 |
| | | | bottom | $Z_2$ | -0,35625 | 794 |
| | | 90 | top | $Z_2$ | -0,35625 | 48 |
| | | | bottom | $Z_3$ | -0,2375 | 32 |
| | 2 | 0 | top | $Z_3$ | -0,2375 | 529 |
| | | | bottom | $Z_4$ | -0,11875 | 264 |
| | | 90 | top | $Z_4$ | -0,11875 | 17 |
| | | | bottom | $Z_5$ | 0 | 0 |

Table 4.8. continued.

| | | | | | | |
|---|---|---|---|---|---|---|
| MT3 | *Neutral axis (Z=0, Stress=0)* | | | | | |
| | 3 | 0 | top | $Z_5$ | 0 | 0 |
| | | | bottom | $Z_6$ | 0,11875 | -264 |
| | | 90 | top | $Z_6$ | 0,11875 | -17 |
| | | | bottom | $Z_7$ | 0,2375 | -32 |
| | 4 | 0 | top | $Z_7$ | 0,2375 | -529 |
| | | | bottom | $Z_8$ | 0,35625 | -794 |
| | | 90 | top | $Z_8$ | 0,35625 | -48 |
| | | | bottom | $Z_9$ | 0,475 | -64 |
| MT4 | 1 | 0 | top | $Z_1$ | -0.45 | 1157 |
| | | | bottom | $Z_2$ | -0.3375 | 868 |
| | | 90 | top | $Z_2$ | -0.3375 | 53 |
| | | | bottom | $Z_3$ | -0.225 | 35 |
| | 2 | 0 | top | $Z_3$ | -0.225 | 579 |
| | | | bottom | $Z_4$ | -0.1125 | 289 |
| | | 90 | top | $Z_4$ | -0.1125 | 16 |
| | | | bottom | $Z_5$ | 0 | 0 |
| | *Neutral axis (Z=0, Stress=0)* | | | | | |
| | 3 | 0 | top | $Z_5$ | 0 | 0 |
| | | | bottom | $Z_6$ | 0.1125 | -289 |
| | | 90 | top | $Z_6$ | 0.1125 | -16 |
| | | | bottom | $Z_7$ | 0.225 | -35 |
| | 4 | 0 | top | $Z_7$ | 0.225 | -579 |
| | | | bottom | $Z_8$ | 0.3375 | -868 |
| | | 90 | top | $Z_8$ | 0.3375 | -53 |
| | | | bottom | $Z_9$ | 0.45 | -70 |
| MT5 | 1 | 0 | top | $Z_1$ | -0.41 | 1155 |
| | | | bottom | $Z_2$ | -0.3075 | 866 |
| | | 90 | top | $Z_2$ | -0.3075 | 50 |
| | | | bottom | $Z_3$ | -0.205 | 33 |
| | 2 | 0 | top | $Z_3$ | -0.205 | 577 |
| | | | bottom | $Z_4$ | -0.1025 | 288 |
| | | 90 | top | $Z_4$ | -0.1025 | 16 |
| | | | bottom | $Z_5$ | 0 | 0 |
| | *Neutral axis (Z=0, Stress=0)* | | | | | |
| | 3 | 0 | top | $Z_5$ | 0 | 0 |
| | | | bottom | $Z_6$ | 0.1025 | -288 |
| | | 90 | top | $Z_6$ | 0.1025 | -16 |
| | | | bottom | $Z_7$ | 0.205 | -33 |
| | 4 | 0 | top | $Z_7$ | 0.205 | -577 |
| | | | bottom | $Z_8$ | 0.3075 | -866 |
| | | 90 | top | $Z_8$ | 0.3075 | -50 |
| | | | bottom | $Z_9$ | 0.41 | -67 |

The internal stresses calculated for the beams in Table 4.8 are shown in Figures 4.17-4.21 according to z-axis coordinates by the zig-zag method. At the layer interfaces there were sudden stress transitions between the layers in an increasing or decreasing manner. However, since each layer is considered homogeneous, the stress change between the top and bottom surfaces changed

linearly. It is clear from the figures and Table 4.8 that warp tows assumed to be $0^0$ carry the highest stress while fill tows assumed to be $90^0$ carry the lowest stress.

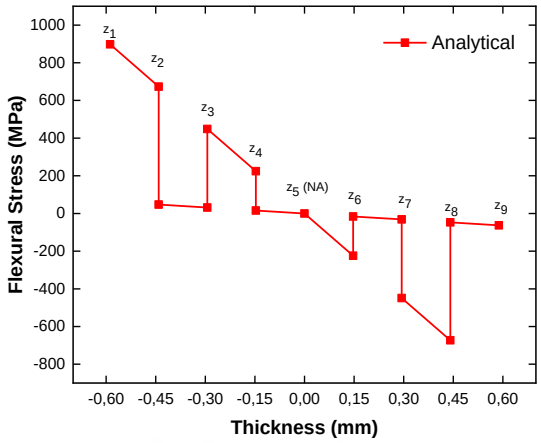



Figure 4.17. Internal stress distribution along the thickness of the MT1 plate was obtained with the practical engineering approach

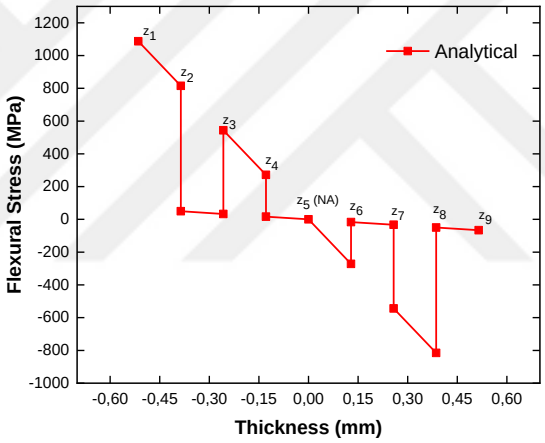



Figure 4.18. Internal stress distribution along the thickness of the MT2 plate was obtained with the practical engineering approach

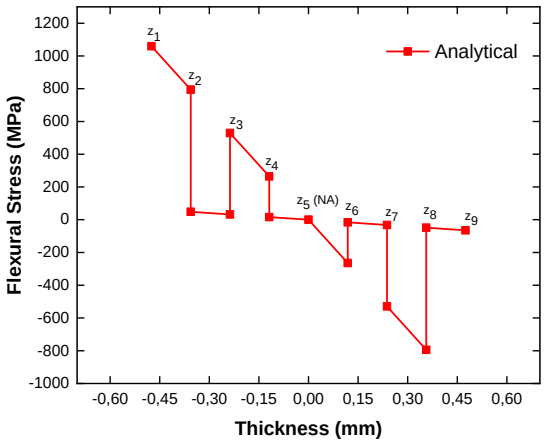



Figure 4.19. Internal stress distribution along the thickness of the MT3 plate was obtained with the practical engineering approach

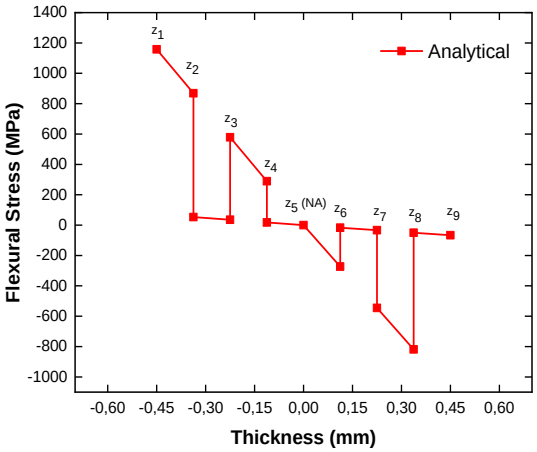



Figure 4.20. Internal stress distribution along the thickness of the MT4 plate was obtained with the practical engineering approach

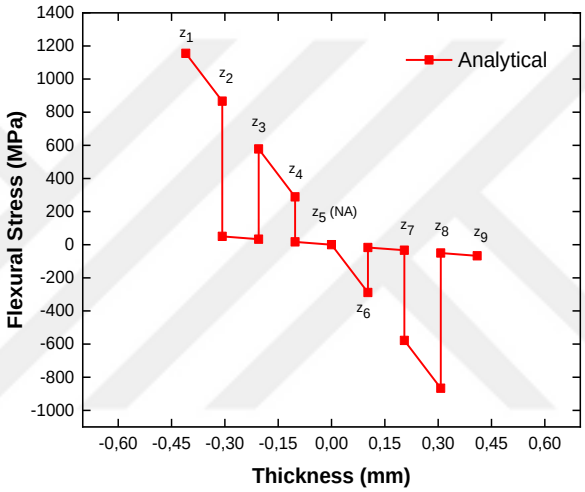



Figure 4.21. Internal stress distribution along the thickness of the MT5 plate was obtained with the practical engineering approach

### 4.1.2. The results of sandwich beam models

The properties of sandwich beams consisting of plain woven fabric composite facesheet and PVC foam core were calculated using the engineering approaches developed in Chapter 3. These properties, such as sandwich bending stiffness, linear elastic limit load (core shear), load-deflection curves in the linear region, failure mode, and maximum carrying load, were determined with developed engineering approaches according to three-point bending load conditions.

*Analytical flexural stiffness results of sandwich beams*

The mechanical properties of four-layer plain woven fabric composite plates were predicted in the practical engineering approach based on the volume fraction values obtained from five different manufacturing methods. The bending stiffness terms of a sandwich structure are calculated by equation 3.58 and are presented in Table 4.9.

The core materials' thicknesses were assumed to be 10 mm, 20 mm, and 30 mm according to the cores used in the sandwich configurations in Table 3.4. Face material was assumed to be produced from composite plates with eight and four layers. The stiffness properties of the four-ply composite plates were obtained from Tables 4.1 and 4.2. The stiffness properties of the eight-ply plate assumed as a sixteen-layer cross-ply were calculated with Equations 3.15 and 3.29. The width of the sandwich beams was also taken to be 50 mm.

Table 4.9. Analytical results of the flexural stiffness sandwich plates for the five manufacturing methods

| **Prod. method** | **Sand. Conc.** | **Core thick.** | **Facesheet thickness** | **$(t_c+t_f)/2$** | **Sand. width** | **Facesheet stiffness terms** | | **Sandwich flexural Stiffness terms** | |
|---|---|---|---|---|---|---|---|---|---|
| | | **$t_c$** | **$t_f$** | **d** | **b** | **$A_{11}$** | **$D_{11}$** | **$D_s^f$** | **$D_s^f b$** |
| | | **mm** | **mm** | **mm** | **mm** | **N/mm$^2$** | **N.mm** | **N.mm** | **N.mm$^2$** |
| | | | | | | **x10$^4$** | | **x10$^5$** | **x10$^7$** |
| MT1 | Con1 | 10 | 1.19 | 5.595 | 50 | 4.16 | 4871 | 26.14 | 13.07 |
| | Con2 | 20 | 1.19 | 10.595 | 50 | 4.16 | 4871 | 93.49 | 46.74 |
| | Con3 | 30 | 1.19 | 15.595 | 50 | 4.16 | 4871 | 202.44 | 101.20 |
| | Con4 | 20 | 2.38 | 11.190 | 50 | 8.32 | 39276 | 209.14 | 104.60 |
| MT2 | Con5 | 10 | 1.03 | 5.515 | 50 | 4.10 | 3628 | 25.03 | 12.51 |
| | Con6 | 20 | 1.03 | 10.515 | 50 | 4.10 | 3628 | 90.82 | 45.41 |
| | Con7 | 30 | 1.03 | 15.515 | 50 | 4.10 | 3628 | 197.65 | 98.82 |
| | Con8 | 20 | 2.06 | 11.030 | 50 | 8.21 | 28880 | 200.30 | 100.10 |
| MT3 | Con9 | 10 | 0.95 | 5.475 | 50 | 4.25 | 3193 | 25.51 | 12.75 |
| | Con10 | 20 | 0.95 | 10.475 | 50 | 4.25 | 3193 | 93.22 | 46.61 |
| | Con11 | 30 | 0.95 | 15.475 | 50 | 4.25 | 3193 | 203.37 | 101.70 |
| | Con12 | 20 | 1.90 | 10.950 | 50 | 8.49 | 25543 | 204.10 | 102.10 |
| MT4 | Con13 | 10 | 0.90 | 5.450 | 50 | 4.13 | 2324 | 24.60 | 12.30 |
| | Con14 | 20 | 0.90 | 10.450 | 50 | 4.13 | 2324 | 90.33 | 45.16 |
| | Con15 | 30 | 0.90 | 15.450 | 50 | 4.13 | 2324 | 197.40 | 98.70 |
| | Con16 | 20 | 1.80 | 10.900 | 50 | 8.27 | 22321 | 196.91 | 98.45 |
| MT5 | Con17 | 10 | 0.82 | 5.410 | 50 | 4.17 | 2336 | 24.45 | 12.22 |
| | Con18 | 20 | 0.82 | 10.410 | 50 | 4.17 | 2336 | 90.42 | 45.21 |
| | Con19 | 30 | 0.82 | 15.410 | 50 | 4.17 | 2336 | 198.09 | 99.04 |
| | Con20 | 20 | 1.64 | 10.820 | 50 | 8.34 | 18630 | 195.64 | 97.82 |

*Modified analytical model results for elastic limits (Core yield load) of the sandwich beams*

The core yield force is one of the most critical load thresholds because the force-deflection curve of the sandwich beam is in the linear region up to this threshold. However, when this loading threshold is exceeded, the sandwich beam loses its elastic properties, such as flexural stiffness. Therefore, the core yield force must be predicted well for the sandwich beam to operate in the linear region. This force value could be determined with the approach developed by Soden. Although this method could make accurate predictions, it was insufficient for fiber-reinforced composite faces. This is because the approach depends on the fiber-reinforced composite plate's elastic modulus, which could be obtained from experimental tests or the properties of similar face plates in the literature. In the present study, Equation 2.21 was modified to predict the core yield strength of the

sandwich with composite face-sheets analytically. The final form of the equation is presented in Equation 3.71. The calculated core yield force values are presented in Table 4.10 for the sandwich configurations planned to be produced, and details are given in Table 3.4. The mechanical properties of the core material were obtained from Table 3. Facesheet width was 50 mm. Face layer longitudinal bending stiffness terms ($D_{11}$) values were taken from Table 4.9. Since the planned sandwiches are to be produced by vacuum bagging with a high vacuum capacity pump, the MT5 composite properties are assumed to be the same as the sandwich beam face materials.

Table 4.10. Analytical core yield force results of sandwich configurations

| **Sandwich configuration** | **Configuration code** | **Core yield Load ( $P_1$, N)** |
|---|---|---|
| 1 | D48T10F4L100 | 378.90 |
| 2 | D48T20F4L100 | 450.55 |
| 3 | D48T30F4L100 | 499.61 |
| 4 | D48T10F4L250 | 378.90 |
| 5 | D48T20F4L250 | 450.55 |
| 6 | D48T30F4L250 | 499.61 |
| 7 | D75T10F4L100 | 643.06 |
| 8 | D75T20F4L100 | 764.73 |
| 9 | D75T30F4L100 | 846.30 |
| 10 | D75T10F4L250 | 643.06 |
| 11 | D75T20F4L250 | 764.73 |
| 12 | D75T30F4L250 | 846.30 |
| 13 | D130T10F4L100 | 1309.99 |
| 14 | D130T20F4L100 | 1557.84 |
| 15 | D130T30F4L100 | 1724.03 |
| 16 | D130T10F4L250 | 1309.99 |
| 17 | D130T20F4L250 | 1557.84 |
| 18 | D130T30F4L250 | 1724.03 |
| 19 | D48T20F8L100 | 729.03 |
| 20 | D75T20F8L100 | 1438.19 |
| 21 | D130T20F8L100 | 2902.52 |

From the table, it can be seen that the core yield loads are equal at the sandwiches with the same properties except for the span length. Results show that the force does not depend on the span length. The core yield loads increased with core thickness. Moreover, the load increased with the increase in core material density. By increasing the thickness of the face layer or by increasing the number of layers, $D_{11}$ was increased and there was an increase in the loads. For example, for the D75t20F4L100 configuration, the load is 764 N. To increase the load capacity of this configuration at the same span length, it may be preferable to increase the core thickness, face thickness, and core density. For these modifications, the load values for the D75T30F4L100, D75T20F8L100, and D130T20F4L100 configurations are 846.30 N, 1438.19 N, and 1557.84 N, respectively. When the results are analyzed, the improvement made by increasing the $D_{11}$ with facesheet thickness or increasing the core density resulted in higher loading values.

*Analytical load mid-span deflection results of sandwich beams in the elastic region*

The load-deflection curves of the sandwich beams using Equation 3.68 for three-point bending loading are presented in Figures 4.22-4.28. The curves are plotted up to the core yield loads where the linear region ends. The curves of the three sandwich configurations are presented in the figures. Figures 4.22-4.27 show the results with the same parameters except for the core thickness, while Figure 4.28 is for the eight-layer facesheet.

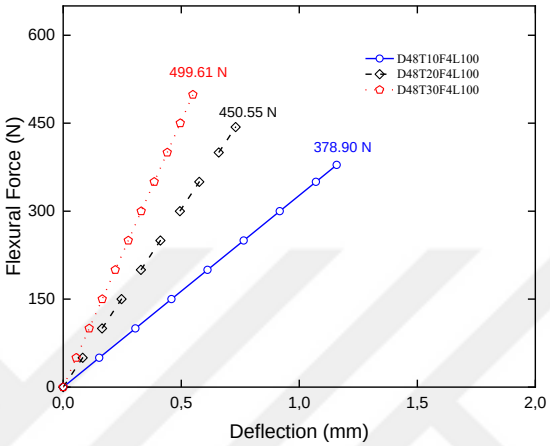



Figure 4.22. Load-displacement curves of sandwiches designed with 48 kg/m$^3$ density core and 4-ply plain woven fabric composite at 100 mm span range under three-point bending

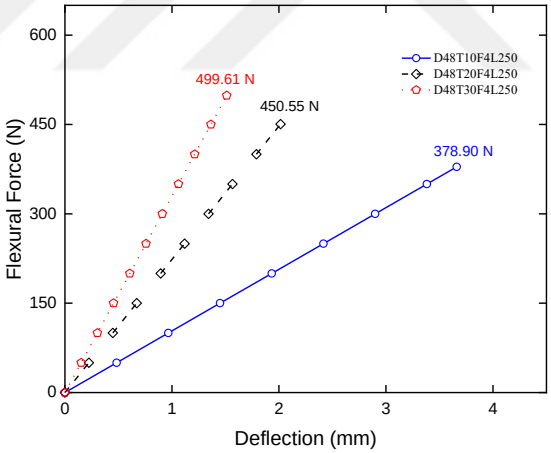



Figure 4.23. Load-displacement curves of sandwiches designed with 48 kg/m$^3$ density core and 4-ply plain woven fabric composite at 250 mm span range under three-point bending

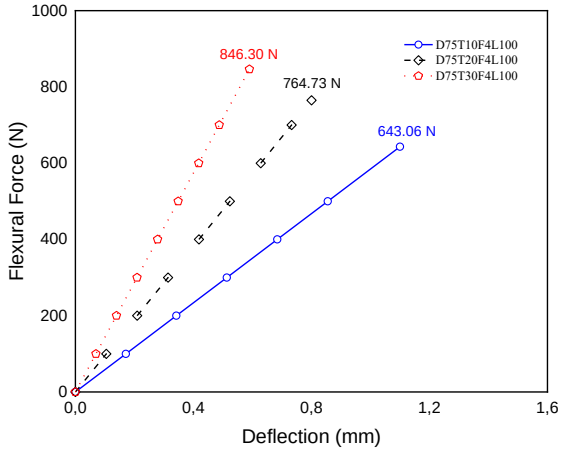



Figure 4.24. Load-displacement curves of sandwiches designed with 80 kg/m$^3$ density core and 4-ply plain woven fabric composite at 100 mm span range under three-point bending

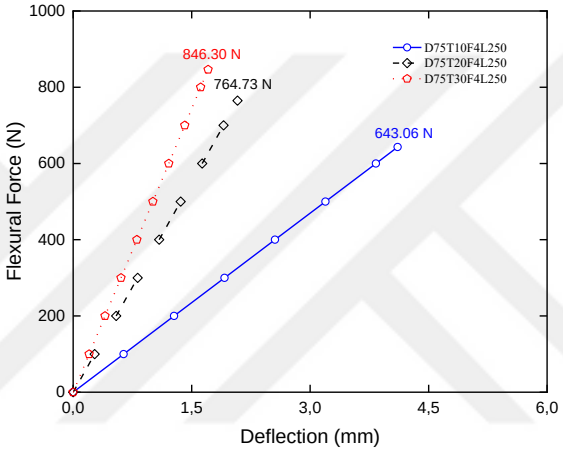



Figure 4.25. Load-displacement curves of sandwiches designed with 80 kg/m$^3$ density core and 4-ply plain woven fabric composite at 250 mm span range under three-point bending

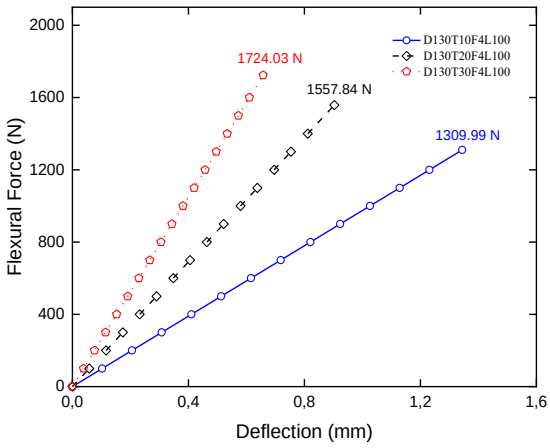



Figure 4.26. Load-displacement curves of sandwiches designed with 130 kg/m$^3$ density core and 4-ply plain woven fabric composite at 100 mm span range under three-point bending

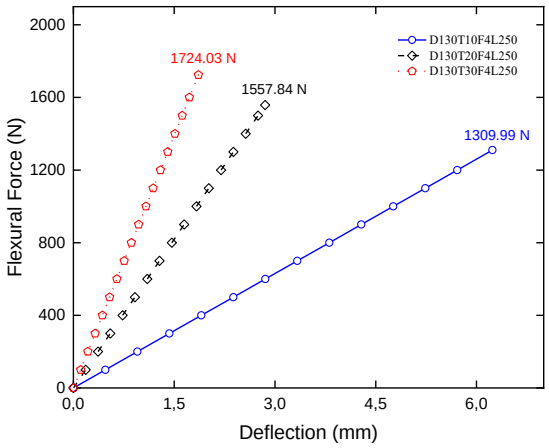



Figure 4.27. Load-displacement curves of sandwiches designed with 130 kg/m$^3$ density core and 4-ply plain woven fabric composite at 250 mm span range under three-point bending

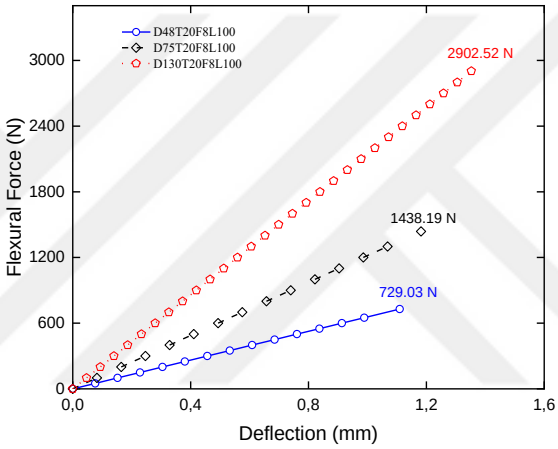



Figure 4.28. Load-displacement curves of sandwiches designed with 20 mm thickness cores and 8-ply plain woven fabric composite at 100 mm span range under three-point bending

The figures show that the load-deflection characteristics of any sandwich configuration (composed of a composite facesheet) for the linear region can be obtained simply with the developed engineering approach and the modified equation giving the core yield load. Thus, designing a sandwich beam according to the loading and boundary conditions is possible. In this design procedure, a sandwich was not designed by separately producing the facesheet, performing mechanical tests, and then collecting the data obtained.

*Analytical results of the sandwich failure loads*

Although sandwich beams lose their linear properties when the core yield load capacity is reached, they continue to carry the load with a nonlinear increase. They fail when they reach the maximum load they can carry. The sandwich structure fails in different failure modes depending on material type, size, and span length. Due to the characteristics of the composite and PVC foam materials referenced in the study, the sandwich beams given in the configurations are not expected

to fail in face yield and wrinkling failure modes. Core shear or indentation failure usually occurs in sandwich beams formed from such materials. Therefore, the sandwich configurations designed in this study were assumed to fail in core shear or indentation failure modes.

- Core shear loads of sandwich beams

Deflection depends on the bending stiffness of the sandwich due to the elastic properties of the face material and the shear modulus of the core material. The core fails when the load values reach the shear strength of the core material. The core shear failure mode depends on the mechanical and cross-sectional area of the core material; the core shear maximum load is calculated using Equation 2.18., and the values are presented in Table 4. 11.

- The results of sandwich indentation loads obtained with the modified analytical model

The estimated maximum indentation loads of the sandwich configurations in the study were calculated with the modified equation 3.74. The results are given in Table 4.11.

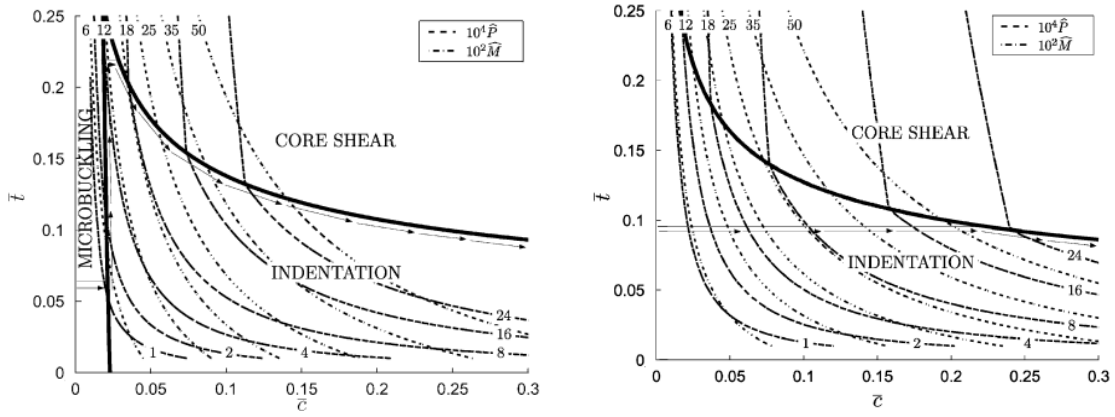
- The decision of failure mode of sandwich beams

The results of the maximum loads that the sandwich configurations can carry in core shear and indentation failure modes are presented in Table 4.11. The smallest load value from the two load results was selected when deciding whether a selected configuration fails in core shear or indentation failure mode. When the configuration's failure mode and load results are analyzed, the loads (core shear and indentation) calculated for the D48T10F4L250 and D75T10F4L100 configurations are very close (differences between 1.2 and 1.6 percent). Therefore, the failure modes of these configurations are in the indentation and core shear transition zone, and it is unclear in which mode they fail. The results obtained from the configurations show that the core shear forces varied with core thickness and core material. However, core thickness and core material also influenced indentation loads, while span length and facesheet thicknesses also affected the calculations. Using a higher-density core and increasing the thickness of the core increased both failure mode loads. Increasing the face thickness increased the indentation forces drastically while increasing the span length decreased them. These changes in design parameter resulted in failure mode variations between similar configurations. For example, the core thickness changed between configurations 1 and 2. The facesheet thickness is different between configurations 2 and 19. For example, the core thickness is different between configurations 1 and 2. The thickness is different between configurations 2 and 19. The span length is different between configurations 1 and 4. Finally, the core density is different between configurations 1 and 13. Due to all these changes, the failure modes of the configurations have changed, as represented in Table 4.11.

Table 4.11. Analytical failure mode force results and expected failure modes of sandwich configurations

| Sandwich conf. | Configuration code | Core Shear Load $P_1$ (N) | Indentation Load $P_2$ (N) | Expected Failure Mode |
|---|---|---|---|---|
| 1 | D48T10F4L100 | 525 | 703.90 | Core Shear |
| 2 | D48T20F4L100 | 1050 | 886.81 | Indentation |
| 3 | D48T30F4L100 | 1575 | 1015.15 | Indentation |
| 4 | D48T10F4L250 | 525 | 518.61 | Indentation or Core Shear |
| 5 | D48T20F4L250 | 1050 | 653.41 | Indentation |
| 6 | D48T30F4L250 | 1575 | 747.97 | Indentation |
| 7 | D75T10F4L100 | 1100 | 1117.31 | Indentation or Core Shear |
| 8 | D75T20F4L100 | 2200 | 1407.72 | Indentation |
| 9 | D75T30F4L100 | 3300 | 1611.45 | Indentation |
| 10 | D75T10F4L250 | 1100 | 823.25 | Indentation |
| 11 | D75T20F4L250 | 2200 | 1159.42 | Indentation |
| 12 | D75T30F4L250 | 3300 | 1327.20 | Indentation |
| 13 | D130T10F4L100 | 2100 | 1982.57 | Indentation |
| 14 | D130T20F4L100 | 4200 | 2497.88 | Indentation |
| 15 | D130T30F4L100 | 6600 | 3145.59 | Indentation |
| 16 | D130T10F4L250 | 2100 | 1460.77 | Indentation |
| 17 | D130T20F4L250 | 4200 | 1840.46 | Indentation |
| 18 | D130T30F4L250 | 6600 | 2106.80 | Indentation |
| 19 | D48T20F8L100 | 1050 | 1877.63 | Core shear |
| 20 | D75T20F8L100 | 2200 | 3103.50 | Core shear |
| 21 | D130T20F8L100 | 4200 | 4990.65 | Core shear |

One of the methods to roughly estimate the failure modes of sandwiches is failure mechanism maps. (Ashby et al., 2002) these maps were first developed for sandwiches designed from metallic face and metal foam core materials. Later, (Steeves and Fleck, 2004a) developed sandwiches designed from composite face and high and medium-density PVC foam core materials with the maps given in Figure 4.29. Maps in the figure are created with horizontal axes based on core thickness/span length ($\bar{c}$) ratio and vertical axes based on facesheet thickness/core thickness ($\bar{t}$) ratio. The results of the current study given in Table 4.11 can be interpreted in general according to these failure maps. Since $\bar{c}$ decreases as the span length increases, a sandwich fractured in core shear will fracture in indentation failure mode. For example, the sandwich in configuration 1 failed in core shear mode, while in configuration 4, where the span length was increased, it failed in the transition zone between indentation and core shear. Configuration 7 is in the transition zone of core shear and indentation failure, while configuration 10, with a longer span length, is in indentation failure. Moreover, when the thickness of the face is increased, $\bar{t}$ will increase, and a sandwich core that fails in indentation will fail in shear failure mode. Again, judging from the results in Table 4.11, configurations 2,8,14 were predicted to fail in indentation mode. Configurations 19, 20, and 21 are the same, only with increased facesheet thickness. These configurations were predicted to have core shear failure. If the core thickness is increased, the value of $\bar{t}$ will decrease, and a transition from core shear to indentation failure mode is expected. Such a situation was predicted in the results for the transition from configuration 1 to 2.




(a) (b)

Figure 4.29. Failure mechanism maps of sandwich beams designed from (a) high-density and (b) medium-density PVC foam core (Steeves and Fleck, 2004b)

The results of the Table and the maps drawn from the literature show that the transition from a sandwich's undesired to desired failure mode is possible. The dimensional parameters that affect these are span length, facesheet thickness, and core thickness. Moreover, the failure modes predicted for the configurations by the preferred method in Table 4.11 confirms itself with the examples described by the relationship presented in the maps.

## 4.2. Comparison and validation of developed analytical engineering approaches with experimental results and models in the literature

Tests of laboratory-produced sandwich and composite plates were conducted to test the reliability and accuracy of the engineering approaches developed in this study. These tests are tensile and three-point bending tests for the composite plates. Three-point bending tests were performed for the sandwiches whose configuration details are in Table 3.4. Compression tests were also conducted on PVC foam core materials for sandwiches. Experimental results were compared with the results obtained from the engineering approaches developed for the composite plate and sandwich beam for verification. Comparisons are also made with the reliable models available in the literature.

### 4.2.1. Comparison of the results of practical engineering approach for plain woven fabric composite face layer

The Axial ($A_{11}^s$) and bending ($D_{11}^s$) stiffnesses of single-layer plain woven fabric composite results were compared using both the practical engineering approach and SAM. Tensile specimens obtained from composite plates were tested. A total of twenty-five tensile test results were obtained, five from each group. The analytical results of the developed approach were compared with the experimental results.

*Comparison of mechanical properties obtained from practical engineering approach with the literature*

In this study, axial ($A_{11}^s$) and bending ($D_{11}^s$) stiffness of single-ply plain woven fabric composite was determined by applying both SAM and CLT (cross-ply (0-90) is assumed). The same yarn volume fraction was considered for two approaches. The results are presented and compared in Tables 4.12 and 4.13.

Table 4.12. Axial Stiffness ($A_{11}^s$) of UD cross-play (0-90) and single-ply plain woven fabric composite (lamina)

| **Sample Code** | $\mathbf{V_f^o}$ | $\mathbf{V_f^y}$ | **UD cross-ply $\mathbf{A_{11}^s}$ (Nm) (a)** | **WPFC $\mathbf{A_{11}^s}$ (Nm) (b)** | **a/b** |
|---|---|---|---|---|---|
| MT1 | 0.34 | 0.52 | 2.14 e7 | 1.02 e7 | 2.09 |
| MT2 | 0.38 | 0.60 | 2.11 e7 | 1.01 e7 | 2.07 |
| MT3 | 0.43 | 0.68 | 2.15 e7 | 1.07 e7 | 2.01 |
| MT4 | 0.45 | 0.70 | 2.11 e7 | 1.06 e7 | 1.98 |
| MT5 | 0.50 | 0.78 | 2.10 e7 | 1.10 e7 | 1.90 |

Table 4.13. Bending Stiffness ($D_{11}^s$) of UD cross-play (0-90) and single-ply plain woven fabric composite (lamina)

| **Sample Code** | $\mathbf{V_f^o}$ | $\mathbf{V_f^y}$ | **UD cross-ply $\mathbf{D_{11}^s}$ (Nm) (a)** | **WPFC $\mathbf{D_{11}^s}$ (Nm) (b)** | **a/b** |
|---|---|---|---|---|---|
| MT1 | 0.34 | 0.52 | 1.48 e-1 | 7.60 e-2 | 1.94 |
| MT2 | 0.38 | 0.60 | 1.24 e-1 | 5.96 e-2 | 2.08 |
| MT3 | 0.43 | 0.68 | 1.06 e-1 | 5.25 e-2 | 2.01 |
| MT4 | 0.45 | 0.70 | 8.57 e-2 | 4.59 e-2 | 1.86 |
| MT5 | 0.50 | 0.78 | 7.30 e-2 | 3.83 e-2 | 1.90 |

When both Tables are analyzed, it is seen that the a/b ratio is approximately two. This ratio indicates a two-to-one ratio between the stiffness properties of cross-ply and plain woven fabric composite plates with equal yarn volume fractions. This is attributed to the undulation angle and the elliptical cross-sectional area of the yarn negatively affect the stiffness. The proportional comparisons in Tables 4.12 and 4.13 inspire a new approach called a practical engineering approach (PEA). Thus, the stiffness values of the single-ply composite plate are presented in Tables 4.14 and 4.15 using the reliable SAM model from the literature and the PEA. The values obtained from both models are compared in percentages in both tables. The percentage differences are less than five percent. This result shows that the model developed in this study can be an alternative to the existing models, and its solution depends on the known and highly established CLT.

Table 4.14. Comparison of SAM and the practical approach for axial stiffness ($A_{11}^{s}$) of single-ply plain woven fabric composite plate

| **Sample Code** | $\mathbf{V_f^O}$ | $\mathbf{V_f^y}$ | $\mathbf{V_f^E}$ | **Slice Array Model $A_{11}^{s}$(N/m) x10$^7$** | **Practical Approach $A_{11}$ (N/m) x10$^7$** | **Difference (%)** |
|---|---|---|---|---|---|---|
| MT 1 | 0.34 | 0.52 | 0.26 | 1.023 | 1.070 | 4.5 |
| MT 2 | 0.38 | 0.60 | 0.30 | 1.018 | 1.050 | 3.4 |
| MT 3 | 0.43 | 0.68 | 0.34 | 1.072 | 1.080 | 0.4 |
| MT 4 | 0.45 | 0.70 | 0.35 | 1.065 | 1.054 | 1.1 |
| MT 5 | 0.50 | 0.78 | 0.39 | 1.101 | 1.050 | 4.7 |

Table 4.15. Comparison of bending stiffness ($D_{11}^{s}$) of single-ply plain woven fabric composite plate based on SAM and the developed practical approach

| **Sample Code** | $\mathbf{V_f^O}$ | $\mathbf{V_f^y}$ | $\mathbf{V_f^E}$ | **Slice Array Model $D_{11}^{s}$(Nm) x10$^{-2}$** | **Practical Approach $D_{11}$(Nm) x10$^{-2}$** | **Difference (%)** |
|---|---|---|---|---|---|---|
| MT1 | 0.34 | 0.52 | 0.26 | 7.60 | 7.95 | 4.4 |
| MT2 | 0.38 | 0.60 | 0.30 | 5.96 | 6.22 | 4.2 |
| MT3 | 0.43 | 0.68 | 0.34 | 5.25 | 5.28 | 0.4 |
| MT4 | 0.45 | 0.70 | 0.35 | 4.59 | 4.54 | 1.1 |
| MT5 | 0.50 | 0.78 | 0.39 | 3.83 | 3.67 | 4.3 |

The proposed approach utilized the strength data by providing a pair of components: a warp and a fill ($\sigma_{warp}^{T}$ and $\sigma_{fill}^{T}$). The strength values are computed according to the Tsai Wu failure theory, which indicates that the fill and warp are assumed to be $90^0$ and $0^0$, respectively. While the plain woven fabric composite can still carry loads in its longitudinal direction, fractures appear in the transverse section. Due to the residual stresses, the structure eventually breaks before reaching its maximum strength. Instead of giving a single breaking point for the composite, this approach considers the various safe and unsafe loading ranges. The structure will remain in the safe range until the value of the fill yarn strength. Even if the warp yarn carries a load, the composite will still break before it reaches its breaking point. Wang et al. (2019) presented a model designed to calculate the strength of plain weave fabrics. They assumed that the composite was a three-layer structure. Depending on the empirical approach, the model used the effective fiber volume fraction to determine its tensile strength. The coefficients for the strength and stiffness of fill and warp yarns were also included in the calculations. They were able to determine the coefficients by conducting tensile test procedures. They then used these in their suggested model. Table 4.9 summarizes the literature examples (Naik and Ganesh, 1996; Tabiei et al., 2003; Wang et al., 2018; Zhen, 2013) that were derived from the experiments carried out using the suggested model and those presented by (Wang et al., 2019). In addition, the study results were also obtained using the practical engineering approach suggested by the present thesis in Table 4.16. As can be seen from the table, the experimental strength results given in the literature are between the warp and fill strength values, determined by the practical engineering approach.

Table 4.16. Comparison of tensile strength values between the experimental literature examples and the present approach

| **Literature Examples**[Wang et al., 2019] | | | | **Application of the present practical approach** | | |
|---|---|---|---|---|---|---|
| **Material** | $\mathbf{V_f^O}$ | $\boldsymbol{\sigma_{exp}^T}$ **N/mm²** | $\boldsymbol{\sigma_{model}^T}$ **N/mm²** | $\mathbf{V_f^E}$ | $\boldsymbol{\sigma_{warp}^T}$ **N/mm²** | $\boldsymbol{\sigma_{fill}^T}$ **N/mm²** |
| EL306/T300-3K[Wang et al., 2019] | 0.52 | 639.5 | 617 | 0.40 | 789 | 348 |
| 1004/T300-3K[Zhen, 2013] | 0.40 | 476 | 434 | 0.31 | 595 | 435 |
| LY556/E-glass[Naik and Ganesh, 1996] | 0.43 | 320 | 332 | 0.33 | 377 | 177 |
| Vinylester/E-glass[Tabiei et al., 2003] | 0.22 | 133 | 142 | 0.17 | 283 | 110 |

*Comparison of analytical results under axial loading obtained from practical engineering approach with experimental results*

This section compares the engineering approach with experimental results to ensure its accuracy and reliability. These comparisons include tensile load-deflection curves, stress-strain curves, elastic modulus, and strengths.

- Tensile load-extension curves

Figure 4.30 to Figure 4.34 show the force-extension curves obtained from tensile tests of the composite plates according to ASTM D 3039. The results of five tests for each production method are presented in the figures. The four-ply fabric test specimens reached to maximum loads between 7500 N and 9000 N. The extension of the specimens was also between 1.8 mm and 2.4 mm. All composite test specimens showed brittle material characteristics, and all curves are of a linear form. The specimens overlapped until micro fractures and cracks occurred, after which the linear curves had minimal differences and divergences. There are also differences in the maximum load values that specimens can reach. These are due to the differences in stress distribution on the warp and fill yarns. As the specimens begin to fail at loads that the fill yarns can carry, they try to reach the load level that the warp yarns can carry. However, due to the differences in the stress distributions occurring in the fill yarns, the maximum load levels that the specimens can carry are different.

Figures also show the force-extension curves obtained from the practical engineering approach. The experimental and analytical curves overlap. Maximum loads are also presented in Table 4.17.

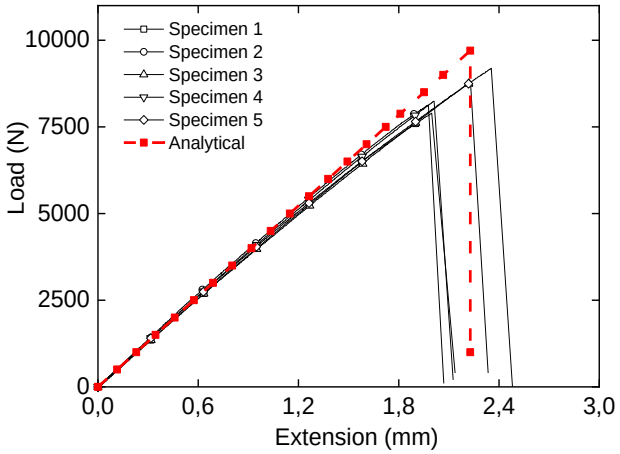



Figure 4.30. Load-extension curves of MT1 (manufactured with hand lay-up) specimens

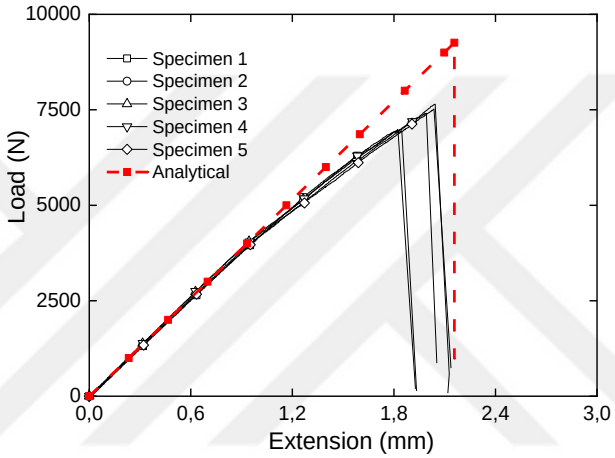



Figure 4.31. Load-extension curves of MT2 (manufactured in the vacuum bag with a low-capacity vacuum pump) specimens

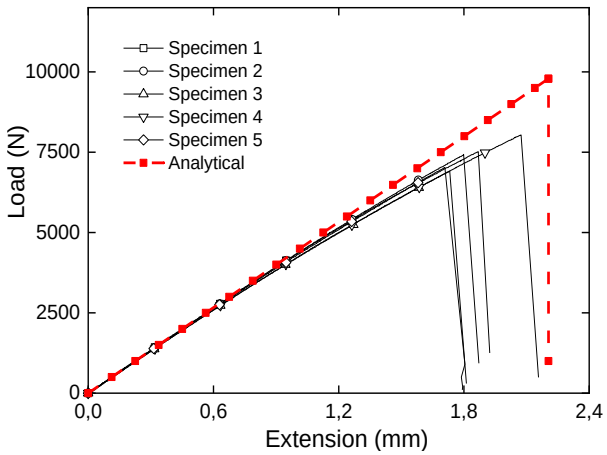



Figure 4.32. Load-extension curves of MT3 (manufactured with vacuum-assisted resin infusion) specimens

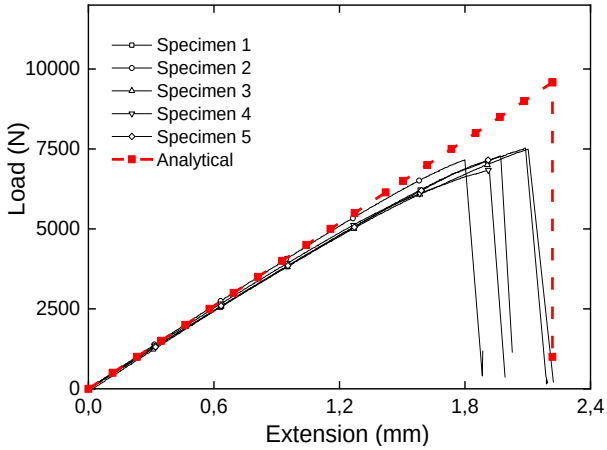



Figure 4.33. Load-extension curves of MT4 (manufactured with compression molding) specimens

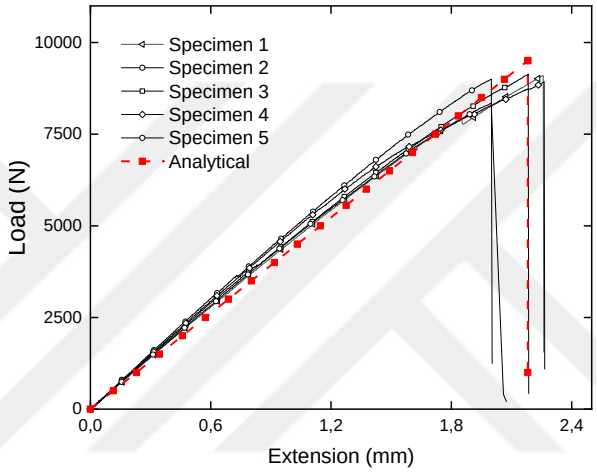



Figure 4.34. Load-extension curves of MT5 (manufactured in the vacuum bag with a high-capacity vacuum pump) specimens

Table 4.17. Maximum tensile loads obtained from experimental and practical engineering approach

| **Laminate code** | **Experimental result** | **Practical engineering approach result** | |
|---|---|---|---|
| | **Maximum tensile Load (N)** | **Warp yarn maximum tensile load (N)** | **Fill yarn maximum tensile load (N)** |
| MT1 | 8407±520 | 9890 | 7854 |
| MT2 | 7555±450 | 9252 | 6860 |
| MT3 | 7481±330 | 9789 | 6489 |
| MT4 | 7168±270 | 9585 | 6142 |
| MT5 | 8789±280 | 9507 | 5560 |

When the figures and Table 4.17 are examined, the load-carrying properties of warp and fill yarns can be explained. The maximum loads obtained experimentally are between the analytical warp and fill yarn results. The linearity of the experimental curves started to disappear around the fill yarn load-carrying capacity. Epoxy carried the stress transfer from fiber to fiber in fill yarns. Since the epoxy strength is much lower than the fiber's load capacity, micro fractures and separations begin in the fill yarn.

On the other hand, in the warp half, where the load bearing is longitudinal on the fiber, the plate failed before reaching the maximum load expected to be carried. The reason for this phenomenon is the negative effect of stress concentration on the warp yarn due to fill yarns and undulation. Another inference is that processing from the MT1 to the MT5 production method increased the fiber volume fraction. While the MT1 experimental maximum force result is closer to the fill yarn force value, MT5 is closer to the warp yarn prediction result.

- Tensile stress-strain curves

Stress-strain curves were generated from the data that constituted the tensile test force-extension curves and are presented in Figures 4.35 to 4.39. The stress-strain curves in the figures are similar in form to the force-displacement curves in terms of overlapping, or slight differences are available between the specimens in the groups. All stress-strain curves were linear in form and failed at the maximum stress level they could bear, with complete stress loss at rupture. The stresses forming the curves were calculated using force/cross sectional area. The width of the specimens with the rectangular area is 15 mm, while the thicknesses are different due to the production methods. The thicknesses of the specimens are given in Table 3.4. Strain is the extension/first length of the specimen. The gauge length of the specimens is 138 mm when the tab lengths are subtracted. The data forming the stress-strain curves were calculated in this way.

The curves for linear elastic behavior of the experimental and analytical models also overlap in the Figures (dashed red line: analytical approach). Although composite material is assumed to be elastic, its linearity starts to deteriorate in experiments after reaching a certain tensile stress value. This is due to the micro failure of matrix materials and fibers. This phenomenon can be seen in the figures. As indicated in the figures, the analytical solution includes two stress levels. Since the main component of the fiber architecture was a plain weave fabric, the fill and warp strength measurements were included. The strength values of cross-laminated composites can vary depending on their longitudinal and transverse orientations. This is why their fill and warp strengths are provided separately. Cross-ply fabrics are commonly used in commercial applications. The failure originates from the fill yarn, and the warp yarns have a tensile load. (Hu et al., 2017) noted that the composites in the warp directions exhibited higher failures than those in the fill directions. (Udhayaraman and Mulay, 2019) also showed that the ultimate tension of the yarns caused the failure of the warp and fill plies. Figures 4.82 to 4.86 show that the laminate ultimately failed in the experiments due to the stress concentrations produced by the fill and undulation yarns. In the study, the indicated fill and warp strength values were obtained using the local software (Yildirim and Tutuncu, 2014).

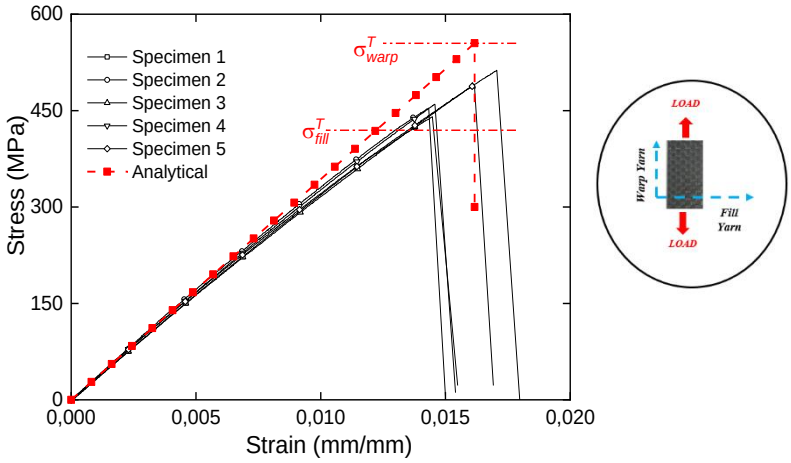



Figure 4.35. Stress-strain curves of MT1 (manufactured with hand lay-up) specimens

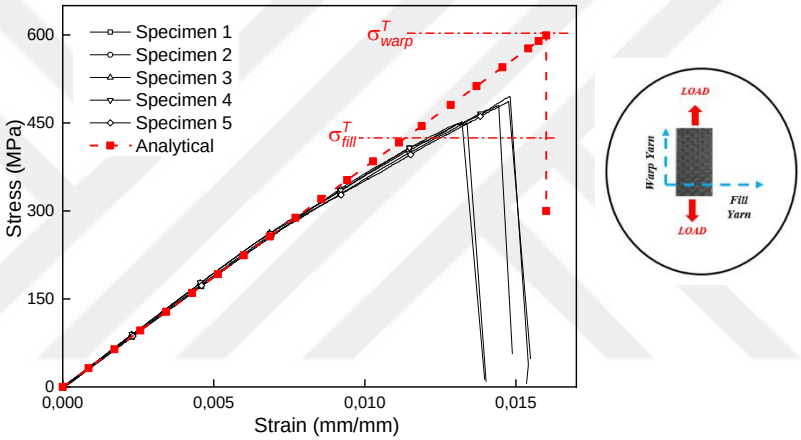



Figure 4.36. Stress-strain curves of MT2 (manufactured in the vacuum bag with a low-capacity vacuum pump) specimens

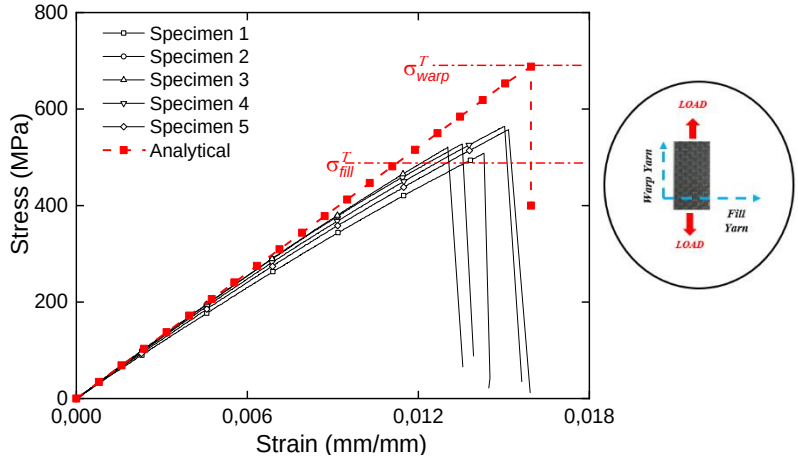



Figure 4.37. Stress-strain curves of MT3 (manufactured with vacuum-assisted resin infusion) specimens

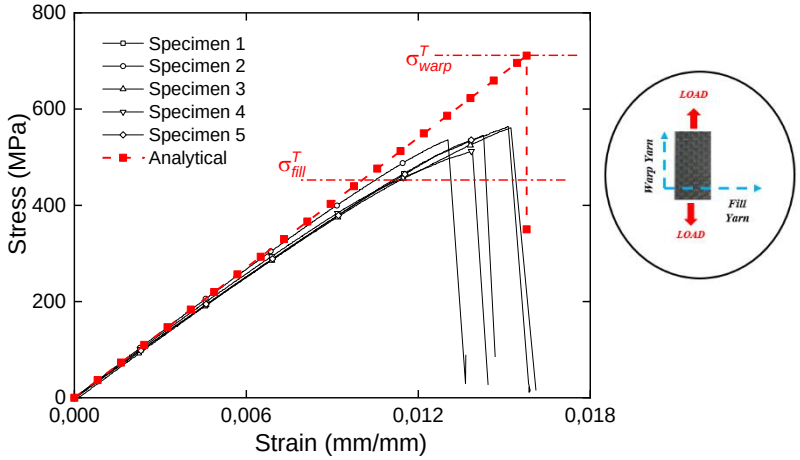



Figure 4.38. Stress-strain curves of MT4 (manufactured with compression molding) specimens

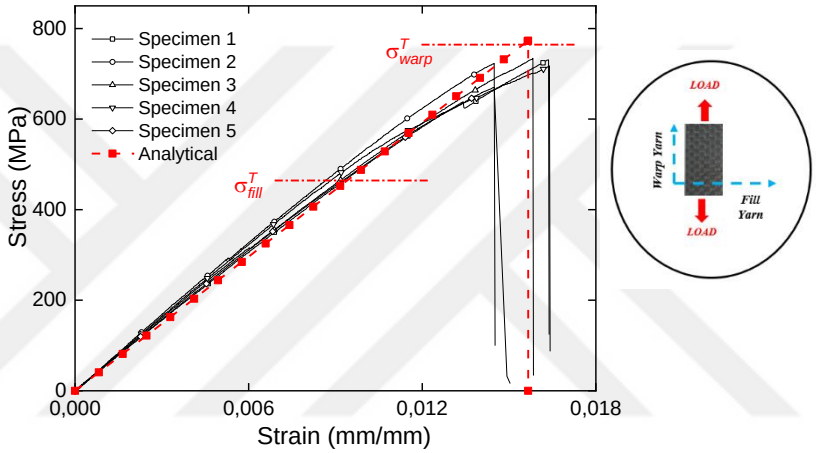



Figure 4.39. Stress-strain curves of MT5 (manufactured in the vacuum bag with a high-capacity vacuum pump) specimens

- Tensile modulus of elasticity and strength properties

The tensile elastic modulus and tensile strength results of the composites are presented in Tables 4.18 and 4.19. Since the dimensional and structural properties of the fill and warp yarns of the fabric are the same, the elastic moduli in the x and y axes are considered the same. When the tables are examined, it is seen that a significant improvement in strength and modulus values as we progress from MT1 to the MT5 method. Table 4.18 shows the percentage comparison of the analytical and experimental elastic modulus results, while Table 4.19 shows the relationship between the strengths.

Table 4.18. Comparison of tensile modulus data obtained from both experiments and analytical approach for four-layer plain woven fabric composite plate

| **Laminate code** | **Experimental Study** | **Practical Engineering Approach** | **Difference** |
|---|---|---|---|
| | **Ex=Ey (GPa)** | **$E_{av}$= Ex=Ey (GPa)** | **%** |
| MT1 | 33.8 ±1.1 | 34.8 | 1.5 |
| MT2 | 37.8 ± 1.1 | 37.4 | 1.0 |
| MT3 | 41.6 ± 1.5 | 43.3 | 3.9 |
| MT4 | 43.0 ± 1.7 | 45.0 | 4.5 |
| MT5 | 50.2 ± 2.6 | 49.3 | 1.8 |

Table 4.19. Comparison of the experimental strength results with the proposed practical approach for four-layer plain woven fabric composite plate

| **Laminate code** | **Experimental Study** | **Practical Engineering Approach** | |
|---|---|---|---|
| | **$\sigma_e^T$ (N/mm$^2$)** | **$\sigma_{warp}^T$ (N/mm$^2$)** | **$\sigma_{fill}^T$ (N/mm$^2$)** |
| MT1 | 471 ± 29 | 554 | 440 |
| MT2 | 489 ± 29 | 599 | 444 |
| MT3 | 525 ± 23 | 687 | 455 |
| MT4 | 531 ± 20 | 710 | 455 |
| MT5 | 674 ± 13 | 773 | 452 |

According to Table 4.18, the difference between the experimental and analytical elastic moduli of all plates is less than five percent. This ratio shows how small the error of the analytical results obtained with the developed approach. According to the comparative stress-strain curves and the data in this table, the approach is compelling to predict the behavior of composites under tensile loads.

The strength values in Table 4.19 show that the developed approach provides tensile strength values for the yarns forming the fabric structure. These are yarn and fill yarn tensile strengths. However, according to the calculations dictated by the technical standards, the maximum tensile strength of the material is obtained from the maximum tensile load in the experimental data. Although this maximum stress before fracture cannot be obtained with this approach, it can be predicted that the material will not reach the warp strength, where it will exceed the fill stress. In addition to this table, the data in Table 4.8 shows that the material will fail between two stresses.

*Comparison of analytical results under flexural loading obtained from practical engineering approach with experimental results*

As in tensile tests, the composites were subjected to three-point bending tests according to ASTM D790. Twenty-five specimens, five from each experimental group, were tested, and the results were obtained. The analytical and experimental flexural results were also compared to prove that the model can predict flexural loads as well as tensile loads. These comparisons include flexural load-deflection curves, elastic modulus, and internal stress distribution.

- Flexural load-midspan deflection curves

Load deflection curves were drawn from Figure 4.40 to 4.44 from the data obtained from the specimens tested. Five different figures were created for each production method, containing the test results of five specimens each. Analyzing the curves, it is concluded that the specimens overlapped for each group. In addition, the maximum loads the specimens can carry and the maximum loads at which fracture occurs are very close.

These curves obtained from the present approach were also compared with the experimental curves in the Figures (dashed red line: analytical approach). The experimental and analytical curves are well-matched in the linear region. The maximum load values are also very close to each other. MT4 (Figure 4.43) provides an example of the interpretation of the curves. The experimental and analytical curves of MT4 are linear and overlap up to 45 N. After that, however, the linearity of the experimental curve did not persist. The maximum loading is around 65 N in both curves. Returning to Figure 4.15, 45.1 N is defined as the point of failure load on the compression side. It shows that while the experimental curve was linear up to around 45 N and the behavior of the beam was elastic, at this load and beyond, failure started on the compression side of the beam, and the elastic property was lost. Finally, the beam failed when the tensile side reached the expected maximum force value. The other figures are similar.

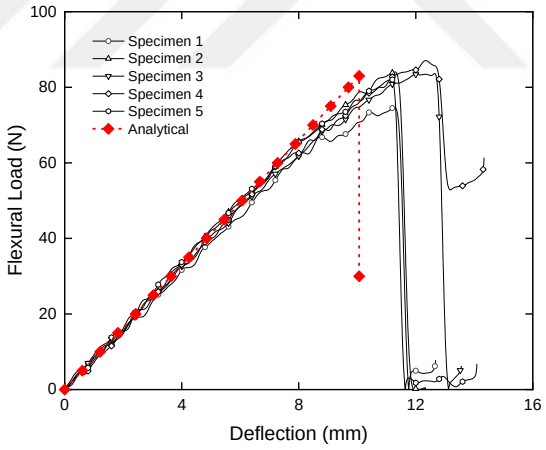



Figure 4.40. Flexural load-deflection curves of MT1 (manufactured with hand lay-up) specimens

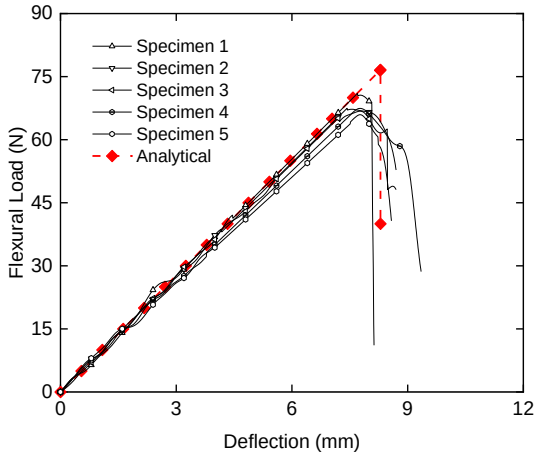



Figure 4.41. Flexural load-deflection curves of MT2 (manufactured in the vacuum bag with a low-capacity vacuum pump) specimens

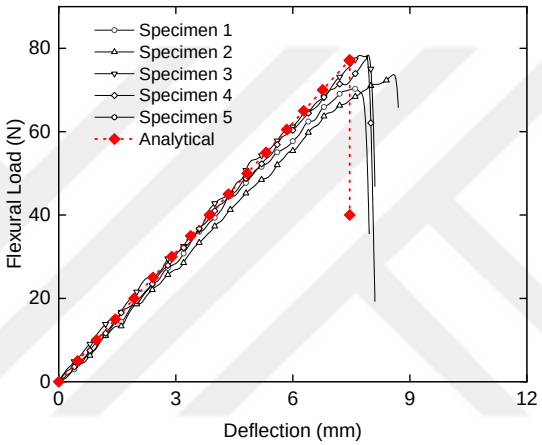



Figure 4.42. Flexural load-deflection curves of MT3 (manufactured with vacuum-assisted resin infusion) specimens

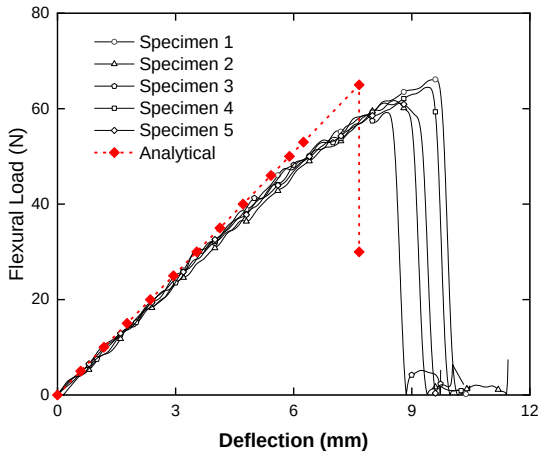



Figure 4.43. Flexural load-deflection curves of MT4 (manufactured with compression molding) specimens

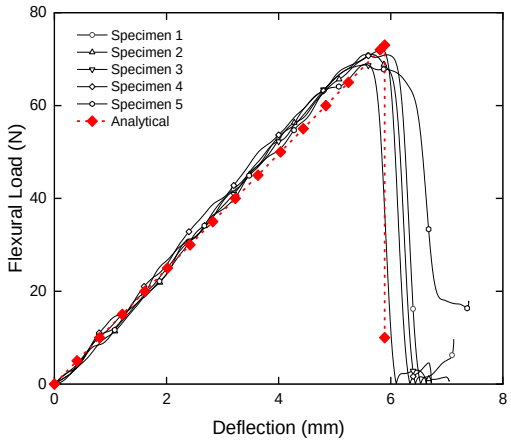



Figure 4.44. Flexural load-deflection curves of MT5 (manufactured in the vacuum bag with a high-capacity vacuum pump) specimens

The successful result in the figures shows that the propsed approach can make accurate predictions in the linear region and is also successful in predicting the maximum flexural loads. The experimental and analytical maximum flexural load results of the beams are presented in Table 4.20. According to these results, the experimental failures are between the loads given in the analytical method and are closer to the failure load on tensile results.

Table 4.20. Experimental and analytical maximum flexural load results of plain woven fabric composite plates

| **Laminate code** | **Experimental results** | **Practical engineering approach results** | |
|---|---|---|---|
| | **Maximum Flexural Load (N)** | **Failure load on compression side (N)** | **Failure load on tensile side (N)** |
| MT1 | 82.3±4.6 | 50.9 | 83.8 |
| MT2 | 62.2±2.1 | 50.3 | 76.5 |
| MT3 | 80.5±3.2 | 41.8 | 77.1 |
| MT4 | 62.5±2.7 | 45.1 | 65.4 |
| MT5 | 70.3±1.5 | 40.3 | 73.2 |

- Experimental flexural stress-strain curves

The stress-strain curves of the composite plates are presented in Figures 4.45 and 4.49. The curves were obtained by calculation according to ASTM D790. The equations used in the calculation of stress and strain are as follows:

$$\varepsilon_f = \frac{6Dt}{L^2} \tag{4.1}$$

$$\sigma_f = \frac{3PL}{2bt^2} \tag{4.2}$$

The figures show that the flexural stress-strain curves are similar to the flexural load-deflection curve profiles.

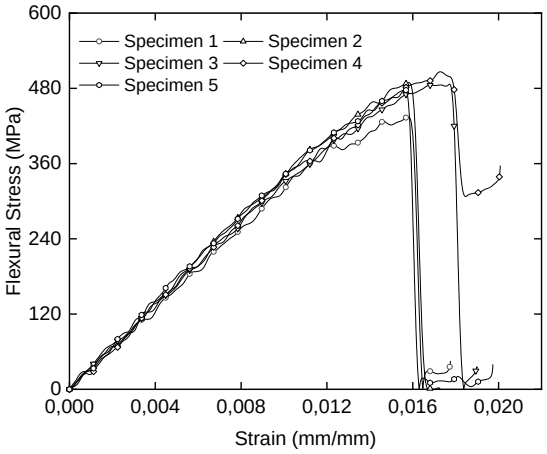



Figure 4.45. Flexural stress-strain curves of MT1 (manufactured with hand lay-up) specimens

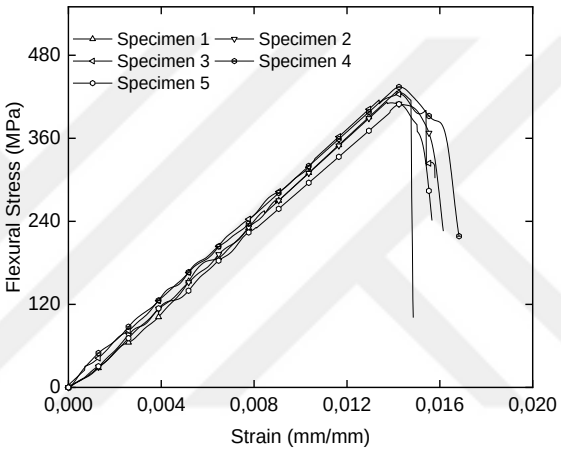



Figure 4.46. Flexural stress-strain curves of MT2 (manufactured in the vacuum bag with a low-capacity vacuum pump) specimens

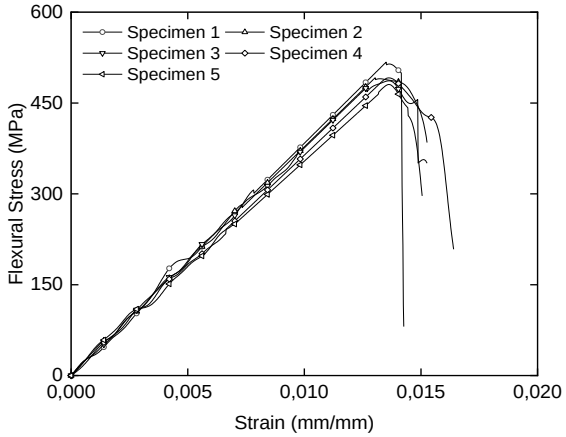



Figure 4.47. Flexural stress-strain curves of MT3 (manufactured with vacuum-assisted resin infusion) specimens

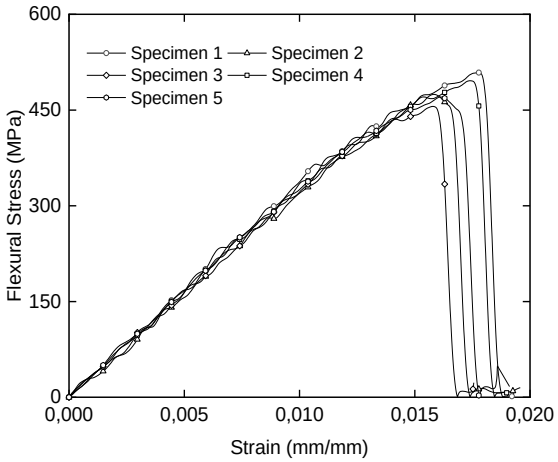



Figure 4.48. Flexural stress-strain curves of MT4 (manufactured with compression molding) specimens

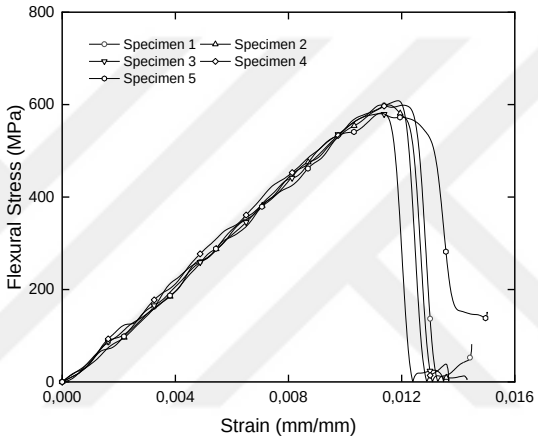



Figure 4.49. Flexural stress-strain curves of MT5 (manufactured in the vacuum bag with a high-capacity vacuum pump) specimens

Experimental maximum flexural stress obtained from all fabrication methods are presented in Table 4.21. When the mechanical properties of the plates were analyzed, MT5 production provided the best mechanical performance. MT5's high vacuum production minimizes excess epoxy and voids in the layers. In addition, due to the vacuum effect, the bonding between the interfaces is better.

Table 4.21. Experimental flexural strength results of plain woven fabric composite

| **Laminate code** | **Results of the flexural experimental tests** | |
|---|---|---|
| | **Maximum Flexural Load (N)** | **$\sigma_e^F$ (MPa)** |
| MT1 | 82.3±4.6 | 479±26 |
| MT2 | 62.2±2.1 | 417±13 |
| MT3 | 67.7±1.7 | 493±12 |
| MT4 | 62.5±2.7 | 455±20 |
| MT5 | 70.3±1.5 | 593±12 |

- Flexural modulus of elasticity properties

Table 4.22 compares five different beams' experimental and analytical flexural modulus values. The difference in MT1 is 5.82 percent, while the others are less than three percent. Especially for MT5, the percentage difference in the comparison is almost negligible. This proves how successful the developed approach is in force-deflection and maximum load predictions as well as in flexural elastic modulus prediction. According to Table 4.22 and Figures 4.40-4.44, the approach yielded successful results in the elastic region.

Table 4.22. Experimentally and analytically obtained flexural properties of four-ply woven plain fabric composite laminate beams

| **Laminate code** | **Experimental tests** | **Practical Engineering Approach** | **Difference** |
|---|---|---|---|
| | **$E_x$=$E_y$ (GPa)** | **$E_{av}^{f}$ (GPa)** | **%** |
| MT1 | 32.6±1.8 | 34.5 | 5.82 |
| MT2 | 37.6±0.7 | 38.4 | 2.3 |
| MT3 | 42.5±1.0 | 43.0 | 1.2 |
| MT4 | 37.5±1.9 | 38.5 | 2.66 |
| MT5 | 51.1±1.6 | 50.9 | 0.03 |

- Flexural internal stress distribution

In layered composite beams, the stress distribution does not vary linearly from the neutral axis to the outer face. While each layer has a continuity within itself, there are stress changes in between layers. These stress differences between layers are due to material differences and fiber angle. Since the plain woven fabric is considered cross-ply in the study, there is a stress difference in each layer transition in the approach. For example, there is a significant decrease in the stress value when moving from the longitudinal ($0^0$) layer to the transition ($90^0$) layer. The experimental results, obtained according to ASTM D790, show the stress on the outer surface at the maximum fracture load and the stress at the neutral axis (0 MPa). The stress in the intermediate layers is unknown and can only be assumed as if there is a linear stress change from the center outward. However, the internal stress distribution relationship obtained by ASTM D790 and the zigzag method can be explained by the relation between Figures 4.50 and 54.

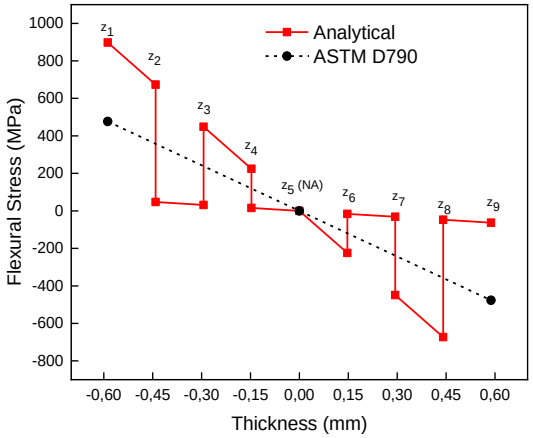



Figure 4.50. Internal stress distribution along the thickness of MT1 specimens manufactured with hand lay-up

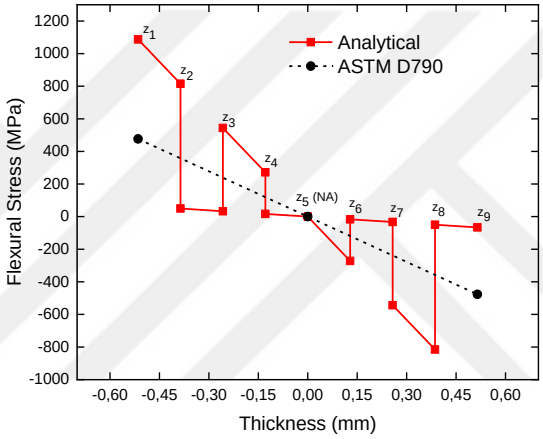



Figure 4.51. Internal stress distribution along the thickness of MT2 specimens manufactured in the vacuum bag with a low-capacity vacuum pump

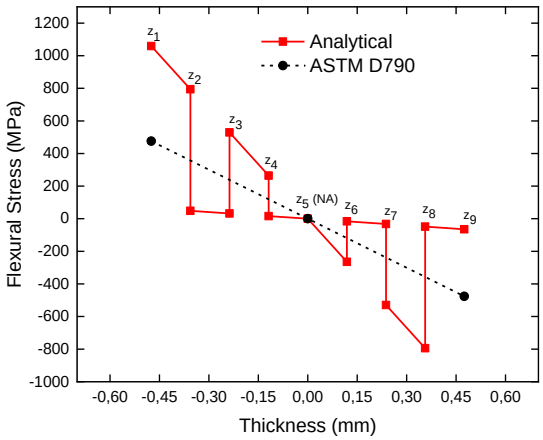



Figure 4.52. Internal stress distribution along the thickness of MT3 specimens manufactured with vacuum-assisted resin infusion specimens

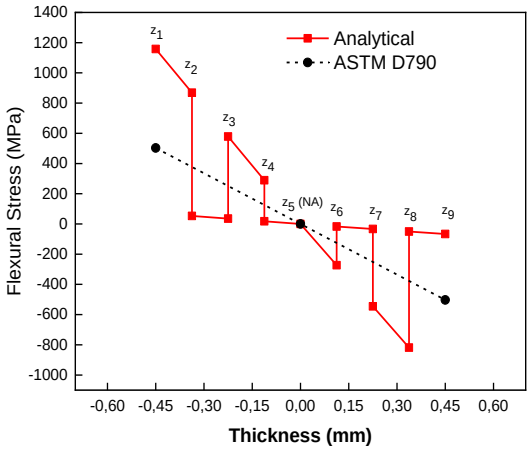



Figure 4.53. Internal stress distribution along with the thickness of MT4 specimens manufactured with compression molding

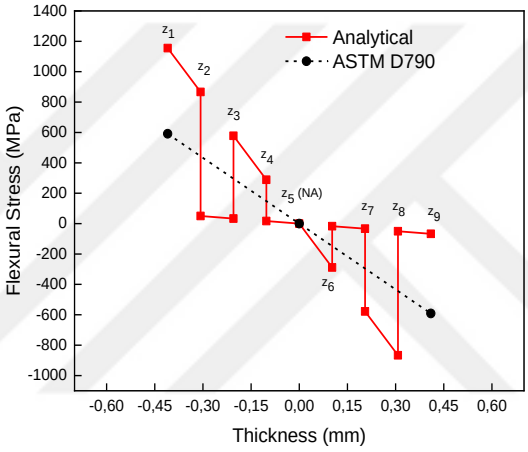



Figure 4.54. Internal stress distribution along with the thickness of MT5 specimens manufactured in the vacuum bag with a high-capacity vacuum pump

The curve generated from the ASTM D790 is linear from the neutral axis outward to the outer surface at maximum stress, while the curves obtained analytically by the zigzag method are nonlinear. There are significant differences in stress values, especially in the transition between layers. In these transitions, the angle of the fibers is different ($0^0$ or $90^0$). When the fiber angle changed, the stress changed. However, the average of the two different stress values indicated in the analytical curve at the layer transition is very close to the assumed stress value of the ASTM D790 curve at that point. When the two curves are matched, the experimental curve is like a linear average of the analytical zigzag curve. The result shows that with the data from the developed model, the zigzag method can obtain internal stress distributions of the composite plates. The experimental results in the figures confirm the analytical results. The developed approach successfully predicted the stress distribution.

### 4.2.2. The comparison of compression test results of foam core with the data sheet of the core

PVC foam core material with three different densities are used in sandwich plates. The supplier-provided mechanical properties of these materials are given in Table 3.1. However, when the Table is examined, there is a wide range between the minimum and average values between the densities and mechanical properties of the foam materials. For example, PVC foam with a density of 48 $km^3$ has a maximum density of 55 $kg/m^3$ and a minimum density of 43 $kg/m^3$. The difference between the average value and the densities at the extremes is 14.5 percent. Considering the compressive modulus as mechanical properties, the average value for the same foam is 48 $N/mm^{2,}$ while the minimum value is 35 $N/mm^2$. The difference is 27 percent, and this value is relatively high. Therefore, the foams were subjected to compression tests to determine which mechanical range was closer to the foam materials supplied in the present study. The stress-strain curves presented in Figures 4.55, 4.56, and 4.57 were obtained from the force-extension data obtained from the compression tests.

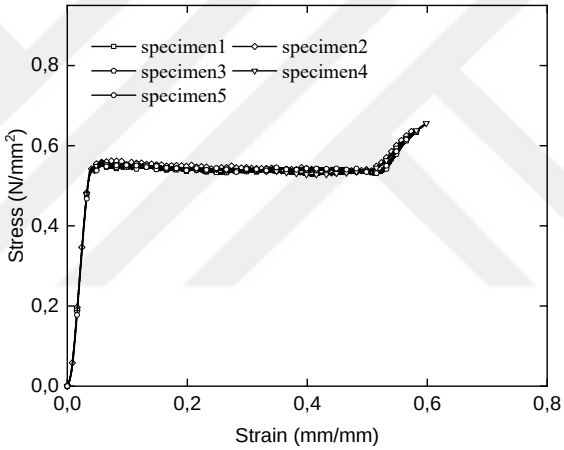



Figure 4.55. 48 $kg/m^3$ density PVC foam compression stress-strain curve

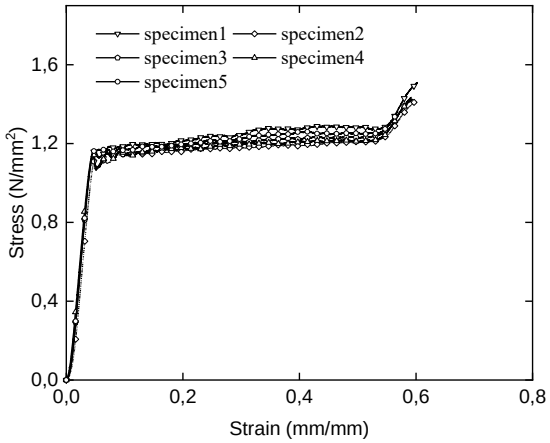



Figure 4.56. 80 $kg/m^3$ density PVC foam compression stress-strain curve

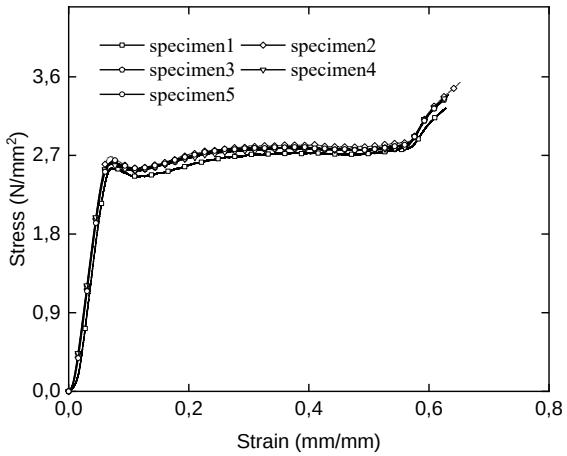


Figure 4.57. 130 kg/m$^3$ density PVC foam compression stress-strain curve

In the curve in Figure 4.55, the compressive strength and modulus values of PVC foam with a density of 48 kg/m$^3$ were obtained as 0.55 MPa and 42 MPa, respectively. In Table 3.1, these values correspond to the average of the lower and average values. Therefore, the other mechanical properties of this PVC foam material given in the table were accepted as the values corresponding to the average and the middle of the lower limit. In Figure 4.56, the compressive strength and modulus of 80 kg/m$^3$ density foam were calculated from the stress-strain curve as 1.2 MPa and 82 MPa, respectively. These values correspond to the lower limit of the values in Table 3.1. Therefore, the other mechanical properties of the material were considered to be at the lower limit. Finally, in Table 4.57, the compressive strength and modulus of the foam material with a density of 130 kg/m$^3$ were obtained as 2.6 MPa and 145 MPa, respectively. These values are equal to the lower limits of the values in the table. Therefore, other mechanical properties of this foam material were assumed to have lower values.

These test data were used to determine the relatively accurate mechanical properties of the PVC foam materials used in this thesis. Because the properties of the core material directly affect the mechanical performance of the sandwich, such as flexural deformation and failure loads, compression tests were carried out for PVC foams. The foams' experimental results were used to analytically obtain the sandwich beams' flexural properties. Thus, the sandwich's experimental and analytical verification errors, which may occur due to the mechanical inconsistency of PVC foam materials, were minimized.

### 4.2.3. Comparison and validation of developed engineering approaches for sandwich beams with flexural test results and models in the literature

In order to validate the analytical models developed in this thesis for the flexural properties of sandwich beams, 21 different groups of sandwich beams were created from different combinations of core PVC foam density, sandwich thickness, span length, and face-sheet thickness. A total of 105 sandwich beam specimens, five specimens from each group, were subjected to three-point bending

tests. Flexural load-deflection curves were obtained from the test data of these beams. Validation was also made with results obtained from models available in the literature. Flexural properties of sandwich beams, such as flexural stiffness, elastic limit load (core yield), force-deflection curves, and maximum flexural load due to failure modes, are compared. The curves were analyzed under two separate headings as short and long sandwich beams referring to two different span lengths.

*Comparison of flexural stiffness obtained from the developed approach with experiments and the literature model*

Flexural stiffness was obtained with the approach (Equation 2.11) developed by Allen to compare with the developed approach. The elastic moduli of face material obtained experimentally are given in Table 4.18. The results presented in Table 4.23 were obtained using both analytical methods and compared in percentage. All the sandwich beams designed in Table 3.4 were produced with the MT5 production method, and experimental tests were carried out. In this context, Table 4.23 shows that the results of the configurations (con17-con20) designed according to MT5 are close for both methods. The percentage differences are 1.4 percent or less. According to these results, it can be said that the developed engineering approach provides results close to the most used approach in the literature without the need for experimental tests of face materials.

The experimental flexural stiffnesses were also obtained according to the ASTM D 7250 standard, which works with experimental data from a three-point bending test and two different span lengths. The flexural stiffness equation in the Standards according to the specified requirements is as follows.

$$EI = D = \frac{P_1 S_1^3 (1 - S_2^2/S_1^2)}{48\Delta_1 (1 - P_1 S_1 \Delta_2 / P_2 S_2 \Delta_1)} \tag{4.3}$$

This thesis work tested beams with the same properties and two different span lengths (100 mm and 250 mm) in three-point bending tests. The *EI* results of the sandwich plates obtained experimentally are presented in Table 4.24.

The experimental results are compared separately with the two analytical approaches, and the differences are presented in percentages in Table 4.25. According to the results displayed, the developed approach provides results closer to the experimental results, and the difference is less than five percent.

Table 4.23. Comparison of flexural stiffness of sandwich plates configuration obtained by engineering approach (developed approach), and Allen's method in literature

| Prod. Meth. | Sand. Con. | Sandwich Properties | | | Developed approach | | Allen's model in literature | | Diff. |
|---|---|---|---|---|---|---|---|---|---|
| | | Core thick. | Faces. Thick. | Sand. width | Sandwich flexural Stiffness terms | | Sandwich flexural stiffness | | |
| | | $t_c$ | $t_f$ | b | $D_s^f$ | $D_s^f b$ | $E_f$ | EI | % |
| | | mm | mm | mm | N.mm | $N.mm^2$ | $N/mm^2$ | $N.mm^2$ | |
| | | | | | $x10^5$ | $x10^7$ | $x10^4$ | $x10^7$ | |
| MT1 | Con1 | 10 | 1.19 | 50 | 26.14 | 13.07 | 3.38 | 12.6 | 3.6 |
| | Con2 | 20 | 1.19 | 50 | 93.49 | 46.74 | 3.38 | 45.2 | 3.4 |
| | Con3 | 30 | 1.19 | 50 | 202.44 | 101.20 | 3.38 | 97.8 | 3.3 |
| | Con4 | 20 | 2.38 | 50 | 208.55 | 104.30 | 3.38 | 10.1 | 3.6 |
| MT2 | Con5 | 10 | 1.03 | 50 | 25.03 | 12.51 | 3.78 | 11.8 | 5.4 |
| | Con6 | 20 | 1.03 | 50 | 90.82 | 45.41 | 3.78 | 43.0 | 5.2 |
| | Con7 | 30 | 1.03 | 50 | 197.65 | 98.82 | 3.78 | 93.7 | 5.1 |
| | Con8 | 20 | 2.06 | 50 | 199.86 | 99.93 | 3.78 | 94.7 | 5.4 |
| MT3 | Con9 | 10 | 0.95 | 50 | 25.51 | 12.75 | 4.16 | 11.8 | 7.1 |
| | Con10 | 20 | 0.95 | 50 | 93.22 | 46.61 | 4.16 | 43.4 | 6.9 |
| | Con11 | 30 | 0.95 | 50 | 203.37 | 101.70 | 4.16 | 94.6 | 6.9 |
| | Con12 | 20 | 1.90 | 50 | 203.72 | 101.90 | 4.16 | 94.8 | 7.1 |
| MT4 | Con13 | 10 | 0.90 | 50 | 24.60 | 12.30 | 4.30 | 11.5 | 6.5 |
| | Con14 | 20 | 0.90 | 50 | 90.33 | 45.16 | 4.30 | 42.3 | 6.4 |
| | Con15 | 30 | 0.90 | 50 | 197.40 | 98.70 | 4.30 | 92.4 | 6.4 |
| | Con16 | 20 | 1.80 | 50 | 196.55 | 98.27 | 4.30 | 92.0 | 6.5 |
| MT5 | Con17 | 10 | 0.82 | 50 | 24.45 | 12.22 | 5.02 | 12.0 | 1.4 |
| | Con18 | 20 | 0.82 | 50 | 90.42 | 45.21 | 5.02 | 44.6 | 1.3 |
| | Con19 | 30 | 0.82 | 50 | 198.09 | 99.04 | 5.02 | 97.8 | 1.3 |
| | Con20 | 20 | 1.64 | 50 | 195.37 | 97.68 | 5.02 | 96.4 | 1.4 |

Table 4.24. Experimental flexural stiffness results of sandwich plates

| Sandwich Configuration | | | Located Load | | Span Length | | Flexural Deflection | | Flexural Stiffness |
|---|---|---|---|---|---|---|---|---|---|
| Plate | Beam 1 | Beam 2 | $P^1$ | $P^2$ | $S^1$ | $S^2$ | $\Delta^1$ | $\Delta^2$ | EI (D) |
| | | | N | N | mm | mm | mm | mm | $Nmm^2x10^7$ |
| D48T10F4 | D48T10F4L100 | D48T10F4L250 | 190.1 | 190.4 | 100 | 250 | 0.49 | 1.64 | 12.55 ±0.28 |
| D48T20F4 | D48T20F4L100 | D48T20F4L250 | 230.4 | 230.5 | 100 | 250 | 0.38 | 1.10 | 46.52±0.63 |
| D48T30F4 | D48T30F4L100 | D48T30F4L250 | 250.6 | 250.3 | 100 | 250 | 0.37 | 0.99 | 102.82±2.39 |
| D75T10F4 | D75T10F4L100 | D75T10F4L250 | 330.3 | 331.4 | 100 | 250 | 0.50 | 1.98 | 12.63±0.19 |
| D75T20F4 | D75T20F4L100 | D75T20F4L250 | 381.1 | 380.1 | 100 | 250 | 0.41 | 1.25 | 47.40±0.91 |
| D75T30F4 | D75T30F4L100 | D75T30F4L250 | 420.4 | 420.9 | 100 | 250 | 0.30 | 0.88 | 103.25±1.39 |
| D130T10F4 | D130T10F4L100 | D130T10F4L250 | 650.3 | 650.3 | 100 | 250 | 0.59 | 2.86 | 12.70±0.19 |
| D130T20F4 | D130T20F4L100 | D130T20F4L250 | 750.7 | 750.4 | 100 | 250 | 0.38 | 1.38 | 47.25±0.78 |
| D130T30F4 | D130T30F4L100 | D130T30F4L250 | 802.2 | 801.1 | 100 | 250 | 0.30 | 0.97 | 101.37±2.22 |

Table 4.25. Comparison of flexural stiffness of sandwich plates obtained by experiment, engineering approach, and Allen's method

| **Sandwich Plate** | **Experimental result** | **Developed Approach results** | | **Allen approach results** | |
|---|---|---|---|---|---|
| | **Flexural Stiffness** | **Flexural Stiffness** | **Diff.** | **Flexural Stiffness** | **Diff.** |
| | **D (Nmm$^2$) x10$^7$** | **Db (Nmm$^2$) x10$^7$** | **%** | **EI (Nmm$^2$) x10$^7$** | **%** |
| D48T10F4 | 12.55 ±0.28 | 12.22 | 2.6 | 12.04 | 4.1 |
| D48T20F4 | 46.52±0.63 | 45.21 | 2.9 | 44.60 | 4.2 |
| D48T30F4 | 102.82±2.39 | 99.04 | 3.8 | 97.75 | 5.1 |
| D75T10F4 | 12.63±0.19 | 12.22 | 3.2 | 12.04 | 4.8 |
| D75T20F4 | 47.40±0.91 | 45.21 | 4.8 | 44.60 | 6.2 |
| D75T30F4 | 103.25±1.39 | 99.04 | 4.2 | 97.75 | 5.6 |
| D130T10F4 | 12.70±0.19 | 12.22 | 3.9 | 12.04 | 5.4 |
| D130T20F4 | 47.25±0.78 | 45.21 | 4.5 | 44.60 | 5.9 |
| D130T30F4 | 101.37±2.22 | 99.04 | 2.3 | 97.75 | 3.7 |

In conclusion, according to the comparative results in Tables 4.23 and 4.25, the engineering approach is quite successful. It proved reliable and accurate in predicting the flexural stiffness of sandwiches. More importantly, in achieving this success, no experimental testing of the fiber-reinforced composite face material was required. With this approach, a sandwich designer or researcher can design a sandwich with the desired properties if they know the mechanical properties of the core, fiber fabric, and matrix material.

*Comparison of modified analytical model results for elastic limits (Core yield load) of the sandwich beams with experimental results and model in the literature*

The results obtained with the modified approach are compared with the Soden model results in Table 4.26 for reliability. The elastic modulus of composite face material required in the Soden model is obtained from Table 4.18. According to the results presented, the model difference is less than 0.5 percent. The results obtained from both models are almost identical. Table 4.27 compares the results obtained from both analytical approaches with the experimental results. There is a good agreement between the experimental results and the models; the differences are around and mostly below five percent.

Table 4.26. Comparison of core yield loads obtained from the original and modified models

| **Sandwich conf.** | **Configuration code** | **Literature model** | **Modified approach** | |
|---|---|---|---|---|
| | | **Core yield Load ( $P_1$, N)** | **Core yield Load ( $P_1$, N)** | **Diff %** |
| 1 | D48T10F4L100 | 377.67 | 378.90 | 0.3 |
| 2 | D48T20F4L100 | 449.13 | 450.55 | 0.3 |
| 3 | D48T30F4L100 | 497.03 | 499.61 | 0.5 |
| 4 | D48T10F4L250 | 377.67 | 378.90 | 0.3 |
| 5 | D48T20F4L250 | 449.13 | 450.55 | 0.3 |
| 6 | D48T30F4L250 | 497.03 | 499.61 | 0.5 |
| 7 | D75T10F4L100 | 641.01 | 643.06 | 0.3 |
| 8 | D75T20F4L100 | 762.31 | 764.73 | 0.3 |
| 9 | D75T30F4L100 | 843.63 | 846.30 | 0.3 |
| 10 | D75T10F4L250 | 641.01 | 643.06 | 0.3 |
| 11 | D75T20F4L250 | 762.31 | 764.73 | 0.3 |
| 12 | D75T30F4L250 | 843.63 | 846.30 | 0.3 |
| 13 | D130T10F4L100 | 1305.83 | 1309.99 | 0.3 |
| 14 | D130T20F4L100 | 1552.90 | 1557.84 | 0.3 |
| 15 | D130T30F4L100 | 1718.57 | 1724.03 | 0.3 |
| 16 | D130T10F4L250 | 1305.83 | 1309.99 | 0.3 |
| 17 | D130T20F4L250 | 1552.90 | 1557.84 | 0.3 |
| 18 | D130T30F4L250 | 1718.57 | 1724.03 | 0.3 |
| 19 | D48T20F8L100 | 728.39 | 729.03 | 0.1 |
| 20 | D75T20F8L100 | 1434.90 | 1438.19 | 0.2 |
| 21 | D130T20F8L100 | 2895.52 | 2902.52 | 0.2 |

Table 4.27. Comparison of core yield loads obtained from the original and modified models with experimental results

| Sand. conf. | Configuration code | Experimental result | Modified approach | | Literature model | |
|---|---|---|---|---|---|---|
| | | Core yield Load ($P_1$, N) | Core yield Load ($P_1$, N) | Diff % | Core yield Load ($P_1$, N) | Diff % |
| 1 | D48T10F4L100 | 382±5 | 378.90 | 0.8 | 377.67 | 1.1 |
| 2 | D48T20F4L100 | 454±3 | 450.55 | 0.8 | 449.13 | 1.1 |
| 3 | D48T30F4L100 | 498±12 | 499.61 | 0.3 | 497.03 | 0.2 |
| 4 | D48T10F4L250 | 380±4 | 378.90 | 0.3 | 377.67 | 0.6 |
| 5 | D48T20F4L250 | 466±30 | 450.55 | 3.3 | 449.13 | 3.6 |
| 6 | D48T30F4L250 | 476±22 | 499.61 | 5.0 | 497.03 | 4.4 |
| 7 | D75T10F4L100 | 669±14 | 643.06 | 3.9 | 641.01 | 4.2 |
| 8 | D75T20F4L100 | 768±13 | 764.73 | 0.4 | 762.31 | 0.7 |
| 9 | D75T30F4L100 | 857±13 | 846.30 | 1.2 | 843.63 | 1.6 |
| 10 | D75T10F4L250 | 648±4 | 643.06 | 0.8 | 641.01 | 1.1 |
| 11 | D75T20F4L250 | 756±14 | 764.73 | 1.2 | 762.31 | 0.8 |
| 12 | D75T30F4L250 | 843±17 | 846.30 | 0.4 | 843.63 | 0.1 |
| 13 | D130T10F4L100 | 1304±12 | 1309.99 | 0.5 | 1305.83 | 0.1 |
| 14 | D130T20F4L100 | 1570±23 | 1557.84 | 0.8 | 1552.90 | 1.1 |
| 15 | D130T30F4L100 | 1770±25 | 1724.03 | 2.6 | 1718.57 | 2.9 |
| 16 | D130T10F4L250 | 1323±43 | 1309.99 | 1.0 | 1305.83 | 1.3 |
| 17 | D130T20F4L250 | 1481±31 | 1557.84 | 5.2 | 1552.90 | 4.9 |
| 18 | D130T30F4L250 | 1615±52 | 1724.03 | 6.8 | 1718.57 | 6.4 |
| 19 | D48T20F8L100 | 764±20 | 729.03 | 4.6 | 728.39 | 4.7 |
| 20 | D75T20F8L100 | 1385±122 | 1438.19 | 3.8 | 1434.90 | 3.6 |
| 21 | D130T20F8L100 | 2938±21 | 2902.52 | 1.2 | 2895.52 | 1.4 |

*Short-span length sandwich beams load-deflection curves*

All sandwiches in this group were tested at a span of 100 mm. There are twelve groups in total. The first nine groups contain specimens consisting of a four-layer plain woven fabric composite. Three different PVC foam densities and three different core thicknesses differentiate the groups. The test results are presented in Figures 4.58-4.66. The remaining three groups (Figures 4.67, 68, 69) include sandwich beams formed with a plain woven fabric composite with eight layers. The face thickness distinguishes this group from the others, while the difference is in PVC foam core density. Core thickness is kept constant. In this section, the curves are quite compatible when the figures are analyzed by considering the harmony of the specimens within themselves. Especially in the linear region, the curves of the specimens overlap. However, minimal divergences in the curves were observed for some groups beyond the linear region. It may be due to local inconsistencies in the material characteristics of the PVC foams used in the core material. The differences can be seen in Figures 4,60, 4,61, 4,562, 4,64, and 4,69.

The figures also include analytical curves obtained with the Allen model and developed analytical model (engineering approach), which are given in dotted blue lines and dashed red lines, respectively. When the curves are analyzed, it is seen that the curves obtained from the Allen model

and the developed model overlap. The experimental curves overlap with these two analytical models. However, in Figures 4.60, 4.63, and 4.6, the models differ only slightly from the experimental curves. Looking at the flexural stiffnesses presented in Table 4.25 for the sandwich beams (D48T30F4, D75T30F4, and D130T30F4) that make up these figures, the maximum difference from the experimental stiffnesses is 4.2 percent. This value is close to the differences in other sandwiches. Therefore, the increase in the difference between the experiment and the model in the force-deflection curves may be attributed to the deformation value resulting from the core shear deflection rather than the bending deflection. Core shear deflection may be due to dimensional variations or variations in the properties of the core material. When looking at the core yield load comparisons of these sandwiches in Table 4.27, the differences are less than three percent. Therefore, we can conclude that this difference is related to dimensions. Although the sandwich beams in these figures have different densities, they are dimensionally identical. For example, all three beams have a 30 mm thickness core. Another common point of the three figures is that the analytical models are slightly more rigid. From this, it can be concluded that as the core thickness increases, the core shear deflection is higher than expected.

On the other hand, the figures show that at the core yield loads, which are the analytical curves' endpoint, the experimental curves' linear forms end and transform into non-linear forms. Figures show that the prediction of force-deflection curves of sandwich beams under short span length with the developed method in the linear region is quite successful. The method proves very reliable, achieving this success for different structure variations such as core thickness, core density, and face-sheet thickness. Remarkably accurate predictions are obtained without fiber-reinforced composite face material or other experimental tests.

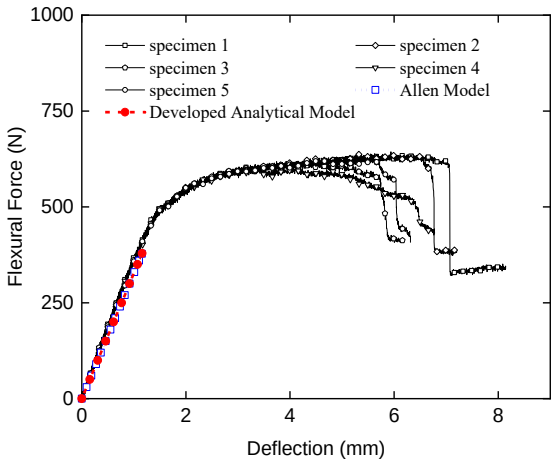


Figure 4.58. Comparison of experimental and analytical force-deflection curves of D48T10F4L100 coded sandwich beam

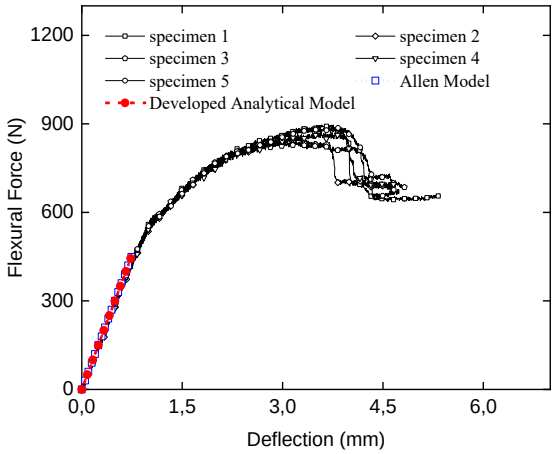



Figure 4.59. Comparison of experimental and analytical force-deflection curves of D48T20F4L100 coded sandwich beam

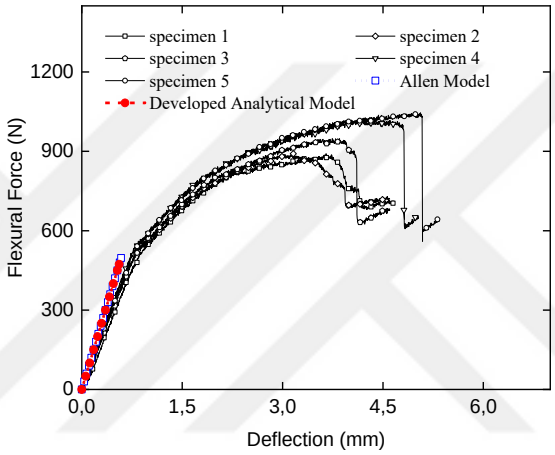



Figure 4.60. Comparison of experimental and analytical force-deflection curves of D48T30F4L100 coded sandwich beam

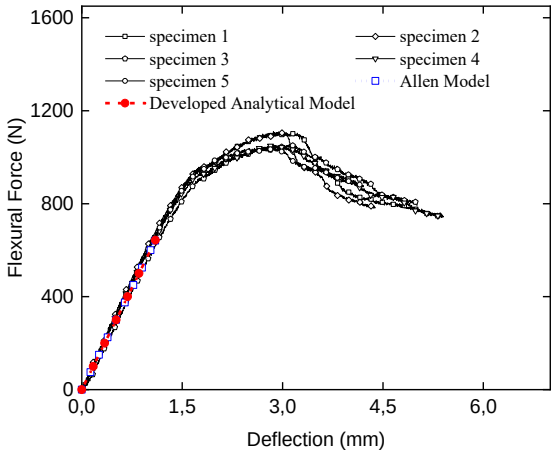



Figure 4.61. Comparison of experimental and analytical force-deflection curves of D75T10F4L100 coded sandwich beam

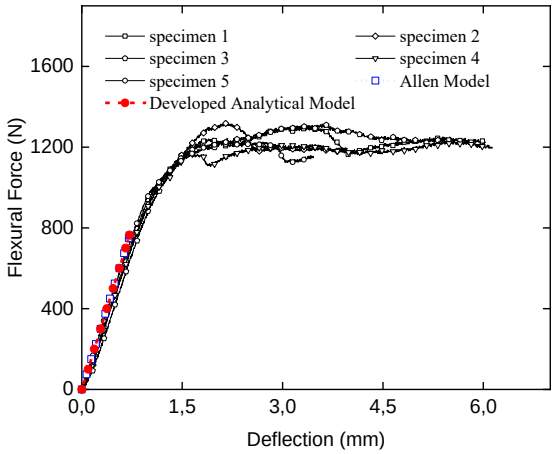



Figure 4.62. Comparison of experimental and analytical force-deflection curves of D75T20F4L100 coded sandwich beam

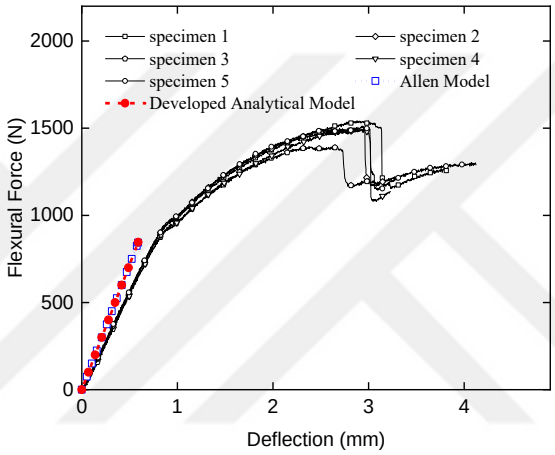



Figure 4.63. Comparison of experimental and analytical force-deflection curves of D75T30F4L100 coded sandwich beam

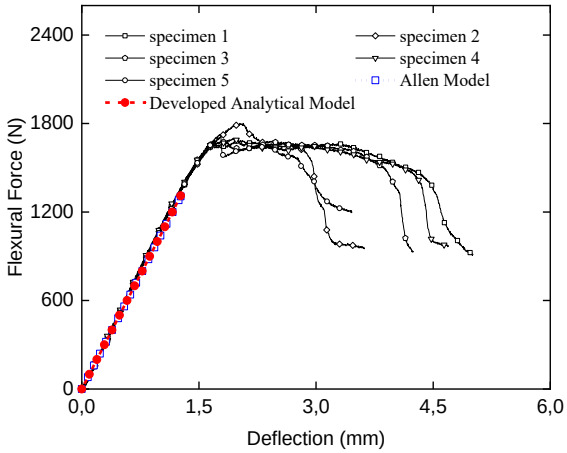



Figure 4.64. Comparison of experimental and analytical force-deflection curves of D130T10F4L100 coded sandwich beam

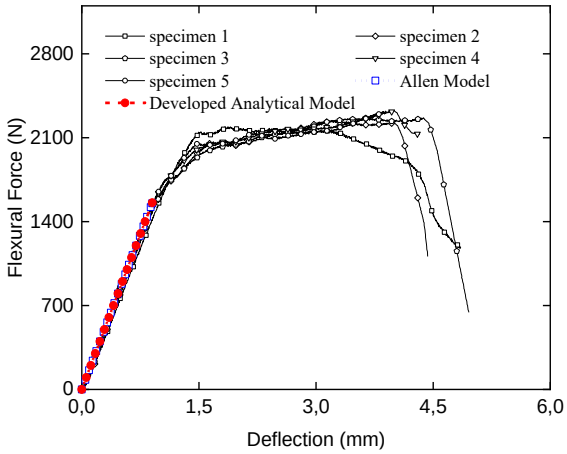



Figure 4.65. Comparison of experimental and analytical force-deflection curves of D130T20F4L100 coded sandwich beam

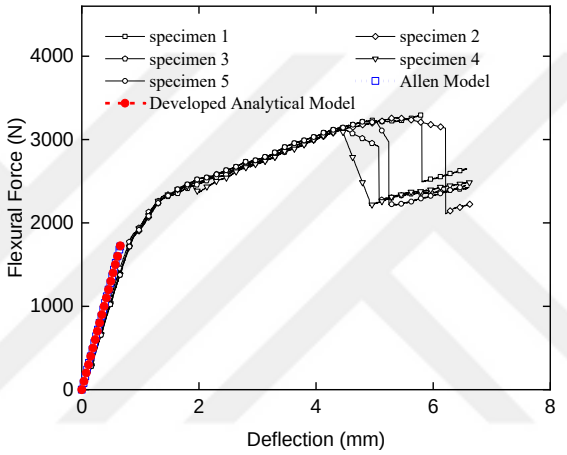



Figure 4.66. Comparison of experimental and analytical force-deflection curves of D130T30F4L100 coded sandwich beam

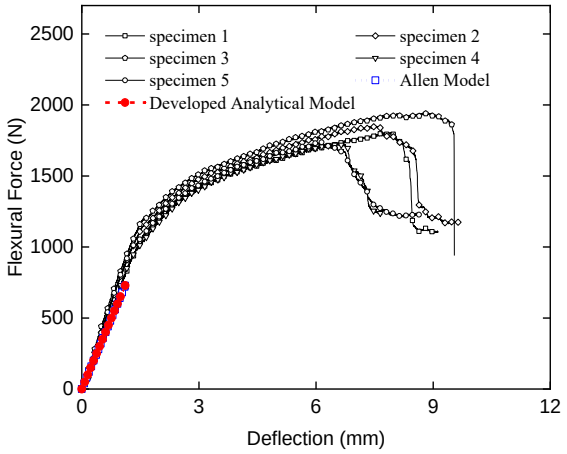



Figure 4.67. Comparison of experimental and analytical force-deflection curves of D48T20F8L100 coded sandwich beam

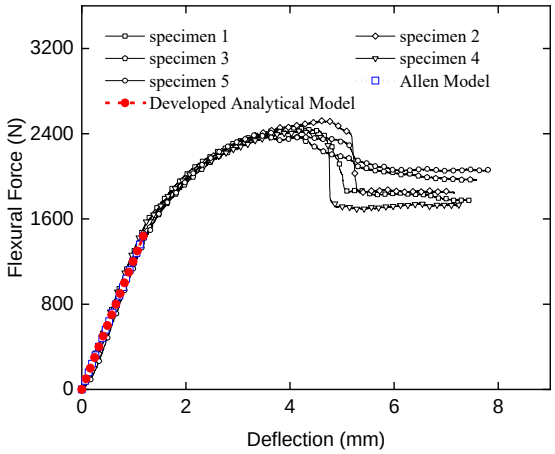



Figure 4.68. Comparison of experimental and analytical force-deflection curves of D75T20F8L100 coded sandwich beam

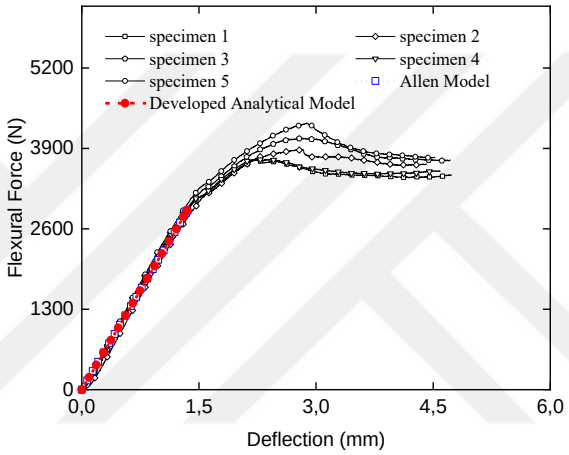



Figure 4.69. Comparison of experimental and analytical force-deflection curves of D130T20F8L100 coded sandwich beam

*Long-span length sandwich beams load-deflection curves.*

The specimens in the group defined as long sandwiches were tested at 250 mm span length. Nine groups provided structural differences in sandwich structures, such as core thickness and core density, except for facesheet thickness. The flexural load-deflection curves were generated from the test results and presented in Figures 4.70 - 4.78. When the groups are analyzed within themselves, there is a high degree of harmony between the specimens. Especially in the linear regions, the curves overlap quite well. However, as in the short-span samples, there are groups where minor differences occur after the linear region. For example, Figures 4.70 and 4.75 are noteworthy.

The figures also include analytical curves obtained with the Allen model and developed analytical model (engineering approach), which are given as dotted blue lines and dashed red lines, respectively. The analytical curves almost completely overlapped in these figures as well. There was also a perfect overlap with the experimental curves. Only in Figure 4.76, it can be said that there is an insignificant difference between the models and the experimental average. Also, the experimental curve of the beam in this figure failed at the core yield strength.

As in the case of the beams analyzed in the short span length, the analytical approach developed here allowed a successful force-displacement curve up to the core yield loading point. Similarly, the experimental curves changed from linear to non-linear after the core yield point. Results again show that the developed model is suitable for obtaining reliable force-displacement curves in the linear region despite the structural differences in long-span length.

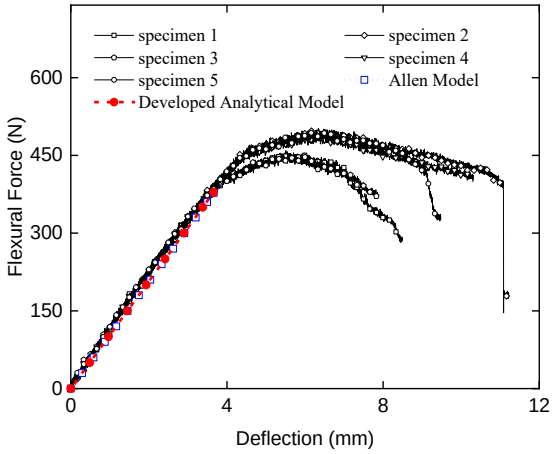



Figure 4.70. Comparison of experimental and analytical force-deflection curves of D48T10F4L250 coded sandwich beam

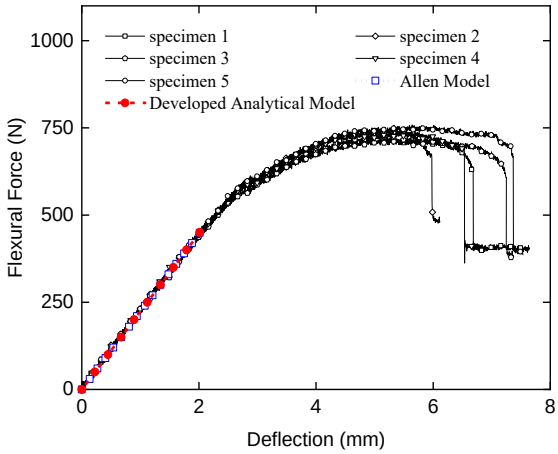



Figure 4.71. Comparison of experimental and analytical force-deflection curves of D48T20F4L250 coded sandwich beam

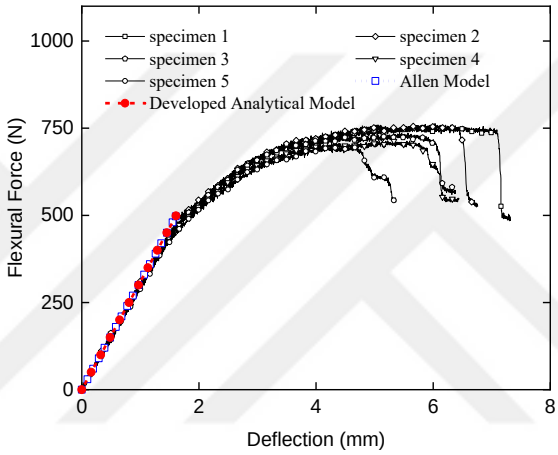



Figure 4.72. Comparison of experimental and analytical force-deflection curves of D48T30F4L250 coded sandwich beam

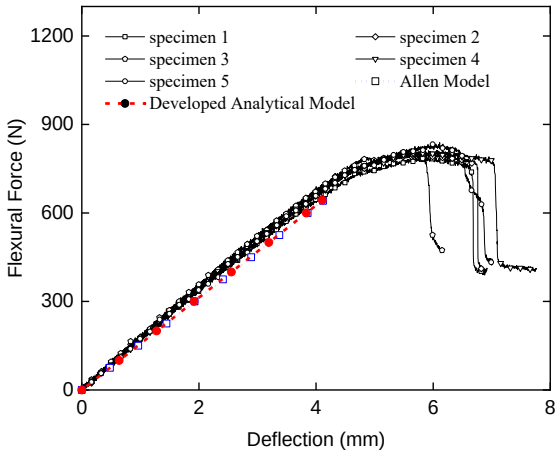



Figure 4.73. Comparison of experimental and analytical force-deflection curves of D75T10F4L250 coded sandwich beam

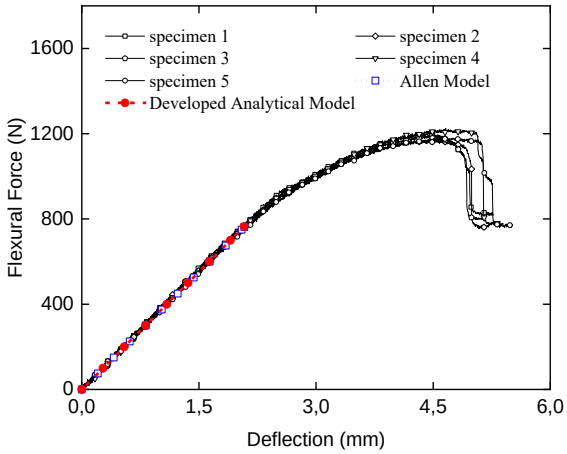



Figure 4.74. Comparison of experimental and analytical force-deflection curves of D75T20F4L250 coded sandwich beam

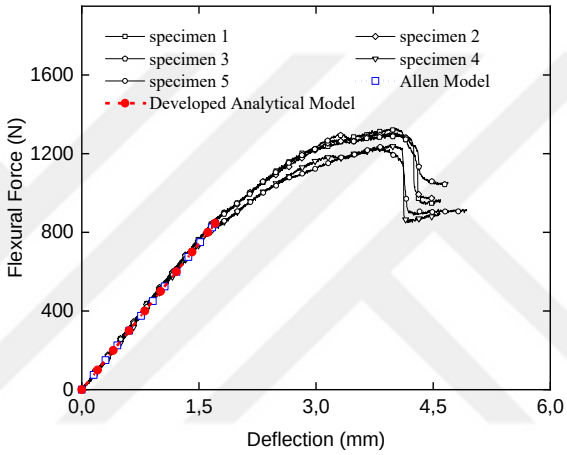



Figure 4.75. Comparison of experimental and analytical force-deflection curves of D75T30F4L250 coded sandwich beam

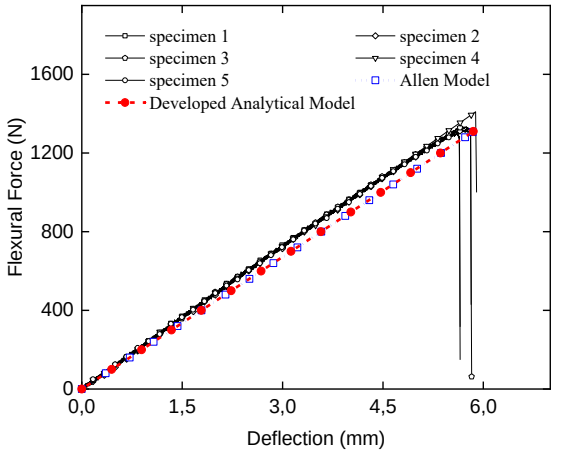



Figure 4.76. Comparison of experimental and analytical force-deflection curves of D130T10F4L250 coded sandwich beam

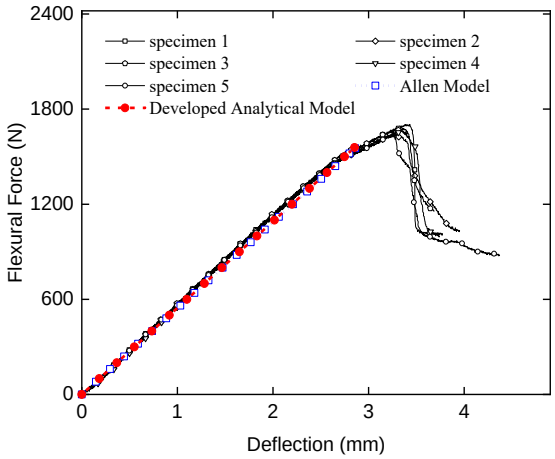



Figure 4.77. Comparison of experimental and analytical force-deflection curves of D130T20F4L250 coded sandwich beam

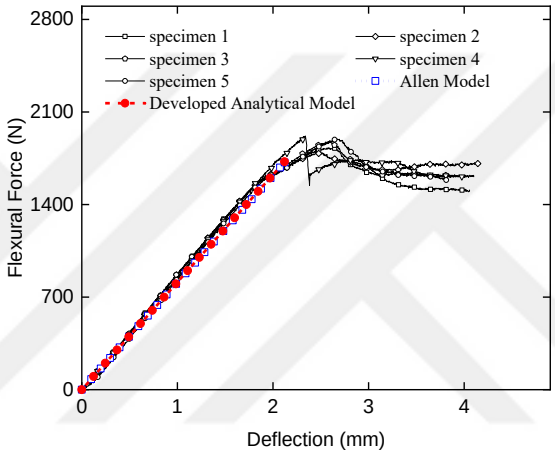



Figure 4.78. Comparison of experimental and analytical force-deflection curves of D130T30F4L250 coded sandwich beam

*Relationship between the flexural behaviors of short and long span length sandwiches*

Noticeably, differences exist between the flexural load-deflection curves for short and long sandwiches. Compared to the sandwich beams tested at short span length, the deflection values of those tested at long span length increased while the slopes of the curves decreased. Also, the maximum failure load values decreased. However, the force values at which they reached the linear limit remained the same. For example, beam D48T20F4L250 2.2 mm reached its linear limit at 466 N and failed at 739 N at maximum load. The beam D48T20F4L100 was at its linear limit at 0.8 mm and 454 N and failed at 870 N.

A different phenomenon that distinguished the specimens tested with long-span lengths from those with short-span lengths occurred in specimens made of PVC foam core materials with a 130 kg/m$^3$ density. Except for these specimens (in Figures 4.71, 4.72, and 4.73), the specimens have curved forms that reach the linear limit and then increase nonlinearly to reach the maximum failure loads. The curves forming these figures fail at the linear limit or immediately after increasing slightly with a lower slope after the linear limit. The specimens of D130T10F4L250 beams especially failed

when they had linear curve forms. D130T20F4L250 and D130T30F4L250 do not have a nonlinear form like other beams, although they increase at a slightly different slope after reaching the linear limit. In order to explain the reason for these differences, pictures of the beams with the same sandwich properties except for the span length at fracture are presented in Figures 4.74, 4.75, and 4.76.

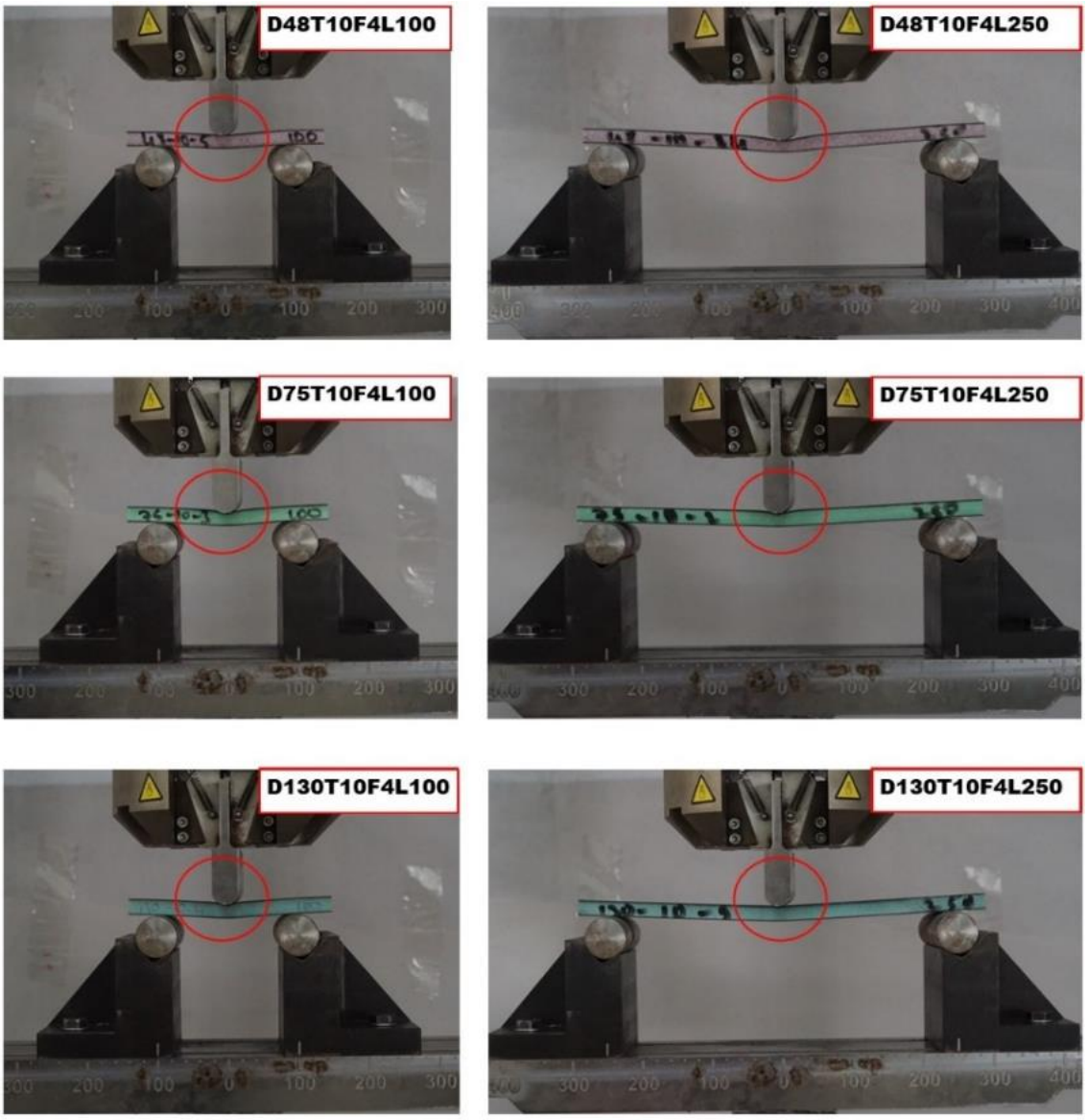



Figure 4.79. Images of sandwiches with 10 mm core thickness and four-ply plain woven fabric composite facesheet at failure under three-point bending load

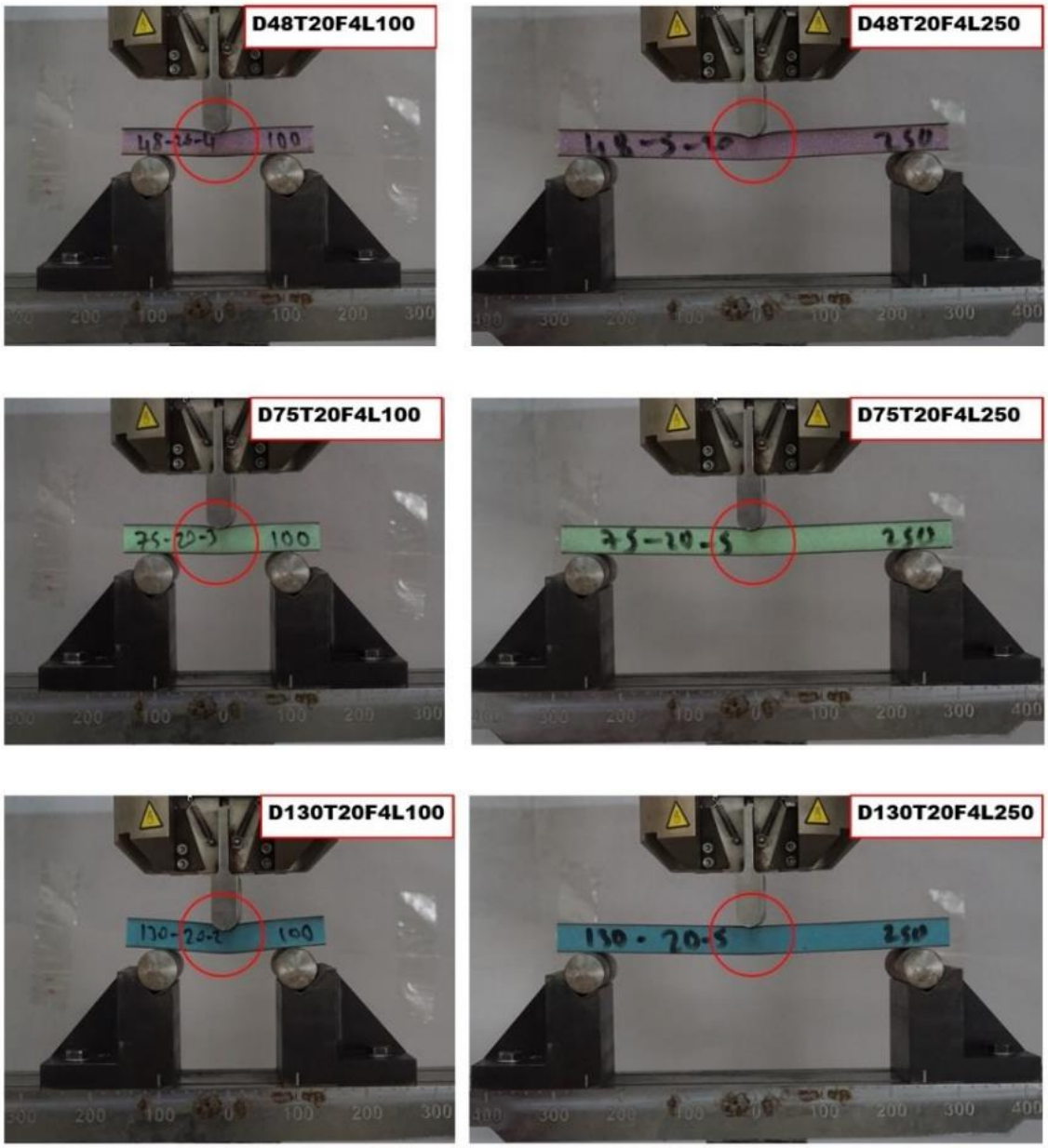



Figure 4.80. Images of sandwiches with 10 mm core thickness and four-ply plain woven fabric composite facesheet at failure under three-point bending load

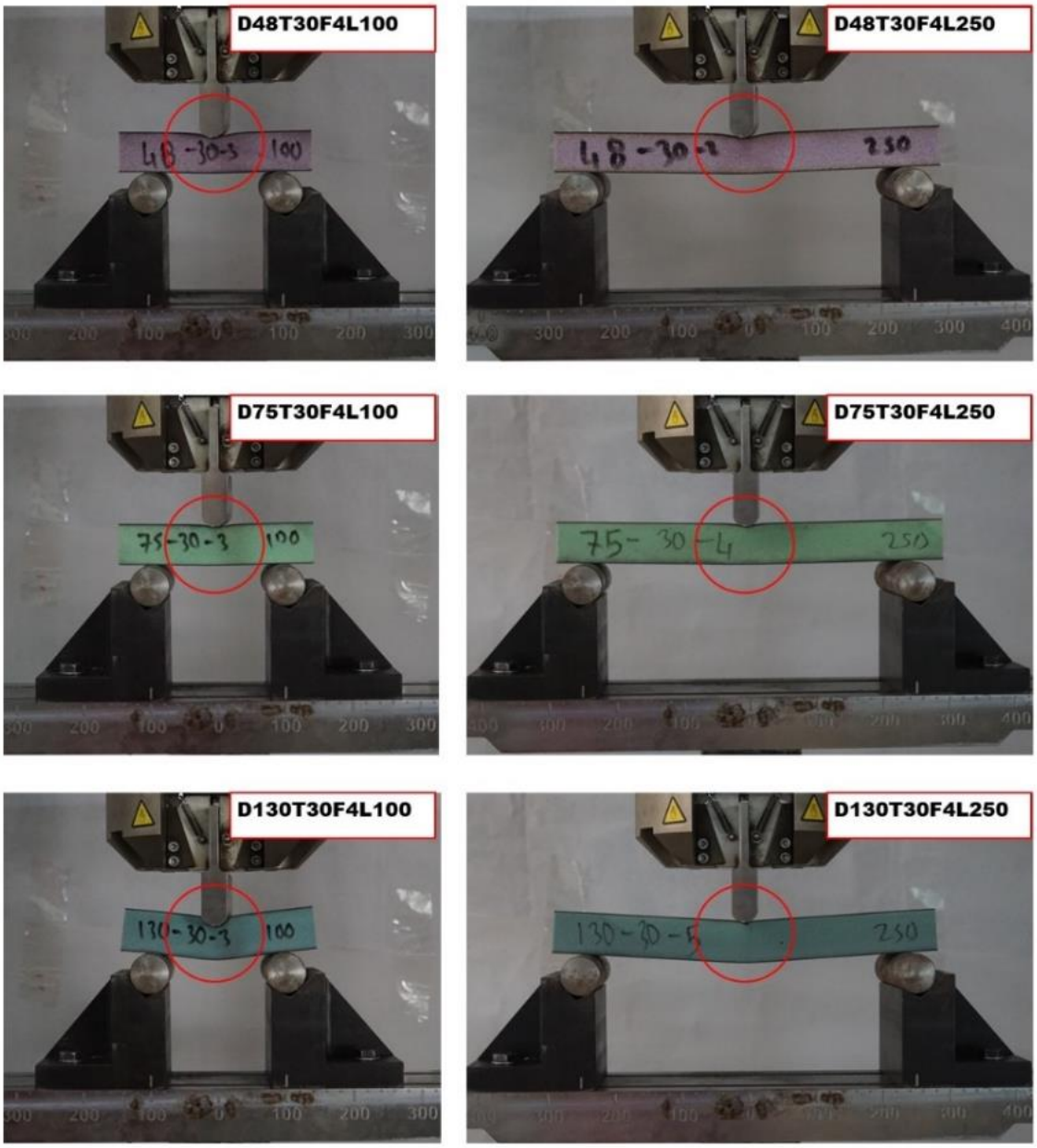


Figure 4.81. Images of sandwiches with 10 mm core thickness and four-ply plain woven fabric composite facesheet at failure under three-point bending load

As seen in the figures, the emphasis is on the interface where the indenter contacts the specimens tested in long and short span lengths. 48- and 75 kg/m3 density PVC foam core sandwiches have similar indenters at fracture and sandwich interface positions in both span lengths. For example, when the D48T30F4L100 and D48T30F4L250 in Figure 4.76 are examined, the failure pattern in the sandwich around the indenter is similar in both: the core is slightly reduced due to the indenter, and the indenter has formed a cavity there. This relationship is similar in other comparisons. However, there is a difference in the failure pictures of short and long-span lengths for the specimen made of PVC foam core material with a density of 130 kg/m$^3$. When the specimens tested at short span length failed, the indenter locally crushed the core material. However, in the pictures of the

specimens tested at a long span length at the time of fracture, there is no local crushing of the core material caused by the indenter.

In summary, the difference and similarity in the forms of all load-deflection curves in the nonlinear region is the crushing damage caused by the indenter on the core. The local crushing of the indenter on the core caused a nonlinear form in the forms of the curves after the linear limit. However, the force-displacement curves of the specimens without local crushing of the core material did not have a nonlinear form after the linear limit force. The specimens failed at or just after the linear limit force with a slight increase in force.

*Comparison of modified analytical model results for failure loads with experimental results and literature models*

Sandwiches have failure modes according to their fracture patterns. For the sandwiches designed and manufactured in the study, the failure modes predicted in Table 4.11 are core shear or indentation failure modes. In this table, the maximum load obtained from analytical models, smaller than the other one, was accepted as failure mode. The closer loads were assumed to be in the transition range of the two failure modes. According to this table, the sandwich beams that may have core shear failure are compared with the experimental results in Table 4.28. There are six sandwich beams where core shear failure is predicted to occur. However, when the percentage differences with the experimental results were examined, it was revealed that four of them differed by ten percent or less. While these sandwich beams can be said to have failed under core shear failure load, the percentage differences for the D48T10F4L100 and D48T20F8L100 beams are sixteen and forty-two percent, respectively. These two beams may not have failed in the core shear failure mode as high percent difference in Table 4.29indicate. These beams' analytically-estimated indentation failure loads were also compared with experimental results.

Table 4.28. Comparison of core shear loads obtained from analytical models with experimental results

| **Configuration code** | **Expected Failure Mode** | **Analytical Core Shear Load** | **Experimental Maximum Load** | **Diff.** |
|---|---|---|---|---|
| | | **N** | **N** | **%** |
| D48T10F4L100 | Core Shear | 525 | 627±13 | 16.3 |
| D48T10F4L250 | Indentation or core shear | 525 | 480±22 | 9.4 |
| D75T10F4L100 | Indentation or Core Shear | 1100 | 1072±30 | 2.6 |
| D48T20F8L100 | Core shear | 1050 | 1815±80 | 42.1 |
| D75T20F8L100 | Core shear | 2200 | 2445±45 | 10.0 |
| D130T20F8L100 | Core shear | 4200 | 3943±222 | 6.5 |

According to the analytical predictions in Table 4.11, failure modes of the other configurations for D48T10F4L250 and D75T10F4L100 beams given in Table 4.30 are predicted to be at the transition boundary between the two failure modes. The differences between the analytical core shear load and experimental results for these two beams are less than ten percent. The type of failure modes, which may be core shear or indentation failure, can be determined by scrutinizing the differences in load results. Analytical and experimental indentation load differences in higher percentages should be determined. Consequently, from the comparisons in Table 4.29 and analytical predictions in 4.11, it can be concluded that beams coded D75T20F8L100 and D130T20F8L100 fail in core shear failure mode.

On the other hand, for the remaining 19 of the 21 beams, the analytically-predicted indentation loads needed to be compared with the experimental results. The indentation forces for these beams were obtained analytically and given in Table 4.29. The table shows the analytical results obtained with the modified equation and the original model equation developed by Fleck and Steves. The difference in the results obtained from the two analytical approaches is less than 0.5 percent. The results show that the modified approach adopted in this thesis work is successful. In addition, it has eliminated the experimental tests required for the composite face materials. It can be said that successful engineering approaches developed in this work for sandwich beams can be used to determine flexural stiffness, core yield, and indentation loads without needing composite face material experimental test data.

The analytical results presented in Table 4.29 are compared with the experimental results in Table 4.30. Both models are compared with the experimental results separately, and the load differences are given in percentages. The percentage differences in comparing analytical approaches with experimental results are close to each other. The experimental and analytical indentation load differences of the five sandwich beams in the table, shown in "*", are between ten and fifteen percent. The percentage differences for six beams in the table shown in "♣" are between five and ten percent, and for eight beams, they are less than five percent.

Table 4.29. Comparison of indentation loads obtained from the original and modified models

| Configuration code | Expected Failure Mode | Original model | Modified model | Diff. |
|---|---|---|---|---|
| | | Indentation load | Indentation load | |
| | | $P_2$ (N) | $P_2$ (N) | % |
| D48T10F4L100 | Indentation | 700.90 | 703.87 | 0.42 |
| D48T20F4L100 | Indentation | 883.07 | 886.81 | 0.42 |
| D48T30F4L100 | Indentation | 1010.87 | 1015.15 | 0.42 |
| D48T10F4L250 | Indentation or Core Shear | 516.42 | 518.61 | 0.42 |
| D48T20F4L250 | Indentation | 650.65 | 653.41 | 0.42 |
| D48T30F4L250 | Indentation | 744.81 | 747.97 | 0.42 |
| D75T10F4L100 | Indentation or Core Shear | 1112.60 | 1117.31 | 0.42 |
| D75T20F4L100 | Indentation | 1401.80 | 1407.72 | 0.42 |
| D75T30F4L100 | Indentation | 1604.64 | 1611.45 | 0.42 |
| D75T10F4L250 | Indentation | 819.77 | 823.25 | 0.42 |
| D75T20F4L250 | Indentation | 1154.52 | 1159.42 | 0.42 |
| D75T30F4L250 | Indentation | 1321.60 | 1327.20 | 0.42 |
| D130T10F4L100 | Indentation | 1974.21 | 1982.57 | 0.42 |
| D130T20F4L100 | Indentation | 2487.35 | 2497.88 | 0.42 |
| D130T30F4L100 | Indentation | 3132.32 | 3145.59 | 0.42 |
| D130T10F4L250 | Indentation | 1454.61 | 1460.77 | 0.42 |
| D130T20F4L250 | Indentation | 1832.70 | 1840.46 | 0.42 |
| D130T30F4L250 | Indentation | 2097.91 | 2106.80 | 0.42 |
| D48T20F8L100 | Indentation | 1766.14 | 1771.80 | 0.32 |

When experimental and analytical results in Tables 4.28 and 4.30 are compared, a more accurate prediction can be obtained for beams with unclear or undetermined failure modes. For beam coded D48T10F4L100, the core shear load difference (16.3%) is larger than the indentation load difference (12.25%), when compared to the experimental result. Accordingly, the failure mode of the beam is closer to indentation. There is a similar situation for the D48T10F4L100 coded beam. The core shear difference is 42.1%, much higher than the indentation difference (2.42%). It is obvious that this beam failed by indentation. Although the two beams are expected to fail in core shear failure mode according to the results in Table 4.11, they fail due to the indentation according to the experimental results in Tables 4.28 and 4.30. However, the expectation of core shear failure in the analytical predictions in Table 4.11 cannot be ignored. This is because the core shear load predictions are smaller than the experimental maximum loads. Hence, it can be said that this provides safe and better predictions in the sandwich design. For D48T10F4L250 and D75T10F4L100 beams, whose core shear and indentation load predictions are close to each other in Table 4.11, the differences with the experimental results in Table 4.28 and Table 4.30 are close to each other. Thus, the inference made for these beams in the transition zone of core shear and indentation failure is supported by the comparison with the experimental results in the tables.

Table 4.30. Comparison of indentation loads obtained from the original and modified models with experimental results

| Sandwich Conf. code | Experimental | Original model | | Modified model | |
|---|---|---|---|---|---|
| | Maximum failure load | Indentation load | Diff. | Indentation load | Diff. |
| | N | N | % | N | % |
| D48T10F4L100* | 627±13 | 700.90 | 11.80 | 703.87 | 12.25 |
| D48T20F4L100 | 870±20 | 883.07 | 1.50 | 886.81 | 1.93 |
| D48T30F4L100♣ | 958±63 | 1010.87 | 5.52 | 1015.15 | 5.97 |
| D48T10F4L250♣ | 480±22 | 516.42 | 7.59 | 518.61 | 8.04 |
| D48T20F4L250* | 739±14 | 650.65 | 11.96 | 653.41 | 11.58 |
| D48T30F4L250 | 734±24 | 744.81 | 1.47 | 747.97 | 1.90 |
| D75T10F4L100 | 1072±30 | 1112.60 | 3.79 | 1117.31 | 4.23 |
| D75T20F4L100♣ | 1281±38 | 1401.80 | 9.43 | 1407.72 | 9.89 |
| D75T30F4L100♣ | 1489±50 | 1604.64 | 7.77 | 1611.45 | 8.22 |
| D75T10F4L250 | 810±15 | 819.77 | 1.21 | 823.25 | 1.64 |
| D75T20F4L250 | 1194±18 | 1154.52 | 3.31 | 1159.42 | 2.90 |
| D75T30F4L250 | 1282±36 | 1321.60 | 3.09 | 1327.20 | 3.53 |
| D130T10F4L100* | 1722±43 | 1974.21 | 14.65 | 1982.57 | 15.13 |
| D130T20F4L100♣ | 2286±75 | 2487.35 | 8.81 | 2497.88 | 9.27 |
| D130T30F4L100 | 3210±67 | 3132.32 | 2.42 | 3145.59 | 2.01 |
| D130T10F4L250♣ | 1336±38 | 1454.61 | 8.88 | 1460.77 | 9.34 |
| D130T20F4L250* | 1663±27 | 1832.70 | 10.20 | 1840.46 | 10.67 |
| D130T30F4L250* | 1876±30 | 2097.91 | 11.83 | 2106.80 | 12.30 |
| D48T20F8L100 | 1815±80 | 1766.14 | 2.70 | 1771.80 | 2.42 |

♣ The six sandwich beams differences are between five and ten percent
* The five sandwich beams differences are between ten and fifteen percent

On the other hand, there are failure maps where the failure modes of sandwich beams can be determined; for example, the maps for PVC foam core sandwich beams are presented in Figure 4.28. The figure contains maps for high-density and medium-density PVC foam cores. Both maps are similar in form. As the ratio of core thickness to span length decreases, indentation failure is effective, while as the ratio of facesheet thickness to core thickness increases, core shear failure is effective, as detailed in Figure 4.82. If the failure modes of several beams are analyzed from this perspective, the map's guidance can be better understood. Beam D75T10F4L100 failed in the transition zone between core shear and indentation failure, as given in Table 4.28. Since beam D75T10F4L250 has a longer span length (250 mm) than beam D75T10F4L100, the ratio of core thickness to span length for beam D75T10F4L250 is lower. The long beam failed in the indentation failure mode, as given in Table 4.31. D75T2F4L100 coded beam failed in the indentation failure mode according to the results in Table 4.30. Since the facesheet thickness of the beam D75T2F8L100 coded beam is higher than that of beam D75T2F4L100, the facesheet core thickness ratio for coded beam D75T2F8L100 is increased. Therefore, beam coded D75T2F8L100 is expected to have core shear failure differently from the beam D75T2F4L100. This beam also failed in core shear, according to the results in Table 4.28.

The collapse maps of sandwich beams given in Figure 4.28 and described in Figure 4.82 depend on the span length, core thickness, and surface layer thickness. These maps are essential but may differ for each core material, such as low-density, medium-density, and high-density PVC foam. For example, coded beams of D48T20F8L100 and D75T20F8L100 have the same sizes but different core densities. The experimental results of beam D48T20F8L100 were closer to the indentation predictions, while beam D75T20F8L100 had the core shear failure. It shows that although the maps obtained for PVC cores have a similar form (Figure 4.29), the location of the boundary curve may vary according to the numerical ratios.

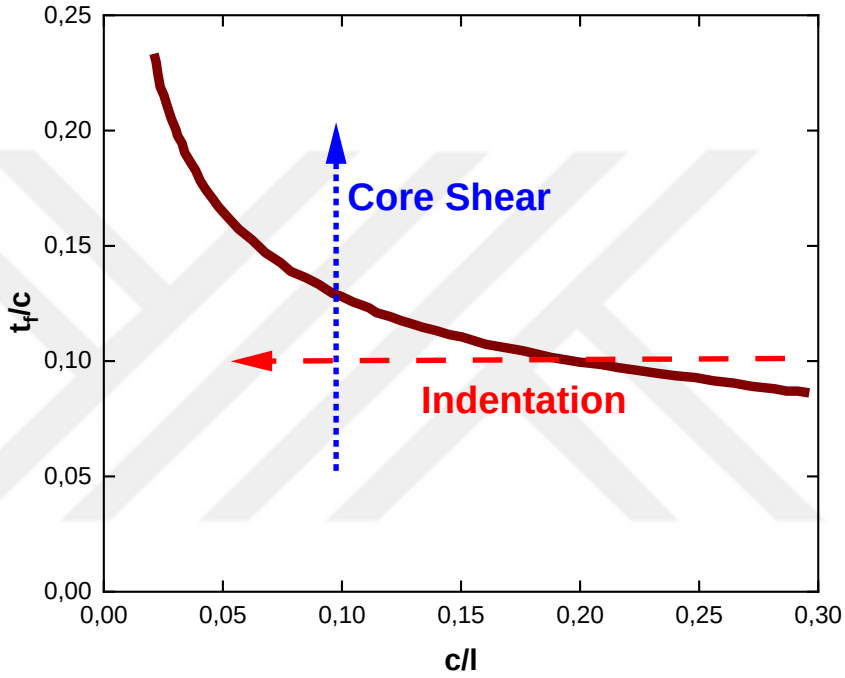



Figure 4.82. Demonstration of the use of failure maps of sandwich beams made of PVC foam core material

The experiments produced five different composite plates with five different production methods. This section compares analytical approaches for predicting the maximum ultimate bearing capacity of sandwich beams and the new approach obtained by modifying the model for predicting the indentation loading with the experimental results. The functionality of failure maps is also discussed. However, although the results obtained with the existing indentation model and the modified approach are quite close, they cannot predict the maximum load value of several beams. These beams are D48T10F4L100, D48T20F4L250, D130T10F4L100, D130T20F4L250, and D130T30F4L250. Although the modified model eliminates the need for experimental testing of the composite face materials, the original analytical model formulation was not fully successful in predicting maximum loads.

Therefore, there is a need to develop a new, reliable, robust, and definite analytical model formulation that can predict the indentation forces better than the original model. Fiber-reinforced composite properties obtained by composite mechanics can be used for a new indentation approach, which may be developed in the future. Because the modified approach results show that the face properties can be predicted by composite mechanics when predicting the indentation failure load of sandwich beams.

## 5. CONCLUSIONS

This study has proposed engineering approaches to predict the flexural performance of sandwich beams with plain woven fabric composite and PVC foam materials. Firstly, a practical engineering approach was developed to predict the mechanical properties of the face layer. This approach defines an engineering fiber volume fraction to eliminate the complex analytical assumptions due to undulation and elliptical yarn cross-sectional area of the fabric. The engineering fiber volume fraction was used to obtain the mechanical properties ($E_1$, $E_2$, $v_{12}$, $G_{12}$) of the composite considered cross-ply. The stiffness matrices and average moduli of elasticity of the layered plate were obtained by classical laminate theory. Secondly, flexural stiffness, core yield, indentation, and core shear failure loads of sandwich beams were obtained analytically. The sandwich's stiffness matrices were obtained depending on the sandwich thickness and the stiffness matrices of the composite face material. Then, the flexural stiffness of the sandwich beam was obtained with the beam's bending stiffness term and width. In the core yield and indentation analytical approaches, the flexural stiffness $(E_f I_f)$ of the face material is replaced by the bending stiffness $(D_{11}b)$. So, the necessity for experimental tests for the face material were eliminated.

The engineering approaches developed are compared with experimental and reliable models available in the literature. Based on five different production methods, five different composite plates were produced for experiments: hand lay-up, low vacuum, infusion, mold compression, and high vacuum. Bending and axial tensile test specimens were obtained from the composite plates and tested. The test results were compared with the practical engineering approach. The approach is also compared with the Slice Array Model (SAM) provided by Naik and Ganesh (1992) for single-ply composite plates.

For sandwich beams, twenty-one different sandwich plates were produced depending on parameters such as core density (48 kg/m$^3$, 80 kg/m$^3$, 130 kg/m$^3$), thickness (10 mm, 20 mm, 30 mm), face layer (four layers and eight layers), and span length (100 mm and 250 mm). The flexural test results of the sandwich beam were compared with the developed models for the sandwich beam. The model developed for flexural stiffness was compared with the Allen (1969) model in the literature, whereas the modified approaches for core yield and indentation loads are compared with Shuaeib&Soden's (1997) and Steeves&Fleck's (2004a) model results, respectively.

The conclusions obtained from the study can be summarized in two main groups as follows;

The practical engineering approach was first developed for plain woven fabric composite plates is summarized in the following points,

- The approach is compared to the Slice Array Model (SAM) (Naik and Ganesh, 1992). Both methods for single-ply fabric composite plates obtained the stiffness matrices. When the results obtained for the axial stiffness term ($A_{11}$) were compared, the differences between

both models were 4.7% and less. When the bending stiffness term ($D_{11}$) results are compared, the differences are 4.4% and below. The difference in the results of the stiffness terms obtained from the models is less than 5%. Results show that the practical engineering approach is usable for the design of single-ply composite plates.

- The approach predicts the strength properties of composite plates as tensile warp ($\sigma_{warp}^{T}$) and fill ($\sigma_{fill}^{T}$) strength. The approach states that micro fractures will start with the $\sigma_{fill}^{T}$ of the plate under tensile load, and the plate will fail before reaching the $\sigma_{warp}^{T}$ strength. The practical engineering approach was compared with the empirical model results, validated with experimental data presented by Wang et al. (2019) in the literature. The tensile strength results presented in the literature are found to be between the ($\sigma_{warp}^{T}$) and ($\sigma_{fill}^{T}$) strengths obtained with the approach. This comparison also supported the failure interpretation as suggested by the present approach.
- Axial tensile test results of four-ply composite plates were compared with the analytical results obtained from the approach. Elastic modulus, strength, load extension, and stress-strain curves were evaluated. The difference between the experimental and analytical average elastic modulus obtained from the approach is 4.5% or less. Experimental tensile strength results are between the fill ($\sigma_{\text{fill}}^{\text{T}}$) and warp ($\sigma_{\text{warp}}^{\text{T}}$) strengths obtained by the approach. Experimental tensile strength values are between $\sigma_{\text{warp}}^{\text{T}}$ and $\sigma_{\text{fill}}^{\text{T}}$ strength as suggested by the present approach.
- The success of the approach in bending was also validated by subjecting four-ply fabric composite plates to flexural tests. The difference in the average flexural elastic modulus results obtained from the experimental and the developed analytical approach is 5.82% or less. The maximum load values obtained experimentally and by the presently proposed approach are very close. Accordingly, the load-deflection curves approximately overlapped with slight error. The stress distributions between the layers under maximum bending loads were compared experimentally and by the zigzag method. Fill yarn and warp yarn stress transitions between the layers are presented analytically by the zigzag method. In the zigzag method, the average stress values at the transition between the layers equal to the calculated experimental stress according to ASTM D790.

Secondly, the concluding remarks on the engineering approaches developed for sandwich beams are summarized as follows,

- In the developed engineering model, the flexural stiffness of the sandwiches was obtained from the bending stiffness of composite face materials. They were compared to prove the accuracy of the developed model with results obtained with Allen Model in the literature (Allen, 1969a). Although the maximum difference in the comparison was

7.1%, it is possible to reduce it depending on the manufacturing quality or increased $V_f$ (the difference is only 1.4% for MT5 product). While the developed model does not require the experimental data of the face material, the Allen model relies on test results of composite plates.

- The flexural stiffness of the sandwich beams subjected to three-point bending tests was obtained experimentally and then compared with developed engineering approach and Allen model. The approach provided close predictions, which the maximum difference with the experiments is 4.5% and 6.2% for Allen model.
- This study modified the core yield load model which was presented by Shuaeib and Soden (1997). After the modification, the core yield load of the sandwich beam can be predicted without the need for experimental data of composite face material. The core yield forces of the sandwich beams produced and designed in the study were obtained with the modified model. The results were compared with the results obtained from the original model. The difference between the results obtained from the two models is 0.5% or less. Moreover, the experimental results validated both models with close approximations
- The study obtained load-displacement curves with engineering approaches that can predict flexural stiffness and core yield load without the need for experimental data of the composite face materials. The curves were obtained up to the point where the linear region ends. Similarly, load-displacement curves were drawn with the help of the results obtained from the Allen and Shuaeib&Soden models available in the literature. When the curves obtained by both analytical methods were compared with the experimental findings, it was seen that the analytical curves overlap and are in good agreement with the experimental curve for each beam.
- As in the core yield model, the indentation model provided by Steeves and Fleck (2004a) was modified with stiffness terms of composite face material. When the results obtained with the modified and original models are compared, the difference is 0.42%. The results are quite close to each other.
- The analytical results obtained from the modified and original indentation models were compared with the maximum experimental loads. The differences with the modified model were between %15.13 and %1.64, whereas the differences with the original model were between %14.65 and %1.50. Although the percent differences of the models with the experimental results are similar, the range between the maximum and minimum difference obtained for both models is extensive (%15.13 -%1.64 and %14.65-%1.50).

***Following studies can be considered for future research works:***

- The practical engineering approach can be used to predict the mechanical properties of plain woven fabric composite with different fiber materials and cell size properties.
- The developed engineering approaches can be used to predict the flexural performances of sandwich beams with composite face materials with different layer configurations.
- The flexural performance of cantilevered and/or four-point bending sandwich beams in flexural loading can be obtained with the developed engineering approach.
- A new approach, which utilizes the stiffness terms of the composite face material, can be developed to predict the indentation load with the low error percentages.

**REFERENCES**


Abdelal, N., Donaldson, S.L., 2017. Comparison of methods for the characterization of voids in glass fiber composites. Journal of Composite Materials 52, 487-501.

Adumitroaie, A., Barbero, E.J., 2012. Stiffness and Strength Prediction for Plain Weave Textile Reinforced Composites. Mechanics of Advanced Materials and Structures 19, 169-183.

Agarwal, B.D., Broutman, L.J., Chandrashekhara, K., 2017. Analysis and Performance of Fiber Composites. Wiley.

Ahmed, U., Tariq, A., Nawab, Y., Shaker, K., Khaliq, Z., Umair, M., 2020. Comparison of Mechanical Behavior of Biaxial, Unidirectional and Standard Woven Fabric Reinforced Composites. Fibers and Polymers 21, 1308-1315.

Akkerman, R., 2005. Laminate mechanics for balanced woven fabrics. Composites Part B: Engineering 37, 108-116.

Ali, I., Qi, S., Shi, P., Ammar, M., Ali, A., 2021. Investigation of mass distribution between core and face sheet on bending energy absorption of self-reinforced PP sandwich beams. Thin-Walled Structures 159, 107283.

Aljibori, H., Alosfur, F., Ridha, N., Salim, M., 2016. A Study on Thermal Diffusivity and Dielectric Properties of Epoxy Matrix Reinforced by Fibers Material. 14, 42-53.

Allen, H.G., 1969. Chapter 2 - Sandwich Beams, in: Allen, H.G. (Ed.), Analysis and Design of Structural Sandwich Panels. Pergamon, pp. 8-47.

Allen, H.G., Neal, B.G., 2013. Analysis and Design of Structural Sandwich Panels: The Commonwealth and International Library: Structures and Solid Body Mechanics Division. Elsevier Science.

Ashby, M., Evans, A., Fleck, N., Gibson, L., Hutchinson, J., Wadley, H.N.G., 2002. Metal Foams: a Design Guide. Materials & Design 23, 119.

Ashby, M.F., 2016. Materials Selection in Mechanical Design. Elsevier Science.

Ashraf, W., Ishak, M.R., Zuhri, M.Y.M., Yidris, N., Ya'acob, A.M., 2021. Experimental Investigation on the Mechanical Properties of a Sandwich Structure Made of Flax/Glass Hybrid Composite Facesheet and Honeycomb Core. International Journal of Polymer Science 2021, 8855952.

ASTM, I., 2017. Standard Test Methods for Flexural Properties of Unreinforced and Reinforced Plastics and Electrical Insulating Materials, ASTM D790-17, West Conshohocken, PA,.

Awad, Z.K., Aravinthan, T., Manalo, A., 2012. Geometry effect on the behaviour of single and glue-laminated glass fibre reinforced polymer composite sandwich beams loaded in four-point bending. Materials & Design 39, 93-103.

Balıkoğlu, F., Demircioğlu, T.K., 2022. Flexural behaviour of the composite sandwich beams with grid-scored foam: Experimental and theoretical approach. Thin-Walled Structures 171, 108691.

Banghai, J., Zhibin, L., Fangyun, L., 2015. Failure mechanism of sandwich beams subjected to three-point bending. Composite Structures 133, 739-745.

Betts, D., Sadeghian, P., Fam, A., 2021. Post-impact residual strength and resilience of sandwich panels with natural fiber composite faces. Journal of Building Engineering 38, 102184.

Bey, K., Tadjine, K., Khelif, R., Chemami, A., Benamira, M., Azari, Z., 2015. Mechanical Behavior of Sandwich Composites Under Three-Point Bending Fatigue. Mechanics of Composite Materials 50, 747-756.

Bhattacharjee, A., Roy, H., 2020. Assessment of tensile and damping behaviour of hybrid particle/woven fibre/polymer composites. Composite Structures 244, 112231.

Birman, V., Lee, J., 2019. Wrinkling in sandwich panels with bi-modular core. ZAMM - Journal of Applied Mathematics and Mechanics. 1, 44-2267

Budiansky, B. ,1983. Micromechanics. Computers & Structures, 16,1-4, 3-12.

Buschow, K.H.J., 2001. Encyclopedia of Materials: Science and Technology. Elsevier.

Cai, L., Zhang, D., Zhou, S., Xu, W., 2018. Investigation on Mechanical Properties and Equivalent Model of Aluminum Honeycomb Sandwich Panels. Journal of Materials Engineering and Performance 27, 6585-6596.

Callister, W.D., Rethwisch, D.G., 2012. Fundamentals of Materials Science and Engineering: An Integrated Approach. Wiley.

Callister, W.D., Rethwisch, D.G., 2016. Fundamentals of Materials Science and Engineering: An Integrated Approach, 5th Edition. Wiley.

Carlsson, L.A., Kardomateas, G.A., 2011. Structural and Failure Mechanics of Sandwich Composites. Springer Netherlands.

Chen, C., Harte, A.M., Fleck, N.A., 2001. The plastic collapse of sandwich beams with a metallic foam core. International Journal of Mechanical Sciences 43, 1483-1506.

Chen, J., Fang, H., Liu, W., Qi, Y., Zhu, L., 2018. Experimental and Numerical Analysis of Nonlinear Flexural Behaviour of Lattice-Web Reinforced Foam Core Composite Sandwich Panels. Advances in Civil Engineering 2018, 2972931.

Chen, S., McGregor, O.P.L., Harper, L.T., Endruweit, A., Warrior, N.A., 2016. Defect formation during preforming of a bi-axial non-crimp fabric with a pillar stitch pattern. Composites Part A: Applied Science and Manufacturing 91, 156-167.

Cox, B., Flanagan, G., 1997. Handbook of Analytical Methods for Textile Composites.

Crupi, V., Epasto, G., Guglielmino, E., 2012. Collapse modes in aluminium honeycomb sandwich panels under bending and impact loading. International Journal of Impact Engineering 43, 6-15.

Crupi, V., Montanini, R., 2007. Aluminium foam sandwiches collapse modes under static and dynamic three-point bending. International Journal of Impact Engineering 34, 509-521.

Çetin, A., Uzay, Ç., Geren, N., Bayramoğlu, M., Tütüncü, N., 2023. A practical approach to predict the flexural properties of woven plain carbon fiber/epoxy laminates. Mechanics of Advanced Materials and Structures 30, 1801-1811.

Daniel, I., Gdoutos, E., 2010. Failure Modes of Composite Sandwich Beams, pp. 197-227.

Daniel, I.M., Gdoutos, E.E., Rajapakse, Y.D.S., 2009. Major Accomplishments in Composite Materials and Sandwich Structures: An Anthology of ONR Sponsored Research. Springer Netherlands.

Daniel, I.M., Gdoutos, E.E., Wang, K.A., Abot, J.L., 2002. Failure Modes of Composite Sandwich Beams. International Journal of Damage Mechanics 11, 309-334.

Dariushi, S., Sadighi, M., 2013. A study on flexural properties of sandwich structures with fiber/metal laminate face sheets. Applied Composite Materials. 20, 839-855.

Darzi, S., Karampour, H., Bailleres, H., Gilbert, B.P., Fernando, D., 2020a. Load bearing sandwich timber walls with plywood faces and bamboo core. Structures 27, 2437-2450.

Darzi, S., Karampour, H., Bailleres, H., Gilbert, B.P., McGavin, R.L., 2020b. Experimental study on bending and shear behaviours of composite timber sandwich panels. Construction and Building Materials 259, 119723.

Darzi, S., Karampour, H., Gilbert, B.P., Bailleres, H., 2018. Numerical study on the flexural capacity of ultra-light composite timber sandwich panels. Composites Part B: Engineering 155, 212-224.

Davies, J.M., 2001. Lightweight Sandwich Construction. Wiley.

Delawa, U., 1990. Delaware Composites Design Encyclopedia: Processing and Fabriactaion Technology. Taylor & Francis.

Dixit, A., Mali, H.S., Misra, R.K., 2014. A Micromechanical Unit Cell Model of 2 × 2 Twill Woven Fabric Textile Composite for Multi Scale Analysis. Journal of The Institution of Engineers (India): Series E Chemical and Textile Engineering.

Dost Kimya, 2009. Laminating Resin MGSTM L160 and Hardener H160, Hexion, Technical Data Sheet, The Netherlands.

Dost Kimya, 2014. Technical Data Sheet, Carbon Fabric – 200gr/sqm 3K Plain. Rev.2.2, Turkey, 1.

Endruweit, A., Gommer, F., Long, A.C., 2013. Stochastic analysis of fibre volume fraction and permeability in fibre bundles with random filament arrangement. Composites Part A: Applied Science and Manufacturing 49, 109-118.

Fadaee, M., 2019. Exact solution for shear deformable model of free damped vibration of magnetorheological fluid sandwich beam. Mechanics Based Design of Structures and Machines 47, 1-15.

Funari, M.F., Spadea, S., Lonetti, P., Lourenço, P.B., 2021. On the elastic and mixed-mode fracture properties of PVC foam. Theoretical and Applied Fracture Mechanics 112, 102924.

Gao, J., Chen, W., Yu, B., Fan, P., Zhao, B., Hu, J., Zhang, D., Fang, G., Peng, F., 2019. A multi-scale method for predicting ABD stiffness matrix of single-ply weave-reinforced composite. Composite Structures 230, 111478.

Gargano, A., Das, R., Mouritz, A.P., 2022. Comparative experimental study into the explosive blast response of sandwich structures used in naval ships. Composites Communications 30, 101072.

Gdoutos, E., Daniel, I., 2010. Failure of Sandwich Structures. Bulgarian Journal of Theoretical and Applied Mechanics 40, 35-46.

Gdoutos, E.E., Daniel, I.M., Wang, K.A., 2002. Indentation failure in composite sandwich structures. Experimental Mechanics 42, 426-431.

Geren, N., Acer, D.C., Uzay, C., Bayramoglu, M., 2021. The effect of boron carbide additive on the low-velocity impact properties of low-density foam core composite sandwich structures. Polymer Composites 42, 2037-2049.

Gibson, R.F., 2011. Principles of Composite Material Mechanics, Third Edition. Taylor & Francis.

Gibson, R.F., 2016. Principles of Composite Material Mechanics. CRC Press.

Gopinath, G., Batra, R.C., 2018. A common framework for three micromechanics approaches to analyze elasto-plastic deformations of fiber-reinforced composites. International Journal of Mechanical Sciences 148, 540-553.

Haldar, S., Bruck, H.A., 2014. Mechanics of composite sandwich structures with bioinspired core. Composites Science and Technology 95, 67-74.

Harizi, W., Anjoul, J., Acosta Santamaría, V.A., Aboura, Z., Briand, V., 2021. Mechanical behavior of carbon-reinforced thermoplastic sandwich composites with several core types during three-point bending tests. Composite Structures 262, 113590.

Hashin, Z., 1983. Analysis of Composite Materials—A Survey. Journal of Applied Mechanics 50, 481-505.

Hashin, Z., Pennsylvania, U.o., Center, L.R., 1972. Theory of Fiber Reinforced Materials. National Aeronautics and Space Administration [For sale by the National Technical Information Service, Springfield, Va.].

Hause, T.J., 2021. Sandwich Structures: Theory and Responses. Springer International Publishing.

Heyman, J., 1998. Structural Analysis: A Historical Approach. Cambridge University Press.

Hoff, N.J., Mautner, S.E., 1945. The Buckling of Sandwich-Type Panels. Journal of the Aeronautical Sciences 12, 285-297.

Hosur, M.V., Abdullah, M., Jeelani, S., 2005. Manufacturing and low-velocity impact characterization of foam filled 3-D integrated core sandwich composites with hybrid face sheets. Composite Structures 69, 167-181.

Hu, J., Gao, C., He, S., Chen, W., Li, Y., Zhao, B., Shi, T., Yang, D., 2017. Effects of on-axis and off-axis tension on uniaxial mechanical properties of plain woven fabrics for inflated structures. Composite Structures 171, 92-99.

Hull, D., 1981. An Introduction to Composite Materials. Cambridge University Press.

International, A., 2016a. Standard Test Method for Core Shear Properties of Sandwich Constructions by Beam Flexure. ASTM International.

International, A., 2016b. Standard Test Method for Flatwise Compressive Properties of Sandwich Cores: Designation: C365/C365M - 16. ASTM International.

International, A., 2017a. Standard Test Method for Tensile Properties of Polymer Matrix Composite Materials, ASTM D3039 / D3039M-17.

International, A., 2017b. Test Methods for Constituent Content of Composite Materials, ASTM Standard D 3171-99.

Ishikawa, T., Chou, T.-W., 1983a. Nonlinear Behavior of Woven Fabric Composites. Journal of Composite Materials 17, 399-413.

Ishikawa, T., Chou, T.-W., 1983b. One-dimensional micromechanical analysis of woven fabric composites. AIAA Journal. 21, 1714-1721.

Ishikawa, T., Chou, T.W., 1982. Stiffness and strength behaviour of woven fabric composites. Journal of Materials Science 17, 3211-3220.

Ivañez, I., Santiuste, C., Sanchez-Saez, S., 2010. FEM analysis of dynamic flexural behaviour of composite sandwich beams with foam core. Composite Structures 92, 2285-2291.

Jahan, I., 2017. Effect of fabric structure on the mechanical properties of woven fabrics. Advance Research in Textile Engineering. 2, 1018-1012.

Jones, R.M., 1998. Mechanics Of Composite Materials. Taylor & Francis.

Jose, J.P., Joseph, K., 2012. Advances in Polymer Composites: Macro- and Microcomposites – State of the Art, New Challenges, and Opportunities, Polymer Composites, pp. 1-16.

Kar, K.K., 2016. Composite Materials: Processing, Applications, Characterizations. Springer Berlin Heidelberg.

Karahan, M., Gul, H., Karahan, N., Ivens, J.J.J.o.R.P., Composites, 2013. Static behavior of three-dimensional ıntegrated core sandwich composites subjected to three-point bending. 32, 664-678.

Karkkainen, R.L., Sankar, B.V., 2006. A direct micromechanics method for analysis of failure initiation of plain weave textile composites. Composites Science and Technology 66, 137-150.

Karlsson, K.F., TomasÅström, B., 1997. Manufacturing and applications of structural sandwich components. Composites Part A: Applied Science and Manufacturing 28, 97-111.

Kavermann, S.W., Bhattacharyya, D., 2019. Experimental investigation of the static behaviour of a corrugated plywood sandwich core. Composite Structures 207, 836-844.

Kaw, A.K., 2005. Mechanics of Composite Materials. CRC Press.

Khan, T., Acar, V., Aydin, M.R., Hülagü, B., Akbulut, H., Seydibeyoğlu, M.Ö., 2020. A review on recent advances in sandwich structures based on polyurethane foam cores. Polymer Composites 41, 2355-2400.

Kheirikhah, M.M., Khalili, S.M.R., Malekzadeh, K., Parsafar, S., 2012. High Order Analytical and 3D Finite Element Solution for Biaxial Wrinkling Analysis of Composite-Faced Sandwich Plates With Soft Core.

Krishnasamy, S., Muthukumar, C., Thiagamani, S.M.K., Rangappa, S.M., Siengchin, S., 2022. Sandwich Composites: Fabrication and Characterization. CRC Press.

Kubo, G., Matsuda, T., Sato, Y., 2018. A novel basic cell modeling method for elastic-viscoplastic homogenization analysis of plain woven laminates with nesting. International Journal of Mechanical Sciences 146-147, 497-506.

Li, Z., Wang, Z., Wang, X., Zhou, W., 2020. Bending behavior of sandwich beam with tailored hierarchical honeycomb cores. Thin-Walled Structures 157, 107001.

Lim, T.S., Lee, C.S., Lee, D.G., 2004. Failure Modes of Foam Core Sandwich Beams under Static and Impact Loads. Journal of Composite Materials 38, 1639-1662.

Liu, C., Zhang, Y.X., Li, J., 2017. Impact responses of sandwich panels with fibre metal laminate skins and aluminium foam core. Composite Structures 182, 183-190.

Liu, J., Xiang, L., Kan, T., 2015. The effect of temperature on the bending properties and failure mechanism of composite truss core sandwich structures. Composites Part A: Applied Science and Manufacturing 79, 146-154.

Logan, D.L., 2002. A First Course in the Finite Element Method. Brooks/Cole.

Ma, W., Elkin, R., 2021. Sandwich Structural Composites: Theory and Practice. CRC Press.

MacDonnell, L., Sadeghian, P., 2020. Experimental and analytical behaviour of sandwich composites with glass fiber-reinforced polymer facings and layered fiber mat cores. Journal of Composite Materials 54, 4875-4887.

Mahbod, M., Asgari, M., 2019. Elastic and plastic characterization of a new developed additively manufactured functionally graded porous lattice structure: Analytical and numerical models. International Journal of Mechanical Sciences 155, 248-266.

Mallikarachchi, H.M.Y.C., 2019. Predicting mechanical properties of thin woven carbon fiber reinforced laminates. Thin-Walled Structures 135, 297-305.

Mamalis, A.G., Spentzas, K.N., Pantelelis, N.G., Manolakos, D.E., Ioannidis, M.B., 2008. A new hybrid concept for sandwich structures. Composite Structures 83, 335-340.

Manalo, A.C., Aravinthan, T., Karunasena, W., Islam, M.M., 2010. Flexural behaviour of structural fibre composite sandwich beams in flatwise and edgewise positions. Composite Structures 92, 984-995.

Materials, ASTM., Testing, Materials, International, A., 2009. Standard Test Methods for Flexural Properties of Unreinforced and Reinforced Plastics and Electrical Insulating Materials. ASTM International.

Materials, ASTM., Testing, Materials, 2020. Standard Test Method for Core Shear Properties of Sandwich Constructions by Beam Flexure.

McCormack, T.M., Miller, R., Kesler, O., Gibson, L.J., 2001. Failure of sandwich beams with metallic foam cores. International Journal of Solids and Structures 38, 4901-4920.

Mehdikhani, M., Gorbatikh, L., Verpoest, I., Lomov, S.V., 2018. Voids in fiber-reinforced polymer composites: A review on their formation, characteristics, and effects on mechanical performance. Journal of Composite Materials 53, 1579-1669.

Mei, J., Liu, J., Huang, W., 2022. Three-point bending behaviors of the foam-filled CFRP X-core sandwich panel: Experimental investigation and analytical modelling. Composite Structures 284, 115206.

Mei, J., Tan, P.J., Bosi, F., Zhang, T., Liu, J.Y., Wang, B., Huang, W., 2021. Fabrication and mechanical characterization of CFRP X-core sandwich panels. Thin-Walled Structures 158, 107144.

Metyx, C., 2020. Core materials Airex C70.

Minakuchi, S., Uezono, T., Takeda, N., 2012. Formation and relaxation of residual facesheet dent on foam-core sandwich structures by localized transverse loading. Journal of Sandwich Structures & Materials 15, 71-91.

Mines, R.A.W., Alias, A., 2002. Numerical simulation of the progressive collapse of polymer composite sandwich beams under static loading. Composites Part A: Applied Science and Manufacturing 33, 11-26.

Mohamed, M., Anandan, S., Huo, Z., Birman, V., Volz, J., Chandrashekhara, K., 2015. Manufacturing and characterization of polyurethane based sandwich composite structures. Composite Structures 123, 169-179.

Mohan, K., Hon, Y.T., Idapalapati, S., Seow, H.P., 2005. Failure of sandwich beams consisting of alumina face sheet and aluminum foam core in bending. Materials Science and Engineering: A 409, 292-301.

Mostafa, A., Shankar, K., Morozov, E.V., 2014. Experimental, Theoretical and Numerical Investigation of the Flexural Behaviour of the Composite Sandwich Panels with PVC Foam Core. Applied Composite Materials 21, 661-675.

Mostafa, A., Shankar, K., Morozov, E.V., 2015. Behaviour of PU-foam/glass-fibre composite sandwich panels under flexural static load. Materials and Structures 48, 1545-1559.

Naik, R., Kempaiah, U.N., Santhosh, N., 2013. Development and Charecterization of High Performance Reinforced Carbon-Fiber and Glass-Fiber Composites. International Journal of Advanced and Innovative Research 99, 2278-7844.

Naik, N.K., Ganesh, V.K., 1992. Prediction of on-axes elastic properties of plain weave fabric composites. Composites Science and Technology 45, 135-152.

Naik, N.K., Ganesh, V.K., 1995. An analytical method for plain weave fabric composites. Composites 26, 281-289.

Naik, N.K., Ganesh, V.K., 1996. Failure Behavior of Plain Weave Fabric Laminates under On-Axis Uniaxial Tensile Loading: I—Analytical Predictions. Journal of Composite Materials 30, 1779-1822.

Naik, N.K., Kumar, R.S., 1999. Compressive strength of unidirectional composites: evaluation and comparison of prediction models. Composite Structures 46, 299-308.

Naik, R.A., 1994. Analysis of Woven and Braided Fabric Reinforced Composites, NASA Contractor Report 194930.

Najafi, M., Eslami, F.R., Khalili, S., 2012. Comparison of compressive properties between vacuum infusion and hand lay-up method toward balsa core sandwich composites.

Newaz, G., Dhaliwal, G.S., Phadatare, A., Hailat, M., 2019. Effect of padding on flexural response of sandwich composites. Journal of Sandwich Structures & Materials 23, 1253-1271.

Oterkus, E., Diyaroglu, C., De Meo, D., Allegri, G., 2016. 4 - Fracture modes, damage tolerance and failure mitigation in marine composites, in: Graham-Jones, J., Summerscales, J. (Eds.), Marine Applications of Advanced Fibre-Reinforced Composites. Woodhead Publishing, pp. 79-102.

Öchsner, A., 2021. Classical Beam Theories of Structural Mechanics. Springer International Publishing.

Pandita, S.D., Nishiyabu, K., Verpoest, I., 2003. Strain concentrations in woven fabric composites with holes. Composite Structures 59, 361-368.

Peliński, K., Smardzewski, J., 2020. Bending Behavior of Lightweight Wood-Based Sandwich Beams with Auxetic Cellular Core. 12, 1723.

Pruez, J., Shoukry, S., William, G., Shoukry, M., 2013. Lightweight Composite Materials for Heavy Duty Vehicles.

Qi, Y., Fang, H., Shi, H., Liu, W., Qi, Y., Bai, Y., 2017. Bending performance of GFRP-wood sandwich beams with lattice-web reinforcement in flatwise and sidewise directions. Construction and Building Materials 156, 532-545.

Quispitupa, A., Berggreen, C., Carlsson, L.A., 2009. Design Analysis of the Mixed Mode Bending Sandwich Specimen. Journal of Sandwich Structures & Materials 12, 253-272.

Raju, I., Wang, J., 1994. Classical laminate theory models for woven fabric composites. Journal of Composites Technology and Research 16, 289-303.

Rapp, H., 1992. Non-homogeneous bars under tension, pure bending and thermal loads. Composites Science and Technology 44, 21-28.

Russell, B., Liu, T., Fleck, N., Deshpande, V.S., 2011a. Quasi-Static Three-Point Bending of Carbon Fiber Sandwich Beams With Square Honeycomb Cores. Journal of Applied Mechanics 78.

Sadighi, M., Pouriayevali, H., 2008. Quasi-Static and Low-Velocity Impact Response of Fully Backed or Simply Supported Sandwich Beams. Journal of Sandwich Structures & Materials 10, 499-524.

Sandifer, R.H., 1969. Analysis and Design of Structural Sandwich Panels. H. G. Allen. Pergamon Press, London. 1969. 284 pp. Illustrated. 35s. The Aeronautical Journal (1968) 73, 982-982.

Selver, E., Kaya, G., 2019. Flexural properties of sandwich composite laminates reinforced with glass and carbon Z-pins. 53, 1347-1359.

Sharaf, T., Fam, A., 2012. Numerical modelling of sandwich panels with soft core and different rib configurations. Journal of Reinforced Plastics and Composites 31, 771-784.

Shi, S., Sun, Z., Hu, X., Chen, H., 2014. Flexural strength and energy absorption of carbon-fiber–aluminum-honeycomb composite sandwich reinforced by aluminum grid. Thin-Walled Structures 84, 416-422.

Shokrieh, M.M., Kamali Shahri, S.M., 2021. 6 - Modeling residual stresses in composite materials, in: Shokrieh, M.M. (Ed.), Residual Stresses in Composite Materials (Second Edition). Woodhead Publishing, pp. 193-213.

Shuaeib, F.M., Soden, P.D., 1997. Indentation failure of composite sandwich beams. Composites Science and Technology 57, 1249-1259.

Song, X.R., 2003. Vacuum Assisted Resin Transfer Molding (VARTM): Model Development and Verification.

Staal, R.A., Mallinson, G.D., Jayaraman, K., Horrigan, D.P.W., 2009. Predicting Failure Loads of Undamaged Sandwich Honeycomb Panels Subject to Bending. Journal of Sandwich Structures & Materials 11, 73-104.

Steeves, C., Fleck, N., 2004a. Collapse mechanisms of sandwich beams with composite faces and a foam core, loaded in three-point bending. Part I: Analytical models and minimum weight design. International Journal of Mechanical Sciences. 46, 561-583.

Steeves, C., Fleck, N., 2004b. Collapse mechanisms of sandwich beams with composite faces and a foam core, loaded in three-point bending. Part II: Experimental investigation and numerical modelling. International Journal of Mechanical Sciences 46, 585-608.

Stier, B., Simon, J.W., Reese, S., 2015. Comparing experimental results to a numerical meso-scale approach for woven fiber reinforced plastics. Composite Structures 122, 553-560.

Studziński, R., Pozorski, Z.J.J.o.S.S., Materials, 2018. Experimental and numerical analysis of sandwich panels with hybrid core. 20, 271-286.

Tabiei, A., Song, G., Jiang, Y., 2003. Strength Simulation of Woven Fabric Composite Materials with Material Nonlinearity Using Micromechanics Based Model. Journal of Thermoplastic Composite Materials. 16, 5-20.

Tagarielli, V.L., Fleck, N.A., Deshpande, V.S., 2004. Collapse of clamped and simply supported composite sandwich beams in three-point bending. Composites Part B: Engineering 35, 523-534.

Taghipoor, H., Eyvazian, A., ghiaskar, A., Praveen Kumar, A., Magid Hamouda, A., Gobbi, M., 2020. Experimental and numerical study of lattice-core sandwich panels under low-speed impact. Materials Today: Proceedings 27, 1487-1492.

Taghizadeh, S.A., Farrokhabadi, A., Liaghat, G., Pedram, E., Malekinejad, H., Mohammadi, S.F., Ahmadi, H., 2019. Characterization of compressive behavior of PVC foam infilled composite sandwich panels with different corrugated core shapes. Thin-Walled Structures 135, 160-172.

Tan, P., Tong, L., Steven, G.P., 1999. Micromechanics models for the elastic constants and failure strengths of plain weave composites. Composite Structures 47, 797-804.

Tang, X., Whitcomb, J.D., 2003. Progressive Failure Behaviors of 2D Woven Composites. Journal of Composite Materials 37, 1239-1259.

Tanov, R., Tabiei, A., 2000. Computationally Efficient Micromechanical Models for Woven Fabric Composite Elastic Moduli. Journal of Applied Mechanics 68, 553-560.

Testing, ASTM., Materials, 2008. Standard Test Method for Tensile Properties of Polymer Matrix Composite Materials. ASTM International.

Theotokoglou, E.E., 1996. Analytical determination of the ultimate strength of sandwich beams. Applied Composite Materials 3, 345-353.

Thiagarajan, S., Munusamy, R., 2022. Experimental and numerical study of composite sandwich panels for lightweight structural design. International Journal of Crashworthiness 27, 747-758.

Timoshenko, S., 1941. Strength of materials. D. Van Nostrand Company, inc.

Timoshenko, S.P., 1921. LXVI. On the correction for shear of the differential equation for transverse vibrations of prismatic bars. The London, Edinburgh, and Dublin Philosophical Magazine and Journal of Science 41, 744-746.

Truong, T.C., Vettori, M., Lomov, S., Verpoest, I., 2005. Carbon composites based on multi-axial multi-ply stitched preforms. Part 4. Mechanical properties of composites and damage observation. Composites Part A: Applied Science and Manufacturing 36, 1207-1221.

Tsai, S.W., Wu, E.M., 1971. A General Theory of Strength for Anisotropic Materials. Journal of Composite Materials 5, 58-80.

Tutuncu, N., 1995. Effect of anisotropy on stresses in rotating discs. International Journal of Mechanical Sciences 37, 873-881.

Udhayaraman, R., Mulay, S.S., 2017. Multi-scale approach based constitutive modelling of plain woven textile composites. Mechanics of Materials 112, 172-192.

Udhayaraman, R., Mulay, S.S., 2019. Multi-scale damage framework for textile composites: Application to plain woven composite. Eur J Mech a-Solid 77.

Umer, R., Waggy, E. M., Haq, M., Loos, A. C., 2012. Experimental and numerical characterizations of flexural behavior of VARTM-infused composite sandwich structures. Journal of Reinforced Plastics and Composites. 31, 67-76.

Uzay, Ç., Acer, D.C., Geren, N., 2022a. A method for the optimal design of low-density polymer foam core sandwiches using FEA and multiobjective optimization of design variables. 42, 75-84.

Uzay, Ç., Çetin, A., Geren, N., 2022b. Physical and mechanical properties of laminar composites depending on the production methods: an experimental investigation. Sādhanā 47, 262.

Uzay, Ç., Çetin, A., Geren, N., Bayramoğlu, M., Tütüncü, N., 2023. Predicting the tensile stiffness and strength properties of plain woven carbon fiber/epoxy laminates: a practical analytical approach and experimental validations. Mechanics of Advanced Materials and Structures, 1-16.

Uzay, Ç., Geren, N., 2020a. Effect of stainless-steel wire mesh embedded into fibre-reinforced polymer facings on flexural characteristics of sandwich structures. Journal of Reinforced Plastics and Composites 39, 613-633.

Uzay, Ç., Geren, N., 2022. Chpt 11:Enhanced Failure Behavior for Sandwiches with Hybrid Wire Mesh/FRP Face Sheets, in: Senthilkumar Krishnasamy, Chandrasekar Muthukumar, Senthil Muthu Kumar Thiagamani, Sanjay Mavinkere Rangappa, Siengchin, S. (Eds.), Sandwich Composites, Fabrication and Characterization. CRC Press, p. 406.

Uzay, Ç., Geren, N., 2020b. Failure Analysis of Low-density Polymer Foam Core Sandwich Structures under Three-point Bending Loading. University of Cukurova Journal of the Faculty of Engineering 35, 49-58.

Vahidi Bidhendi, M., Rahimi, G.H., Gazor, M.S., Zangoei, A.R., 2022. Experimental and numerical investigation of debonding in the composite sandwich structures with a foam-composite core under TPSB test. Journal of the Brazilian Society of Mechanical Sciences and Engineering 44, 604.

Vidal-sallé, E., Boisse, P., 2012. 2D Textile Composite Reinforcement Mechanical Behavior, Polymer Composites, pp. 363-392.

Vinson, J.R., Sierakowski, R.L., 2008. Beams Columns and Rods of Composite Materials, in: Vinson, J.R., Sierakowski, R.L. (Eds.), The Behavior Of Structures Composed Of Composite Materials. Springer Netherlands, Dordrecht, pp. 155-213.

Vitale, J.P., Francucci, G., Xiong, J., Stocchi, A., 2017. Failure mode maps of natural and synthetic fiber reinforced composite sandwich panels. Composites Part A: Applied Science and Manufacturing 94, 217-225.

Vocke, W., 1967. F. J. Plantema, Sandwich Construction. XX + 246 S. m. Fig. New York/London/Sydney 1966. John Wiley & Sons, Inc. Preis geb. 115 s. ZAMM - Journal of Applied Mathematics and Mechanics / Zeitschrift für Angewandte Mathematik und Mechanik 47, 138-138.

Wadsworth, D.J., Horrigan, D.P.W., Moltschaniwskyj, G., Collins, I., 2009. Facesheet Wrinkling of Damaged Honeycomb Sandwich Structures. Journal of Sandwich Structures & Materials 11, 105-131.

Wang, B., Zhou, Y., Tong, C., (2015a). Failure mechanism of PMI foam core sandwich beam in bending. International Journal for Simulation and Multidisciplinary Design Optimization. 6, A8, 10-1051.

Wang, B., Wu, L., Jin, X., Du, S., Sun, Y., Ma, L., 2010. Experimental investigation of 3D sandwich structure with core reinforced by composite columns. Materials & Design 31, 158-165.

Wang, L., Liu, W., Fang, H., Wan, L., 2015b. Behavior of sandwich wall panels with GFRP face sheets and a foam-GFRP web core loaded under four-point bending. 49, 2765-2778.

Wang, L., Zhao, B., Wu, J., Chen, C., Zhou, K., 2018. Experimental and numerical investigation on mechanical behaviors of woven fabric composites under off-axial loading. International Journal of Mechanical Sciences 141, 157-167.

Wang, Q., Sun, L., Yang, W., Zhan, B., Yang, X., 2019. An analytical approach for predicting the tensile strength of plain weave fabric composites. Polymer Composites 40, 2391-2399.

Wang, X., Shi, X.-l., Meng, Q.-k., Hu, Y.-c., Wang, L.-h., 2020. Bending behaviors of three grid sandwich structures with wood facing and jute fabrics/epoxy composites cores. Composite Structures 252, 112666.

Wei, X., Wu, Q., Gao, Y., Xiong, J., 2020. Bending characteristics of all-composite hexagon honeycomb sandwich beams: experimental tests and a three-dimensional failure mechanism map. Mechanics of Materials 148, 103401.

Wen, P., Aliabadi, M.H., 2011. Mesh-free micromechanical model for woven fabric composite elastic moduli. Journal of Multiscale Modelling 01.

Xie, H., Shen, C., Fang, H., Han, J., Cai, W., 2022. Flexural property evaluation of web reinforced GFRP-PET foam sandwich panel: Experimental study and numerical simulation. Composites Part B: Engineering 234, 109725.

Xiong, J.J., Shenoi, R.A., Cheng, X., 2009. A modified micromechanical curved beam analytical model to predict the tension modulus of 2D plain weave fabric composites. Composites Part B: Engineering 40, 776-783.

Yang, Y., Zeng, P., 2018. A computationally efficient model to predict the uniaxial tensile loading response for dry woven fabrics. Composite Structures 201, 434-445.

Yazici, M., Wright, J., Bertin, D., Shukla, A., 2014. Experimental and numerical study of foam filled corrugated core steel sandwich structures subjected to blast loading. Composite Structures 110, 98-109.

Yildirim, S., Tutuncu, N., 2014. Analysis of Composite Plates by Kompro. International Journal of Arts&Sciences.

Yu, Y., Hou, W.-b., Hu, P., Yang, H., Jia, X., 2019. Failure analysis and bending performance of carbon fiber composite sandwich structures with corrugated cores. Journal of Sandwich Structures & Materials 23, 1427-1452.

Yuan, H., Zhang, J., Sun, H., 2022. The failure behavior of double-layer metal foam sandwich beams under three-point bending. Thin-Walled Structures 180, 109801.

Yurgartis, S.W., 1987. Measurement of small angle fiber misalignments in continuous fiber composites. Composites Science and Technology. 30, 279-29.

Zenkert, D., 1995. An Introduction to Sandwich Construction. Engineering Materials Advisory Services.

Zenkert, D., Fund, N.I., 1997. The Handbook of Sandwich Construction. Engineering Materials Advisory Services.

Zenkert, D., Shipsha, A., Persson, K., 2004. Static indentation and unloading response of sandwich beams. Composites Part B: Engineering 35, 511-522.

Zhang, F., Liu, W., Fang, H., Jia, Z., 2019. Flexural behavior of composite sandwich beams with different kinds of GFRP ribs in flatwise and edgewise positions. Composites Part B: Engineering 156, 229-239.

Zhang, J., Qin, Q., Ai, W., Li, H., Wang, T.J., 2014. The Failure Behavior of Geometrically Asymmetric Metal Foam Core Sandwich Beams Under Three-Point Bending. Journal of Applied Mechanics 81.

Zhang, J., Qin, Q., Ai, W., Wang, Z., Wang, T.J., 2016. Indentation of Metal Foam Core Sandwich Beams: Experimental and Theoretical Investigations. Experimental Mechanics. 56, 771-784.

Zhang, J., Supernak, P., Mueller-Alander, S., Wang, C.H., 2013. Improving the bending strength and energy absorption of corrugated sandwich composite structure. Materials & Design. (1980-2015) 52, 767-773.

Zhang, W., Qin, Q., Li, J., Li, K., Poh, L.H., Li, Y., Zhang, J., Xie, S., Chen, H., Zhao, J., 2020a. Deformation and failure of hybrid composite sandwich beams with a metal foam core under quasi-static load and low-velocity impact. Composite Structures. 242, 112175.

Zhang, W., Qin, Q., Li, J., Su, B., Zhang, J., 2020b. A comparison of structural collapse of fully clamped and simply supported hybrid composite sandwich beams with geometrically asymmetric face sheets. Composites Part B: Engineering 201, 108398.

Zhen, M.J., 2013. A Multiscale modeling Approach for the Progressive Failure Analysis of Textile Composites. National University of Singapore.

Zhu, D., Shi, H., Fang, H., Liu, W., Qi, Y., Bai, Y., 2018. Fiber reinforced composites sandwich panels with web reinforced wood core for building floor applications. Composites Part B: Engineering. 150, 196-211.

Zingone, G., 1968. Limit analysis of a beam in bending immersed in an elastoplastic medium. Meccanica. 3, 48-56.

**CURRICULUM VITAE**

Ahmet ÇETİN, completed his high school education at Anamur Anatolian High School in 2008. 2014, he graduated from Çukurova University Automotive Engineering Department with highest grade point average. As part of his double-major program, he also obtained the Bachelor of Science degree in Mechanical Engineering in the same year. In 2017, he completed his Master's degree at Çukurova University, Department of Mechanical Engineering. He started his PhD education in the same department in 2018. In 2014, he started working as a research assistant at Adıyaman University. Since 2015, he has worked as a research assistant at Çukurova University, Faculty of Engineering, Department of Mechanical Engineering.